BONE-DERIVED HYDROXYAPATITE TOOTHPASTE FOR SUSTAINABLE PHARMACEUTICAL AND BIOMEDICAL APPLICATIONS

ARTICLES FOR FACULTY MEMBERS

Antibacterial activity of natural-based toothpaste incorporated with nano-hydroxyapatite from fish bone against dental caries bacteria / Hasan, M. R., Ghazali, M. S. M., & Mohtar, N. F.

Food Research
Volume 8 Issue 2 (2024) Pages 192–200
https://doi.org/10.26656/fr.2017.8(2).119
(Database: Rynnye Lyan Resources)

Bovine cancellous hydroxyapatite toothpaste enhances enamel remineralization / Octarina, O., Kurniawan, F. L., Falatehan, N., Sofiana, K., Siregar, G. M., Maulana, I. N., & Surboyo, M. D. C.

International Dental Journal
Volume 76 Issue 1 (2026) 109308 Pages 1-9
https://doi.org/10.1016/j.identj.2025.109308
(Database: ScienceDirect)

Comparative assessment of the remineralization characteristics of nano-hydroxyapatite extracted from fish scales and eggshells / Mkhize, S. C., Onwubu, S. C., Mokhothu, T. H., Mdluli, P. S., & Mishra, A. K.

Journal of Applied Biomaterials and Functional Materials
Volume 21 (2023) Pages 1-10
https://doi.org/10.1177/22808000231180390
(Database: Sage Journals)

BONE-DERIVED HYDROXYAPATITE TOOTHPASTE FOR SUSTAINABLE PHARMACEUTICAL AND BIOMEDICAL APPLICATIONS

ARTICLES FOR FACULTY MEMBERS

Hydroxyapatite recovery from fish byproducts for biomedical applications / Hernández-Ruiz, K. L., López-Cervantes, J., Sánchez-Machado, D. I., Martínez-Macias, M. del R., Correa-Murrieta, M. A., & Sanches-Silva, A.

Sustainable Chemistry and Pharmacy
Volume 28 (2022) 100726 Pages 1-14
https://doi.org/10.1016/j.scp.2022.100726
(Database: ScienceDirect)

Marine bioceramic generation for bone tissue regeneration: Sea urchin (echinometra mathaei) exoskeleton-derived calcium carbonate as a precursor for hydroxyapatite synthesis, incorporated into chitosan based-hydrogel and 3d-printed PCL scaffold for osteogenic differentiation / Jamshidizadeh, S., Amrollahi Biuki, N., & Zarei, M.

Marine Biotechnology
Volume 28 Issue 25 (2026) Pages 1-19
https://doi.org/10.1007/s10126-025-10555-5
(Database: Springer Nature Link)

Microwave-assisted hydrothermal synthesis of hydroxyapatite from fermented fish by-product for removal of lead from contaminated water / Chaiyachet, W., Junggoth, R., Donprajum, T., Yasaka, S., Chaiyachet, R., & Kanchanatip, E.

Beni-Suef University Journal of Basic and Applied Sciences
Volume 14 Issue 116 (2025) Pages 1-22
https://doi.org/10.1186/s43088-025-00704-z
(Database: Springer Nature Link)

BONE-DERIVED HYDROXYAPATITE TOOTHPASTE FOR SUSTAINABLE PHARMACEUTICAL AND BIOMEDICAL APPLICATIONS

ARTICLES FOR FACULTY MEMBERS

Natural sources of hydroxyapatite for biomedical applications / Suresh, N., Sweety, V. K., Suresh, N., Suraj, A. R., Waltimo, T., & Anil, S.

Ceramics International
Volume 52 Issue 2 (2026) Pages 1383-1391
https://doi.org/10.1016/j.ceramint.2025.12.019
(Database: ScienceDirect)

Physicochemical analysis and application of sardinella fimbriata-derived hydroxyapatite in toothpaste formulations / Anwar, A. I., Ruslin, M., Marlina, E., & Hasanuddin, H.

BMC Oral Health
Volume 25 Issue 195 (2025) Pages 1-9
https://doi.org/10.1186/s12903-025-05557-7
(Database: Springer Nature Link)

Preparation and characterization of hydroxyapatite obtained from bovine bones / Alvarado, C., Alfaro, A., Cisneros, M., & Alvarado-Quintana, H.

Proceedings of the 21st LACCEI International Multi-Conference for Engineering, Education and Technology
(2023) Pages 1-6
https://doi.org/10.18687/laccei2023.1.1.590
(Database: Latin American and Caribbean Consortium of Engineering Institutions)

ARTICLES FOR FACULTY MEMBERS

BONE-DERIVED HYDROXYAPATITE TOOTHPASTE FOR SUSTAINABLE PHARMACEUTICAL AND BIOMEDICAL APPLICATIONS

Antibacterial activity of natural-based toothpaste incorporated with nano-hydroxyapatite from fish bone against dental caries bacteria / Hasan, M. R., Ghazali, M. S. M., & Mohtar, N. F.

Food Research
Volume 8 Issue 2 (2024) Pages 192–200
https://doi.org/10.26656/fr.2017.8(2).119
(Database: Rynnye Lyan Resources)

Food Research 8 (2) : 192 - 200 (April 2024)
Journal homepage: https://www.myfoodresearch.com

FOOD RESEARCH

RESEARCH PAPER

Antibacterial activity of natural-based toothpaste incorporated with nano-hydroxyapatite from fish bone against dental caries bacteria

[1]Hasan, M.R., [2]Ghazali, M.S.M. and [1,*]Mohtar, N.F.

[1]*Faculty of Fisheries and Food Science, Universiti Malaysia Terengganu, 21030 Kuala Nerus, Terengganu, Malaysia*

[2]*Faculty of Science and Marine Environment, Universiti Malaysia Terengganu, 21030 Kuala Nerus, Terengganu, Malaysia*

Article history:
Received: 19 March 2022
Received in revised form: 26 April 2022
Accepted: 4 September 2022
Available Online: 26 March 2024

Keywords:
Hydroxyapatite,
Toothpaste,
Essential oil,
Antibacterial,
Dental caries

DOI:
https://doi.org/10.26656/fr.2017.8(2).119

Abstract

Toothpaste formulation development has become important due to dental health problems. There has been a large array of improvements in the formulation including fluoride and microbeads (MBs) incorporation. However, the typical problems of the current toothpaste formulation are caused due to the fluoride and MBs toxicity issues on consumer health and aquatic animals. There is an urgent need to rectify this problem through the development of environmentally friendly hydroxyapatite (HAp) toothpaste using different natural components. This study was set out to determine the optimum gelling agent in toothpaste formulation and to investigate the effect of different combinations of the components in HAp-based toothpaste against *Streptococcus mutans*. The antibacterial activity of the developed toothpaste formulation was investigated using a well-diffusion method and the optimum concentration of the gelling agent (Arabic gum) was determined using a rheometer. One of the most significant findings in the study was the optimum concentration of the gelling agent was found at 55% and a combination of formulation with clove oil (CO) demonstrated the largest size of inhibition against *S. mutans* (CO = 24 mm, CO with formulation = 11 mm) compared to the other tested components. Findings from this study have suggested that the combination of formulation in HAp-based toothpaste with CO demonstrated the best bacterial inhibitory effect and the optimum gelling agent was at 55%. The overall finding is particularly important in the formulation development of HAp-based toothpaste, thus contributing to an increased supply of HAp in meeting its demand in the Halal market.

1. Introduction

There has been a growing recognition that more concern should be made to toothpaste formulation development as a result of dental health issues, particularly dental caries. Dental caries is a chronic infectious illness that affects tooth hard tissue, which has influenced toothpaste formulation (Takahashi and Nyvad, 2011; Cheng *et al*., 2017). The deposition of acidic metabolites such as glucose leads to a pH decline underneath the critical pH, at which tooth hard-tissue demineralization begins (Takahashi and Nyvad, 2011; Cheng *et al*., 2017). Recently, there has been a resurgence of interest in fluoride toothpaste, which has been discovered as an extremely effective caries preventative agent with numerous benefits (Marinho *et al*., 2013; Marinho *et al*., 2015; Marinho *et al*., 2016; Fontana, 2016; Bijle *et al*., 2018; Walsh *et al*., 2019). Preventive treatments for caries are mostly performed by decreasing bacterial acid production or by altering the mineralization imbalance (Buzalaf *et al*., 2011; Bijle *et al*., 2018).

Fluoride is widely accepted as a functional anti-caries agent in the dental industry (Hardwick *et al*., 2000; Loveren, 2001; Koo, 2008; Featherstone, 2009; Cheng *et al*., 2017). It is rapidly becoming a critical component of tooth treatment as an efficient preventative measure against dental caries. Caries prevention is mostly achieved by brushing with fluoride toothpaste, but the efficacy varies depending on the dosage (Walsh *et al*., 2019). Despite its safety and effectiveness, fluoride toothpaste has some significant disadvantages. Fluoride toothpaste's widespread use may result in inadvertent ingestion during toothbrushing, resulting in dental fluorosis (Zohoori *et al*., 2012). Fluoride usage

*Corresponding author.
Email: *fazliyana@umt.edu.my*

eISSN: 2550-2166
Published by Rynnye Lyan Resources

has increased toxicity and the evolution of fluoride-resistant *Streptococcus mutans* and other oral bacterial species (Liao *et al*., 2017; Bijle *et al*., 2018). Excess fluoride administration can cause dental fluorosis, a persistent discoloration of the tooth enamel (Carwile *et al*., 2020). Intentional intake of a high amount of sodium fluoride has been claimed to result in severe bleeding and cardiac failure (Bridwell *et al*., 2019). In addition, synthetic microbeads (MBs) with diameters ranging from 5 mm to 1 mm have become extremely prevalent in toothpaste formulations (King *et al*., 2017; Nam and Park, 2020). MBs used in facial cleansers and toothpaste pose a huge public health issue and are hazardous to marine, agricultural, and freshwater habitats (Ding *et al*., 2020). Due to their non-biodegradability and durability in the marine ecosystem, these compounds are frequently settled in marine creatures (Nam and Park, 2020). MBs may be chronically hazardous to organisms due to their polymer constituents, characteristics, and tiny size (Sun *et al*., 2019; Ding *et al*., 2020). It tends to absorb endocrine-disrupting compounds (EDCs), medicines, and personal care products in aqueous conditions (Carr *et al*., 2016). Previous studies have proven the detrimental effects of MBs on several marine creatures, including the growth of medaka (Chisada *et al*., 2019), planktonic crustaceans (Gambardella *et al*., 2017), floating freshwater plants (Kalčíková *et al*., 2017), and chronic toxicity on freshwater zebra mussels (Magni *et al*., 2018). As a consequence, various substitute compounds, such as theobromine (Nakamoto *et al*., 2016; Premnath *et al*., 2019; Golfeshan *et al*., 2021), caffeine (Golfeshan *et al*., 2021), plant extract (Annisa *et al*., 2022) and hydroxyapatite (Sharma *et al*., 2015) are being identified as promising active ingredients in the protection of hypersensitivity and dental cavities. Preliminary research suggests that using hydroxyapatite (HAp) in toothpaste can minimize dental caries-causing dentine hypersensitivity (Sharma *et al*., 2015).

HAp is one of the most widely researched biomaterials in medicine and dentistry due to its biocompatibility (Balhuc *et al*., 2021). It has been employed as an additive material to strengthen currently utilized dental materials, particularly in preventative applications (Balhuc *et al*., 2021). HAp can enhance crystallite formation and proliferation, resulting in enamel remineralization (Oubenyahya, 2021). The use of HAp is justified since it would obliterate the open dentinal tubules and merge in with them, lessening the pain of dentine hypersensitivity (Vano *et al*., 2018). Over the last decade, substantial research has been undertaken on the integration of HAp into toothpaste formulations due to its potential beneficial effect (Esteves-Oliveira *et al*., 2016; Hiller *et al*., 2018; Vano *et al*., 2018; Amaechi *et al*., 2019; Bossù *et al*., 2019; Jumanca *et al*., 2019; Meyer and Enax, 2019; Hasan *et al*., 2020; Ionescu *et al*., 2020; Körner *et al*., 2020; Rifada *et al*., 2020; Sarembe *et al*., 2020; Steinert *et al*., 2020; Hasan *et al*., 2021a, 2021b; O'Hagan-Wong *et al*., 2021). Although the majority of research implies that toothpaste containing HAp has the potential to prevent dental caries, lesions, and microbial viability, this topic is still disputed.

There has been little consensus on the effectiveness of HAp as a fluoride replacement, signalling the need for additional research, particularly on the role of HAp against the leading cause of dental caries. It is well-known that the *S. mutans* species is the most prevalent strain related to teeth problems and diseases (Nachu *et al*., 2022). However, there seems to be a lack of prior research on the effect of HAp toothpaste on dental *S. mutans* bacteria. There is certainly a significant need to investigate the relevance of HAp-based toothpaste as a fluoride-free alternative for dental caries prevention. Other than that, the synthesis of HAp from fishery by-products can significantly contribute to better management of such waste. It is well-known that such by-products such as the skin, bone and internal organs contain high protein and biopolymers that can be utilized into high-value added products (Zhou *et al*., 2006; Karim and Bhat, 2009; Mohtar *et al*., 2010; Boutinguiza *et al*., 2012; Fan *et al.*, 2017; Chew *et al*., 2020; Hasan *et al*., 2020; Hasan *et al*., 2021a, 2021b; Alves *et al*., 2022; Dermawan *et al*., 2022; Derkach *et al*., 2022; Nie *et al*., 2022; Sockalingam *et al*., 2022). Therefore, the primary aim of this study was to evaluate the optimal gelling agent for toothpaste formulation and to assess the antimicrobial activity of various component combinations in HAp-based toothpaste against *S. mutans*. This study is an ideal opportunity to explore the combined effect of HAp and a few selected essential oils in toothpaste formulations against the aforementioned bacteria associated with dental caries.

2. Materials and methods

2.1 Preparation of raw materials and extraction of hydroxyapatite

Fish bones were collected from the local fish processing industries and were processed according to Hasan *et al*. (2020). They were then washed thoroughly and boiled to remove excess meat. They were then dried in an oven for 24 hrs. The dried bones were then heated in a furnace (Carbolite ELF 11/14B/301, UK) at temperatures ranging from 600 to 1000°C, with a heating rate of 10°C/min for 5 hrs and it was cooled isothermally for 3 hrs. The calcined bones were milled using the ball-mill (Retsch PM 100, Germany). The extraction was carried out based on the method of Boutinguiza *et al*.

https://doi.org/10.26656/fr.2017.8(2).119

(2012).

2.2 Preparation of toothpaste formulation

The preparation of toothpaste formulations was formulated based on the method of Ogboji *et al*. (2017). The abrasive agent and binder were weighed using fine balance before the binder was premixed with water at room temperature with continuous mixing until the jelly structure gradually formed. The gel was mixed with an abrasive agent with continuous stirring. The formed gel was mixed with oil components such as peppermint, clove, and neem oils at 40°C with continuous stirring to form an emulgel. This step is crucial step to ensure a homogeneous emulgel. The emulgel was next mixed with glycerine and olive oil and the homogeneous paste was deaerated and stored at 4°C for 24 hrs. The ingredients used for the formulation of the toothpaste are outlined in Table 1.

Table 1. List of ingredients used in the formulation of toothpaste in this study and their respective functions.

Components	Function	Percentage (%)
Arabic gum	Binder/emulsifier	55.0
HAp	Abrasive/active	3.0
Glycerine	Humectant	3.0
Olive oil	surfactant	1.5
Peppermint oil	Flavouring	1.5
Clove/Neem oils	Antibacterial	5.0
Water	Medium	31.0

2.3 Rheological analysis

The rheometer was used to measure the rheological properties of toothpaste formulations. All toothpaste formulations were kept at 25°C before they were analyzed using a rheometer (Hybrid Discovery HR-2, USA) with spindle no. 34 at speeds ranging from 10 to 100 rpm. The device was initially analyzed using a blank sample before the analysis as a control. A small amount of toothpaste sample was mounted on a sample disc and pressed with constant pressure. Experimental data was automatically recorded via a computer connected to a rheometer through Rheocalc software. Each experiment was carried out three times.

2.4 Evaluation of antibacterial

2.4.1 Preparation of medium culture

The nutrient agar (NA) and tryptone soy broth (TSB) were used for the subculturing medium of bacteria in this study. The agar and broth mediums were prepared by dissolving 28 g of NA powder and 30 g of TSB in 1 L of distilled water. Both of the mediums were then proceeded to the sterilization process using an autoclave at 121°C for 45 mins. The sterile NA solution was poured directly onto Petri dishes with an average of 25 mm thickness and a centrifuge tube for TSB. The poured agar solution was then left for 20 mins in the laminar flow for the solidification process. The Bunsen burner was used throughout the process to avoid any cross-contamination. The culture mediums were then kept at 4° C until further used.

2.4.2 Preparation of bacteria culture

The cross-streaking method was used in this study for the sub-culturing process of bacteria. The freeze-dried bacteria were purchased from a supplier and sub-cultured three times to obtain a pure culture. The process was carried out in a biological safety cabinet (BSC) and sprayed with 70% ethanol before the process. The inoculation loop was burned and a few colonies of single species of bacteria were inoculated and streaked onto the NA. The cultures were cultivated at 37°C for 40 to 48 hrs. The pure culture bacteria were then stored at -80°C in glycerol stock with a ratio of 1:1 until further use.

2.4.3 Antibacterial assay

2.4.3.1 Preparation of turbidity standard

A few colonies of bacteria on the surface of nutrient agar (NA) were inoculated and suspended into sterile and tryptone soy broth (TSB) and mixed well using a vortex for homogeneous suspension. The bacterial suspension was measured optically using an Ultraviolet-Visible Spectrophotometer (UV-Vis) at 550 nm wavelength. It was then diluted several times until reached the reading of 0.125 of optical density (OD) which is equivalent to the 0.5 McFarland turbidity standards.

2.4.3.2 Well diffusion

A toothpaste solution was prepared by mixing 3 g of toothpaste in 3 mL of distilled water (1:1 dilution). An amount of 0.2 mL of the mixture was incorporated into a nutrient agar (NA) plate using a micropipette and left for 1 hr. A sterile cork borer with a 6 mm diameter was used to form wells before the sample solutions were introduced on the surface of the agar. Gentamycin was used as the positive control while the formulation without oil was for the negative control. All of the plates were cultivated for 40 to 48 hrs at 37°C. The inhibition zone was then determined after the cultivation period.

2.5 Statistical analysis

One-way Analysis of Variance (ANOVA) and multiple comparisons (Post hoc test) were applied for all analyses and experiments in this study. A significant level was applied at $\alpha = 0.05$. The analyses were conducted using SPSS for Windows (Version 23.0).

https://doi.org/10.26656/fr.2017.8(2).119

3. Results and discussion

3.1 Rheological properties of the toothpaste formulation

The rheological property of the toothpaste formulation is important as it may influence the character of the formulation system. Determination of the rheological behaviour of three toothpaste formulations with various concentrations of Arabic gum (AG) was carried out using the rheometer. By using spindle no. 34 at a temperature of 25°C and rotational speed ranging from 10 to 100 rpm, the viscosity profiles of the three formulations of toothpaste samples were determined. Based on the results obtained, the results revealed that the difference in the viscosity profile of toothpaste samples was influenced by the combination of all ingredients and the concentration of the gelling agent. The viscosity analysis was conducted to determine the optimum concentration of gelling agent that was compatible to be applied in toothpaste formulation as a comparable concentration with standard toothpaste. Figure 1 shows a comparison of the viscosity of toothpaste formulation samples compared with standard toothpaste (ST) for clove and neem formulations.

The analysis of data shows that all of the toothpaste samples disobeyed the Newtonian interaction between viscosity, shear rate, and shear stress. This phenomenon can be considered as non-Newtonian fluids due to the decreasing value of viscosity over shear rate. The result demonstrated that C30 and N30 showed the lowest viscosity value compared to the others. This phenomenon could be due to poor network structure (Liu *et al.*, 2015). Meanwhile, C60 and N60 demonstrated the highest viscosity value and can be considered the most viscous and stable formulations. However, C55 has a viscosity value which was comparable to ST. Different concentrations and different components in toothpaste formulations could be significant contributors to the changes in the rheological behaviour of those formulations (Cai *et al*., 2017). According to Liu *et al*. (2015), different types of commercial toothpaste have different viscosity values; Darlie (3.4 kPa/s), Colgate (4.2 kPa/s), and Ynby (4.8 kPa/s). They added a point that the viscosity values of the three toothpaste formulation samples were significantly decreased as the shear rate increased which indicated that all samples follow shear-thinning behaviour. According to the Newtonian rule, a liquid can be considered Newtonian if its viscosity varies linearly with the shear rate (Ahuja and Potanin, 2018). This indicated that the viscosity of all toothpaste samples in the present study followed a non-Newtonian behaviour which had pseudoplastic properties, aligned with the theoretical viscosity behaviour of toothpaste and other such gelling agents (Carboxy-methyl cellulose and xanthan gum) (Barros *et al.,* 2022). This situation could be due to the aggregation of molecules in the sample which started to be destroyed and deformed when the molecules moved on the spindle surface. Based on the rheological properties, the optimum concentration of the AG was found to be 55% and it was used in the formulation for further analysis.

3.2 Antibacterial properties of the toothpaste formulation

The antibacterial test was carried out to discover the bacterial inhibitory properties of the toothpaste formulation against gram-positive *S. mutans*. This species of bacteria was chosen due to the species' domination on teeth and it is usually related to mouth diseases such as gingivitis and periodontitis. The test was

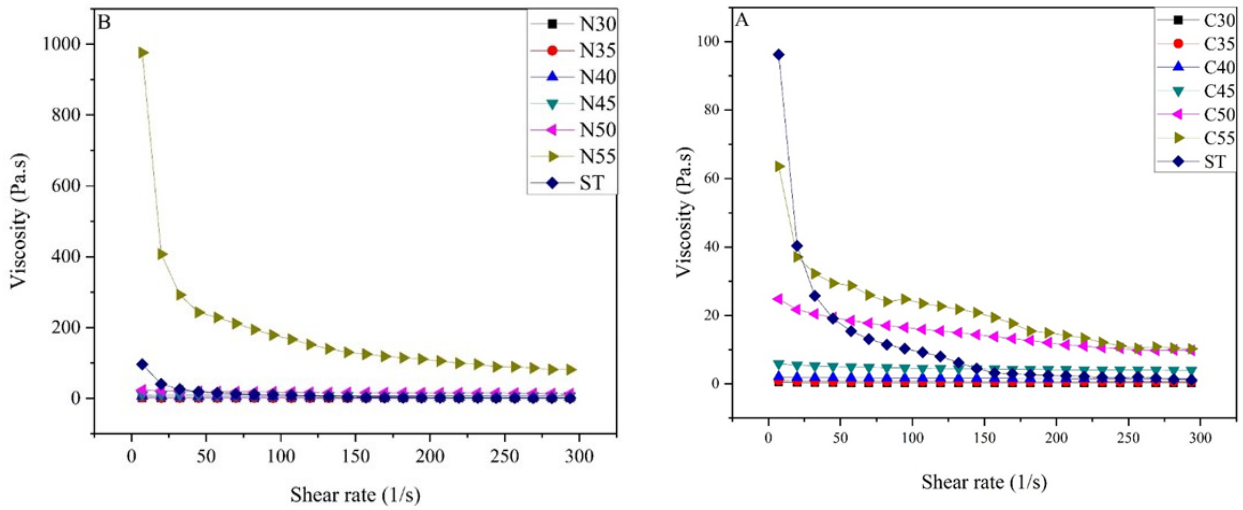

Figure 1. Comparison of the viscosity of toothpaste formulation with the addition of (A) clove and (B) neem and comparison with ST.

C30, C35, C40, C45, C50, and C55 represent toothpaste formulation with the addition of clove oil 30%, 35%, 40%, 45%, 50% and 55%, respectively.

N30, N35, N40, N45, N50, N55 represent toothpaste formulation with the addition of neem oil 30%, 35%, 40%, 45%, 50% and 55%, respectively.

https://doi.org/10.26656/fr.2017.8(2).119

carried out on hydroxyapatite (HAp), clove oil (CO), neem oil (NO), HAp + formulation (HF), clove oil + formulation (CF), and neem oil + formulation (NF). The size of the inhibition zones is presented in Table 2.

The most interesting aspect of the result was that the CO formulation had the largest size of inhibition (21 mm) compared to the other tested components followed by the CF formulation (11 mm). In Table 2, there is a clear trend of the size of inhibition which decreased with the combination of the formulation. Further statistical tests revealed the significant difference in the inhibition zone demonstrated by the CO. However, no significant difference was observed in the size of inhibition for other samples. The most surprising aspect of the data is that the size of inhibition decreased with the combination of the formulation. The combination of different ingredients of toothpaste formulation resulted in the interaction of the components occurring, hence reducing the antibacterial effect.

Table 2. Size of inhibition zone of the samples against *S. mutans* species.

Samples	Size of inhibition (mm)
Clove oil	21±3.06[a]
Neem oil	11±3.61[b]
HAp	10±1.53[b]
Clove with formulation	11±2.65[b]
Neem with formulation	7±2.52[b]
HAp with formulation	9±2.00[b]
Gentamycin	28±1.53[c]

Values are presented as mean±SD of triplicates. Values with different superscripts are statistically significantly different ($p<0.05$).

Dental caries are the specific damage of susceptible dental hard tissues induced by acidic by-products of bacterial fermentation of dietary carbohydrates. These plaques can attract the presence of anaerobic bacteria such as *S. mutans* to surround the plaque area. These bacteria could carry anaerobic respiration by metabolizing the sugar from the plaque. Anaerobic respiration is necessary for their survival through the production of cellular energy in the form of adenosine triphosphate (ATP). However, the anaerobic glycolysis process of the bacteria could cause the release of lactic acid as a by-product. The demineralization of enamel, dentine, or cementum happens when the pH drops below a threshold range. Therefore, the present study was designed to determine the effect of a different combination of the components in HAp-based toothpaste against *S. mutans.*

The current study found that the inhibition size of the tested toothpaste formulation in this study ranged from 7 mm to 21 mm, with CO exhibiting the highest size of inhibition zone against *S. mutans*. This also accords with earlier findings from Yumas *et al.* (2022), which showed that the inhibition size against *S. mutans* of the tested toothpaste formulation containing different concentrations of unfermented cocoa powder ranged from 18 mm to 21 mm. One unanticipated finding was that the combination of the different components has resulted in the reduction of the antibacterial effect of the samples. This finding is consistent with that of Sunitha *et al.* (2015) who found that toothpaste containing different ingredient-based (neem = 16.66 mm, Vicco Vajradanti = 15.6 mm, Himalaya Herbal = 16.66 mm Colgate Herbal = 18 mm, Dabur Red = 17.33 mm, and Dabur Babool = 19 mm) demonstrates the different size of inhibition against *S. mutans*. This finding broadly supports the work of other studies in this area which suggested that different combinations of toothpaste ingredients had different antibacterial effects. A possible explanation for these results may be due to the interaction of the components, thus minimizing the antibacterial effect of the oil. The antibacterial effect of the CO was mainly contributed by the primary active compounds which consisted of eugenol and eugenol acetate. Cloves' chemical composition has been found to exhibit 81 to 84% eugenol, 3 to 4% ß-caryophyllene, and 81 to 86% eugenol (Sohilait, 2015).

The underlying mechanism is believed to be the penetration of the active compound into the cytoplasmic membrane which then inhibits the normal synthesis of deoxyribonucleic acid (DNA) and proteins that are required for bacterial growth. Essential oils (EO) can infiltrate bacterium cells, altering the regular functions of cells due to volatility and water solubility (Nair *et al.,* 2022). It destroys cell walls and membranes, next causing the loss of vital intracellular materials, which finally results in the apoptosis of bacteria cells (Xu *et al*., 2016). However, the combination of the components has ceased and reduced the penetration of the active compound to the bacteria cell. This result is suggestive of a link between the combination of different components in toothpaste formulation and the inhibition effect on bacteria which provides an insight into the toothpaste product research and development. However, the finding in this study is somehow limited to revealing the inhibitory effect of different concentrations of samples which indicates future studies on this matter are therefore recommended.

4. Conclusion

This study revealed that a combination of formulation with CO had the largest size of inhibition against *S. mutans* compared to the other tested

https://doi.org/10.26656/fr.2017.8(2).119

components. This finding suggests that the combination of formulation with CO in HAp toothpaste demonstrated the best bacterial inhibitory effect. This work contributes to the existing knowledge of toothpaste formulation development particularly HAp-based toothpaste products by providing a different angle of knowledge in which, a synergistic effect of HAp-based toothpaste with different EO had shown improved antibacterial properties. Overall, this finding implies that both single component and combination effects should be taken into account when developing a toothpaste formulation due to the different degrees of effectiveness.

Conflicts of interest

The authors have no financial or commercial conflicts of interest in this paper.

Acknowledgements

The authors would like to acknowledge the Faculty of Fisheries and Food Science (FPSM) and Centre of Research and Field Services (CRaFS) of Universiti Malaysia Terengganu for the support of facilities and materials in carrying out the research. This work did not receive any specific grant from funding agencies in the public, commercial, or not-for-profit sectors.

References

Ahuja, A. and Potanin, A. (2018). Rheological and sensory properties of toothpastes. *Rheologica Acta*, 57(6), 459–471. https://doi.org/10.1007/s00397-018-1090-z

Alves, A.L., Fraguas, F.J., Carvalho, A.C., Valcárcel, J., Pérez-Martín, R.I., Reis, R.L., Vázquez, J.A. and Silva, T.H. (2022). Characterization of codfish gelatin: A comparative study of fresh and salted skins and different extraction methods. *Food Hydrocolloids,* 124(Part A), 107238. https://doi.org/10.1016/j.foodhyd.2021.107238

Amaechi, B.T., Ahmed, A.P., Alshareif, D.O., Shehata, M.A., Sampaio, L.P.P.C., Abdollahi, A., Kalkhorani, P.S. and Evans, V. (2019). Comparative efficacy of a hydroxyapatite and a fluoride toothpaste for prevention and remineralization of dental caries in children. *British Dental Journal Open*, 5, 18. https://doi.org/10.1038/s41405-019-0026-8

Annisa, M., Kanina, P.A.R., Hamid, N.L. and Nuryanti, A. (2022). Effectiveness of green tea, bay leaf, and lime peel extracts as toothpastes active agents for extrinsic stain removal on teeth, artificial teeth, and denture base. *Padjadjaran Journal of Dentistry,* 34 (1), 47-56. https://doi.org/10.24198/pjd.vol34no1.32236

Balhuc, S., Campian, R., Labunet, A., Negucioiu, M., Buduru, S. and Kui, A. (2021). Dental applications of systems based on hydroxyapatite nanoparticles-An evidence-based update. *Crystals*, 11(6), 674-693. https://doi.org/10.3390/cryst11060674

Barros, P.L., Ein-Mozaffari, F. and Ali Lohi. (2022). Gas dispersion in non-Newtonian fluids with mechanically agitated systems: A review. *Processes*, 10(2), 275-304. https://doi.org/10.3390/pr10020275

Bijle, M.N.A., Ekambaram, M., Lo, E.C.M. and Yiu, C.K.Y. (2018). The combined enamel remineralization potential of arginine and fluoride toothpaste. *Journal of Dentistry*, 76, 75–82. https://doi.org/10.1016/j.jdent.2018.06.009

Bossù, M., Saccucci, M., Salucci, A., Di Giorgio, G., Bruni, E., Uccelletti, D., Sarto, M.S., Familiari, G., Relucenti, M. and Polimeni, A. (2019). Enamel remineralization and repair results of biomimetic hydroxyapatite toothpaste on deciduous teeth: An effective option to fluoride toothpaste. *Journal of Nanobiotechnology*, 17, 17. https://doi.org/10.1186/s12951-019-0454-6

Boutinguiza, M., Pou, J., Comesaña, R., Lusquiños, F., Carlos, A. and León, B. (2012). Biological hydroxyapatite obtained from fish bones. *Materials Science and Engineering: C*, 32(3), 478–486. https://doi.org/10.1016/j.msec.2011.11.021

Bridwell, R.E., Carius, B.M., Tomich, E.B. and Maddry, J.K. (2019). Intentional toxic ingestion of sodium fluoride: a case report. *Cureus*, 11(6), 5025-5027. https://doi.org/10.7759/cureus.5025

Buzalaf, M.A.R., Pessan, J.P., Honório, H.M. and Cate, J.M. (2011). Mechanisms of action of fluoride for caries control. *Fluoride and the Oral Environment*, 22, 97–114. https://doi.org/10.1159/000325151

Cai, H., Li, Y. and Chen, J. (2017). Rheology and tribology study of the sensory perception of oral care products. *Biotribology*, 10, 17–25. https://doi.org/10.1016/j.biotri.2017.03.001

Carr, S.A., Liu, J. and Tesoro, A.G. (2016). Transport and fate of microplastic particles in wastewater treatment plants. *Water Research*, 91, 174–182. https://doi.org/10.1016/j.watres.2016.01.002

Carwile, J.L., Ahrens, K.A., Seshasayee, S.M., Lanphear, B. and Fleisch, A.F. (2020). Predictors of plasma fluoride concentrations in children and adolescents. *International Journal of Environmental Research and Public Health*, 17(24), 9205-9220. https://doi.org/10.3390/ijerph17249205

Cheng, X., Liu, J., Li, J., Zhou, X., Wang, L., Liu, J. and Xu, X. (2017). Comparative effect of a stannous fluoride toothpaste and a sodium fluoride toothpaste on a multispecies biofilm. *Archives of Oral Biology*,

74, 5–11. https://doi.org/10.1016/j.archoralbio.2016.10.030

Chew, R.M., Zin, Z.M, Ahmad, A., Mohtar, N.F., Rusli, N.D. and Zainol, M.K. (2020). Physicochemical and sensory properties of deep fried battered squid containing Brownstripe red snapper (*Lutjanus vitta*) protein hydrolysate. *Food Research,* 4(4), 1245 - 1253. https://doi.org/10.26656/fr.2017.4(4).083

Chisada, S., Yoshida, M. and Karita, K. (2019). Ingestion of polyethylene microbeads affects the growth and reproduction of medaka, *Oryzias latipes*. *Environmental Pollution*, 254, 113094-113103. https://doi.org/10.1016/j.envpol.2019.113094

Derkach, S.R., Kolotova, D.S., Kuchina, Y.A. and Shumskaya, N.V. (2022). Characterization of fish gelatin obtained from atlantic cod skin using enzymatic treatment. *Polymers*, 14(4), 751-768. https://doi.org/10.3390/polym14040751

Dermawan, S.K., Ismail, Z.M.M., Jaffri, M.Z. and Abdullah, H.Z. (2022). Effect of the calcination temperature on the properties of hydroxyapatite from black tilapia fish bone. *Journal of Physics: Conference Series*, 2169, 012034. https://doi.org/10.1088/1742-6596/2169/1/012034

Ding, N., An, D., Yin, X. and Sun, Y. (2020). Detection and evaluation of microbeads and other microplastics in wastewater treatment plant samples. *Environmental Science and Pollution Research*, 27(13), 15878–15887. https://doi.org/10.1007/s11356-020-08127-2

Esteves-Oliveira, M., Santos, N.M., Meyer-Lueckel, H., Wierichs, R.J. and Rodrigues, J.A. (2016). Caries-preventive effect of anti-erosive and nano-hydroxyapatite-containing toothpastes in vitro. *Clinical Oral Investigations*, 21(1), 291–300. https://doi.org/10.1007/s00784-016-1789-0

Fan, H., Dumont, M.-J. and Simpson, B.K. (2017). Extraction of gelatin from salmon (*Salmo salar*) fish skin using trypsin-aided process: Optimization by Plackett–Burman and response surface methodological approaches. *Journal of Food Science and Technology*, 54(12), 4000–4008. https://doi.org/10.1007/s13197-017-2864-5

Featherstone, J.D.B. (2009). Remineralization, the Natural Caries Repair Process-The Need for New Approaches. *Advances in Dental Research*, 21(1), 4–7. https://doi.org/10.1177/0895937409335590

Fontana, M. (2016). Enhancing Fluoride: Clinical Human Studies of Alternatives or Boosters for Caries Management. *Caries Research*, 50(1), 22–37. https://doi.org/10.1159/000439059

Gambardella, C., Morgana, S., Ferrando, S., Bramini, M., Piazza, V., Costa, E., Garaventa, F. and Faimali, M. (2017). Effects of polystyrene microbeads in marine planktonic crustaceans. *Ecotoxicology and Environmental Safety*, 145, 250–257. https://doi.org/10.1016/j.ecoenv.2017.07.036

Golfeshan, F., Mosaddad, S.A. and Ghaderi, F. (2021). The effect of toothpastes containing natural ingredients such as theobromine and caffeine on enamel microhardness: An in vitro study. *Evidence-Based Complementary and Alternative Medicine*, 2021(1), 012034. https://doi.org/10.1155/2021/c

Hardwick, K., Barmes, D., Writer, S. and Richardson, L.M. (2000). International collaborative research on fluoride. *Journal of Dental Research*, 79(4), 893–904. https://doi.org/10.1177/00220345000790040301

Hasan, M.R., Yasin, N.S.M., Ghazali, M.S.M. and Mohtar, N.F. (2020). Proximate and morphological characteristics of nano hydroxyapatite (Nano HAp) extracted from fish bone. *Journal of Sustainability Science and Management*, 15(8), 9–21. https://doi.org/10.46754/jssm.2020.12.002

Hasan, M.R., Ghazali, M.S.M. and Mohtar, N.F. (2021a). Correlation of heating profile with calcination temperature for the extraction of nano hydroxyapatite (Nano-HAp) derived from bone. *Journal of Mechanical Engineering and Sciences*, 15(1), 7807–7823. https://doi.org/10.15282/jmes.15.1.2021.15.0615

Hasan, M.R., Ghazali, M.S.M. and Mohtar, N.F. (2021b). Nitrogen sorption isotherms of biologically synthesized non-stoichiometric hydroxyapatite nanoparticles (HAp NPs) extracted from fish bones. *Global Journal of Science Frontier Research*, 21(2), 25–37. https://doi.org/10.34257/GJSFRCVOL21IS2PG25

Hiller, K.-A., Buchalla, W., Grillmeier, I., Neubauer, C. and Schmalz, G. (2018). In vitro effects of hydroxyapatite containing toothpastes on dentin permeability after multiple applications and ageing. *Scientific Reports*, 8, 4888. https://doi.org/10.1038/s41598-018-22764-1

Ionescu, A.C., Cazzaniga, G., Ottobelli, M., Garcia-Godoy, F. and Brambilla, E. (2020). Substituted nano -hydroxyapatite toothpastes reduce biofilm formation on enamel and resin-based composite surfaces. *Journal of Functional Biomaterials*, 11(2), 36-53. https://doi.org/10.3390/jfb11020036

Jumanca, D., Matichescu, A., Galuscan, A., Balean, O. and Rusu, L.C. (2019). The effect of hydroxyapatite from various toothpastes on tooth enamel. *Revista de Chimie*, 70(7), 2604–2607. https://doi.org/10.37358/RC.19.7.7388

Kalčíková, G., Žgajnar Gotvajn, A., Kladnik, A. and Jemec, A. (2017). Impact of polyethylene microbeads on the floating freshwater plant duckweed Lemna

minor. *Environmental Pollution*, 230, 1108–1115. https://doi.org/10.1016/j.envpol.2017.07.050

Karim, A.A. and Bhat, R. (2009). Fish gelatin: Properties, challenges, and prospects as an alternative to mammalian gelatins. *Food Hydrocolloids*, 23(3), 563 –576. https://doi.org/10.1016/j.foodhyd.2008.07.002

King, C.A., Shamshina, J.L., Zavgorodnya, O., Cutfield, T., Block, L.E. and Rogers, R.D. (2017). Porous chitin microbeads for more sustainable cosmetics. *ACS Sustainable Chemistry and Engineering*, 5(12), 11660–11667. https://doi.org/10.1021/acssuschemeng.7b03053

Koo, H. (2008). Strategies to enhance the biological effects of fluoride on dental biofilms. *Advances in Dental Research*, 20(1), 17–21. https://doi.org/10.1177/154407370802000105

Körner, P., Schleich, J.A., Wiedemeier, D.B., Attin, T. and Wegehaupt, F.J. (2020). Effects of additional use of bioactive glasses or a hydroxyapatite toothpaste on remineralization of artificial lesions in vitro. *Caries Research*, 54(4), 336–342. https://doi.org/10.1159/000510180

Liao, Y., Brandt, B.W., Li, J., Crielaard, W., Loveren, V.C. and Deng, D.M. (2017). Fluoride resistance in *Streptococcus mutans*: A mini review. *Journal of Oral Microbiology*, 9(1), 1344509. https://doi.org/10.1080/20002297.2017.1344509

Liu, Z., Liu, L., Zhou, H., Wang, J. and Deng, L. (2015). Toothpaste microstructure and rheological behaviours including aging and partial rejuvenation. *Korea-Australia Rheology Journal*, 27(3), 207–212. https://doi.org/10.1007/s13367-015-0021-0

Loveren, V.C. (2001). Antimicrobial activity of fluoride and its in vivo importance: identification of research questions. *Caries Research*, 35(1), 65–70. https://doi.org/10.1159/000049114

Magni, S., Gagné, F., André, C., Della Torre, C., Auclair, J., Hanana, H., Parenti, C.C., Bonasoro, F. and Binelli, A. (2018). Evaluation of uptake and chronic toxicity of virgin polystyrene microbeads in freshwater zebra mussel *Dreissena polymorpha* (Mollusca: Bivalvia). *Science of The Total Environment*, 631-632, 778–788. https://doi.org/10.1016/j.scitotenv.2018.03.075

Marinho, V.C.C., Chong, L.-Y., Worthington, H.V. and Walsh, T. (2016). Fluoride mouthrinses for preventing dental caries in children and adolescents. *Cochrane Database of Systematic Reviews*, 7, CD002284. https://doi.org/10.1002/14651858.CD002284.pub2

Marinho, V.C.C., Worthington, H.V., Walsh, T. and Chong, L.-Y. (2015). Fluoride gels for preventing dental caries in children and adolescents. *Cochrane Database of Systematic Reviews*, 6, CD002280. https://doi.org/10.1002/14651858.CD002280.pub2

Marinho, V.C.C., Worthington, H.V., Walsh, T. and Clarkson, J.E. (2013). Fluoride varnishes for preventing dental caries in children and adolescents. *Cochrane Database of Systematic Reviews*, 11(7), 1-22. https://doi.org/10.1002/14651858.CD002279.pub2

Meyer, F. and Enax, J. (2019). Hydroxyapatite in Oral Biofilm Management. *European Journal of Dentistry*, 13(2), 287–290. https://doi.org/10.1055/s-0039-1695657

Mohtar, N.F., Perera, C. and Quek, S.-Y. (2010). Optimisation of gelatine extraction from hoki (*Macruronus novaezelandiae*) skins and measurement of gel strength and SDS–PAGE. *Food Chemistry*, 122 (1), 307–313. https://doi.org/10.1016/j.foodchem.2010.02.027

Nachu, S., Ravoori, S. and Pachava S. (2022). Antiplaque efficacy of toothpaste – A systematic review and meta-analysis of randomized controlled trials. *Journal of Indian Association of Public Health Dentistry*, 20 (1), 16-24. https://doi.org/10.4103/jiaphd.jiaphd_140_21

Nair, A., Mallya, R., Suvarna, V., Khan, T.A., Momin, M. and Omri, A. (2022). Nanoparticles-Attractive carriers of antimicrobial essential oils. *Antibiotics*, 11 (1), 1-45. https://doi.org/10.3390/antibiotics11010108

Nakamoto, T., Falster, A.U. and Simmons, W.B. (2016). Theobromine: A safe and effective alternative for fluoride in dentifrices. *Journal of Caffeine Research*, 6, 1–9. https://doi.org/10.1089/jcr.2015.0023

Nam, H.C. and Park, W.H. (2020). Eco-friendly poly (lactic acid) microbeads for cosmetics via melt electrospraying. *International Journal of Biological Macromolecules*, 157, 734–742. https://doi.org/10.1016/j.ijbiomac.2019.11.240

Nie, Y., Chen, J., Xu, J., Zhang, Y., Yang, M., Yang, L., Wang, X. and Zhong, J. (2022). Vacuum freeze-drying of tilapia skin affects the properties of skin and extracted gelatins. *Food Chemistry*, 374, 1-10. https://doi.org/10.1016/j.foodchem.2021.131784

O'Hagan-Wong, K., Enax, J., Meyer, F. and Ganss, B. (2021). The use of hydroxyapatite toothpaste to prevent dental caries. *Odontology,* 110, 223-230. https://doi.org/10.1007/s10266-021-00675-4

Ogboji, J., Chindo, I.Y., Jauro, A., Boryo, D.E.A. and Lawal, N.M. (2017). Formulation, physicochemical evaluation and antimicrobial activity of green toothpaste on streptococcus mutans. *International Journal of Advanced Chemistry*, 6(1), 108-113. https://doi.org/10.14419/ijac.v6i1.10808

Oubenyahya, H. (2021). Nano hydroxyapatite toothpaste as a treatment for dentine hypersensitivity: A systematic review. *Saudi Journal of Oral Sciences*, 8 (3), 122-128. https://doi.org/10.4103/sjoralsci.sjoralsci_27_21

Premnath, P., John, J., Manchery, N., Subbiah, G.K., Nagappan, N. and Subramani, P. (2019). Effectiveness of theobromine on enamel remineralization: A comparative in-vitro study. *Cureus*, 11(9), 5686-5696. https://doi.org/10.7759/cureus.5686

Rifada, A., Af'idah, B.M., Aufia, W., Vibriani, A., Maghdalena, M., Saputro, K.E., Nugroho, D.W., Iskandar, M.A., Cahyanto, A., Noviyanto, A. and Rochman, N.T. (2020). Effect of nano hydroxyapatite in toothpaste on controlling oral microbial viability. *IOP Conference Series: Materials Science and Engineering*, 924, 012010. https://doi.org/10.1088/1757-899X/924/1/012010

Sarembe, S., Enax, J., Morawietz, M., Kiesow, A. and Meyer, F. (2020). In vitro whitening effect of a hydroxyapatite-based oral care gel. *European Journal of Dentistry*, 14(3), 335–341. https://doi.org/10.1055/s-0040-1714759

Sharma, D.S., Vyavhare, S. and Kulkarni, V.K. (2015). Effect of three different pastes on remineralization of initial enamel lesion: An in vitro study. *The Journal of Clinical Pediatric Dentistry*, 39(2), 149-160. https://doi.org/10.17796/jcpd.39.2.yn2r54nw24l03741

Sockalingam, K., Abdullah, H.Z. and Idris, M.I. (2022). Alteration of physico-mechanical properties of black tilapia scale gelatins using UVA and UVC irradiation. *International Journal of Integrated Engineering*, 14 (1), 150-156. https://doi.org/10.30880/ijie.2022.14.01.013

Sohilait, H.J. (2015). Chemical composition and antibacterial activity of the essential oils from different parts of *Eugenia caryophylata*, thunb grown in Amboina island. *Science Journal of Chemistry*, 3 (6), 95-99. https://doi.org/10.11648/j.sjc.20150306.13

Steinert, S., Zwanzig, K., Doenges, H., Kuchenbecker, J., Meyer, F. and Enax, J. (2020). Daily application of a toothpaste with biomimetic hydroxyapatite and its subjective impact on dentin hypersensitivity, tooth smoothness, tooth whitening, gum bleeding, and feeling of freshness. *Biomimetics*, 5(2), 17-28. https://doi.org/10.3390/biomimetics5020017

Sun, J., Dai, X., Wang, Q., Loosdrecht, V.M.C.M. and Ni, B.-J. (2019). Microplastics in wastewater treatment plants: detection, occurrence and removal. *Water Research*, 152, 21–37. https://doi.org/10.1016/j.watres.2018.12.050

Sunitha, J., Ananthalakshmi, R., Jeeva, J., Jeddy, N., Dhakshininamoorthy, S. and Meenakshi, R.M.M. (2015). Antimicrobial effect of herbal dentifrices: An in vitro study. *Journal of Pharmacy and Bioallied Sciences*, 7(2), 628-631. https://doi.org/10.4103/0975-7406.163575

Takahashi, N. and Nyvad, B. (2011). The role of bacteria in the caries process. *Journal of Dental Research*, 90 (3), 294–303. https://doi.org/10.1177/0022034510379602

Vano, M., Derchi, G., Barone, A., Pinna, R., Usai, P. and Covani, U. (2018). Reducing dentine hypersensitivity with nano-hydroxyapatite toothpaste: A double-blind randomized controlled trial. *Clinical Oral Investigations*, 22(1), 313–320. https://doi.org/10.1007/s00784-017-2113-3

Walsh, T., Worthington, H.W., Glenny, A., Marinho, V.C. and Jeroncic, A. (2019). Fluoride toothpastes of different concentrations for preventing dental caries. *Cochrane Database of Systematic Reviews*, 3, CD007868. https://doi.org/10.1002/14651858.CD007868.pub3

Xu, J.-G., Liu, T., Hu, Q.-P. and Cao, X.-M. (2016). Chemical composition, antibacterial properties and mechanism of action of essential oil from clove buds against *Staphylococcus aureus*. *Molecules*, 21(9), 1194-1207. https://doi.org/10.3390/molecules21091194

Yumas, M., Loppies, J.E., Khaerunnisa, Ramlah, S., Rosniati, and Lullung, A. (2022). Characterization of toothpaste made with unfermented cocoa powder (*Theobroma cacao L*) against bacteria *Streptococcus mutans*. *Environment, Energy and Earth Science Web of Conferences,* 344, 01002. https://doi.org/10.1051/e3sconf/202234401002

Zhou, P., Mulvaney, S.J. and Regenstein, J.M. (2006). Properties of alaska pollock skin gelatin: a comparison with tilapia and pork skin gelatins. *Journal of Food Science*, 71(6), 313-321. https://doi.org/10.1111/j.1750-3841.2006.00065.x

Zohoori, F.V., Ralph M., Omid, D.N., O'Hare, W.T. and Maguire, A. (2012). Fluoridated toothpaste: Usage and ingestion of fluoride by 4- to 6-yr-old children in England. *European Journal of Oral Sciences*, 120(5), 415–421. https://doi.org/10.1111/j.1600-0722.2012.00984.x

ARTICLES FOR FACULTY MEMBERS

BONE-DERIVED HYDROXYAPATITE TOOTHPASTE FOR SUSTAINABLE PHARMACEUTICAL AND BIOMEDICAL APPLICATIONS

Bovine cancellous hydroxyapatite toothpaste enhances enamel remineralization / Octarina, O., Kurniawan, F. L., Falatehan, N., Sofiana, K., Siregar, G. M., Maulana, I. N., & Surboyo, M. D. C.

International Dental Journal
Volume 76 Issue 1 (2026) 109308 Pages 1-9
https://doi.org/10.1016/j.identj.2025.109308
(Database: ScienceDirect)

Scientific Research Report

Bovine Cancellous Hydroxyapatite Toothpaste Enhances Enamel Remineralization

Octarina Octarina [a], *Florencia Livia Kurniawan* [a*], *Niko Falatehan* [b], *Karen Sofiana* [c], *Gladys Mawarni Siregar* [c], *Ilman Nafi Maulana* [c], *Meircurius Dwi Condro Surboyo* [d]

[a] *Department of Dental Material, Faculty of Dentistry, Universitas Trisakti, Jakarta, Indonesia*
[b] *Department of Prosthodontics, Faculty of Dentistry, Universitas Trisakti, Jakarta, Indonesia*
[c] *Faculty of Dentistry, Universitas Trisakti, Jakarta, Indonesia.*
[d] *Department of Oral Medicine, Faculty of Dental Medicine, Universitas Airlangga, Surabaya, Indonesia*

ARTICLE INFO

Article history:
Received 1 October 2025
Received in revised form
4 November 2025
Accepted 8 November 2025
Available online 11 December 2025

Key words:
Hydroxyapatite
Bovine cancellous bone
Enamel remineralization
Antimicrobial
Toothpaste

ABSTRACT

Background: Hydroxyapatite (HA) is a biomimetic material capable of promoting enamel remineralization and exhibiting antimicrobial properties. Bovine cancellous bone is a promising HA source due to its bioactivity, biocompatibility, and cost-effectiveness. This study evaluated the effects of toothpaste formulations containing varying concentrations of bovine cancellous HA (1%, 3%, and 5%) on enamel remineralization, antimicrobial activity, abrasivity, and biocompatibility.

Methods: Toothpaste formulations were prepared with bovine cancellous HA at 1%, 3%, and 5%, alongside a base formulation and a commercial control. Physical properties (pH, viscosity, homogeneity, stability) and organoleptic characteristics (odour, taste, texture, colour) were assessed. Enamel remineralization was evaluated via Vickers microhardness testing and surface roughness analysis after simulated brushing. Antimicrobial activity was assessed against *Staphylococcus aureus* and *Candida albicans*.

Results: All formulations exhibited slightly alkaline pH, stable viscosity, uniform homogeneity, and no phase separation over 30 days. Sensory evaluation indicated that 3% HA toothpaste provided the optimal balance between functionality and acceptability. Brushing with HA toothpaste increased enamel microhardness in a dose-dependent manner, with 3% and 5% HA toothpaste showing superior remineralization (Vickers Hardness Number: 327.6 ± 14.0 and 319.4 ± 19.9, respectively) compared to 1% (226.9 ± 11.1). Surface roughness was minimized with HA incorporation, indicating protective effects against enamel wear. Antimicrobial assays demonstrated concentration-dependent inhibition of *S. aureus*, with the 5% HA toothpaste (9.1 ± 0.06 mm) comparable to commercial toothpaste (9.4 ± 0.1 mm), whereas inhibition of *C. albicans* was highest at 1% HA (9.7 ± 1.2 mm).

Conclusion: Bovine cancellous HA toothpaste effectively enhances enamel remineralization, reduces abrasivity, exhibits antimicrobial potential, and demonstrates excellent biocompatibility. The 3% to 5% HA toothpaste provide a balanced combination of efficacy, safety, and user acceptability, supporting their potential for translational applications in preventive oral care.

* *Corresponding author*. Department of Dental Material, Faculty of Dentistry, Universitas Trisakti, Jalan Kyai Tapa No.260, Kecamatan Grogol Petamburan, Kota Jakarta Barat, Daerah Khusus Ibukota, Jakarta 11440, Indonesia.
E-mail address: florencia@trisakti.ac.id (F.L. Kurniawan).
Octarina Octarina: http://orcid.org/0000-0002-8764-8365
Niko Falatehan: http://orcid.org/0000-0002-3690-8438
Karen Sofiana: http://orcid.org/0009-0008-6329-5690
Gladys Mawarni Siregar: http://orcid.org/0009-0009-1041-8279
Ilman Nafi Maulana: http://orcid.org/0009-0006-1745-2443
Meircurius Dwi Condro Surboyo: http://orcid.org/0000-0002-6052-2287
https://doi.org/10.1016/j.identj.2025.109308

Introduction

Caries prevention is primarily achieved through regular toothbrushing with toothpaste, a daily-use product designed to maintain oral hygiene and dental health.[1-3] Conventional toothpaste typically contains abrasives, humectants, thickeners, detergents, sweeteners, and therapeutic active ingredients such as fluoride, which functions as an anticaries agent by forming fluorapatite.[4-6] Fluorapatite exhibits low solubility, rendering enamel more resistant to acid attacks. However, fluoride-mediated remineralization depends on the availability of calcium and phosphate ions at the enamel surface; insufficient levels of these ions can limit the remineralization process.[7] Additionally, excessive abrasives in toothpaste may erode enamel and increase tooth sensitivity, highlighting the need for innovative formulations that enhance remineralization while minimizing abrasivity and providing antimicrobial protection.[7]

Hydroxyapatite (HA) ($Ca_{10}(PO_4)_6(OH)_2$) is a biomimetic material with a chemical structure and mineral composition similar to dental enamel.[8-11] Its nanoscale particles can penetrate and fill microporosities in demineralized enamel, restoring tissue integrity.[7,12] The binding mechanism involves electrostatic interactions between enamel surface charges and salivary pellicle proteins, allowing HA to integrate more deeply than fluoride, which primarily acts on the surface.[13] Bovine cancellous bone is widely explored as a natural HA source because its crystal structure and composition closely resemble human enamel. It demonstrates high bioactivity and biocompatibility and offers practical advantages such as scalability and cost-efficiency for oral care applications.[14-16] Cancellous bone was selected over dense cortical bone due to its naturally porous microarchitecture, which provides a greater surface area for ion exchange and biological interaction, enhancing enamel adhesion and remineralization potential. Although natural HA may exhibit variability in particle size, this can be effectively controlled through milling and sieving techniques. Importantly, HA also exhibits antimicrobial activity against *Staphylococcus aureus* and *C. albicans*, providing dual protection against caries.[15,17,18]

Toothpaste formulations incorporating bovine cancellous HA typically use concentrations of 1%, 3%, and 5%.[19] The 1% concentration is considered minimally effective for children, 5% is commonly applied for adults, and 3% serves as an intermediate concentration to evaluate optimal efficacy. Previous studies have demonstrated that even lower concentrations (0.7%-1.5%) can enhance enamel remineralization and reduce abrasivity; therefore, higher concentrations are expected to further improve remineralization and antimicrobial effects.[20] Comprehensive evaluation of HA-based toothpaste should assess physical properties (pH, viscosity, homogeneity, stability), sensory attributes (odour, taste, texture, colour), enamel protection (abrasivity, microhardness, surface morphology), antimicrobial activity, and biocompatibility with oral soft tissues.

Based on this rationale, the present study investigates toothpaste formulations containing varying concentrations of bovine cancellous HA to determine their effects on enamel remineralization, antimicrobial activity against *S. aureus* and *C. albicans*, abrasivity, and biocompatibility. The results aim to provide robust preliminary evidence supporting HA as a safe and effective active ingredient for innovative preventive dental care.

Accordingly, the null hypothesis of this study was that HA toothpaste formulations (1%, 3%, and 5%) would not demonstrate significant differences in enamel remineralization, surface abrasivity, antimicrobial activity, sensory acceptability, or biocompatibility compared with control toothpaste. The alternative hypothesis was that incorporation of bovine cancellous HA at these concentrations would improve these outcomes relative to the control.

Materials and methods

Preparation of HA from bovine bone

Fresh bovine bone shafts were sectioned into small fragments and deproteinized with hydrogen peroxide (H_2O_2). Samples were sonicated at 60°C, rinsed thoroughly with distilled water, and air-dried. They were then calcined at 1000°C for 1 hour in a muffle furnace. To reduce residual impurities and potential toxicity, the calcined bone was washed three to four times with distilled water, oven-dried at 60 to 100°C, ground into powder, and sieved to obtain particles <150 μm.[15,21]

Toothpaste formulation

HA toothpaste was prepared with bovine cancellous HA at three concentrations (1%, 3%, and 5%) to evaluate their effects on enamel remineralization. The base formulation contained standard toothpaste excipients including abrasives, humectants, binders, surfactants, fluoride, and flavouring agents. Ingredients were thoroughly mixed to ensure homogeneity, and HA was incorporated according to the target concentration (Figure 1). The detailed composition of each formulation is presented in Table 1.

Organoleptic test

Sensory evaluation was performed with 30 random adult men or women who assessed odour, taste, texture, and colour. Each participant tested five formulations: commercial toothpaste, base formulation, and HA formulations at 1%, 3%, and 5%. Samples were evaluated using a 5-point hedonic scale (1 = strongly dislike, 2 = dislike, 3 = neutral, 4 = like, 5 = strongly like).

Evaluation of physical properties

Five formulations were tested: HA toothpastes (1%, 3%, 5%), the base formulation (negative control), and a commercial toothpaste (positive control).

- **pH measurement**: One gram of toothpaste was diluted in 20 mL distilled water, and pH was determined with a digital pH meter (Aquasearcher, Ohaus) in three different point observation. The acceptable range was 7 to 10. pH evaluations were performed according to the Indonesian National Standard for dentifrices (SNI 12-3524-1995).
- **Viscosity**: Samples (25-100 g) were measured with a rotational viscometer (K447-BL-CP, Cole-Parmer) at room temperature and expressed in centipoise (cP). Viscosity evaluations were performed according to the Indonesian National Standard for dentifrices (SNI 12-3524-1995).

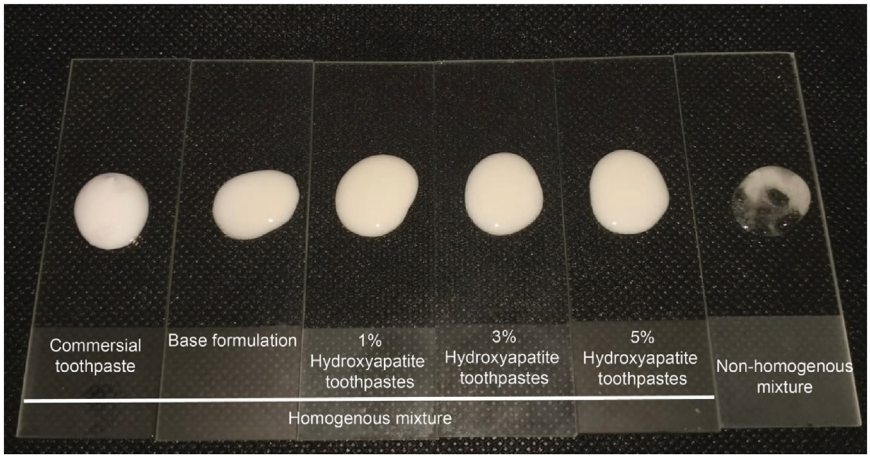

Fig. 1 – Visual assessment of toothpaste homogeneity across formulations. All hydroxyapatite formulations display uniform texture and consistent appearance without visible phase separation. In contrast, the nonhomogeneous sample exhibits clumping and watery separation, demonstrating inadequate mixing.

Table 1 – Toothpaste formulation with bovine cancellous hydroxyapatite.

		Compositions		
Ingredient	Function	1% hydroxyapatite toothpaste	3% hydroxyapatite toothpaste	5% hydroxyapatite toothpaste
Bovine cancellous HA	Remineralization	1%	3%	5%
Calcium carbonate	Abrasive	20%	20%	20%
Sorbitol	Humectant	30%	30%	30%
Glycerine	Humectant, sweetener	15%	15%	15%
Arabic gum	Binder	1,2%	1,2%	1,2%
Na-CMC	Binder, thickener	1,2%	1,2%	1,2%
Sodium Fluoride	Anticaries	0,02%	0,02%	0,02%
Citric acid	pH regulator	3%	3%	3%
SLS	Surfactant	2%	2%	2%
Zinc oxide	Antimicrobial	3%	3%	3%
Propylene glycol	Humectant	5%	5%	5%
Peppermint oil	Flavouring	0,5%	0,5%	0,5%
Water	Solvent	21%	19%	16%

- **Homogeneity**: One gram of toothpaste was spread on a glass slide and examined under light for coarse particles, clumps, or bubbles. Preparations without irregularities were considered homogeneous.
- **Stability**: Samples were stored at 40 ± 2°C for 30 days and evaluated on days 0, 10, 20, and 30 for colour, odour, and phase separation. Colour was assessed visually under consistent natural lighting and compared with the reference commercial toothpaste. Odour evaluation was performed qualitatively by three trained laboratory assessors familiar with sensory assessment procedures. Phase separation was monitored by visual inspection for any stratification, liquid separation, or textural inconsistency. Samples that exhibited no detectable changes in these parameters during the observation period were classified as stable.

Abrasivity test

Caries-free permanent maxillary incisors were sectioned at the cementoenamel junction and embedded vertically in acrylic resin. Brushing was performed with an electric toothbrush under 50 g load, twice daily for 2 minutes over 3 weeks (28, 56, and 84 minutes cumulative). Surface roughness was measured with a tester (Surtronic S128, Taylor Hobson) and expressed as Ra (μm). Measurements were recorded at baseline, after brushing without toothpaste, and after brushing with test formulations. Controls included brushing without toothpaste (negative) and with commercial toothpaste (positive).

Enamel microhardness test

Caries-free maxillary incisors were sectioned at the cementoenamel junction and mounted in acrylic resin with the labial enamel exposed. The labial enamel surface was gently flattened using 400-grit silicon-carbide abrasive paper under water irrigation to obtain a smooth and uniform testing area without excessive enamel removal. Baseline Vickers microhardness was measured, followed by demineralization with 37% phosphoric acid. Remineralization was simulated by brushing with test formulations for 2 minutes, twice daily,

over 14 days under 50 g load using an electric toothbrush. The teeth were stored in artificial saliva in a sealed container at room temperature to prevent enamel dehydration. During the experimental period, samples were taken out only for brushing and testing. At each evaluation point (days 1, 7, and 14), the enamel surface was gently rinsed with distilled water, air-dried, and Vickers microhardness measurements were performed immediately. Microhardness was evaluated on the central labial surface using a Vickers Hardness Tester (Shimadzu HMV-30) and expressed as Vickers Hardness Number (VHN).

Antimicrobial test

Antimicrobial activity was evaluated against *S. aureus* and *C. albicans*. Mueller–Hinton Agar was used for *S. aureus*, and Sabouraud Dextrose Agar (SDA) for *C. albicans*. Microbial suspensions were standardized to 0.5 McFarland ($\approx 1.5 \times 10^8$ CFU/mL) in 0.9% NaCl, and 0.1 mL was spread onto agar. Wells (6 mm) were filled with 50 μL of test solutions: distilled water (negative control), commercial HA toothpaste, and experimental formulations (1%, 3%, 5%). In addition, chloramphenicol (100 ppm) was used as the positive control for S. aureus and nystatin (5000 IU/mL) as the positive control for *C. albicans*. Plates were incubated at 37°C for 24 hours. Inhibition zones were measured, and activity was calculated as W = T − D, where W = inhibition width, T = clear zone diameter, and D = well diameter.

Statistical analysis

All data were expressed as mean ± standard deviation (SD). The effects of bovine cancellous HA concentration and treatment conditions on pH, enamel surface hardness, surface roughness, and antimicrobial activity were analysed using two-way analysis of variance (ANOVA). When significant interactions or main effects were observed, multiple comparisons were performed using Tukey's post hoc test. A significance level of $P < .05$ was considered statistically significant. Statistical analyses were performed using GraphPad Prism version 10 (GraphPad Software).

Results

Organoleptic evaluation

The sensory characteristics of the toothpaste formulations were evaluated using a 5-point hedonic scale (1 = strongly dislike, 5 = strongly like) for odour, taste, texture, and colour. The commercial control toothpaste consistently received the highest scores across all parameters, indicating strong overall acceptability. Among the experimental formulations, 3% HA toothpaste achieved the most balanced sensory profile, with moderate scores for odour, taste, texture, and colour. In contrast, formulations containing 1% and 5% HA were less preferred, particularly for taste and odour. The base toothpaste exhibited intermediate acceptability (Table 2).

Table 2 – Organoleptic evaluation of toothpaste formulations.

Formula	Hedonic scores* (Mean)			
	Odour	Taste	Texture	Colour
Commercial toothpaste	4.37	4.45	4.53	4.60
1% hydroxyapatite toothpaste	2.43	2.53	2.45	2.43
3% hydroxyapatite toothpaste	3.22	3.57	2.85	2.62
5% hydroxyapatite toothpaste	2.37	1.95	2.53	2.62
Base toothpaste	2.62	2.50	2.63	2.72

* Measured from 30 samples.

pH, viscosity, homogeneity, and stability

All HA toothpaste formulations-maintained pH within the optimal oral health range (7-10), indicating reduced risk of enamel demineralization. The 3% and 5% HA toothpaste exhibited the most stable pH over 30 days, whereas the 1% HA toothpaste and base showed minor fluctuations (Figure 2).

Viscosity measurements confirmed compliance with the Indonesian National Standard (20,000-50,000 cP). The commercial toothpaste showed the highest and most stable viscosity, while the 1% and 3% HA toothpaste experienced moderate fluctuations. The 5% HA toothpaste and base formulations demonstrated overall increases without compromising rheological properties (Table 3). Homogeneity testing confirmed uniform distribution in all formulations, and stability assessments under accelerated storage (40 ± 2°C) revealed no changes in colour, odour, or phase separation over 30 days (Tables 4 and 5).

Enamel microhardness

Vickers microhardness testing showed that brushing with HA formulations increased enamel hardness over the 14-day period (Figure 3A). The 3% and 5% HA toothpaste achieved superior remineralization compared to 1%, with day 14 VHN of 327.6 ± 14.0 and 319.4 ± 19.9, respectively, vs 226.9 ± 11.1 for 1%. The commercial control also exhibited high remineralization (VHN 353 ± 28.7). These results indicate a dose-dependent effect of HA on enamel surface hardness.

Surface roughness

Surface roughness testing revealed that brushing increased Ra values across all groups over 3 weeks (Figure 3B). The 3% and 5% HA toothpaste minimized surface roughness progression more effectively than 1% HA toothpaste and the negative control, indicating protective effects against enamel abrasion. The commercial toothpaste also effectively reduced roughness increases.

Antimicrobial activity

HA toothpaste formulations exhibited measurable inhibitory effects against *S. aureus* and *C. albicans*. For *S. aureus*, all HA formulations produced inhibition zones significantly larger than the negative control (****, $P < .0001$) (Figure 4A). The 5% HA toothpaste

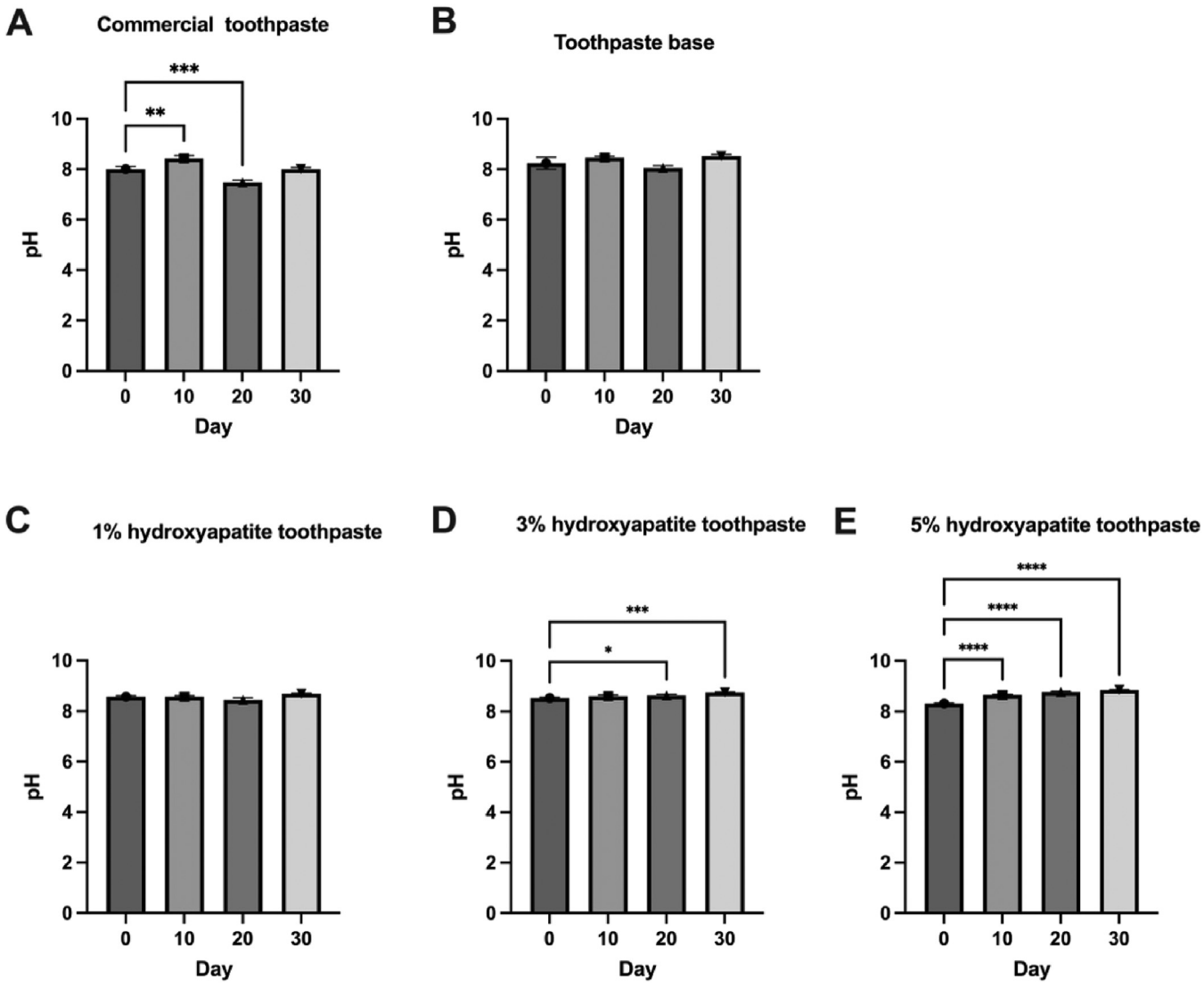

Fig. 2 – All formulations-maintained pH within the optimal oral health range. (A) Commercial toothpaste, (B) toothpaste base, (C) 1% hydroxyapatite toothpaste, (D) 3% hydroxyapatite toothpaste, and (E) 5% hydroxyapatite toothpaste. Data are presented as mean ± SD ($n = 3$). Statistical analysis was performed using one-way ANOVA followed by Tukey's post hoc test. $^{*}P < .05$, $^{**}P < .01$, $^{***}P < .001$, $^{****}P < .0001$.

Table 3 – Viscosity of toothpaste formulations (cP).

Formula	D 0	D 10	D 20	D 30
Commercial toothpaste	-	-	-	-
1% hydroxyapatite toothpaste	28,279	29,164	29,069	28,400
3% hydroxyapatite toothpaste	26,424	30,801	38,955	41,176
5% hydroxyapatite toothpaste	30,716	53,079	39,871	31,942
Base toothpaste	26,362	31,779	27,434	31,134

showed the highest inhibition, comparable to the commercial toothpaste, while the 1% and 3% formulations yielded slightly smaller zones. As expected, chloramphenicol (100 ppm) demonstrated the strongest inhibition ($P < .0001$ vs all test groups).

For *C. albicans*, nystatin (5000 mg/L) produced the largest inhibition ($P < .0001$), followed by the HA formulations (Figure 4B). The 1% HA toothpaste achieved the greatest antifungal effect ($P < .05$), while the 3% and 5% formulations

Table 4 – Homogeneity test results.

Formula	D 0	D 10	D 20	D 30
Commercial toothpaste	Homogeneous	Homogeneous	Homogeneous	Homogeneous
1% hydroxyapatite toothpaste	Homogeneous	Homogeneous	Homogeneous	Homogeneous
3% hydroxyapatite toothpaste	Homogeneous	Homogeneous	Homogeneous	Homogeneous
5% hydroxyapatite toothpaste	Homogeneous	Homogeneous	Homogeneous	Homogeneous
Base toothpaste	Homogeneous	Homogeneous	Homogeneous	Homogeneous

Table 5 – Stability test results.

Formula	D 0	D 10	D 20	D 30
Commercial toothpaste	Stable	Stable	Stable	Stable
1% hydroxyapatite toothpaste	Stable	Stable	Stable	Stable
3% hydroxyapatite toothpaste	Stable	Stable	Stable	Stable
5% hydroxyapatite toothpaste	Stable	Stable	Stable	Stable
Base toothpaste	Stable	Stable	Stable	Stable

showed slightly lower inhibition. The commercial toothpaste demonstrated moderate activity, and the negative control showed no inhibition.

All HA toothpaste formulations showed no microbial growth when cultured, indicating the absence of unintended bacterial or fungal contamination during preparation and storage. Notably, the results indicate that HA concentration influences antibacterial activity against *S. aureus*, whereas antifungal activity against *C. albicans* is not strictly dose dependent.

Discussion

The present study demonstrates that bovine cancellous HA can be effectively incorporated into toothpaste formulations to enhance enamel remineralization while maintaining biocompatibility and physical stability. The slightly alkaline pH observed across all formulations supports a protective environment for dental enamel, minimizing the risk of demineralization and contributing to oral health.[12,22] The progressive increase in pH observed in HA-containing formulations, particularly at higher concentrations, likely reflects the inherent buffering capacity of HA, which releases calcium and phosphate ions capable of stabilizing the local environment.[23,24] This property aligns with prior evidence that HA particles can modulate oral pH and provide a favourable milieu for enamel remineralization.

Viscosity and physical stability data indicate that HA can be incorporated at 1% to 5% without compromising formulation integrity. Notably, higher concentrations (5%) influenced rheological behaviour, likely due to particle aggregation and increased interparticle interactions, which is consistent with previous reports on HA's effect on gel matrices.[23] Nevertheless, all formulations demonstrated homogeneity and maintained stability over 30 days, indicating that the preparation method and excipient selection were adequate to prevent phase separation or sedimentation.[23,25] These findings reinforce the feasibility of producing stable HA-based toothpastes that are safe for routine use.

Sensory evaluation highlighted that a 3% HA toothpaste strikes a balance between functional efficacy and consumer acceptability. While higher concentrations may enhance remineralization, they can introduce sensory drawbacks such as altered taste, odour, and texture due to the bone-derived material.[26] These observations emphasize the importance of optimizing HA concentration to ensure both therapeutic efficacy and patient compliance.

The enamel microhardness results confirm the remineralization potential of HA toothpaste, showing a dose-

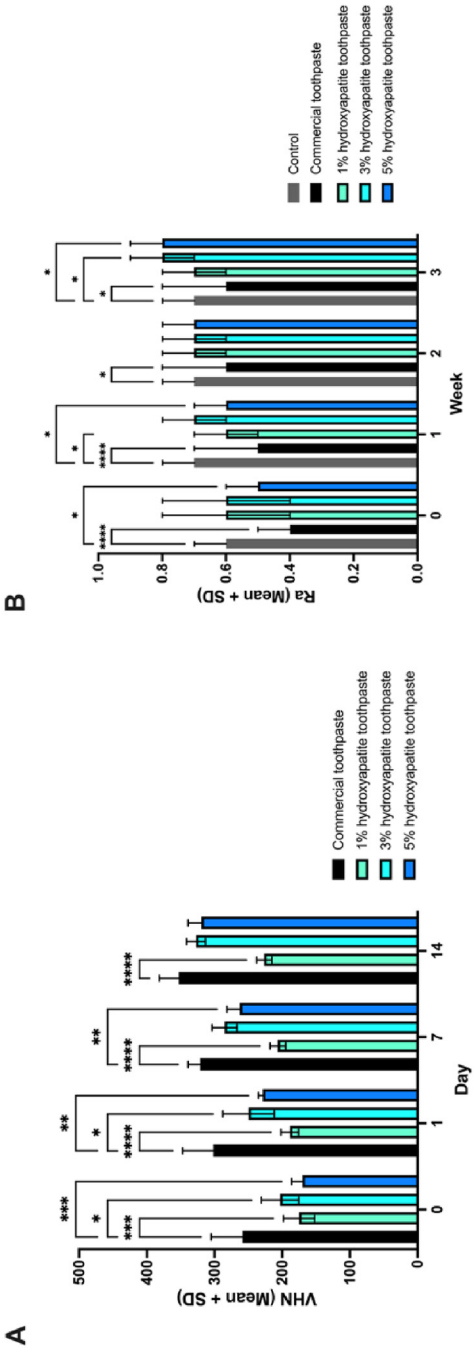

Fig. 3 – Effects of bovine cancellous hydroxyapatite toothpaste on enamel microhardness and surface roughness. (A) Vickers microhardness number (VHN) over 14 days of brushing. Both 3% and 5% hydroxyapatite toothpaste significantly increased enamel hardness compared with 1% hydroxyapatite toothpaste, approaching the commercial toothpaste control. (B) Surface roughness over 3 weeks of brushing. Hydroxyapatite formulations, particularly at 3% and 5%, reduced roughness progression relative to the negative control, showing protective effects comparable to commercial toothpaste. Each groups consist 3 samples. Statistical analysis was performed using one-way ANOVA followed by Tukey's post hoc test. $^{*}P < .05$, $^{**}P < .01$, $^{***}P < .001$, $^{****}P < .0001$.

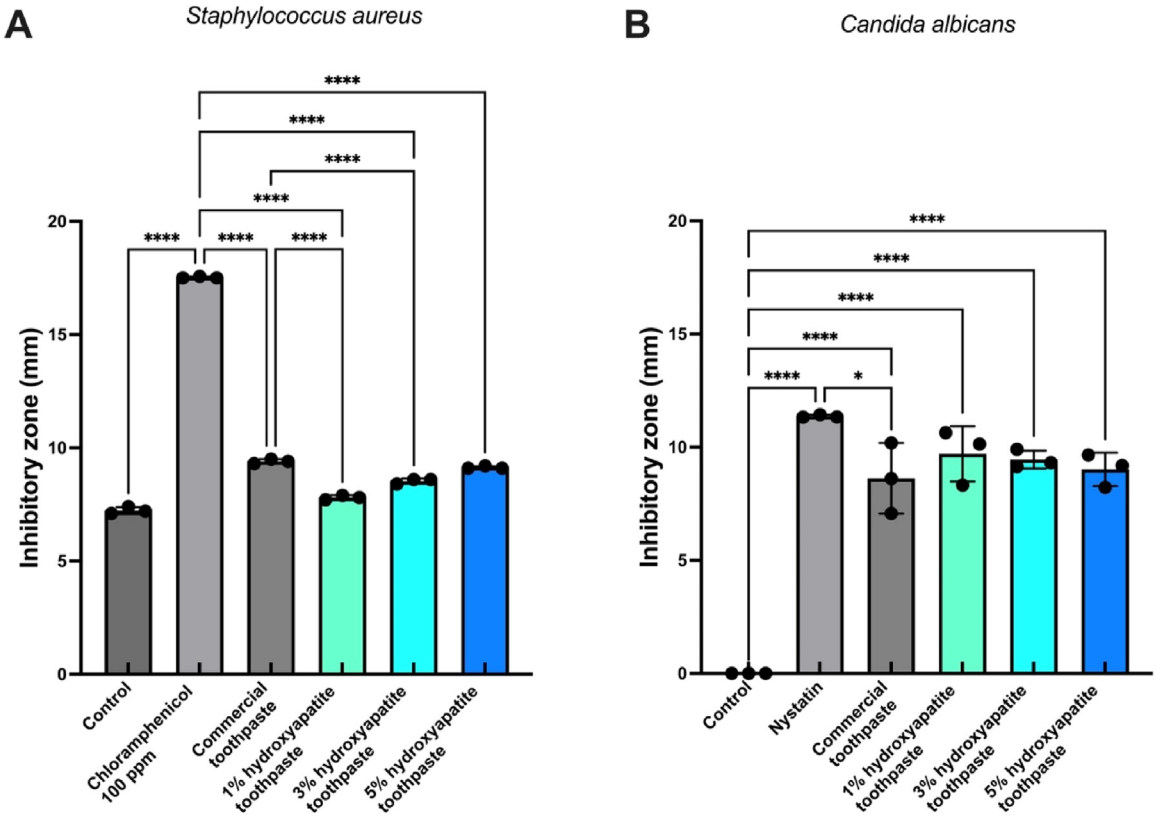

Fig. 4 – Antimicrobial activity of bovine cancellous hydroxyapatite toothpaste formulations. (A) Inhibition zones against *Staphylococcus aureus*. Hydroxyapatite formulations (1%-5%) exhibited significant inhibitory effects compared with the negative control, with the 5% formulation showing activity comparable to the commercial toothpaste. Chloramphenicol (100 ppm) served as the positive control. (B) Inhibition zones against *Candida albicans*. The 1% hydroxyapatite formulation demonstrated the strongest antifungal activity, significantly higher than the commercial toothpaste. Nystatin (5000 mg/L) was used as the positive control. Data are presented as mean ± SD ($n = 3$). Statistical analysis was performed using two-way ANOVA followed by Tukey's post hoc test. $^{*}P < .05$, $^{**}P < .01$, $^{***}P < .001$, $^{****}P < .0001$.

dependent improvement in hardness over the 14-day brushing period. This effect is attributable to the deposition of calcium and phosphate ions from HA onto demineralized enamel surfaces, effectively restoring structural integrity and increasing resistance to acid challenges.[27,28] Complementary surface roughness measurements further indicate that HA not only reinforces enamel but also mitigates abrasive wear during toothbrushing, preserving enamel smoothness and reducing the risk of microdamage.

The present findings are consistent with previous studies demonstrating the remineralization potential of HA-containing dentifrices. Similar to our results, Huang et al reported dose-dependent increases in enamel microhardness with increasing HA concentration, particularly within the 1% to 5% range.[29] Likewise, Amaechi et al showed that biomimetic HA toothpaste performed comparably to fluoride in enhancing surface microhardness and reducing early enamel erosion.[30] Our observation that the 3% concentration provided the most desirable balance between remineralization efficacy and user acceptability aligns with studies indicating that moderate HA concentrations optimize enamel surface deposition and texture while avoiding sensory burden from excessive mineral content.

From a microbiological standpoint, the HA-containing formulations showed no detectable bacterial or fungal growth, indicating the absence of unintended microbial contamination and supporting their suitability for oral use. Moreover, they exhibited antimicrobial activity, particularly against *S. aureus*, with higher HA concentrations enhancing inhibition. The antifungal activity against *C. albicans* was less straightforward, suggesting that antimicrobial effects are influenced by microbial characteristics in addition to HA concentration. These findings indicate that HA toothpaste can confer dual benefits: mechanical protection and a degree of antimicrobial support, complementing its remineralization function.[31]

Overall, the study establishes that bovine cancellous HA is a safe and effective functional ingredient for toothpaste. Incorporation at concentrations of 3% to 5% maximizes enamel remineralization, maintains favourable physical properties, and contributes to antimicrobial potential as demonstrated in microbial inhibition assays, without compromising biocompatibility as supported by cytocompatibility testing and the absence of microbial contamination in the formulations. Sensory properties should be optimized at moderate concentrations to ensure consumer acceptability while retaining therapeutic benefits.

Despite these promising results, several limitations should be acknowledged. First, the study relied on in vitro models, which cannot fully replicate the complex dynamics of the oral environment, including salivary flow, dietary acids, and microbial biofilms. Second, the short-term evaluation (2-3 weeks) does not capture long-term efficacy or potential cumulative effects of repeated use. Third, antimicrobial testing was limited to *S. aureus* and *C. albicans*, whereas the oral microbiome is highly diverse. Fourth, organoleptic testing was performed on a small panel, limiting the generalizability of sensory acceptability findings. Fifth, while pH remained within the acceptable range during the 30-day stability test, the upward trend indicates the need for longer-term pH monitoring to fully assess formulation stability over time. Finally, this study served as a pilot formulation assessment and did not include a formal sample size calculation. Some experiments used limited sample numbers due to feasibility constraints. Larger powered studies are required to validate these preliminary findings and support clinical application.

Future studies should explore the clinical efficacy of HA toothpaste in vivo, including its effects on caries prevention, enamel remineralization, and biofilm modulation over extended periods. Investigations into HA interactions with complex oral biofilms and synergistic effects with other active ingredients, such as fluoride or xylitol, could provide insights into optimizing antimicrobial efficacy. Additionally, enhancing flavour and texture profiles could improve consumer acceptability of higher HA concentrations, expanding the potential for broader population use.

Bovine cancellous HA toothpaste has potential as a biomimetic preventive oral care product, suitable for enhancing enamel remineralization, reducing hypersensitivity, and offering antimicrobial benefits. Its biocompatibility and physical stability make it applicable for paediatric and geriatric populations, and it could be formulated into alternative oral hygiene products such as gels, mouth rinses, or coatings for targeted enamel protection.

Conclusion

Bovine cancellous HA toothpaste demonstrates enhanced enamel remineralization, protective effects against surface wear, antimicrobial potential, and excellent biocompatibility. Formulations containing 3% to 5% HA achieve a favourable balance between efficacy and user acceptability, supporting their potential as safe, functional oral care products. These findings provide a strong basis for further development and clinical evaluation of HA-based toothpastes as an effective strategy for maintaining dental health.

Author contributions

Conceptualization: Octarina, Florencia Livia Kurniawan, Niko Falatehan. Methodology: Octarina, Florencia Livia Kurniawan, Niko Falatehan. Validation: Octarina, Florencia Livia Kurniawan, Niko Falatehan, Meircurius Dwi Condro Surboyo. Formal analysis: Octarina, Florencia Livia Kurniawan, Niko Falatehan. Investigation: Karen Sofiana, Gladys Mawarni Siregar, Ilman Nafi Maulana. Writing – original draft: Karen Sofiana, Gladys Mawarni Siregar, Ilman Nafi Maulana. Writing – review and editing: Octarina, Florencia Livia Kurniawan, Niko Falatehan, Meircurius Dwi Condro Surboyo. Visualization: Octarina, Meircurius Dwi Condro Surboyo. Supervision: Octarina, Florencia Livia Kurniawan, Niko Falatehan. Funding acquisition: Octarina, Florencia Livia Kurniawan.

Declaration of generative AI and AI-assisted technologies in the writing process

During the preparation of this work, the author used ChatGPT in order to check the language. After using this tool/service, the authors reviewed and edited the content as needed and takes full responsibility for the content of the published article.

Ethics statement

This study was approved by the Ethics Committee of the Faculty of Dentistry, Universitas Trisakti (Approval No. 921/S1/KEPK/FKG/6/2025).

Conflict of interest

The authors declare that they have no known competing financial interests or personal relationships that could have appeared to influence the work reported in this article.

Acknowledgements

The authors would like to express their gratitude to the Directorate General of Research and Development, Ministry of Higher Education, Science, and Technology, for the financial support provided through the BIMA Research Grant Program 2025 under Contract Numbers: 124/C3/DT.05.00/PL/2025 and 1014/LL3/AL.04/2025.

REFERENCES

1. Unterbrink P, Wiesche ESZ, Meyer F, Fandrich P, Amaechi BT, Enax J. Prevention of dental caries: a review on the improvements of toothpaste formulations from 1900 to 2023. Dent J (Basel) 2024;12(3):64.
2. MacHiulskiene V, Campus G, Carvalho JC, et al. Terminology of dental caries and dental caries management: consensus report of a workshop organized by ORCA and Cariology Research Group of IADR. Caries Res 2020;54:7–14.
3. Warreth A. Dental caries and its management. Int J Dent 2023;2023:9365845.
4. Lippert F. An introduction to toothpaste – its purpose, history and ingredients. Monogr Oral Sci 2013;23:1–14.
5. Martu M, Stoleriu S, Pasarin L, et al. Toothpastes composition and their role in oral cavity hygiene. Rom J Med Dent Educ 2021;10:6–15.
6. Hegde MN, Hegde NN, Shetty P, Hegde NN, Vittal CL, Ravinanthan M. Effect of medicated toothpastes and tooth mousse on

cariogenic microbes of the oral cavity: an in vitro study. J Conserv Dent Endod 2024;27(9):983–7.
7. Chen L, Al-Bayatee S, Khurshid Z, Shavandi A, Brunton P, Ratnayake J. Hydroxyapatite in oral care products—a review. Materials (Basel) 2021;14:4865.
8. Octarina O, Munadziroh E, Razak FA, Handharyani E, Surboyo MDC. The role of bovine amniotic membrane and hydroxyapatite for the ridge preservation. Int J Biomater 2024;2024:4053527.
9. Octarina O, Munadziroh E, Octarina MS. Potential of bovine amniotic membrane and hydroxyapatite as biocomposite materials for enhanced bone formation. Malays J Med Health Sci 2021;17(supp 6):124–6.
10. Octarina, Kurniawan FL, Larosa FA, Komala ON, Surboyo MDC. Physicochemical properties of demineralized bone matrix and calcium hydroxide composites used as bone graft material. Crystals (Basel) 2025;15(6):564.
11. Meyer F, Schulze Zur Wiesche E, Amaechi BT, Limeback H, Enax J. Caries etiology and preventive measures. Eur J Dent 2024;18 (3):766–76.
12. O'Hagan-Wong K, Enax J, Meyer F, Ganss B. The use of hydroxyapatite toothpaste to prevent dental caries. Odontology 2022;110:223–30.
13. Anil A, Ibraheem WI, Meshni AA, Preethanath R, Anil S. Demineralization and remineralization dynamics and dental caries. IntechOpen; 2022.
14. Luthfiyah S, Soegijono B, Susetyo FB, Notonegoro HA. Comparing properties of bovine bone derived hydroxyapatite and synthetic hydroxyapatite. J Appl Sci Eng 2022;25(6):1045–51.
15. Filio P, Octarina FNU, Komariah FNU. Characterization of fabricated bovine hydroxyapatite crystal as socket preservation material: an SEM-EDX and X-ray diffraction study. World J Dent 2022;13(S2):S175–81.
16. Agustantina TH, Munadziroh E, Yuliati A, et al. The characteristics of swelling and biodegradation tests of bovine amniotic membrane-hydroxyapatite biocomposite. Dent J 2023;56(3):172–7.
17. Shetty PJ, Roshni RS, Gomes L. Assessment and comparison of toothpastes for pH and antibacterial effect against Streptococcus mutans. SRM J Res Dent Sci 2021;12(1):8–12.
18. Spatafora G, Li Y, He X, Cowan A, Tanner ACR. The evolving microbiome of dental caries. Microorganisms 2024;12:121.
19. Pawinska M, Paszynska E, Limeback H, et al. Hydroxyapatite as an active ingredient in oral care: an international symposium report. Bioinspir Biomim Nanobiomater 2023; 13(1):1–14.
20. Cahyanto A, Rifada MA. Paten: Formulasi Sediaan Pasta Gigi Anak dengan Nano Hidroksiapatit untuk Meningkatkan Remineralisasi Gigi. Patent ID: IDP000091677. Indonesia; 2020.
21. Octarina, Munadziroh E, Razak FA, Surboyo MDC. Characterisation of bovine amniotic membrane with hydroxyapatite bio-composite. Coatings 2022;12(10):1403.
22. Anwar AI, Ruslin M, Marlina E, Hasanuddin H. Physicochemical analysis and application of sardinella fimbriata-derived hydroxyapatite in toothpaste formulations. BMC Oral Health 2025;25(1):195.
23. Nikfallah A, Mohammadi A, Ahmadakhondi M, Ansari M. Synthesis and physicochemical characterization of mesoporous hydroxyapatite and its application in toothpaste formulation. Heliyon 2023;9(10):195.
24. Ozan Toksoy M, Tugcu-demiröz F, Tirnaksiz F. Evaluation of rheological and textural properties of toothpastes. J Pharm Sci 2013;38(3):135–41.
25. Intannia W, Charlena C, Suparto IH. Hydroxyapatite-ZnO biomimetic toothpaste formulation from rice snail shell waste. Sci Technol Indones 2023;8(3):486–93.
26. Anggresani L, Sari YN, Rahmadevi R. Hydroxyapatite (HAp) from Tenggiri fish bones as abrasive material in toothpaste formula. J Kim Val 2021;7(1):1–9.
27. Amaechi BT, Farah R, Liu JA, et al. Remineralization of molar incisor hypomineralization (MIH) with a hydroxyapatite toothpaste: an in-situ study. BDJ Open 2022;8(1):33.
28. Sudradjat H, Meyer F, Loza K, Epple M, Enax J. In vivo effects of a hydroxyapatite-based oral care gel on the calcium and phosphorus levels of dental plaque. Eur J Dent 2020;14(2):206–11.
29. Huang SB, Gao SS, Yu HY. Effect of nano-hydroxyapatite concentration on remineralization of initial enamel lesion in vitro. Biomed Mater 2009;4:034104.
30. Amaechi BT, AbdulAzees PA, Okoye LO, Meyer F, Enax J. Comparison of hydroxyapatite and fluoride oral care gels for remineralization of initial caries: a pH-cycling study. BDJ Open 2020;6:9.
31. Imran E, Cooper PR, Ratnayake J, Ekambaram M, Mei ML. Potential beneficial effects of hydroxyapatite nanoparticles on caries lesions in vitro—a review of the literature. Dent J 2023;11(2):40.

ARTICLES FOR FACULTY MEMBERS

BONE-DERIVED HYDROXYAPATITE TOOTHPASTE FOR SUSTAINABLE PHARMACEUTICAL AND BIOMEDICAL APPLICATIONS

Comparative assessment of the remineralization characteristics of nano-hydroxyapatite extracted from fish scales and eggshells / Mkhize, S. C., Onwubu, S. C., Mokhothu, T. H., Mdluli, P. S., & Mishra, A. K.

Journal of Applied Biomaterials and Functional Materials
Volume 21 (2023) Pages 1-10
https://doi.org/10.1177/22808000231180390
(Database: Sage Journals)

Original Research Article

JABFM Journal of Applied Biomaterials & Functional Materials

Comparative assessment of the remineralization characteristics of nano-hydroxyapatite extracted from fish scales and eggshells

Journal of Applied Biomaterials & Functional Materials
1–10

DOI: 10.1177/22808000231180390
journals.sagepub.com/home/jbf
Sage

Sandile Cromwell Mkhize, Stanley Chibuzor Onwubu, Thabang Hendrica Mokhothu, Phumlane Selby Mdluli and Ajay Kumar Mishra

Abstract

Objectives: Dentine hypersensitivity (DH) is a common concern in dentistry that has the potential to restrict daily activities and harm a person's quality of life. In this study, the remineralization characteristics of nano-hydroxyapatite (nHAp) extracted from waste eggshells and fish scales were comparatively assessed.

Materials and methods: The extraction methods used to obtain nHAp from both fish scales and eggshells are also described. The effect of the extraction process and bio-waste source on the physicochemical characteristics of the nHAp such as Ca/P ratio, functional groups, crystallinity and phase change, and surface morphology are presented in the study. The remineralization properties were evaluated using dentine models ($n = 15$). A field scanning electron microscope was used to evaluate the effectiveness of the dentine tubules occlusion. The percentage occluded area for all the specimens was evaluated statistically using a one-way analysis of variance ($\alpha = 0.05$).

Results: The results showed that there were variations in the physicochemical characteristics of the nHAp extracted, including the crystallinity, particle size, and surface morphology, and buffering effects against citric acids. The EnHAp extracted from eggshells had higher crystallinity, superior buffering effects, and smaller particle size compared to the nHAp extracted from fish scales, making it a more favourable material for remineralization of teeth. The statistical evidence showed that there were statistically significant differences in the dentine occluding properties measured in the nHAp ($p < 0.001$). The highest mean % occluded area was measured with the EnHAp group.

Conclusions: The findings of this study provide insights into the use of bio-waste materials for the development of sustainable and effective products for oral health care.

Keywords

Bio-waste, eggshells, fish scales, nano-hydroxyapatite, remineralization

Date received: 15 February 2023; revised: 24 April 2023; accepted: 21 May 2023

Highlights

- Dentine hypersensitivity (DH) has been a common concern.
- Remineralization characteristics of nHAp extracted from eggshells and fish scales.
- Physicochemical characteristics of the nHAp extraction.

Department of Chemistry, Durban University of Technology (DUT), Durban, South Africa

Corresponding author:
Stanley Chibuzor Onwubu, Department of Chemistry, Durban University of Technology (DUT), Steve Biko Road, Durban 4001, South Africa.
Email: 21445599@dut4life.ac.za

- EnHAp extracted from eggshells showed higher crystallinity.
- Superior buffering effects and smaller particle size.
- EnHAp shows more favourable material for remineralization of teeth.

Introduction

Recently, the use of bio-based materials has gained popularity and has thus attracted many researchers who aim to explore their potential for biomedical applications.[1,2] The unique properties of these materials such as their non-toxicity, abundant availability, biocompatibility, and biodegradability make them favourable for use in various applications including antimicrobial coatings,[3] drug carriers[4] and adsorbents.[5] Particularly, the healthcare sector has been revolutionized by the use of bio-based materials due to the growing use in a variety of multidisciplinary fields including dentistry.[6] From a dentistry context, the use of bio-based materials has brought about tremendous growth and advantage in dental practice. For example, bio-based materials such as hydroxyapatite have been widely used in preventive and conservative dentistry,[7,8] restorative and periodontal treatment.[9] This makes hydroxyapatite bio-based materials a game-changer in the treatment and management of dental and oral-facial conditions.

In the era of preventive dentistry, the literature suggests periodontal therapy and improved home care practices may result in individuals retaining their teeth for longer, potentially leading to an increase in the number of exposed dentin surfaces.[10] This could result in a condition known as dentine hypersensitivity (DH). DH, a common oral health problem, is defined by the Canadian Association of Dentistry as a 'short, sharp pain arising from exposed dentin in response to stimuli typically thermal, evaporative, tactile, osmotic or chemical, and which cannot be attributed to any other form of dental defect or pathology'.[11]

In an attempt to manage DH, a variety of topical desensitizing toothpastes, which are dentin tubule occluding materials containing materials like potassium oxalates,[12] strontium salts[13] and sodium fluoride[14] among others. The use of hydroxyapatite particles, particularly in the form of nanohydroxyapatite (nHAp), has emerged as a promising material for remineralizing dentin. This is supported by clinical evidence, which suggests that nHAp-based desensitizing agents have shown promising results in improving DH.[7,8] It is important to note that nHAp is a natural component of the human tooth and bones, composing about ~90% of enamel and ~70% of dentine,[15] which thus makes nano-hydroxyapatite ideal for remineralization of damaged dentine tubules.

In our previous studies, we demonstrated the in vitro extraction of nHAp using eggshell waste as substrate and its use in occluding dentin tubules.[16,17] Fish scales can also be a source of nHAp. Fish scales, which are often considered waste, have been shown to contain valuable inorganic and organic components, including collagen (40%–55%) and hydroxyapatite (15%), making them a useful alternative source for hydroxyapatite extraction.[18,19] Thus, fish scale waste has tremendous unexploited potential as a biomaterial that could potentially add value to waste.

The fish market generates a significant amount of waste, which is either discarded or allowed to rot and represents a major environmental threat by acting as bacterial incubators.[20] These wastes generate large amounts of methane and other harmful gases[21] that pose a significant challenge to the environment. Thus, the creation of valuable, sustainable products from fish waste would serve as a dual-purpose strategy, enabling the extraction of nHAp from a sustainable source while also producing a valuable product. Furthermore, using the fish scale in the extraction of nHAp is important in addressing the environmental problem of waste management and towards a circular economy that supports a cleaner and greener environment. The objective of this study was to evaluate the effectiveness of nHAp derived from fish scales in occluding dentinal tubules.

In this study, we compared the characteristics of nHAp extracted from fish scales with that of eggshells. Fish scale nHAp (FnHAp) was extracted from fish scales in two separate batches. In the first batch, we use common chemicals such as sodium hydroxide (NaOH) and acetic acid in the extraction process. Thereafter, the extracted FnHAp were milled using a planetary ball-milling process. We assess the effectiveness of these materials in the remineralization of dentine tubules using the agitation process proposed by Onwubu et al.[22] To the best of our knowledge, there is little evidence in research that has comparatively compared the effectiveness of natural nHAp extracted from eggshell and fish scale wastes in occluding dentine tubules. The study hypothesized that there will be no significant difference in the occluding abilities of the nHAp extracted from eggshells (EnHAp) and fish scales (FnHAp).

Materials and method

Extraction of nHAp from eggshell and fish scale waste

Collected eggshells and fish scale waste from local outlets in South Africa were processed following the recommendations given by Onwubu et al.[23] These were heated in a furnace for 1 h at 300°C, then heated for 3 h at 900°C at a rate of 3°C min^{-1} to produce a white powder. This was a result of the calcium carbonate component of the eggshell waste breaking down to yield a calcium oxide powder.[16] Using the stoichiometric ratio of 1:5, 20 g of the white powder and 13.4 g of sodium triphosphate were wet-milled together in a 250 mL bowl containing 100 mL deionized

water at 500 rpm for 5 h. The mixture was then centrifuged for 30 min at a speed of 1000 rpm and dried in an oven for 5 days at 40°C. Thirty stainless steel balls with a diameter of 10 mm were used in a planetary ball mill (Retsch® PM 100) during the milling process.

The extraction of nHAp from fish scales was carried out in two batches. In the first batch, the scales were immersed in 1M hydrochloric acid (HCl) for 24 h. After 24 h, they were thoroughly rinsed with reverse osmosis water and then soaked in 1M sodium hydroxide (NaOH) for an additional 24 h to remove proteins. The fish scales were then rinsed and placed in a beaker with water, which was boiled for 20 min on a hot plate at 80°C. The fish scales were dried in an oven at 80°C for 2 h, then placed in crucibles and heated in a furnace at 700°C for 2 h. In the second batch, the obtained power (FnHAp) was dry ball-milled at 500 rpm for 2 h using the same milling parameters as explained above to obtain milled fish scale nHAp (mFnHAp).

Characterization

Fourier transform infrared spectroscopy analysis. The functional groups that were present in the prepared powders were determined using a Perkin Elmer Universal ATR. A background investigation was initially conducted before scanning. A small quantity of the prepared sample powders was then placed in a sample holder and scanned between 400 and 4500 cm^{-1} with a resolution of 4 cm^{-1}.

X-ray diffraction analysis. To track any potential changes in the crystallinity of the prepared powders, an X-ray diffraction (XRD) analysis was conducted. The patterns were captured using a diffractometer (D8 Advance BRUKER AXS instrument Germany instrument); Cu-Ka radiation (lKa1 = 1.5406) the patterns were analyzed between 10 and 80 (2 theta). The parameters used were 40 kV of voltage, 40 mA of current and 0.5 s of pass time.

High-resolution transmission electron microscopic analysis. In a high-resolution transmission electron microscope (HRTEM); (model: Philips CM 120) operating at 120 kV, the size, shape, and distribution of the prepared powders were investigated. Before HRTEM observation, tiny amounts of the powders were each dispersed in 10 mL of ethanol and sonicated at 10 kHz for 10 min. Finally, using a Leica microtome (South Africa), thin cross-sections of cryo-microtomed specimens were created and placed on carbon copper grids measuring 100 mm × 100 mm.

Elemental analysis of samples. The calcium to phosphate ratio of the samples was evaluated using the Energy Dispersive X-ray (EDX) technique. The findings were presented as a percentage weight of all the elements. Due to the interest in estimating the calcium to phosphate ratio that exhibits the component of the tooth's hydroxyapatite, data for carbon, oxygen, phosphorus and calcium are presented.

Table 1. Sample groups.

Sample powder	Total
EnHAp	5
FnHAp	5
mFnHAp	5

n = number of bovine teeth.

pH test. A pH metre (BOECO, BT-675, Germany) with a temperature sensor was used to monitor the pH value. About 1.5 g of each of the sample powders (EnHAp, FnHAp and mFnHAp) was put into a beaker containing 50 mL of deionized water. This mixture was stirred continuously for 10 min at a speed of 600 r min^{-1}, with pH readings taken every minute.

Dentin tubule occlusion test

Recently extracted anterior bovine-enamel teeth (15) were acquired at a slaughterhouse in Durban, KwaZulu Natal, South Africa. The bovine teeth were washed thoroughly and sterilized in a solution of 10% chloroxylenol. Using a low-speed water cooling diamond saw, dentin discs measuring 5 mm × 5 mm × 1 mm were cut below the dentin-enamel junction. The generated dentin disc was then wet-processed for 60 s using silicon carbide polishing sheets (600–1000 grits). Before creating the sensitive tooth model, the dentin discs were placed in a resin (AMT composite, South Africa). Afterwards, to open the dentine tubules, the specimens were submerged for 5 min in a citric acid solution with a concentration of 8 wt%. As shown in Table 1, the specimens were randomly allocated into four groups ($n = 5$) and treated using agitation techniques described by Onwubu et al.[16]

SEM evaluation of the occluded specimen. The occluded dentin before and after treatment was evaluated under controlled air conditions using an SEM (field emission, Carl Zeiss) operating at 20 kV. A thin, electrically conductive gold coating was applied to the surface to prevent an electrostatic charge build-up before SEM observation. With the aid of the ImageJ software (National Institute of Health, USA, http://imagej.nih.gov/ij) the ratios of both the occluded and the opened tubules were calculated. The ratios were determined by dividing the area of blocked tubules by the area of all tubules using 10,000 magnification photos ($n = 5$).

Analysis of the data. To study the mean values of the occluded area ratio in the SEM investigation, a one-way analysis of

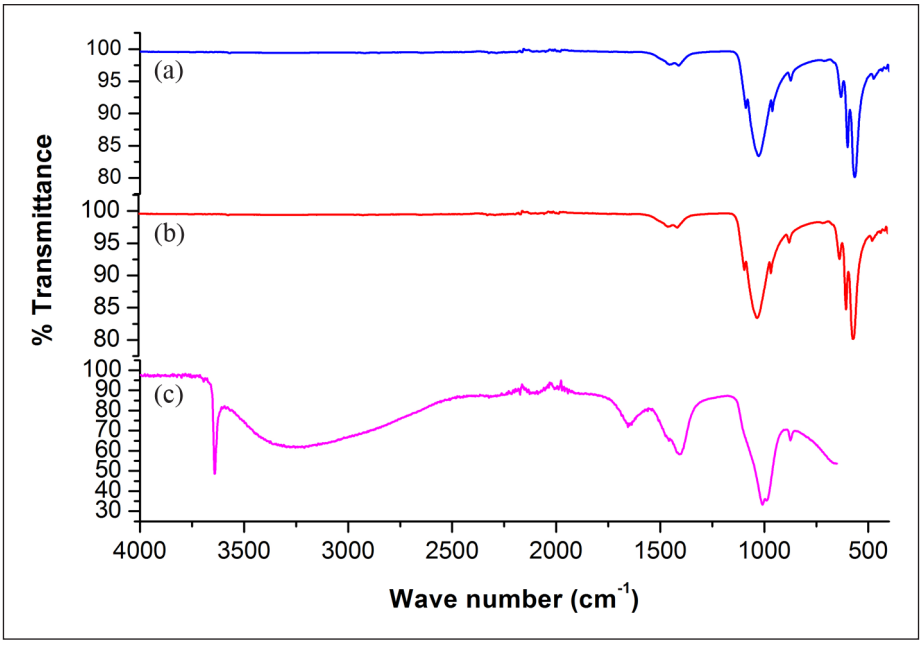

Figure 1. FTIR spectra of: (a) FnHAp, (b) mFnHAp and (c) EnHAp.

variance (ANOVA) was conducted using statistical software (IBM SPSS Statistics v28; IBM Corp). Afterwards, a multi-comparison test with Bonferroni correction (=0.05) was performed. To determine the statistical significance of differences between the groups. The results were considered statistically significant if the *p*-value was less than 0.05. The findings of the SEM investigation were presented as the mean ± standard deviation of the occluded area ratio.

Results

Characterization of the extracted hydroxyapatite samples

The image in Figure 1(a)–(c) shows the characteristic absorption peaks of the extracted nHAp powders as revealed by the FTIR analyses. The absorption bands typical of hydroxyapatite characteristics were observed around ~1000 and ~560 cm^{-1} for all the samples, respectively. This is due to the asymmetrical stretching and asymmetric bending vibrations of the PO_4^{3-} group, as reported in literature.[16,24] While the carbonate bands at 1450 cm^{-1} were evident in all the samples (Figure 1(a)–(c)), the intensity was much more prominent in the EnHAp (Figure 1(c)). The presence of the carbonate group in all the samples is attributable to out-of-plane bending mode and asymmetric stretching of CO_3^{2-} ions in the structure of the nHAp produced.[17] The reason for the carbonate peak found in all the samples may be associated with the substitution of the PO_4^{3-} ions in the structure of nHAp.[24,25] The hydroxyl group (O–H) bending was observed at around ~3750 cm^{-1}, identified by a small absorption peak in samples shown in Figure 1(a) and (b). In contrast, the absorption band for EnHAp (Figure 1(c)) was very visible around 3750 cm^{-1} and it is attributable to the OH stretching.[17] Furthermore, the broadband around ~3450 and 3000 cm^{-1}, and also the sharp band at 1600 cm^{-1} associated with water molecules[16] were evident in EnHAp samples alone (Figure 1(c)). The probable cause for the absence of water molecules in Figure 1(a) and (b) could be related to the alkaline hydrolysis and mechanochemical processes involved in the extraction of nHAp from fish scale.

The image in Figure 2(a)–(c) shows the XRD patterns of the extracted nHAp. The diffraction angles marked at 25.8° (002), 31.8° (121), 32.2° (112), 32.9° (030), 39.8° (310), 46.7° (222) and 49.4° (123), observed in all samples, are indicative of nHAp, according to the international standard (JCP2-76-0694). The peak observed at 29.4° corresponds to calcite, while the peak around 34.1° suggests the presence of Portlandite (20). The crystallinity value of EnHAp (82.19%) was found to be higher when compared to FnHAp (67.48%) and mFHAp (67.22%). The close values in crystallinity between FnHAp and mFnHAp suggest that milling did not impact the crystallinity of the nHAp extracted from fish scales. The Gaussian plot was used to determine the peak area, and the formula below was used to determine the crystallinity.

$$\text{Crystallinity Area of crystalline peak Area} = \text{of all peaks} * 100$$

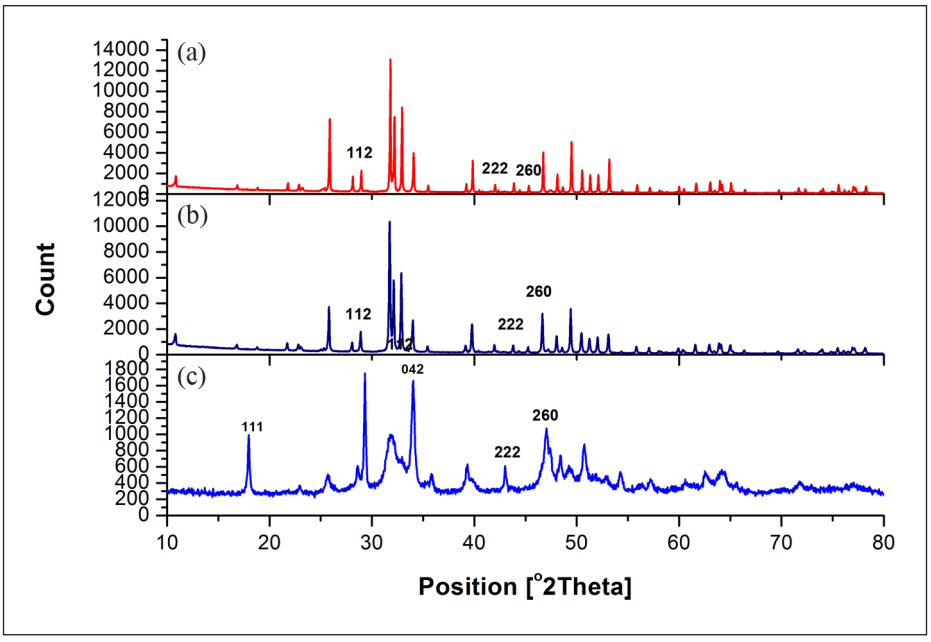

Figure 2. XRD pattern of: (a) FnHAp, (b) mFnHAp and (c) EnHAp.

Table 2. Showing mineral content of the sample powders, as determined by XRD analysis.

Mineral	Chemical formula	FnHAp	mFnHAp	EnHAp
Portlandite	$Ca(OH)_2$	3% (ICDD reference file 96-900-6834)	18% (ICDD reference file 96-100-1788	13.8% (ICDD reference file 98-020-2222)
Calcite	$CaCO_3$	12% (ICDD reference file 96-900-9668	8% (ICDD reference file 96-900-7688	2.5% (ICDD reference file 98-016-4935)
hydroxyapatite	$Ca4(PO4)_6OH_2$	77% (ICDD reference file 96-230-0274)	79% (ICDD reference file 96-230-0274	74.8% (ICDD reference file 96-230-0274)

EnHAp: eggshell nano-hydroxyapatite; FnHAp: fish scale nano-hydroxyapatite; mFnHAp: milled fish scale nano-hydroxyapatite; XRD: X-ray diffraction.
The International Centre for Diffraction Data (ICDD) reference codes were the reference standard used for XRD analyses. These codes guided the identification of organic and inorganic crystalline materials.

The mineralogical content in the different extracted nHAp (FnHAp, mFnHAp and EnHAP) obtained from the XRD analysis is further represented in Table 2. The analysis revealed differences in the mineralogical composition of the key minerals identified by the XRD analysis. The highest composition of hydroxyapatite (79%) and portlandite (18%) were measured in mFnHAp, respectively. By contrast, calcite content was higher in FnHAp (12%) compared to mFnHAp (8%) and FnHAp (2.5%).

The highest concentration of hydroxyapatite in mFnHAp indicates that milling the fish scales improved the mineral content compared to the initial extracted FnHAp. The presence of portlandite in mFnHAp suggests that the milling process could have led to the formation of new phases from the reaction of $Ca(OH)_2$ with CO_2 from the atmosphere. The difference in calcite content between FnHAp and mFnHAp highlights that the milling process might have caused the loss of some of the calcite content during the process. EnHAp showed the lowest content of hydroxyapatite (70%) compared to the other two samples, which suggests that the extraction process using an alkaline solution might have resulted in the loss of some of the hydroxyapatite content. The presence of calcite (2.5%) and portlandite (26%) in EnHAp indicates that the extraction process using an alkaline solution might have led to the formation of new minerals in the sample.

The elements present in the sample groups (FnHAp, mFnHAp and EnHAp) were analyzed by EDX and the results are shown in Table 3. The elements found in the samples were carbon (C), calcium (Ca), oxygen (O), phosphorus (P) and sodium (Na) with the presence of sodium being only evident in mFnHAp and EnHAp. All sample groups had high levels of calcium and phosphorus in the form of carbonate and phosphate. The ratio of calcium to phosphorus (Ca/P) was found to be different for each sample, with mFnHAp having a ratio of 1.9, slightly higher

Table 3. Elemental analysis of the samples.

Element (weight in %)	Sample groups		
	EnHAp	FnHAp	mFnHAp
Carbon (C)	17.5	10.5	15.3
Calcium (Ca)	26.9	66.3	21.4
Oxygen (O)	39	15.6	45
Phosphorus (P)	13	7.9	11.1
Sodium (Na)	3.0	0	4.8
Magnesium	0.6	0	2.4
Ca/P	2.1	2.1	1.9

than the 1.67 ratio found in human bones and teeth. The ratios for FnHAp and EnHAp were slightly different from the stoichiometric ratio of 1.67, which is likely due to the presence of trace elements like sodium and magnesium in natural nHAp.[26,27]

The HRTEM image in Figure 3(a)–(c) shows the surface morphology of the sample powders. There were visible differences in the surface morphology of the nHAp extracted from eggshells and fish scales. The image in Figure 3(a) and (b) shows that the nano-hydroxyapatite from fish scales (FnHAp and mFnHAp) particles presented an irregular morphology. After milling at 500 rpm for 2 h, the mFnHAP (Figure 3(b)) showed an increase in surface smoothness in comparison with FnHAp (Figure 3(a)). By contrast, an irregular-rod-like structure was observed for the eggshell nano-hydroxyapatite (EnHAp). The particles also appeared to assemble into short chains that stuck together into clusters (Figure 3(c)). In addition, the particle size of the sample powder measured using Image J software showed that the EnHAp had a mean diameter of 11.6 ± 2.7 nm. By contrast, the mean diameter measured for FnHAp and mFnHAp were 190 ± 81.8 and 74.6 ± 33.7, respectively.

Figure 4 shows the pH of the sample powders in deionized water and citric acid solution with initial pH of 2.06. The findings indicated that EnHAp had the highest mean pH value in deionized water (13.09), whereas the mFnHAp had the lowest value (10.77). All the sample powder had alkaline characteristics that may be attributable to the elevated calcium content. EnHAp had the best buffering characteristics when compared to both FnHAp and mFnHAp from fish scales in the sample powder study using the citric acid solution at pH 2.06 since it effectively neutralized the pH of the citric acids (Figure 4).

Additionally, it was also noted that the EnHAp showed the greatest buffering capacity as the slope of the EnHAp was the smallest among the sample groups. The results showed that EnHAp was more effective in maintaining the stability of the pH in the citric acid solution compared to FnHAp and mFnHAp. The ability to buffer pH is important in several biological processes and the results suggest that EnHAp may have potential applications in the biomedical field.

Dentine tubule occluding characteristics

FESEM was used to examine the morphological alterations of the occlusion of the dentine tubule before and after treatment (agitation). The samples treated with EnHAp (Figure 5c2) and mFnHAp (Figure 5b2) had more occluded areas than the samples treated with FnHAp (Figure 5a2). All samples show visible evidence of dentine tubule occlusion after agitation. The nanoparticles can be seen on the surface of the dentine specimens, and it can be inferred that the nanoparticles have entered the dentine tubules and have caused the occlusion. The results indicate that the EnHAp and mFnHAp were more effective in occluding the dentine tubules compared to FnHAp, which could be due to the difference in size and surface morphology of the particles. The smaller size and the rod-like structure of the EnHAp particles might have allowed for easier penetration into the dentine tubules, leading to more effective occlusion. On the other hand, the irregular shape of the FnHAp particles might have hindered their penetration into the tubules, resulting in less effective occlusion.

The mean % occluded area of the dentine tubules for the treated specimens is given in Table 4. The ANOVA value shows that the total mean % ratio of the dentine tubules occluded area for the specimens treated with sample powders (EnHAp, FnHAp and mFnHAp) was statistically significant ($p < 0.001$). The results indicate that EnHAp had the highest % mean occluded area ($78.2 \pm 1.5\%$) while the lowest was measured for the FnHAp group ($59.7 \pm 1.7\%$). According to the results of the Bonferroni test, the percentage of tubules occluded for the EnHAp group was statistically higher than that of the FnHAp group and the mFnHAp group ($P = 0.002$ and 0.001, respectively). In comparison to the FnHAp group, the % occluded area measured for the mFnHAp group was higher ($p = 0.001$).

Discussion

The clinical condition of DH has the potential to impede and restrict daily activities, which negatively impacts the person's quality of life.[28] According to Balhuc et al,[29] the use of more complex products and combinations between nano-hydroxyapatite (nHAp) and various compounds is an innovative method for significantly reducing DH and remineralizing dentinal tubules. While synthetic nHAp is commonly used in biomaterial applications, the need for environmental sustainability products has created a market for bio-waste materials. In this present study, we comparatively assessed the remineralization characteristics of nHAp extracted from waste eggshells and fish scales. The

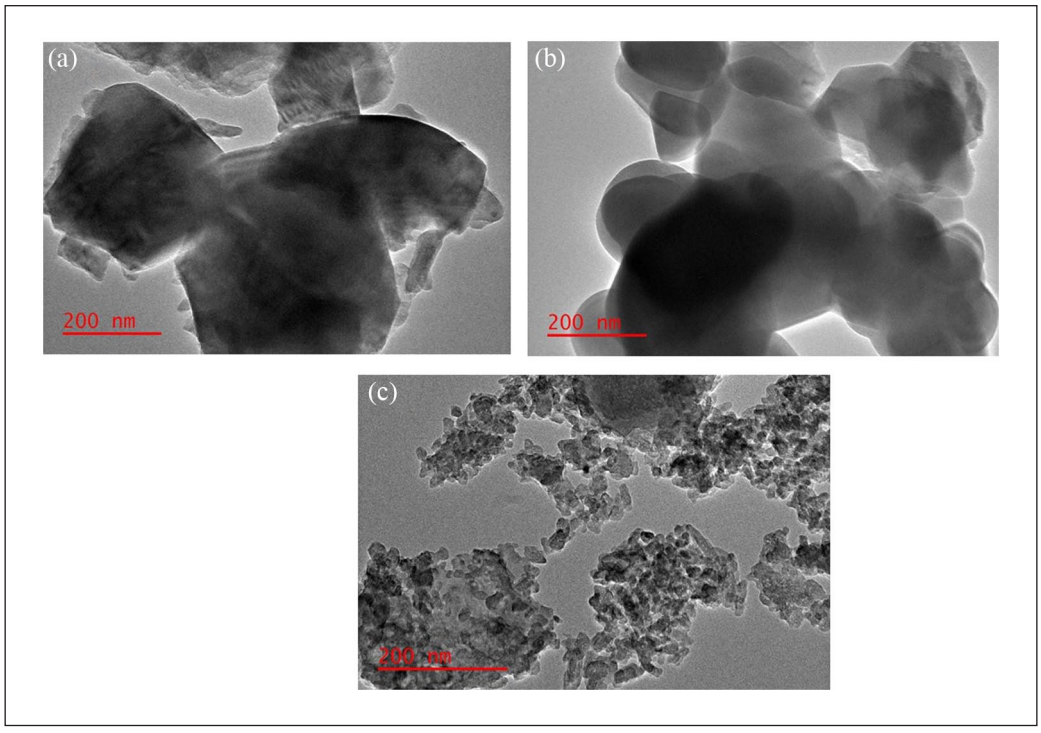

Figure 3. HRTEM micrograph of: (a) FnHAp, (b) mFnHAp and (c) EnHAp.

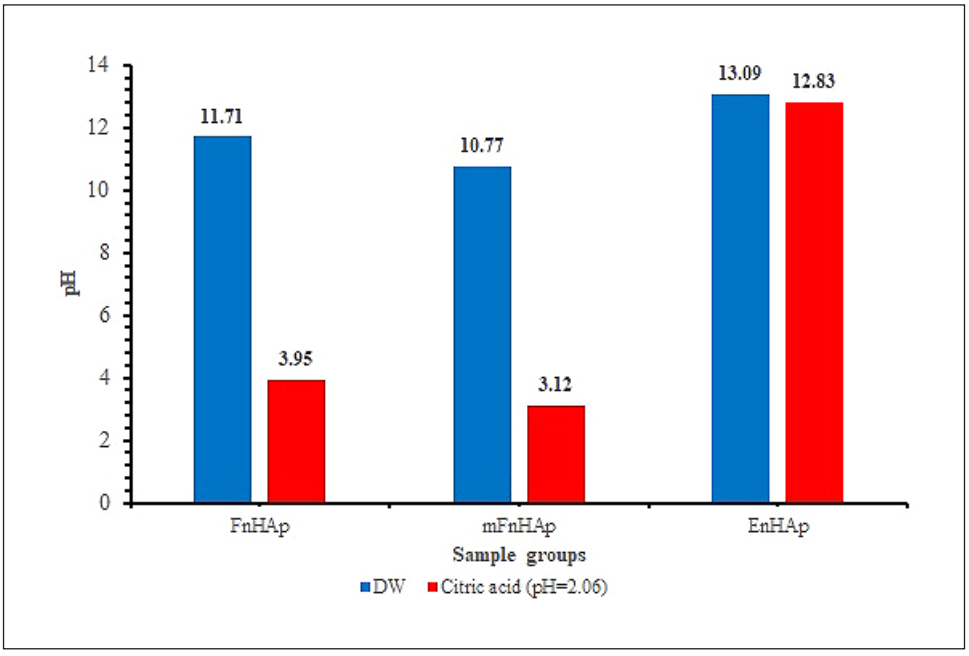

Figure 4. Buffering characteristics of samples.

results showed slight variations in the physicochemical characteristics of the nHAp extracted (Figure 1). While the nHAp from eggshells had higher crystallinity, the mineralogical content of hydroxyapatite was higher in the fish scale nHAp (Table 2).

The surface morphology also revealed variations between the nHAp extracted from eggshells and fish scales (Figure 3). The study results showed that milling the nHAp extracted from the fish scale does not negatively impact the physicochemical characteristics, but the milled fish

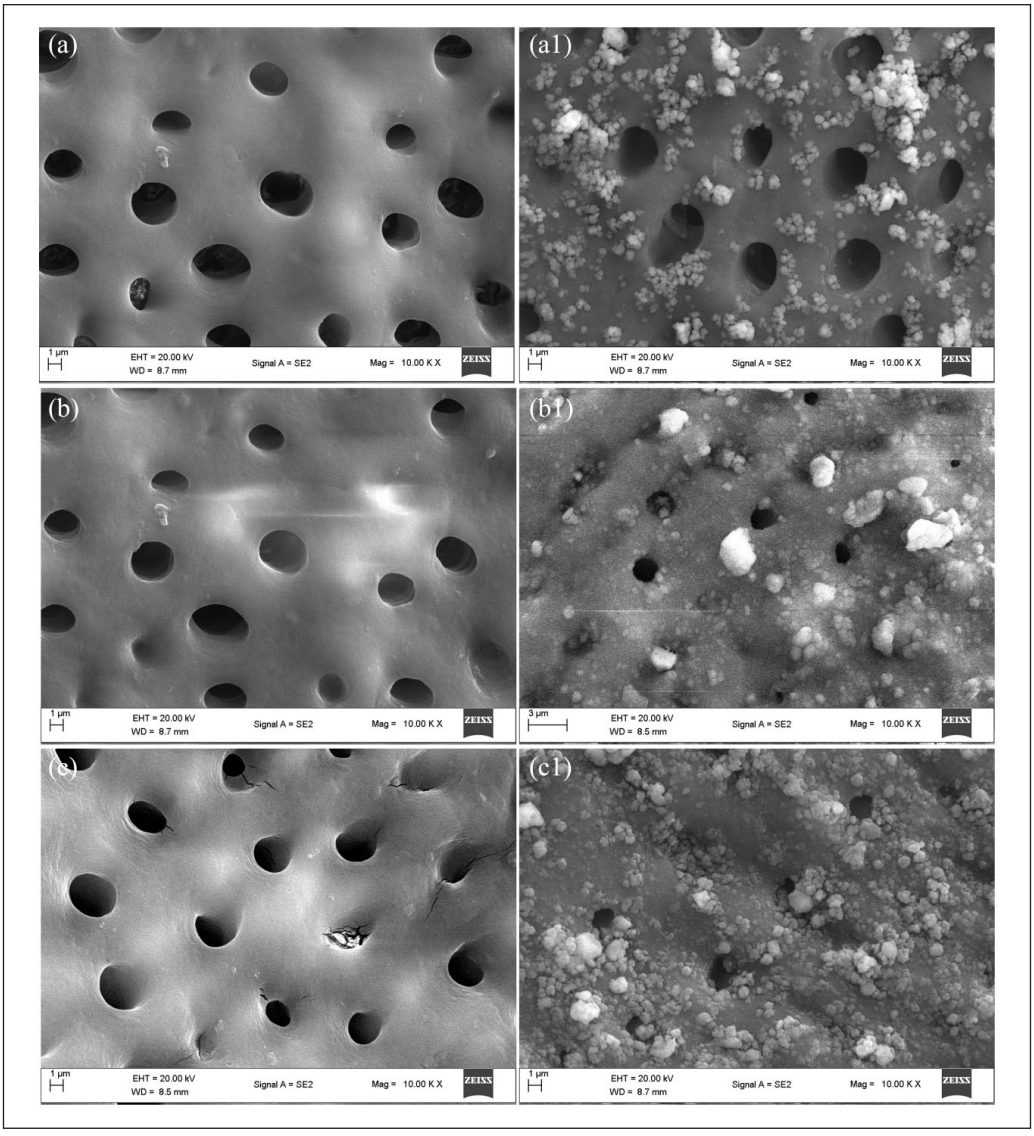

Figure 5. Remineralization test: (a) FnHAp, (b) mFnHAp and (c) EnHAp (1 represents after agitation).

scale nHAp (mFnHAp) had a smoother surface morphology and reduced particle size after milling (Figure 3). This may be due to the effect of the mechanical energy during milling, which could have triggered a transition from aggregated FnHAp to a smoother mFnHAp (Figure 3). Another study reported that milling stimulates transitions of substances due to the impact of mechanical energy.[30] Based on the study results, it can reasonably be assumed that the physicochemical characteristics of the nHAp such as the crystallinity, particle size and surface morphology vary due to the source of bio-waste, method of extraction, pH and temperatures.[31]

Furthermore, the results indicate that the buffering characteristics of eggshell nHAp (EnHAp) against citric acids were superior to those measured for nHAp extracted from fish scales (Figure 4). The reason for EnHAp having higher buffering effects compared to FnHAp and mFnHAp could be due to the differences in the crystal structure and particle size. The irregular rod-like structure and smaller particle size of EnHAp may provide a larger surface area for reaction with the citric acid, allowing it to effectively neutralize the pH of the solution. The higher surface area could lead to a greater number of surface-active sites, resulting in more efficient buffering effects. It is also possible that differences in the chemical composition and the presence of trace elements in each sample group could play a role in the buffering characteristics of the materials. This indicates that EnHAp provides better protection against enamel demineralization from acidic substances by effectively neutralizing citric acid. The implication for oral health are that EnHAp provides high bioavailable calcium that is crucial for tooth remineralization.[17,32] This is

Table 4. ANOVA test comparison of the occluded area.

Treatment group	N	Mean ± SD	Standard error	95% confidence interval		p-Value	Bonferroni's correction
				Lower bound	Upper bound		p-Value
EnHAp	5	78.2 ± 1.5	0.680	76.332	80.108	<0.001	0.002[1,3]
FnHAp	5	59.7 ± 1.7	0.753	57.629	61.811		0.001[1,2]
mFnHAp	5	72.9 ± 2.1	0.939	70.332	75.548		0.001[3,2]

EnHAp: eggshell nanohydroxyapatite; FnHAp: fish scale nanohydroxyapatite; mFnHAp: milled fish scale nanohydroxyapatite; SD: standard deviation. The superscript numbers indicate the mean differences between sample groups.

supported by the FESEM image in Figure 5, which shows that EnHAp had the most increase in dentine tubules occlusion. In agreement with Tschoppe et al,[33] this means that the higher pH values of the nHAp slurries favour tooth remineralization. Statistical results indicate a statistically significant difference in the treated dentine specimens ($p < 0.001$), and the formulated study hypothesis was rejected based on the results obtained.

Overall, the EnHAp group had the highest mean % occluded area of the dentine tubules (Table 4). The plausible difference in the dentine tubules observed may be due to the physicochemical characteristics of the nHAp extracted. This aligns with Kong et al[34] who suggest that the performance of nHAp is influenced by its crystallinity, particle size, and surface morphology. This means that the smaller particle size of EnHAp and the higher pH values favour its remineralization characteristics over the fish scale nHAp. Additionally, the particle sizes measured for the nHAp extracted are smaller than the size of tubules close to the dentine-enamel junction, which is around 3–5 µm.[35] This indicates that smaller nHAp particles can easily be attached to dentinal surfaces and occlude exposed dentine tubules. This may explain the dentine tubule occlusion in all the tested nHAp from both fish scales and eggshells (Figure 5). Another possible reason is the polarity and the large surface proportion of the atomic number of nHAp, which allows the particles to bind to collagen and hydroxyapatite in dentine.[36]

Conclusions

The study we have compared the remineralization characteristics of nano-hydroxyapatite (nHAp) extracted from waste eggshells and fish scales. The results showed that there were variations in the physicochemical characteristics of the nHAp extracted from the two sources. The EnHAp extracted from eggshells had higher crystallinity and superior buffering effects against citric acids compared to the nHAp extracted from fish scales. The smaller particle size and higher pH values of EnHAp favoured its remineralization characteristics. The results showed that EnHAp had superior buffering effects against citric acids and higher mean % occlusion of dentine tubules compared to FnHAp and milled FnHAp (mFnHAp). The ANOVA results also indicated that there was a statistically significant difference ($p < 0.001$) in the dentine tubule occlusion between EnHAp and FnHAp. These findings highlight the potential of nHAp from natural bio-waste as a low-cost alternative for dental applications and warrant further research to optimize its use in clinical practice.

Declaration of conflicting interests

The author(s) declared no potential conflicts of interest with respect to the research, authorship, and/or publication of this article.

Funding

The author(s) disclosed receipt of the following financial support for the research, authorship, and/or publication of this article: The support offered by the National Research Foundation of South Africa (Grant Number: 129492) is acknowledged.

ORCID iD

Stanley Chibuzor Onwubu https://orcid.org/0000-0002-4499-1534

Data availability statement

On reasonable request, the corresponding author will provide the datasets generated during and/or analysed during the current study.

References

1. Antunes A, Faria P, Silva V and Brás A. Rice husk-earth based composites: A novel bio-based panel for buildings refurbishment. *Constr Build Mater* 2019; 221: 99–108.
2. Battegazzore D, Abt T, Maspoch ML and Frache A. Multilayer cotton fabric bio-composites based on PLA and PHB copolymer for industrial load carrying applications. *Compos B Eng* 2019; 163: 761–768.
3. Kalyoncuoglu UT, Yilmaz B and Gungor S. Evaluation of the chitosan-coating effectiveness on a dental titanium alloy in terms of microbial and fibroblastic attachment and the effect of aging. *Mater Technol* 2015; 49: 925–931.
4. Aguilar A, Zein N, Harmouch E, et al. Application of chitosan in bone and dental engineering. *Molecules* 2019; 24: 3009.
5. Tavakolian M, Munguia-Lopez JG, Valiei A, et al. Highly absorbent antibacterial and biofilm-disrupting hydrogels from cellulose for wound dressing applications. *ACS Appl Mater Interfaces* 2020; 12: 39991–40001.

6. Anju S, Prajitha N, Sukanya VS and Mohanan PV. Complicity of degradable polymers in health-care applications. *Mater Today Chem* 2020; 16: 100236.
7. Vano M, Derchi G, Barone A, Pinna R, Usai P and Covani U. Reducing dentine hypersensitivity with nano-hydroxyapatite toothpaste: a double-blind randomized controlled trial. *Clin Oral Investig* 2018; 22: 313–320.
8. Anand S, Rejula F, Sam JVG, Christaline R, Nair MG and Dinakaran S. Comparative evaluation of effect of nano-hydroxyapatite and 8% arginine containing toothpastes in managing dentin hypersensitivity: double blind randomized clinical trial. *Acta Med* 2017; 60: 114–119.
9. Kijartorn P, Wongpairojpanich J, Thammarakcharoen F, Suwanprateeb J and Buranawat B. Clinical evaluation of 3D printed nano-porous hydroxyapatite bone graft for alveolar ridge preservation: a randomized controlled trial. *J Dent Sci* 2022; 17: 194–203.
10. Balcheva G, Balcheva M, Koleva M, Grozdeva D and Panov V. Epidemiology of dentin hypersensitivity. *J Med Dent Pract* 2017; 4: 524–530.
11. Cartwright R. Dentinal hypersensitivity: a narrative review. *Community Dent Health* 2014; 31: 15–20.
12. Cunha-Cruz J, Stout JR, Heaton LJ and Wataha JC. Dentin hypersensitivity and oxalates: a systematic review. *J Dent Res* 2011; 90: 304–310.
13. Saeki K, Marshall GW, Gansky SA, Parkinson CR and Marshall SJ. Strontium effects on root dentin tubule occlusion and nanomechanical properties. *Dent Mater* 2016; 32: 240–251.
14. Pandit N, Gupta R and Bansal A. Comparative evaluation of two commercially available desensitizing agents for the treatment of dentinal hypersensitivity. *Indian J Dent Res* 2012; 23: 778–783.
15. Abou Neel EA, Aljabo A, Strange A, et al. Demineralization-remineralization dynamics in teeth and bone. *Int J Med* 2016; 11: 4743–4763.
16. Onwubu SC, Mhlungu S and Mdluli PS. *In vitro*evaluation of nanohydroxyapatite synthesized from eggshell waste in occluding dentin tubules. *J Appl Biomater Funct Mater* 2019; 17: 1–6.
17. Onwubu SC, Naidoo D, Mkhize SC, Mabaso NLN, Mdluli PS and Thakur S. An investigation in the remineralization and acid resistant characteristics of nanohydroxyapatite produced from eggshell waste via mechanochemistry. *J Appl Biomater Funct Mater* 2020; 18: 2280800020968352.
18. Boaventura T, Peres A, Gil V, Gil C, Oréfice R and Luz R. Reuse of collagen and hydroxyapatite from the waste processing of fish to produce polyethylene composites. *Química Nova* 2020; 43: 168–174.
19. Kulkarni P and Maniyar M. Utilization of fish collagen in pharmaceutical and biomedical industries: waste to wealth creation. *Life Sci Inform Publications* 2020; 6: 11.
20. Aziz U, Haq EU, Rashid M and Nadeem M. Development and characterization of biodegradable fish scale composite using natural binder. *Mater Today Proc* 2021; 47: S22–S27.
21. Mejía-Saulés JE, Waliszewski KN, Garcia MA, et al. The use of crude shrimp shell powder for chitinase production by Serratia marcescens WF. *Food Technol Biotechnol* 2006; 44: 95–100.
22. Onwubu SC, Mdluli PS and Singh S. Evaluating the buffering and acid-resistant properties of eggshell–titanium dioxide composite against erosive acids. *J Appl Biomater Funct Mater* 2019; 17(1): 7.
23. Onwubu SC, Vahed A, Singh S and Kanny KM. Reducing the surface roughness of dental acrylic resins by using an eggshell abrasive material. *J Prosthet Dent* 2017; 117: 310–314.
24. Ronan K and Kannan MB. Novel sustainable route for synthesis of hydroxyapatite biomaterial from biowastes. *ACS Sustain Chem Eng* 2017; 5: 2237–2245.
25. Farzadi A, Bakhshi F, Solati-Hashjin M, Asadi-Eydivand M and Osman NAA. Magnesium incorporated hydroxyapatite: synthesis and structural properties characterization. *Ceram Int* 2014; 40: 6021–6029.
26. Akram M, Ahmed R, Shakir I, Ibrahim WAW and Hussain R. Extracting hydroxyapatite and its precursors from natural resources. *J Mater Sci* 2014; 49: 1461–1475.
27. Milovac D, Gamboa-Martínez TC, Ivankovic M, Gallego Ferrer G and Ivankovic H. PCL-coated hydroxyapatite scaffold derived from cuttlefish bone: in vitro cell culture studies. *Mater Sci Eng C* 2014; 42: 264–272.
28. Bekes K and Hirsch C. What is known about the influence of dentine hypersensitivity on oral health-related quality of life? *Clin Oral Investig* 2013; 17 Suppl 1: S45–S51.
29. Balhuc S, Campian R, Labunet A, Negucioiu M, Buduru S and Kui A. Dental applications of systems based on hydroxyapatite nanoparticles—an evidence-based update. *Crystals* 2021; 11: 674.
30. Baláž M. Ball milling of eggshell waste as a green and sustainable approach: a review. *Adv Colloid Interface Sci* 2018; 256: 256–275.
31. Mohd Pu'ad NAS, Koshy P, Abdullah HZ, Idris MI and Lee TC. Syntheses of hydroxyapatite from natural sources. *Heliyon* 2019; 5: e01588.
32. Macri DV. Implementing a minimally invasive approach. *Dimens Dent Hyg* 2016; 14: 32–37.
33. Tschoppe P, Zandim DL, Martus P and Kielbassa AM. Enamel and dentine remineralization by nano-hydroxyapatite toothpastes. *J Dent* 2011; 39: 430–437.
34. Kong D, Xiao X, Qiu X, et al. Synthesis and characterization of europium ions doping of hydroxyapatite nanorods by the simple two step method. *Funct Mater Lett* 2015; 08: 1550075.
35. Lenzi TL, Guglielmi Cde A, Arana-Chavez VE and Raggio DP. Tubule density and diameter in coronal dentin from primary and permanent human teeth. *Microsc Microanal* 2013; 19: 1445–1449.
36. Enax J, Fabritius H-O, Fabritius-Vilpoux K, Amaechi BT and Meyer F. Modes of action and clinical efficacy of particulate hydroxyapatite in preventive oral health care − state of the art. *Open Dent J* 2019; 13: 274–287.

ARTICLES FOR FACULTY MEMBERS

BONE-DERIVED HYDROXYAPATITE TOOTHPASTE FOR SUSTAINABLE PHARMACEUTICAL AND BIOMEDICAL APPLICATIONS

Hydroxyapatite recovery from fish byproducts for biomedical applications / Hernández-Ruiz, K. L., López-Cervantes, J., Sánchez-Machado, D. I., Martínez-Macias, M. del R., Correa-Murrieta, M. A., & Sanches-Silva, A.

Sustainable Chemistry and Pharmacy
Volume 28 (2022) 100726 Pages 1-14
https://doi.org/10.1016/j.scp.2022.100726
(Database: ScienceDirect)

Sustainable Chemistry and Pharmacy 28 (2022) 100726

Contents lists available at ScienceDirect

Sustainable Chemistry and Pharmacy

journal homepage: www.elsevier.com/locate/scp

Hydroxyapatite recovery from fish byproducts for biomedical applications

Karen Lilián Hernández-Ruiz [a], Jaime López-Cervantes [a], Dalia Isabel Sánchez-Machado [a, *], María del Rosario Martínez-Macias [a], Ma. Araceli Correa-Murrieta [a], Ana Sanches-Silva [b, c]

[a] Technological Institute of Sonora, Ciudad Obregon, MX, 85000, Sonora, Mexico
[b] National Institute of Agrarian and Veterinary Research, Vila do Conde, Portugal
[c] Center for Study in Animal Science (CECA), University of Oporto, Oporto, Portugal

ARTICLE INFO

Keywords:
Hydroxyapatite
Aquatic waste
Biomaterials
Biological properties

ABSTRACT

The solid waste that is generated during industrial fish processing causes environmental deterioration after it is discarded. However, these aquatic materials are a source of valuable compounds such as hydroxyapatite (HAp). HAp is a calcium phosphate with physicochemical and biological properties that are similar to those of native human bone. HAp has been used in biomedical material development because it is biocompatible and does not cause adverse effects. It has been combined with many other chemical compounds to improve their mechanical, structural, and bioactive properties and has noteworthy application benefits in the food supplement, drug delivery, cosmetology, odontology, and bone implant fields. In this review, recent research related to the isolation of HAp and the development of materials with health benefits due to its bioactive properties are discussed. Moreover, the HAp derived from industrial fish processing adds value to the byproduct and reduces the environmental risks caused by aquatic waste disposal in landfills.

1. Introduction

Fish consumption worldwide has increased the amount of waste generated, either from scales or bones. However, these wastes from fish processing have value for bioactive compound extraction. Among these compounds are polymers that have recently been gaining increasing attention, such as collagen, gelatin, starch, and chitosan (Bochicchio et al., 2020; Atef and Ojagh, 2017). Furthermore, aquatic waste contains enzymes, polyunsaturated fatty acids, antioxidant compounds and minerals, such as calcium phosphates (Atef and Ojagh, 2017). Pal et al. (2017) reported that fish waste is an important source of calcium, phosphates, and carbonates.

Calcium phosphates belong to a family of minerals containing both calcium cations (Ca^{+2}) and phosphate anions (Jeong et al., 2019). These materials are of great significance in chemistry, agriculture, medicine, biochemistry and bioengineering because they play an important role in biological calcification. Traditionally, calcium phosphates have been obtained from chemical synthesis. However, these compounds have also been found in different natural sources, such as bovine and goat bones, as well as dental enamel and the shells, scales, and bones of aquatic animals. To date, the calcium phosphate material that has been given the most attention in this research area is hydroxyapatite (HAp) due to its similarities to native human bone and teeth (Li et al., 2019).

* Corresponding author.
E-mail address: dalia.sanchez@itson.edu.mx (D.I. Sánchez-Machado).

https://doi.org/10.1016/j.scp.2022.100726
Received 5 January 2022; Received in revised form 19 April 2022; Accepted 10 May 2022
Available online 21 May 2022

Currently, HAp is the most studied calcium phosphate because it is found in a natural form. On average, HAp represents between 50 and 70% of bone weight, and it has been reported to be a highly osteoconductive, biodegradable, biocompatible, and bioactive material (Khandelwal and Prakash, 2016). In addition, its stability at normal temperatures and pH values between 4 and 12 makes it an optimum material for very diverse uses. Recently, interest in HAp has increased due to its hemostatic properties and bone recovery functions (Pokhrel, 2018). Therefore, several methods have been developed for its extraction while regulating its physical, chemical, and morphological properties for applications in the production of biomaterials.

The extraction and purification of HAp has been studied for many years to improve its quality and increase its applications. Although HAp has been synthesized through chemical methods, its extraction from natural sources, such as human or animal bones, has gained attention in recent years (Muhammad et al., 2016). Additionally, eggshells, seashells and other aquatic wastes (bones and scales) represent promising ways to acquire large quantities of HAp while also reducing environmental pollution (Oladele et al., 2018). However, the extraction efficiency and purity and chemical properties of the extracted HAp will depend on the bone conditions, degree of calcification, and extraction method. HAp has been recovered from the demineralization stage of collagen extraction as an additional product (Nam et al., 2019). Among the extraction methods for the recovery of HAp from natural sources, the most common are acidic, alkaline, and acidic-alkaline hydrolysis, which use HCl and NaOH at different concentrations to eliminate collagen proteins. Additionally, ionic and enzymatic hydrolysis with Protamex (1%) and Alcalase have been reported (Ismail et al., 2019; Nam et al., 2019). Moreover, incineration has been used to extract HAp after washing the fresh material. However, incineration is used as last step in the purification of the final product after deproteinization. Moreover, HAp from natural sources could contain trace elements with important benefits to the human body (Li et al., 2019). Based on this, the recovery of HAp from natural sources represents an alternative to improve its biological properties and chemical characteristics for use in biomedical fields.

Currently, HAp is used in tissue engineering as a bone implant or filling. Likewise, it has been added to products used in dentistry for enamel recovery and dental implants (Vano et al., 2018; Chadda et al., 2016). HAp is employed in biomaterial formulations due to its ability to promote biomineralization. Incorporating HAp into other polymers improves its mechanical and biological properties, thus increasing its applicability. Additionally, the interaction between the polymers could create an ideal environment with interfacial bonding on the surface of the biomaterial to enhance the interaction between the biomaterial and living tissues. Currently, the preparation of biomaterials of natural origin is attractive due to their availability, biocompatibility and biodegradability, which also represents a promising way to reduce the disposal of industrial waste and generate value-added materials (Athinarayanan et al., 2020).

Furthermore, the increase in HAp research has been attributed to its natural abundance and benefits to the human body. Hence, the aim of this work was to provide an exhaustive and updated review on the recovery methods of HAp from aquatic sources and the biological and material development properties of HAp with medical potential. All the knowledge contained herein will expand upon the possible biomedical applications of this mineral isolated from natural sources due to its many biological properties. Although research on the natural sources and methods of extraction and purification of HAp has been carried out to promote the use of this material, the use of natural compounds to produce biomaterials remains a great challenge. Future perspectives on the uses and applicability of HAp will focus on its extraction from natural products and the promotion of eco-friendly and low-cost methods for its recovery to produce safe materials that can be used in biomedical fields.

2. Natural sources of HAp

Calcium phosphate (CaP) compounds belong a specific mineral family that consist of calcium cations (Ca^{+2}) combined with phosphate anions such as orthophosphate, metaphosphate, and pyrophosphate (Eliaz and Metoki, 2017). These compounds have a general formula of $A_4B_6(MO_4)_6X_2$, where A and B represent calcium ions, MO_4 is the phosphate group, and X indicates the presence of –OH groups in the structure. Currently, HAp is the most widely used bioactive calcium phosphate. Its chemical structure is $Ca_{10}(PO_4)_6(OH)_2$, and it has a calcium/phosphorus (Ca/P) molar ratio between 0.5 and 2. Notably, Pu'ad et al. (2019) reported that the ideal HAp Ca/P ratio for good biocompatibility and excellent bioactivity is 1.67.

HAp was discovered in 1926 and has since been widely used for biomedical applications. It has been purified from different sources through several methods to improve its chemical, biological and mechanical properties. Fig. 1 shows the history of the acquisition of this compound from its discovery to the use of natural products for its extraction, which is expected to continue in the future (Perloff and Posner, 1956; Dry and Beebe, 1960; Callan and Rohrer, 1993; Lee et al., 1997; Khalid and Chaudhry, 2019). As mentioned before, HAp can be synthesized from chemical components or extracted from natural organic materials. Some of the most commonly used synthetic techniques are chemical precipitation, radiofrequency thermal plasma, microemulsion and hydrothermal methods (Sathiskumar et al., 2019). Nonetheless, synthetic production requires the use of hazardous chemical compounds that can make the process risky, costly and time consuming (Alhussary et al., 2020). On the other hand, several natural sources have been utilized to isolate HAp, such as mammalian bones (bovine, camel, and horses), aquatic waste (shells, scales, and bones), and eggshells (Pu'ad et al., 2019).

Some authors have reported that fish scales and bones are safe sources for HAp obtention. In addition, this approach reduces environmental risk because it makes use of fishery industry waste (Venkatesan et al., 2015; Alif et al., 2018). Moreover, added value is given to aquatic byproducts through the development of functional foods, drug delivery systems, biomaterials, and biomedical products. Therefore, utilizing the waste generated by the fishing industry to isolate HAp through simple, inexpensive and biologically safe methods that do not require the use of chemicals for processing is a promising alternative (Sathiskumar et al., 2019).

Annually, millions of tons of fish are captured, but only between 50 and 60% are consumed. The remaining fish become solid waste, which has low added value (Paul et al., 2017; Granito et al., 2018). This aquatic waste is composed of organic collagen and in-

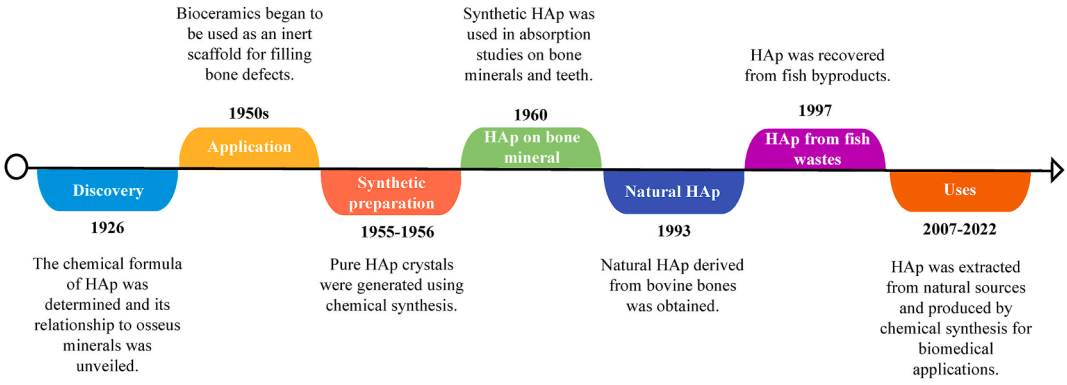

Fig. 1. Historical timeline of the recovery and application of HAp.

organic HAp, with some authors reporting HAp recovery yields of between 50% and 53% (Hasan et al., 2020). Nevertheless, HAp yield ultimately depends on the extraction conditions and methodology.

3. HAp extraction methodologies and quality analysis

The methods reported for HAp extraction from natural sources include the sol-gel process, precipitation techniques, hydrothermal methods, hydrolysis, microwave irradiation and solid-state reactions (Muhammad et al., 2016). It is recommended that the chosen extraction method be effective with a high yield. To produce a high-quality material, it is important to control the composition and purity of the source materials, pH, and temperature (Khoshzaban et al., 2017). Based on published data, three stages have been identified for the isolation of HAp. Initially, the fresh material is cleaned, then the proteins are hydrolyzed, and finally, the solid residue is incinerated. Additional methods for HAp extraction from aquatic waste are documented and detailed in Table 1.

First, impurities such as skin, meat, fat, blood, and salts are removed from the raw material by soaking and boiling in water for 1–24 h, depending on how much material is being used and how dirty the material is (Yamamura et al., 2018; Ayala-Barajas et al., 2020). Granito et al. (2018) reported that any sort of treatment prior to HAp extraction promotes good quality of the final product due to the removal of impurities. This stage is performed using tap and distilled water until the impurities are removed; sometimes, the material must be dried at room temperature or at a temperature up to 80 °C for 24 h.

Subsequently, the solid raw materials are deproteinized by acidic, alkaline, or enzymatic hydrolysis to promote HAp recovery. Several treatment methods have been reported, with the use of 1 N HCl and 1% NaOH for up to 24 h of treatment being among the most common. Then, the remaining material is neutralized and immediately dried at 50–60 °C. Based on the information reported in Table 1, the most widespread method to extract HAp from aquatic sources is through alkaline deproteinization to promote the HAp recovery and purification. During this stage, the organic materials present in the fresh material, such as collagen and noncollagenous proteins, are removed. Notably, the extraction yield after this process is lower than that of other reported methods, which indicates high-quality HAp purification.

Finally, sample incineration is carried out to purify the HAp. It has been found that an increase in temperature modifies the composition, crystallinity, and particle size of HAp. Khoo et al. (2015) reported that these effects are associated with heat absorption from particles. They also found that pores and structural variations are created by the decomposition of organic substances after incineration at higher temperatures, from 700 to 1100 °C. Reported calcination temperatures reported range from 500 to 1400 °C with 1 and 24 h of reaction with a gradual increase in temperature (Ismail et al., 2019). The most commonly used temperatures are between 700 and 800 °C because higher temperatures may diminish the porosity of the final product and affect its bioactivity and interactions with other materials (Bhat et al., 2021). Moreover, the crystallinity, shape and size of the final product vary with increasing temperature during this stage. Thus, temperature is an important factor to consider during the purification of HAp so that a final product with better chemical, morphological and biological characteristics can be produced for biomedical applications.

Incineration is one of the most direct methods to isolate HAp; however, it is laborious and time consuming when the previous steps are not carried out, and impurities may remain in the final product. Therefore, incineration is commonly the last step in HAp purification, occurring after acidic, alkaline and/or enzymatic hydrolysis.

Nevertheless, some research groups have reported using incineration to isolate HAp with minimal fresh material processing. Doğdu et al. (2021) extracted HAp from the teeth of frog fish (*Lagocephalus sceleratus*). The first step was bleaching with H_2O_2 for 1 h followed by filtration and washing with water and finally drying at 105 °C. They reported a Ca/P molar ratio of 1.32 and the presence of carbonate and phosphate ions in oval and plate-shaped particles. Alhussary et al. (2020) isolated HAp from the shells of sea snails by washing with water and incineration at 900 °C for 1 h for purification. The authors identified hydroxyl and phosphate groups in the final product, which indicates the absorption of water. Hasan et al. (2020) washed and boiled sardine bones in water, and the remaining material was dried for 24 h and incinerated at temperatures ranging from 600 to 1000 °C for 5 h. They obtained sphere-shaped nonstoichiometric HAp with a Ca/P molar ratio of 1.64, and the highest yield (53%) was obtained at 600 °C. Paul et al. (2017) boiled carp scales in water for 20–25 min, immersed them in water for an additional 24 h, dried them at 60 °C for 3–4 h, and then incinerated them at 200, 400, 800, 1000 and 1200 °C for 1 h (heating rate: 5 °C/min). Irregularly shaped and agglomerated particles

Table 1
Applied methodologies for HAp recovery from aquatic wastes.

Matrix	Scientific name	Conditions	Results	Reference
Acidic deproteinization				
Scales (carp and tilapia)	*Catla catla Oreochromis niloticus*	Soak in distilled water/deproteinize with 1 N HCl for 30 min/pH neutralization using 6 N NaOH/ boil for 30 min/freeze at −80 °C/dry overnight at 160 °C/incinerate at 800 °C for 2 h	Crystalline-phase HAp was synthesized; phosphate, carbonate, and hydroxyl ions were present; good thermal stability	Al Buraiki et al. (2020)
Scales (rosy barb)	*Puntius conchonius*	Wash with water/deproteinize with 1 N HCl for 24 h at 27 °C/wash with distilled water/dry at 50 °C for 12 h/incinerate at 1000 °C for 4 h	Only scaffold characterization was reported; showed thermal stability; phosphate, carbonate, and hydroxyl groups were present; there was no difference between the HAp powder and scaffold	Deb et al. (2019)
Scales (fish)	*Probarbus jullieni*	Wash with water/deproteinize with 4% HCl for 15 min/neutralize using NaOH/boil at 100 °C for 30 min/dry at 60 °C	Powders had a flat-plate morphology, porous structure, large surface area and roughness; Ca/P ratio of approximately 2.01; presence of carbonate, phosphate and hydroxyl groups; particle size of 23.11 nm; lower crystallinity than synthetic HAp	Pon-On et al. (2016)
Acidic-alkaline deproteinization				
Scales (tilapia)	*Oreochromis niloticus*	Wash with water/deproteinize with 1 M HCl/ wash with distilled water/dry at 60 °C/heat to 100 °C with 5 M NaOH for 1 h/neutralize with distilled water/dry at 80 °C/incinerate at 1200 °C for 2 h	HAp presented a white-blue color after incineration; presence of phosphate and hydroxyl groups; particle size between 20 and 30 nm; high grade of crystallinity; molar Ca/P ratio of 1.83	Zainol et al. (2019)
Scales (fish)	*N.I.*	Remove impurities/dry at room temperature/ deproteinize with 0.1 M HCl/boil for 5–7 h/ treatment with 50% NaOH/filter and neutralize with water/dry at 60 °C/incinerate at 300–1000 °C for 1 h (heating rate: 5 °C/min)	Increase in particle size and crystallinity with higher temperature; presence of phosphate, hydroxyl, and carbonate groups	Alias et al. (2018)
Scales (bass and sea bream)	*Dicentrarchus labrax* L. *Sparus aurata* L.	Wash with water/deproteinize with 0.1 M HCl/ wash with distilled water/heat with 5% (w/v) NaOH for 5 h at 70 °C/wash with distilled water/ dry at 60 °C/add 50% (w/v) NaOH and stir for 1 h at 100 °C/incinerate at 800 °C for 1 h	HAp powder had a spherical morphology; particle size <1 μm; low crystalline phase; phosphate, carbonate, and hydroxyl groups were identified; Ca/P molar ratio of 1.70	Alparslan et al. (2017)
Alkaline deproteinization				
Scales (tilapia)	*Oreochromis niloticus Oreochromis hunteri*	Wash with water/deproteinize with NaOH (1%)/ incinerate	Extraction yield was between 13 and 14.26%; soft blue color and soft pink color for *O. hunteri* and *O. niloticus,* respectively; block-shaped particles with porous and rough surfaces; carbonate, phosphate, and hydroxyl groups were present; Ca/P molar ratios of 2.46 and 2.48, respectively	Ayala-Barajas et al. (2020)
Scales (rohu)	*Labeo rohita*	Wash with water/dry at room temperature/ hydrolyze with 1 N NaOH/wash with distilled water/dry at 40 °C for 12 h/incinerate at 1000 °C for 3 h	No degradation above 800 °C; good thermal stability; the presence of carbonate, phosphate and hydroxyl ions confirmed the formation of HAp	Deb et al. (2018)
Bones (croaker)	*Micropogonias furnieri*	Wash with water/deproteinize with 1 N NaOH for 24 h/wash with water/bleach with 30% H_2O_2 for 24 h/wash with water/incinerate at 800 °C for 5 h	HAp showed good crystallinity; phosphate and carbonate groups were present; Ca/P molar ratio of 1.40	Yamamura et al. (2018)
Bones (salmon)	*Oncorhynchus* sp.	Boil at 200 °C for 4 h/boil with acetone and 2 M NaOH for 1 h at 200 °C/wash with water/ deproteinize with 2 M NaOH for 1 h at 200 °C/ dry at 60 °C/centrifuge (1000 rpm for 5 min)/ neutralize with water/dry at 100 °C	HAp had a light yellow color after deproteinization; nanorod-shaped crystals between 6 and 37 nm; phosphate, carbonate, and hydroxyl groups were observed	Venkatesan et al. (2015)
Enzymatic hydrolysis				
Scales (fish)	*N. S.*	Wash with water/dry at 80 °C for 24 h/boil for 3 h/wash with water/dry at 80 °C for 24 h/ hydrolyze with Protamex (1%) at 40 °C for 3 h (pH 9)/incinerate at 500, 600, 700, 800, 900 and 1000 °C for 4 h	Irregularly shaped particles with different particle sizes; high crystallinity at higher calcination temperatures; hydroxyl, carbonate, and phosphate groups were present	Ismail et al. (2019)
Raw bones (catfish, tilapia, seabass, and yellowfin tuna)	*Pangasius hypophthalmus Oreochoromis* sp. *Lates calcarifer Thunnus albacares*	Wash with water for 5 min/hydrolyze with Alcalase at 60 °C for 9 h/fractionation/wash solid material/dry at 100 °C/incinerate at 600, 700, 800, 900 and 1000 °C for 2 h	Color differed depending on the raw material (from yellow to brown); particles between 50 and 70 nm with porous surfaces; carbonate, phosphate and hydroxyl groups were present; Ca/P molar ratio of 1.80; presence of trace elements (Na, K, Mg, Sr, Zn and Al)	Nam et al. (2019)
Ionic hydrolysis				

(*continued on next page*)

Table 1 (*continued*)

Matrix	Scientific name	Conditions	Results	Reference
Scales (carp)	*Cyprinidae* sp.	Wash with tap and distilled water/dry at room temperature/heat in oil bath with 1-butyl-3-methylimidazolium acetate for 12 h at 100 °C/ add 0.5 NaOH (bring to pH 9)/centrifuge at 11, 000 rpm for 30 min	Extraction yield was 32%; nanoparticles (1050–2900 nm) with different morphologies were obtained; carbonate and phosphate groups were present; a Ca/P molar ratio of 1.60	Muhammad et al. (2016)
Hydrothermal				
Scales (fish)	*Lethrinus lentjan*	Wash with water/dry at room temperature/blend with Milli-Q water (1:50, w/v)/autoclave at 280 °C for 3 h/filter/lyophilize	Rod-shaped nanostructures (8–12 nm in diameter and 50–100 nm long); highly pure HAp was obtained; phosphate, carbonate, and hydroxyl groups were detected; Ca/P molar ratio of 2.33	Athinarayanan et al. (2020)

N.S.: Neither the genus nor species was specified.

ranging from 12 to 92 nm were generated with a Ca/P molar ratio of 1.71, and carbonate, phosphate, and hydroxyl groups were found.

HAp purity is evaluated through analytical techniques such as X-ray diffraction (XRD), with scans from an angular range (2θ) of 10°–80°, and energy dispersive X-ray spectroscopy (EDS) (Pon-On et al., 2016). The structural and morphological characteristics of HAp particles are determined by transmission electron microscopy (TEM) and scanning electron microscopy (SEM). These characteristics vary depending on the HAp source and extraction method (Hasan et al., 2020). Additionally, Fourier transform infrared spectroscopy is utilized to acquire absorption spectra and observe infrared emission as well as determine the functional groups present in the range of 450–4000 cm^{-1} (Khoo et al., 2015; Muhammad et al., 2016). Khallok et al. (2019) observed infrared absorption bands in the following regions: 475, 575, 600, 960, 1040 and 1090 cm^{-1}, which are characteristic of the PO_4^{3-} group present in HAp, as well as vibrations bands at 3570 and 630 cm^{-1} corresponding to OH groups. The Ca/P molar ratio has been analyzed by inductively coupled plasma–optical emission spectrometry (ICP–OES) as well as many other spectrometric methods (Rincón-López et al., 2019). Furthermore, use of the Branaur-Emmett-Teller (BET) method to determine the specific surface area of a solid has been reported (Muhammad et al., 2016).

Based on the data reported in Table 1, the particle size, crystallinity, and morphology of HAp vary depending on the extraction method. Previous authors have reported spherical, block-shaped, and rod-shaped crystals with particle sizes ranging from <1 μm to 2900 nm; the largest size was obtained using ionic hydrolysis. Moreover, increases in crystallinity and porosity have been reported at higher temperatures, which indicates improved HAp bioactivity. Finally, the presence of phosphate, carbonate and hydroxyl groups has been confirmed for HAp with Ca/P molar ratios between 1.40 and 2.48. The presence of hydroxyl groups could be attributed to water absorption by the particles. The effects of these characteristics will be described in the next section.

4. Chemical and biological properties of HAp

HAp is thermodynamically stable at physiological pH (7.4), and its biodegradability depends on other parameters, such as crystallinity, porosity, chemical purity, and surface rugosity (Bohner and Miron, 2019; Li et al., 2019). Moreover, due to its porosity and moisturizing capacity in water and organic solvents, adhesion to drugs, such as antibiotics or other substances, to improve bone healing is possible (Pokhrel, 2018). Ferraris et al. (2020) suggested that the abundance OH groups affects surface hydrophilicity. The isoelectric point, charge and surface ion adsorption of HAp depend on the acidity/basicity of its hydroxyl groups. In a basic environment, the superficial charge becomes negative through H^+ release from the OH groups, while an acidic environment promotes a positive superficial charge through acceptance of H^+ from OH groups.

HAp has received attention because it has a porous structure similar to native human bone and teeth. Additionally, it presents other constructive characteristics, as it does not produce inflammation, is antimutagenic and nontoxic, and has other bioactivities, such as biocompatibility and osseointegration (Ramesh et al., 2018). Moreover, HAp is osteoconductive, bioinert, and stable and does not produce immunological reactions; in Table 2, its chemical and biological properties and their functions are reported (Raghavendra et al., 2017; Aarthy et al., 2019).

It has been reported that HAp can form ionic bonds with living tissue by generating a vascular or invasive cellular network for bone development (Bohner and Miron, 2019; Rincón-López et al., 2019). Likewise, it has been noted that HAp can directly join with host bone tissue because it is absorbed through the actions of osteoclasts (Bosco et al., 2015). HAp also has the capability to create an interfacial apatite layer around tissues and enhance bone regeneration velocity (Pon-On et al., 2016; Pokhrel, 2018). Additionally, it promotes rapid bone regeneration, replacing damaged or degenerated hard tissue in the human body (Li et al., 2019; Feng et al., 2020).

Some researchers have demonstrated that HAp supports osteogenic adhesion, differentiation and proliferation, improving bone tissue integration (Ebrahimi et al., 2017). On bone, HAp is deposited on collagen nanofibers using noncollagen proteins and proteoglycans as cement for mineralization, preventing resting crack formation and ensuring mechanical strength and hardness in the biological environment (Bai et al., 2020). Thus, a favorable environment is required to use the largest cellular number available in biological fluid to stimulate bioactivity (Feng et al., 2020). Currently, HAp can facilitate protein adsorption on implant surfaces through the association of osteoblasts. Additionally, researchers are seeking to facilitate the formation of a transition zone between the implant and tissue through specific cell fixation (Bohner and Miron, 2019).

Table 2
Chemical and biological properties of HAp.

Property	Function(s)
Chemical properties	
Crystallinity	Enhancement in osteointegration properties
Porosity	Cell adhesion and proliferation
Chemical purity	Ca/P molar ratio of 1.67 improves biocompatibility and bioactivity
Surface rugosity	Improves cell adhesion and proliferation
Porosity and moisturizing capacity	Adhesion with other compounds to improve bone healing
Biological properties	
Biomineralization	Promotes proper bonding with bone tissue
Noninflammatory	Enhancement in the functionality of HAp
Nontoxic	Improves the functionality and bioactivity of HAp
Antimutagenic	Suitable for biomedical applications by creating an ideal environment for bone regeneration
Osseointegration	Ability to form ionic bonds with living tissues and enhancement in bone regeneration velocity

(Raghavendra et al., 2017; Ramesh et al., 2018; Aarthy et al., 2019).

Furthermore, the addition of ions such as Sr, Cu, Ag, Zn or Co, which can have anabolic effects on bone metabolism, has been researched. Since the release of these ions in the physiological environment has a favorable effect on human cell behavior, improving HAp bioactivity, specifically in osteogenesis and angiogenesis, through the regulation of bone generation by osteoblast action and bone cell reabsorption by osteoclast function has been explored (Li et al., 2019). However, biomineralization in the bone regeneration process can be affected by sudden changes in pH, with optimal pH values ranging from 7 to 7.5 (Jeong et al., 2019).

5. Biomaterials based on natural HAp

Natural biomedical materials are necessary to reduce toxic effects. Therefore, the isolation of HAp from fish byproducts, such as scales, teeth, and bones, is being investigated (Alif et al., 2018). This type of waste is abundant and has very little added value, so its processing helps to address the related environmental problems (Yamamura et al., 2018). Eliaz and Metoki (2017) reported that HAp in powder, grain, dense or porous block shapes and a variety of composites is the basis of several biomaterials that are used to calcify damaged living tissue (Fig. 2). Thus, the development of biomaterials with a composition and structure similar to those of natural human bone is a promising application of HAp (Li et al., 2019).

Biomaterials based on pure HAp are naturally fragile, which makes them unfit for many applications (Khoshzaban et al., 2017). Therefore, biomaterials based on HAp incorporated with other biopolymers, such as collagen, chitosan, starch, and polylactic acid, have been explored (Ebrahimi et al., 2017). Additionally, other compounds, such as glycolic acid and phosphonic acid, have been integrated to improve the interfacial bonding between HAp and other biopolymers and accelerate biomaterial degradation to improve bioactivity, biodegradability, and osteogenesis abilities (Shuai et al., 2020, 2021). The overall objective is to obtain a biomaterial with optimal properties so that they can be used for biomedical applications (Deb et al., 2019). In general, bioceramic and bioglass materials are biocompatible substances that improve healing and have antibacterial and antifungal activities for use in medicine and

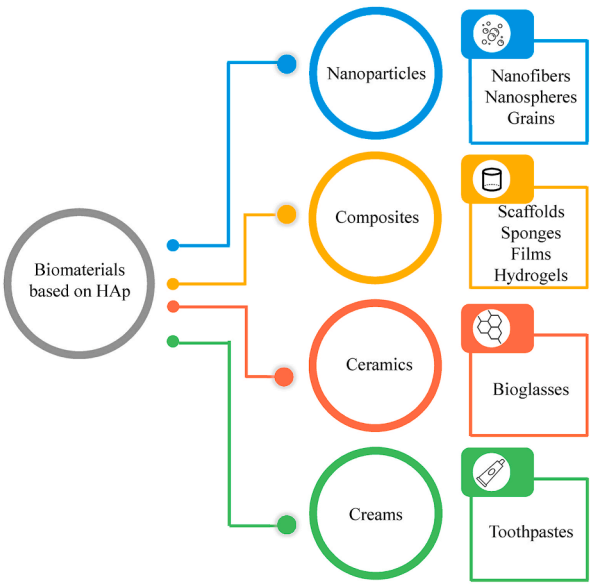

Fig. 2. Biomaterials based on HAp for biomedical applications.

dentistry. These materials may function as adsorbents in human tissues and improve natural tissue regeneration (Raghavendra et al., 2017).

Moreover, the incorporation of diatoms, nanoclays and calcium carbonates has possibly expanded the applicability of biomaterials in several fields (Mustafov et al., 2020; Bhat et al., 2021). These materials can be obtained from abundant natural sources through cost-effective and eco-friendly/green methods. Diatoms, which have been used to induce mineralization, have been reported to have good biocompatibility and other promising results for their application in diverse fields (Rabiee et al., 2021). On the other hand, nanoclays are used to improve the mechanical properties of materials, helping to establish a better interaction with the polymer matrix through porous networks. Moreover, carbonate-based compounds can promote protein absorption through the interaction between carboxylate groups and interface calcium ions (Cantaert et al., 2017; Kundu et al., 2021). Therefore, the use of biomaterials based on HAp is a promising alternative due to its similarity to human bone and the availability of natural sources from which it can be isolated. Additionally, the incorporation of HAp into other polymers could improve biological activity. Finally, natural HAp promotes the isolation of value-added compounds from biowastes.

Venkatesan et al. (2015) reported that the importance of biomaterials based on calcium phosphates and type I collagen is mainly due to their favorable attraction to the bone extracellular matrix. Shams et al. (2020) and Yazdani et al. (2020) reported nanofibers based on bioactive glasses supplemented with HAp, and the bioactivity of the material increased without eliciting cytotoxic effects. According to these studies, modifying biomaterial structures through the incorporation of HAp is an essential way to improve their bioactivity and availability and increase their application.

Seyedmajidi et al. (2018a) developed a foam based on HAp and bioglass and reported the formation of an apatite layer on the foam surface after exposure to simulated biological fluids, which indicates an increase in its bioactivity. In the same year, Seyedmajidi et al. (2018b) developed another foam based on HAp with improved physical and biological properties for use in 3D scaffold creation, suggesting its low toxicity and lack of an inflammatory response after application. These results were achieved by reducing the particle size and increasing the surface area between the biomaterial and body fluids, thus promoting osteoblast function. Table 3 shows different biomaterials that have been developed based on HAp from aquatic byproducts combined with other ingredients. Among these biomaterials are pellets, sponges, scaffolds, foams, films, and coatings, all of which produced good results during their application.

Based on Table 3, the mixture of HAp with other polymers could improve the mechanical and biological activities of biomaterials, as good adhesion and favorable interactions have been shown between the components. The most reported types of biomaterials based on HAp and other polymers are prepared scaffolds and pellets with better mechanical properties and porosity that improve cellular development, adhesion, and proliferation. In addition, these materials show antibacterial activity, lower cytotoxicity, good biocompatibility, and a higher degradation capacity, supporting their application in bone healing or growth (Sathiskumar et al., 2019).

Table 3
Materials based on HAp from aquatic sources mixed with other ingredients.

Composition	Hydroxyapatite source	Results	Reference
Scaffolds			
HAp/polyethylene glycol/ starch	Scales *(Labeo rohita)*	Good mechanical and porosity properties	Deb et al. (2018)
HAp/silica	Fish scales	Improvements in mechanical properties, flexibility and compressive strength	Razali et al. (2018)
HAp/zinc	Scales *(Labeo rohita)*	Prevents bacterial biofilm formation and inhibits *Staphylococcus aureus* and *Escherichia coli*	Sathiskumar et al. (2019)
Sponges			
HAp/gelatin/ carboxymethyl cellulose	Oyster shells	Good porosity and cellular adhesion and nontoxic	Gheysari et al. (2020)
HAp/chitosan/fucoidan	Salmon bones	Reduces water absorption and retention, high biocompatibility and mineralization, good porosity, and improves cellular development	Lowe et al. (2016)
HAp/starch	Fish scales	Good adhesion and cellular proliferation, promotes bone healing in rabbits and nontoxic	Mondal et al. (2016)
Foams			
HAp/starch	Scales	Improves mechanical and thermal conditions and shows good adhesion to components	Chiarathanakrit et al. (2018)
Films			
HAp/polylactic acid	Fish scales	Biodegradable with good biocompatibility and bioactivity	Prasad et al. (2017)
Pellets			
HAp/polymethyl methacrylate	Scales *(Puntius conchonius)*	Good porosity, high degradation capacity, water absorption ability, and bone formation capability	Deb et al. (2019)
HAp/demineralized bone matrix/gelatin	Fish bones	Improves strength and quality, high porosity, low cytotoxicity, and good biocompatibility	Senthil et al. (2018)
HAp/PVA/PEG	Scales *(Oreochromis mossambicus)*	Ability to remove ions	Liu et al. (2017)
HAp	Scales *(Probarbus jullieni)*	Better adherence and cellular proliferation for bone growth	Pon-On et al. (2016)

Miculescu et al. (2017) reported that tridimensional biomaterials developed with HAp and starch can be used as adhesive materials, cements, waxes, and bone implants while ensuring their mechanical stability and nontoxicity to the human body. Doustgani (2015) reported that nanocomposites based on HAp and other polymers are potential substrates for osteoblast proliferation and mineralization, thus improving bone regeneration.

Shuai et al. (2021) reported the addition of glycolic acid into polylactic acid- and HAp-based scaffolds to accelerate their degradation and improve their contact area with body fluids for use as a replacement for damaged bone. Their results revealed that the scaffolds had a porous structure with an improved hydrophilic area, which promotes apatite layer deposition through ion exchange with body fluid, provides a suitable environment for cell growth and proliferation (osteoblast action to promote bone regeneration) and shows potential uses in medicine.

A year later, Shuai et al. (2022a) reported the incorporation of graphene oxide nanosheets into polylactic acid and HAp scaffolds to improve their mechanical properties, bioactivity and osteoconductivity. Their results showed that the hydrophilicity increased with graphene oxide and HAp incorporation, bringing an ideal environment for cell growth, adhesion and proliferation and showing the favorable cytocompatibility of the scaffolds. Therefore, after immersion of the scaffolds in simulated body fluid, the Ca/P molar ratio increased from 1.47 to 1.65, indicating a good ability to induce the formation of an apatite layer and an ideal chemical bond between the scaffold and living bone tissue.

Syusyukina et al. (2017) explored nanofibers based on HAp and polylactic acid and found that HAp incorporation improved surface wetting and that HAp acted as a cellular support. However, the porosity of these fibers was limited, which could affect water diffusion and product degradation. Accordingly, it has been reported that biomaterials based on HAp and polylactic acid have poor interfacial bonding, but the incorporation of other materials, such as poly(D-lactide), could improve both the interfacial bonding and mechanical properties due to the hydroxyl groups of HAp, finally reducing their deterioration (Shuai et al., 2022b). These limitations should be considered for future studies, as they are important factors involved in controlling the biomaterial structure and properties so that the designed compounds can perform their proposed functions. In addition, it is essential to consider the chemical composition of the polymers that will be incorporated to optimize their interactions with HAp and create quality materials.

6. HAp applicability in medicine

HAp can adsorb bioactive molecules, making it an important component for pharmaceutical products, food supplements and biocompatible material preparations used in odontology, cosmetology and the bone implant field, and importantly, it is biocompatible and nontoxic to the human body (Fig. 3).

6.1. Bone implants

Healing bone defects remains a great challenge in the medical field. This is due to the limited availability of materials that can be used to promote bone growth and development and encourage complete fusion with mammalian hard tissue. To address this issue, a tissue engineering strategy has been used to create a tridimensional structure fabricated with suitable materials to work not only as a passive support for bone cells but also as a stimulant for bone formation through the interaction between the biological tissue and biomaterial (Miculescu et al., 2017). Some important features investigate when evaluating the applicability of biomaterials are their capability to induce cellular proliferation, adhesion and dispersion; their antibacterial activity, osteoconductivity, biocompatibility,

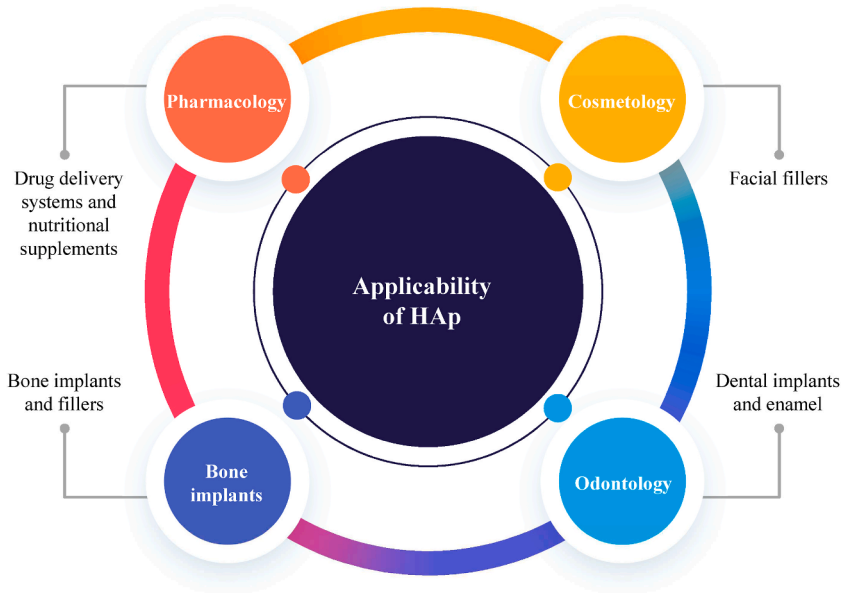

Fig. 3. Biomedical applications of HAp.

and cytocompatibility; their potential during mineralization; and their ability to create a physiological environment. These features depend on the structure, porosity, compressive strength, ion attachment and distribution in the biomaterial, and other mechanical properties that can be modified during biomaterial development (Bhat et al., 2021).

Bone is a complex dynamic tissue composed of two nanoscale majority phases, known as the organic phase, which is composed mainly of proteins (type I collagen), and the inorganic phase, which is composed mainly of minerals (HAp) (Ramesh et al., 2018). Bone tissue is highly vascularized and populated by different kinds of cells that promote its development (osteoblasts, osteoclasts, and osteocytes), giving it the potential for autoregeneration (Bochicchio et al., 2020).

Kovtun et al. (2015) made foams based on HAp, gelatin and soy extract, which were injected directly into rabbits. New bone formed after 12 weeks with noninflammatory effects. In addition, Rodriguez et al. (2016) prepared films composed of HAp, poly (D,L-lactide-*co*-glycolide) and carbon foam, because films allow osteoblast adhesion to material, and demonstrated their application in orthopedics. To confirm the abilities of the foam to support osteoblast adhesion and spreading, this study was performed in rat calvarial osteoblasts for 24 h, and its cytocompatibility and potential use as a bone fixation material were proven. Stipniece et al. (2016) reported that the addition of a polymeric phase to HAp biomaterials exerts additional functions because these biomaterials act as molecular vehicles, growth factors and antibiotics until tissue engineering improves. The authors carried out an *in vitro* analysis to evaluate the bioactivities of the HAp biomaterials in simulated body fluid and MG-63 cells for 3 days. These biomaterials presented good biocompatibility, bioactivity, and low toxicity, which was attributed to the interaction between the biomaterial and living bone tissues. Moreover, material degradation was reduced due to strong chemical interactions between the components.

Shuai et al. (2020) dispersed HAp into a polylactic acid matrix using effective interfacial electrovalent bonding between a phosphonic acid coupling reagent (2-carboxyethylphosphonic acid) and HAp, improving the mechanical and bioactive properties. Adding phosphonic acid to 3D porous scaffolds makes them more hydrophobic, improving the compatibility and dispersion of HAp by decreasing the number of hydrophilic groups (-OH groups) on the scaffolds. These characteristics could enhance cell growth without toxic effects and promote the formation of an apatite layer after immersion of the scaffolds in simulated body fluid after 28 days, thus increasing the Ca/P ratio from 1.58 to 1.66, which indicated an increase in bioactivity.

In the documented investigation, an improvement in the interaction between the biomaterials based on HAp and other polymers was reported, demonstrating their effect on the recovery of bones both *in vitro* and *in vivo* with nontoxic and anti-inflammatory effects through the improvement in cell adhesion, cell proliferation and biological properties.

6.2. Dental biomaterials

Dental caries, enamel erosion and dental sensitivity have been reported as critical problems in dental care worldwide (Poggio et al., 2017; Vano et al., 2018; Bossù et al., 2019). To solve this issue, HAp has been used in odontology as a supplement in pastes, resins, and dental enamels. To date, HAp addition has been demonstrated to improve dental enamel resistance to acidification (Andrade Neto et al., 2016). Bossù et al. (2019) reported that the use of dental pastes supplemented with HAp is a promising alternative to prevent dental caries, promote biomineralization and reduce fluorosis risks by repairing the enamel surface through the deposition of a new apatite layer. Additionally, Vano et al. (2018) found that HAp addition to fluoride-free pastes reduces tooth sensitivity after 2 weeks of application. This result could be attributed to the fact that HAp has been shown to be a suitable material to reduce pain due to its ability to penetrate exposed the dentin tubules responsible for dental sensitivity. Poggio et al. (2017) applied dental paste containing Zn and HAp to patients with enamel erosion and reported beneficial effects on oral health in terms of dental enamel biomineralization and erosion prevention because this can counteract the effects of acidic solutions on dental enamel, promoting a remineralization process on the enamel surface.

HAp has also been used in dental resins. Chadda et al. (2016) incorporated silica and HAp into commercial resins to improve their biocompatibility, showing promising results for possible applications as restorative materials for dental defects. Good biological responses were observed through modification of the mechanical and biological properties, which may allow cell proliferation, without toxic effects. Similarly, Calabrese et al. (2016) reported that HAp addition to silica fillers stimulated the interaction between the dental matrix and filler interface, improving biocompatibility. Poorzandpoush et al. (2017) blended a restorative material with HAp and found when this mineral was present in a ratio of higher than 5%, good coverage was not obtained and filler degradation could be induced during dental brushing.

Based on these reports, the addition of HAp to biomaterials used for dental care could enhance the interaction between HAp and other compounds and promote biomineralization in damaged tissues. The addition of HAp to dental pastes, resins and other materials used in odontology indicates the biocompatibility and cytocompatibility of HAp, suggesting that it is an ideal ingredient for applications in this field.

6.3. Drug delivery systems and nutritional supplements

Currently, drug delivery is prolonged when drugs are administered orally, creating a lag before the material comes into contact with gastrointestinal fluids and the blood to perform its biological functions. Zhang et al. (2018) created foams based on HAp and chitosan using the drug candesartan cilexetil. They generated a porous dimensional structure with high potential for drug delivery due to its increased solubility and availability of less soluble compounds; furthermore, the material did not present cytotoxicity and showed biocompatibility with Caco-2 cells.

Stipniece et al. (2016) covered titanium oxide scaffolds with HAp, improving their porosity, mechanical properties, and bioactivity. The researchers reported that these scaffolds can be used as carriers for drugs such as antibiotics because they improve drug functionality without producing inflammatory effects. In recent research performed by Padmanabhan et al. (2020), HAp and acacia gum nanospheres were created to combine their biocompatibilities and antibacterial activities. The results showed that these bioma-

terials have the potential to be used as carriers for long-term drug release and exert an antibacterial effect for biomedical applications. These results could be attributed to the improvement in the surface and contact areas of these biomaterials and their ability to improve their interactions through hydrogen bonding due to the presence of hydroxyl groups on the hydrophobic materials (Uthappa et al., 2018).

Calcium is an essential element for living organisms. Currently, calcium supplements are consumed to prevent joint problems and improve bone health. Since HAp is a mineral containing calcium ions, it is an ingredient of interest for the development of nutritional supplements. Tokhiriyon and Poznyakovsky (2019) evaluated the effect of a mineral-vitamin complex consisting of HAp, vitamin C, vitamin D3, magnesium, boron, zinc, and manganese on children with long tubular bone defects. Children between 3 and 7 years of age ingested two tablets every day with each meal, while children between the ages of 8 and 14 years ingested three tablets every day. The children were assessed at 14 and 30 days after treatment had started. The researchers observed a positive effect on the bone healing process, recommending 1 tablet every day for the treatment and prevention of joint problems. Additionally, Castelo-Branco et al. (2019) evaluated the effects of a HAp complex on osteoporosis in women between 40 and 50 years of age. Ossein-HAp 830 mg tablets (containing 712 mg of elemental calcium per day) were administered, and the subjects were monitored every 6 months for 36 months. The results showed that the tablets can be applied to safely treat and prevent bone loss.

Sun et al. (2018) designed nanorods based on doxorubicin and HAp with the addition of folic acid and evaluated their effects on antitumor treatment and their ability to improve drug availability to tumors. The efficiency of the biomaterials was measured by evaluating component release in simulated body fluids at pH values mimicking the blood circulation (pH 7.4), tumor cells (pH 6) and endosomes (pH 5.5). The results showed that there was an improvement in drug availability to the tumors. Moreover, they inoculated HepG2 cells into the flank regions of mice to evaluate cancerous tumor degradation, and antitumor efficacy was observed through the capability of the biomaterials to inhibit the tumors by releasing doxorubicin. The nanorods with the strongest effect on tumor growth suppression were those that contained folic acid, indicating their applicability as nanotherapeutic agents against tumors *in vivo*. However, under acidic conditions, the release of doxorubicin was weak due to the weakened interaction with HAp under these conditions.

6.4. Cosmetology

Many studies have demonstrated that HAp can be used in cosmetology to improve cell growth and viability and promote collagen generation (Sani et al., 2019). However, the development of biomaterials based on biopolymers to improve skin defects represents a great challenge because these materials must provide quick, scar-free regeneration of skin layers through interactions with the host tissues. Additionally, these biomaterials must have direct interactions with human cells to improve their adhesion, proliferation, and differentiation while minimizing bacterial growth during their application (Bhat et al., 2021). Da Cunha et al. (2019) reported that HAp is an alternative antiaging esthetic treatment because when it was used as a facial filler, it was able to fade wrinkles and expression lines.

On his own, Jeong et al. (2016) made hydrogels based on hyaluronic acid and HAp and demonstrated an increase in collagen production in the skin after 12 weeks of application, which was caused by cell proliferation. Moreover, Ghorbani et al. (2020) developed hydrogels based on hyaluronic acid, HAp and pullulan, which improved both biological development and *in vitro* cellular adhesion for clinical applications.

6.5. Other applications

Although HAp has mainly been used in biomedical fields, interest in its use in other areas has been pursued. Ismail et al. (2019) obtained HAp from fish waste, and it was applied to remove gallic acid during biodiesel production, eliminating almost 80% of the phenolic compounds. Moreover, Pooladi and Bazargan-Lari (2020) made composites based on chitosan/HAp/nanomagnetite (2:1:1) to remove copper and zinc ions. Both studies showed promising results for the use of HAp as a natural adsorbent with highly efficient ion adsorption for water treatment.

As mentioned before, HAp has been used in many industrial areas. Although the exact interactive mechanism between HAp and biomaterials is not completely understood, exhaustive research in the scientific community on biomaterials and their applications has encouraged many to understand these processes. To date, many HAp products have been commercialized; Fig. 4 shows these products with worldwide distribution that were compiled based on an exhaustive internet search.

7. Future trends in the clinical translation of HAp

Each year, diseases related to bone loss and injury, demineralization, and dental problems affect millions of people worldwide (Rodriguez et al., 2016). Moreover, the production of materials based on biopolymers represents a great challenge for their application in humans because *in vitro* and *in vivo* assays must first be performed to prove their biocompatibility and low toxicity. In recent years, research on the use of HAp to enhance the bioactivity of other materials has been performed. Furthermore, studies in animals and clinical trials in humans using biomaterials based on HAp and other polymers have been reported in the following areas: bone implants (Kovtun et al., 2015), dental care (Poggio et al., 2017; Vano et al., 2018), supplements (Castelo-Branco et al., 2019; Tokhiriyon and Poznyakovsky, 2019), and cosmetology (Jeong et al. 2016; Da Cunha et al., 2019). The HAp used in these research works was obtained through chemical synthesis or commercial products.

On the other hand, HAp from aquatic sources has been used to produce biomaterials, and *in vitro* assays have been reported to show cellular adhesion, a capacity for bone formation and nontoxic effects, representing a future approach for HAp applicability (Deb et al., 2019; Gheysari et al., 2020). However, the clinical use of natural HAp from aquatic sources is limited. In the future, the use of

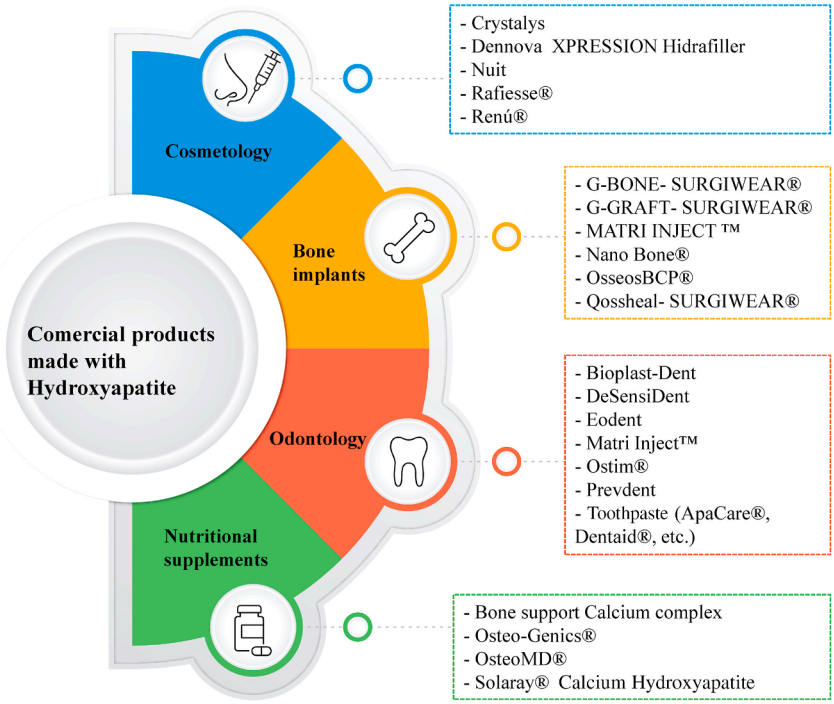

Fig. 4. Commercial products based on HAp.

natural ingredients to produce materials will increase to reduce both costs and pollution. Moreover, the HAp recovered from aquatic sources could contain trace elements that have beneficial effects on the human body. Finally, future works with natural HAp must focus on *in vivo* trials to prove its bioactivities and the advantages of these materials.

8. Conclusions

Considering that the main source of HAp is chemical synthesis, the need to extract this material from natural sources is amplified. Moreover, recent research has promoted and demanded the use of safe materials for various applications. Thus, this review provides examples of HAp recovery from aquatic sources and describes the related methodologies. Many methods have been reported for the recovery of HAp, including chemical synthesis and hydrothermal and hydrolysis processes, with a final incineration step for purification. The acquisition of this compound from natural sources has gained attention, and hydrolysis is the most common method by which it is obtained.

Additionally, HAp has been blended with other chemical compounds to develop materials for medical uses, such as scaffolds, pellets, films, sponges, and foams, to improve their mechanical, biological, and structural properties. Furthermore, research on the applicability of these biomaterials has confirmed their capability to regenerate damaged tissues, prevent defects and promote cellular proliferation. In addition, the uses of HAp have been extended to cosmetology, odontology, and pharmacology, as well as the creation of adsorbents for the removal of environmental pollutants.

The distribution of commercial products based on HAp in the global market is evidence of its applications. Therefore, this review focused on the exploitation of industrial residues for the recovery of this valuable compound and thus supports the reduction in environmental pollution and the acquisition of large quantities of this mineral.

Declaration of competing interest

The authors declare that they have no known competing financial interests or personal relationships that could have appeared to influence the work reported in this paper.

Acknowledgments

K. L. Hernández-Ruiz thanks CONACYT for the doctoral scholarship (no.: 703185). This study was funded by the Technological Institute of Sonora under PROFAPI project CA-2022-0018.

References

Aarthy, S., Thenmuhil, D., Dharunya, G., Manohar, P., 2019. Exploring the effect of sintering temperature on naturally derived hydroxyapatite for bio-medical applications. J. Mater. Sci. Mater. Med. 30 (2), 21. https://doi.org/10.1007/s10856-019-6219-9.

Al Buraiki, N.S.S., Albadri, B.A., Alsheriqi, S., Alshabibi, B., Al-Mammari, S., Premkumar, S., Sah, M.K., Sudhakar, M.S., 2020. Characterization of Catla catla and

Oreochromis niloticus fish scales derived hydroxyapatite scaffolds for regenerative medicine. Mater. Today Proc. 27, 2609–2616. https://doi.org/10.1016/j.matpr.2019.11.074.
Alhussary, B.N., A Taqa, G., Taqa, A.A.A., 2020. Preparation and characterization of natural nano hydroxyapatite from eggshell and seashell and its effect on bone healing. J. Appl. Vet. Sci. 5 (2), 25–32. https://doi.org/10.21608/javs.2020.85567.
Alias, M., Hamzah, S., Saidin, J., 2018. The effect of sintering temperature on characteristic and properties of hydroxyapatite extracted from fish scale bio-waste. Int. J. Eng. Technol. 7 (4), 3726–3730. https://doi.org/10.14419/ijet.v7i4.11939.
Alif, M.F., Aprillia, W., Arief, S., 2018. A hydrothermal synthesis of natural hydroxyapatite obtained from Corbicula moltkiana freshwater clams shell biowaste. Mater. Lett. 230, 40–43. https://doi.org/10.1016/j.matlet.2018.07.034.
Alparslan, Y., Baygar, T., Baygar, T., 2017. Extraction, characterization and antimicrobial activity of hydroxyapatite from seabass and seabream scale. J. Food Health Sci. 3 (3), 90–96. https://doi.org/10.3153/jfhs17012.
Andrade Neto, D., Carvalho, E.V., Rodrigues, E.A., Feitosa, V.P., Sauro, S., Mele, G., Carbone, L., Mazzetto, S.E., Rodrigues, L.K., Fechine, P.B.A., 2016. Novel hydroxyapatite nanorods improve anti-caries efficacy of enamel infiltrants. Dent. Mater. 32 (6), 784–793. https://doi.org/10.1016/j.dental.2016.03.026.
Atef, M., Ojagh, S.M., 2017. Health benefits and food applications of bioactive compounds from fish byproducts: a review. J. Funct.Foods 35, 673–681. https://doi.org/10.1016/j.jff.2017.06.034.
Athinarayanan, J., Periasamy, V.S., Alshatwi, A.A., 2020. Simultaneous fabrication of carbon nanodots and hydroxyapatite nanoparticles from fish scale for biomedical applications. Mater. Sci. Eng. C 117, 111313. https://doi.org/10.1016/j.msec.2020.111313.
Ayala-Barajas, D., González-Vélez, V., Vélez-Tirado, M., Aguilar-Pliego, J., 2020. Hydroxyapatite extraction from fish scales of Tilapia. In: 2020 42nd Annual International Conference of the IEEE Engineering in Medicine & Biology Society (EMBC). IEEE, pp. 2206–2208. https://doi.org/10.1109/EMBC44109.2020.9176479.
Bai, S., Zhang, X., Lv, X., Zhang, M., Huang, X., Shi, Y., Lu, C., Song, J., Yang, H., 2020. Bioinspired mineral–organic bone adhesives for stable fracture fixation and accelerated bone regeneration. Adv. Funct. Mater. 30 (5), 1908381. https://doi.org/10.1002/adfm.201908381.
Bhat, S., Uthappa, U.T., Altalhi, T., Jung, H.Y., Kurkuri, M.D., 2021. Functionalized porous hydroxyapatite scaffolds for tissue engineering applications: a focused review. ACS Biomater. Sci. Eng. https://doi.org/10.1021/acsbiomaterials.1c00438.
Bochicchio, B., Barbaro, K., De Bonis, A., Rau, J.V., Pepe, A., 2020. Electrospun poly (d, l-lactide)/gelatin/glass-ceramics tricomponent nanofibrous scaffold for bone tissue engineering. J. Biomed. Mater. Res. 108 (5), 1064–1076. https://doi.org/10.1002/jbm.a.36882.
Bohner, M., Miron, R.J., 2019. A proposed mechanism for material-induced heterotopic ossification. Mater. Today 22, 132–141. https://doi.org/10.1016/j.mattod.2018.10.036.
Bosco, R., Iafisco, M., Tampieri, A., Jansen, J.A., Leeuwenburgh, S.C., Van Den Beucken, J.J., 2015. Hydroxyapatite nanocrystals functionalized with alendronate as bioactive components for bone implant coatings to decrease osteoclastic activity. Appl. Surf. Sci. 328, 516–524. https://doi.org/10.1016/j.apsusc.2014.12.072.
Bossù, M., Saccucci, M., Salucci, A., Di Giorgio, G., Bruni, E., Uccelletti, D., Sarto, M.S., Familiari, G., Relucenti, M., Polimeni, A., 2019. Enamel remineralization and repair results of Biomimetic Hydroxyapatite toothpaste on deciduous teeth: an effective option to fluoride toothpaste. J. Nanobiotechnol. 17 (1), 1–13. https://doi.org/10.1186/s12951-019-0454-6.
Calabrese, L., Fabiano, F., Currò, M., Borsellino, C., Bonaccorsi, L.M., Fabiano, V., Ientile, R., Proverbio, E., 2016. Hydroxyapatite whiskers based resin composite versus commercial dental composites: mechanical and biocompatibility characterization. Adv. Mater. Sci. Eng. https://doi.org/10.1155/2016/2172365.
Callan, D.P., Rohrer, M.D., 1993. Use of bovine-derived hydroxyapatite in the treatment of edentulous ridge defects: a human clinical and histologic case report. J. Periodontol. 64 (6), 575–582. https://doi.org/10.1902/jop.1993.64.6.575.
Cantaert, B., Kuo, D., Matsumura, S., Nishimura, T., Sakamoto, T., Kato, T., 2017. Use of amorphous calcium carbonate for the design of new materials. ChemPlusChem 82 (1), 107–120. https://doi.org/10.1002/cplu.201600457.
Castelo-Branco, C., Cancelo Hidalgo, M.J., Palacios, S., Ciria-Recasens, M., Fernández-Pareja, A., Carbonell-Abella, C., Manasanch, J., Haya-Palazuelos, J., 2019. Efficacy and safety of ossein-hydroxyapatite complex versus calcium carbonate to prevent bone loss. Climacteric 23 (3), 252–258. https://doi.org/10.1080/13697137.2019.1685488.
Chadda, H., Naveen, S.V., Mohan, S., Satapathy, B.K., Ray, A.R., Kamarul, T., 2016. Cytotoxic evaluation of hydroxyapatite-filled and silica/hydroxyapatite-filled acrylate-based restorative composite resins: an in vitro study. J. Prosthet. Dent 116 (1), 129–135. https://doi.org/10.1016/j.prosdent.2015.12.013.
Chiarathanakrit, C., Riyajan, S.A., Kaewtatip, K., 2018. Transforming fish scale waste into an efficient filler for starch foam. Carbohydr. Polym. 188, 48–53. https://doi.org/10.1016/j.carbpol.2018.01.101.
Da Cunha, M.G., da Cunha, A.L.G., Gonzaga, M., da Veiga, G.L., Alves, B.D.C.A., Fonseca, F.L.A., Machado Filho, C.A., 2019. Treatment of facial aging with calcium hydroxyapatite-filling and lifting concept. Eur. J. Biol. Res. 9 (4), 267–275. https://doi.org/10.5281/zenodo.3569835.
Deb, P., Deoghare, A.B., Barua, E., 2018. Poly ethylene glycol/fish scale-derived hydroxyapatite composite porous scaffold for bone tissue engineering. 1. In: IOP Conference Series: Materials Science and Engineering, vol. 377. 012009. IOP Publishing. https://doi.org/10.1088/1757-899X/377/1/012009.
Deb, P., Barua, E., Deoghare, A.B., Lala, S.D., 2019. Development of bone scaffold using Puntius conchonius fish scale derived hydroxyapatite: physico-mechanical and bioactivity evaluations. Ceram. Int. 45 (8), 10004–10012. https://doi.org/10.1016/j.ceramint.2019.02.044.
Doğdu, S.A., Turana, C., Depci, T., Ayas, D., 2021. Natural hydroxyapatite obtained from pufferfish teeth for potential dental application. J. Ceram. Process. Res. 22 (3), 356–361. https://doi.org/10.36410/jcpr.2021.22.3.356.
Doustgani, A., 2015. Effect of electrospinning process parameters of polycaprolactone and nanohydroxyapatite nanocomposite nanofibers. Textil. Res. J. 85 (14), 1445–1454. https://doi.org/10.1177/0040517514566109.
Dry, M.E., Beebe, R.A., 1960. Adsorption studies on bone mineral and synthetic hydroxyapatite1, 2. J. Phys. Chem. 64 (9), 1300–1304. https://doi.org/10.1021/j100838a042.
Ebrahimi, M., Botelho, M.G., Dorozhkin, S.V., 2017. Biphasic calcium phosphates bioceramics (HA/TCP): concept, physicochemical properties and the impact of standardization of study protocols in biomaterials research. Mater. Sci. Eng. C 71, 1293–1312. https://doi.org/10.1016/j.msec.2016.11.039.
Eliaz, N., Metoki, N., 2017. Calcium phosphate bioceramics: a review of their history, structure, properties, coating technologies and biomedical applications. Materials 10 (4), 334. https://doi.org/10.3390/ma10040334.
Feng, P., Peng, S., Shuai, C., Gao, C., Yang, W., Bin, S., Min, A., 2020. In situ generation of hydroxyapatite on biopolymer particles for fabrication of bone scaffolds owning bioactivity. ACS Appl. Mater. Interfaces 12 (41), 46743–46755. https://doi.org/10.1021/acsami.0c13768.
Ferraris, S., Yamaguchi, S., Barbani, N., Cazzola, M., Cristallini, C., Miola, M., Vernè, E., Spriano, S., 2020. Bioactive materials: in vitro investigation of different mechanisms of hydroxyapatite precipitation. Acta Biomater. 102, 468–480. https://doi.org/10.1016/j.actbio.2019.11.024.
Gheysari, H., Mohandes, F., Mazaheri, M., Dolatyar, B., Askari, M., Simchi, A., 2020. Extraction of hydroxyapatite nanostructures from marine wastes for the fabrication of biopolymer-based porous scaffolds. Mar. Drugs 18 (1), 26. https://doi.org/10.3390/md18010026.
Ghorbani, F., Zamanian, A., Behnamghader, A., Joupari, M.D., 2020. Bioactive and biostable hyaluronic acid-pullulan dermal hydrogels incorporated with biomimetic hydroxyapatite spheres. Mater. Sci. Eng. C 112, 110906. https://doi.org/10.1016/j.msec.2020.110906.
Granito, R.N., Renno, A.C.M., Yamamura, H., de Almeida, M.C., Ruiz, P.L.M., Ribeiro, D.A., 2018. Hydroxyapatite from fish for bone tissue engineering: a promising approach. Int. J. Mol. Cell. Med. 7 (2), 80. https://doi.org/10.22088/IJMCM.BUMS.7.2.80.
Hasan, M.R., Yasin, N.S.M., Mohd, M.S., 2020. Proximate and morphological characteristics of nano hydroxyapatite (nano HAP) extracted from fish bone. J. Sustain. Sci. Manag. 15 (8), 9–21. https://doi.org/10.46754/jssm.2020.12.002.
Ismail, N.F., Hamzah, S., Razali, N.A., Yussof, W.M.H.W., Ali, N., Mohammad, A.W., 2019. Preparation and characterisation of hydroxyapatite extracted from fish scale waste for the removal of gallic acid as inhibitor in biofuel production. Malays. J. Anal. Sci. 23 (6), 938–949. https://doi.org/10.17576/mjas-2019-2306-03.
Jeong, S.H., Fan, Y.F., Baek, J.U., Song, J., Choi, T.H., Kim, S.W., Kim, H.E., 2016. Long-lasting and bioactive hyaluronic acid-hydroxyapatite composite hydrogels for injectable dermal fillers: physical properties and in vivo durability. J. Biomater. Appl. 31 (3), 464–474. https://doi.org/10.1177/0885328216648809.
Jeong, J., Kim, J.H., Shim, J.H., Hwang, N.S., Heo, C.Y., 2019. Bioactive calcium phosphate materials and applications in bone regeneration. Biomater. Res. 23 (1), 1–11. https://doi.org/10.1186/s40824-018-0149-3.
Khalid, H., Chaudhry, A.A., 2019. 4.1 Biological apatite and synthetic hydroxyapatite: differences and similarities. Handbook of Ionic Substituted Hydroxyapatites 85.

Khallok, H., Ojala, S., Ezzahmouly, M., Elouahli, A., Gourri, E.H., Jamil, M., Hatim, Z., 2019. Porous foams based hydroxyapatite prepared by direct foaming method using egg white as a pore promoter. J. Australas. Ceram. Soc. 55 (2), 611–619. https://doi.org/10.1007/s41779-018-0269-1.
Khandelwal, H., Prakash, S., 2016. Synthesis and characterization of hydroxyapatite powder by eggshell. J. Miner. Mater. Char. Eng. 4 (2), 119–126. https://doi.org/10.4236/jmmce.2016.42011.
Khoo, W., Nor, F.M., Ardhyananta, H., Kurniawan, D., 2015. Preparation of natural hydroxyapatite from bovine femur bones using calcination at various temperatures. Procedia Manuf. 2, 196–201. https://doi.org/10.1016/j.promfg.2015.07.034.
Khoshzaban, A., Rakhshan, V., Najafi, F., Aghajanpour, L., Hashemian, S.J., Keshel, S.H., Watanabe, I., Valanejad, A., Kashi, T.S.J., 2017. Effect of sintering temperature rise from 870 to 920° C on physicomechanical and biological quality of nano-hydroxyapatite: an explorative multi-phase experimental in vitro/vivo study. Mater. Sci. Eng. C 77, 142–150. https://doi.org/10.1016/j.msec.2017.03.183.
Kovtun, A., Goeckelmann, M.J., Niclas, A.A., Montufar, E.B., Ginebra, M.P., Planell, J.A., Santin, M., Ignatius, A., 2015. In vivo performance of novel soybean/gelatin-based bioactive and injectable hydroxyapatite foams. Acta Biomater. 12, 242–249. https://doi.org/10.1016/j.actbio.2014.10.034.
Kundu, K., Afshar, A., Katti, D.R., Edirisinghe, M., Katti, K.S., 2021. Composite nanoclay-hydroxyapatite-polymer fiber scaffolds for bone tissue engineering manufactured using pressurized gyration. Compos. Sci. Technol. 202, 108598. https://doi.org/10.1016/j.compscitech.2020.108598.
Lee, C.K., Choi, J.S., Jeon, Y.J., Byun, H.G., Kim, S.K., 1997. The properties of natural hydroxyapatite isolated from tuna bone. Korean J. Fish. Aquat. Sci. 30 (4), 652–659.
Li, T.T., Ling, L., Lin, M.C., Jiang, Q., Lin, Q., Lou, C.W., Lin, J.H., 2019. Effects of ultrasonic treatment and current density on the properties of hydroxyapatite coating via electrodeposition and its in vitro biomineralization behavior. Mater. Sci. Eng. C 105, 110062. https://doi.org/10.1016/j.msec.2019.110062.
Li, Y., Wang, Y., Li, Y., Luo, W., Jiang, J., Zhao, J., Liu, C., 2019. Controllable synthesis of biomimetic hydroxyapatite nanorods with high osteogenic bioactivity. ACS Biomater. Sci. Eng. 6 (1), 320–328. https://doi.org/10.1021/acsbiomaterials.9b00914.
Liu, W.K., Liaw, B.S., Chang, H.K., Wang, Y.F., Chen, P.Y., 2017. From waste to health: synthesis of hydroxyapatite scaffolds from fish scales for lead ion removal. JOM (J. Occup. Med.) 69 (4), 713–718. https://doi.org/10.1007/s11837-017-2270-5.
Lowe, B., Venkatesan, J., Anil, S., Shim, M.S., Kim, S.K., 2016. Preparation and characterization of chitosan-natural nano hydroxyapatite-fucoidan nanocomposites for bone tissue engineering. Int. J. Biol. Macromol. 93, 1479–1487. https://doi.org/10.1016/j.ijbiomac.2016.02.054.
Miculescu, F., Maidaniuc, A., Voicu, S.I., Thakur, V.K., Stan, G.E., Ciocan, L.T., 2017. Progress in hydroxyapatite–starch based sustainable biomaterials for biomedical bone substitution applications. ACS Sustain. Chem. Eng. 5 (10), 8491–8512. https://doi.org/10.1021/acssuschemeng.7b02314.
Mondal, S., Pal, U., Dey, A., 2016. Natural origin hydroxyapatite scaffold as potential bone tissue engineering substitute. Ceram. Int. 42 (16), 18338–18346. https://doi.org/10.1016/j.ceramint.2016.08.165.
Muhammad, N., Gao, Y., Iqbal, F., Ahmad, P., Ge, R., Nishan, U., Rahim, A., Gonfa, G., Ullah, Z., 2016. Extraction of biocompatible hydroxyapatite from fish scales using novel approach of ionic liquid pretreatment. Separ. Purif. Technol. 161, 129–135. https://doi.org/10.1016/j.seppur.2016.01.047.
Mustafov, S.D., Sen, F., Seydibeyoglu, M.O., 2020. Preparation and characterization of diatomite and hydroxyapatite reinforced porous polyurethane foam biocomposites. Sci. Rep. 10 (1), 1–9. https://doi.org/10.1038/s41598-020-70421-3.
Nam, P.V., Van Hoa, N., Trung, T.S., 2019. Properties of hydroxyapatites prepared from different fish bones: a comparative study. Ceram. Int. 45 (16), 20141–20147. https://doi.org/10.1016/j.ceramint.2019.06.280.
Oladele, I.O., Agbabiaka, O.G., Olasunkanmi, O.G., Balogun, A.O., Popoola, M.O., 2018. Non-synthetic sources for the development of hydroxyapatite. J. Appl. Biotechnol. Bioeng 5 (2), 88–95. https://doi.org/10.15406/jabb.2018.05.00122.
Padmanabhan, V.P., Kulandaivelu, R., Nellaiappan, S.N.T., Lakshmipathy, M., Sagadevan, S., Johan, M.R., 2020. Facile fabrication of phase transformed cerium (IV) doped hydroxyapatite for biomedical applications–A health care approach. Ceram. Int. 46 (2), 2510–2522. https://doi.org/10.1016/j.ceramint.2019.09.245.
Pal, A., Paul, S., Choudhury, A.R., Balla, V.K., Das, M., Sinha, A., 2017. Synthesis of hydroxyapatite from Lates calcarifer fish bone for biomedical applications. Mater. Lett. 203, 89–92. https://doi.org/10.1016/j.matlet.2017.05.103.
Paul, S., Pal, A., Choudhury, A.R., Bodhak, S., Balla, V.K., Sinha, A., Das, M., 2017. Effect of trace elements on the sintering effect of fish scale derived hydroxyapatite and its bioactivity. Ceram. Int. 43 (17), 15678–15684. https://doi.org/10.1016/j.ceramint.2017.08.127.
Perloff, A., Posner, A.S., 1956. Preparation of pure hydroxyapatite crystal. Science 124 (3222), 583–584. https://doi.org/10.1126/science.124.3222.583.b.
Poggio, C., Gulino, C., Mirando, M., Colombo, M., Pietrocola, G., 2017. Protective effect of zinc-hydroxyapatite toothpastes on enamel erosion: an in vitro study. J. clin. exp. dent. 9 (1), e118. https://doi.org/10.4317/jced.53068.
Pokhrel, S., 2018. Hydroxyapatite: preparation, properties and its biomedical applications. Adv. Chem. Eng. Sci. 8 (4), 225. https://doi.org/10.4236/aces.2018.84016.
Pon-On, W., Suntornsaratoon, P., Charoenphandhu, N., Thongbunchoo, J., Krishnamra, N., Tang, I.M., 2016. Hydroxyapatite from fish scale for potential use as bone scaffold or regenerative material. Mater. Sci. Eng. C 62, 183–189. https://doi.org/10.1016/j.msec.2016.01.051.
Pooladi, A., Bazargan-Lari, R., 2020. Simultaneous removal of copper and zinc ions by chitosan/hydroxyapatite/nano-magnetite composite. J. Mater. Res. Technol. 9 (6), 14841–14852. https://doi.org/10.1016/j.jmrt.2020.10.057.
Poorzandpoush, K., Omrani, L.R., Jafarnia, S.H., Golkar, P., Atai, M., 2017. Effect of addition of Nano hydroxyapatite particles on wear of resin modified glass ionomer by tooth brushing simulation. J. clin. exp. dent. 9 (3), e372. https://doi.org/10.4317/jced.53455.
Prasad, A., Bhasney, S.M., Sankar, M.R., Katiyar, V., 2017. Fish scale derived hydroxyapatite reinforced poly (lactic acid) polymeric bio-films: possibilities for sealing/locking the internal fixation devices. Mater. Today Proc. 4 (2), 1340–1349. https://doi.org/10.1016/j.matpr.2017.01.155.
Pu'ad, N.M., Koshy, P., Abdullah, H.Z., Idris, M.I., Lee, T.C., 2019. Syntheses of hydroxyapatite from natural sources. Heliyon 5 (5), e01588. https://doi.org/10.1016/j.heliyon.2019.e01588.
Rabiee, N., Khatami, M., Jamalipour Soufi, G., Fatahi, Y., Iravani, S., Varma, R.S., 2021. Diatoms with invaluable applications in nanotechnology, biotechnology, and biomedicine: recent advances. ACS Biomater. Sci. Eng. 7 (7), 3053–3068. https://doi.org/10.1021/acsbiomaterials.1c00475.
Raghavendra, S.S., Jadhav, G.R., Gathani, K.M., Kotadia, P., 2017. Bioceramics in endodontics–a review. J. Istanbul Univ. Fac. Dent. 51 (3 Suppl. 1), S128. https://doi.org/10.17096/jiufd.63659.
Ramesh, N., Moratti, S.C., Dias, G.J., 2018. Hydroxyapatite–polymer biocomposites for bone regeneration: a review of current trends. J. Biomed. Mater. Res. B 106 (5), 2046–2057. https://doi.org/10.1002/jbm.b.33950.
Razali, R.A.C., Rahim, N.A., Zainol, I., Sharif, A.M., 2018. Preparation of dental composite using hydroxyapatite from natural sources and silica. 1. In: Journal of Physics: Conference Series, vol. 1097. 012050. IOP Publishing. https://doi.org/10.1088/1742-6596/1097/1/012050.
Rincón-López, J.A., Hermann-Muñoz, J.A., Cinca-Luis, N., Garrido-Domiguez, B., García-Cano, I., Guilemany-Casadamon, J.M., Alvarado-Orozco, J.M., Munoz-Saldana, J., 2019. Preferred growth orientation of apatite crystals on biological hydroxyapatite enriched with bioactive glass: a biomimetic behavior. Cryst. Growth Des. 19 (9), 5005–5018. https://doi.org/10.1021/acs.cgd.9b00268.
Rodriguez, D.E., Guiza-Arguello, V., Ochoa, O.O., Gharat, T., Sue, H.J., Lafdi, K., Hahn, M.S., 2016. Development of a hydroxyapatite-poly (d, l-lactide-co-glycolide) infiltrated carbon foam for orthopedic applications. Carbon 98, 106–114. https://doi.org/10.1016/j.carbon.2015.10.086.
Sani, N.S., Malek, N.A.N.N., Jemon, K., Kadir, M.R.A., Hamdan, H., 2019. Preparation and characterization of hydroxyapatite incorporated silica aerogel and its effect on normal human dermal fibroblast cells. J. Sol. Gel Sci. Technol. 90 (2), 422–433. https://doi.org/10.1007/s10971-019-04946-z.
Sathiskumar, S., Vanaraj, S., Sabarinathan, D., Bharath, S., Sivarasan, G., Arulmani, S., Preethi, K., Ponnusamy, V.K., 2019. Green synthesis of biocompatible nanostructured hydroxyapatite from Cirrhinus mrigala fish scale–A biowaste to biomaterial. Ceram. Int. 45 (6), 7804–7810. https://doi.org/10.1016/j.ceramint.2019.01.086.
Senthil, R., Vedakumari, S.W., Sastry, T.P., 2018. Hydroxyapatite and demineralized bone matrix from marine food waste–a possible bone implant. American Journal of Materials Synthesis and Processing 3 (1), 1–6. https://doi.org/10.11648/j.ajmsp.20180301.11.
Seyedmajidi, S., Seyedmajidi, M., Zabihi, E., Hajian-Tilaki, K., 2018a. A comparative study on cytotoxicity and genotoxicity of the hydroxyapatite-bioactive glass and fluorapatite-bioactive glass nanocomposite foams as tissue scaffold for bone repair. J. Biomed. Mater. Res. 106 (10), 2605–2612. https://doi.org/10.1002/jbm.a.36452.
Seyedmajidi, S., Seyedmajidi, S., Alaghehmand, H., Hajian-Tilaki, K., Haghanifar, S., Zabihi, E., Rajabnia, R., Seyedmajidi, M., 2018b. Synthesis and characterization of hydroxyapatite/bioactive glass nanocomposite foam and fluorapatite/bioactive glass nanocomposite foam by gel casting method as cell scaffold for bone tissue.

Eurasian. J. Anal. Chem. 13 (3), em17. https://doi.org/10.29333/ejac/85078.
Shams, M., Nezafati, N., Poormoghadam, D., Zavareh, S., Zamanian, A., Salimi, A., 2020. Synthesis and characterization of electrospun bioactive glass nanofibers-reinforced calcium sulfate bone cement and its cell biological response. Ceram. Int. 46 (8), 10029–10039. https://doi.org/10.1016/j.ceramint.2019.12.270.
Shuai, C., Yu, L., Yang, W., Peng, S., Zhong, Y., Feng, P., 2020. Phosphonic acid coupling agent modification of HAP nanoparticles: interfacial effects in PLLA/HAP bone scaffold. Polymers 12 (1), 199. https://doi.org/10.3390/polym12010199.
Shuai, C., Yang, W., Feng, P., Peng, S., Pan, H., 2021. Accelerated degradation of HAP/PLLA bone scaffold by PGA blending facilitates bioactivity and osteoconductivity. Bioact. Mater. 6 (2), 490–502. https://doi.org/10.1016/j.bioactmat.2020.09.001.
Shuai, C., Peng, B., Feng, P., Yu, L., Lai, R., Min, A., 2022a. In situ synthesis of hydroxyapatite nanorods on graphene oxide nanosheets and their reinforcement in biopolymer scaffold. J. Adv. Res. 35, 13–24. https://doi.org/10.1016/j.jare.2021.03.009.
Shuai, C., Yu, L., Feng, P., Peng, S., Pan, H., Bai, X., 2022b. Construction of a stereocomplex between poly (d-lactide) grafted hydroxyapatite and poly (l-lactide): toward a bioactive composite scaffold with enhanced interfacial bonding. J. Mater. Chem. B. https://doi.org/10.1039/D1TB02111G.
Stipniece, L., Narkevica, I., Sokolova, M., Locs, J., Ozolins, J., 2016. Novel scaffolds based on hydroxyapatite/poly (vinyl alcohol) nanocomposite coated porous TiO2 ceramics for bone tissue engineering. Ceram. Int. 42 (1), 1530–1537. https://doi.org/10.1016/j.ceramint.2015.09.101.
Sun, W., Fan, J., Wang, S., Kang, Y., Du, J., Peng, X., 2018. Biodegradable drug-loaded hydroxyapatite nanotherapeutic agent for targeted drug release in tumors. ACS Appl. Mater. Interfaces 10 (9), 7832–7840. https://doi.org/10.1021/acsami.7b19281.
Syusyukina, V.A., Shapovalova, Y., Korotchenko, N.M., Kurzina, I.A., 2017. Structural-phase state and surface properties of composite materials based on polylactide and hydroxyapatite. Russ. J. Appl. Chem. 90 (1), 106–112. https://doi.org/10.1134/S1070427217010165.
Tokhiriyon, B., Poznyakovsky, V.M., 2019. New biocomplex for nutrient-metabolic support of bone tissue. 3. In: IOP Conference Series: Earth and Environmental Science, vol. 315. 032020. IOP Publishing. https://doi.org/10.1088/1755-1315/315/3/032020.
Uthappa, U.T., Brahmkhatri, V., Sriram, G., Jung, H.Y., Yu, J., Kurkuri, N., Aminabhavi, T.M., Altalhi, T., Neelgund, G.M., Kurkuri, M.D., 2018. Nature engineered diatom biosilica as drug delivery systems. J. Contr. Release 281, 70–83. https://doi.org/10.1016/j.jconrel.2018.05.013.
Vano, M., Derchi, G., Barone, A., Pinna, R., Usai, P., Covani, U., 2018. Reducing dentine hypersensitivity with nano-hydroxyapatite toothpaste: a double-blind randomized controlled trial. Clin. Oral Invest. 22 (1), 313–320. https://doi.org/10.1007/s00784-017-2113-3.
Venkatesan, J., Lowe, B., Manivasagan, P., Kang, K.H., Chalisserry, E.P., Anil, S., Kim, D.G., Kim, S.K., 2015. Isolation and characterization of nano-hydroxyapatite from salmon fish bone. Materials 8 (8), 5426–5439. https://doi.org/10.3390/ma8085253.
Yamamura, H., da Silva, V.H.P., Ruiz, P.L.M., Ussui, V., Lazar, D.R.R., Renno, A.C.M., Ribeiro, D.A., 2018. Physico-chemical characterization and biocompatibility of hydroxyapatite derived from fish waste. J. Mech. Behav. Biomed. Mater. 80, 137–142. https://doi.org/10.1016/j.jmbbm.2018.01.035.
Yazdani, I., Movahedi, B., Naeimi, M., Sattary, M., Rafienia, M., 2020. Novel electrospun polyurethane scaffolds containing bioactive glass nanoparticles. Bioinspired, Biomimetic Nanobiomaterials 9 (3), 175–183. https://doi.org/10.1680/jbibn.18.00004.
Zainol, I., Adenan, N.H., Rahim, N.A., Jaafar, C.A., 2019. Extraction of natural hydroxyapatite from tilapia fish scales using alkaline treatment. Mater. Today Proc. 16, 1942–1948. https://doi.org/10.1016/j.matpr.2019.06.072.
Zhang, Y., Dong, K., Wang, F., Wang, H., Wang, J., Jiang, Z., Diao, S., 2018. Three dimensional macroporous hydroxyapatite/chitosan foam-supported polymer micelles for enhanced oral delivery of poorly soluble drugs. Colloids Surf., B 170, 497–504. https://doi.org/10.1016/j.colsurfb.2018.06.053.

ARTICLES FOR FACULTY MEMBERS

BONE-DERIVED HYDROXYAPATITE TOOTHPASTE FOR SUSTAINABLE PHARMACEUTICAL AND BIOMEDICAL APPLICATIONS

Marine bioceramic generation for bone tissue regeneration: Sea urchin (echinometra mathaei) exoskeleton-derived calcium carbonate as a precursor for hydroxyapatite synthesis, incorporated into chitosan based-hydrogel and 3d-printed PCL scaffold for osteogenic differentiation / Jamshidizadeh, S., Amrollahi Biuki, N., & Zarei, M.

Marine Biotechnology
Volume 28 Issue 25 (2026) Pages 1-19
https://doi.org/10.1007/s10126-025-10555-5
(Database: Springer Nature Link)

Marine Biotechnology (2026) 28:25
https://doi.org/10.1007/s10126-025-10555-5

RESEARCH

Marine Bioceramic Generation for Bone Tissue Regeneration: Sea Urchin (*Echinometra mathaei*) Exoskeleton-Derived Calcium Carbonate as a Precursor for Hydroxyapatite Synthesis, Incorporated into Chitosan Based-Hydrogel and 3D-Printed PCL Scaffold for Osteogenic Differentiation

Sara Jamshidizadeh[1] · **Narges Amrollahi Biuki**[1,2] · **Maaroof Zarei**[3,4]

Received: 12 October 2024 / Accepted: 9 December 2025

Abstract

The marine environment is a rich and diverse habitat, home to numerous organisms that serve as valuable sources of biological and pharmacological compounds. The skeletal structures of many marine invertebrates represent precursors for calcium phosphate (CaP) bioceramics. This study demonstrates hydroxyapatite (HA) synthesis from sea urchin (*Echinometra mathaei*) shell and spine, a sustainable $CaCO_3$ source. FTIR and XRD analysis revealed the presence of characteristic peaks associated with hydroxyapatite. SEM-EDS observations indicated that synthesis parameters determined the calcium to phosphorus ratio (Ca/P) and morphology of the derived calcium phosphate bioceramic. HA-based hydrogels play an important role in bone tissue engineering due to their high biocompatibility. The hydrogels were formulated as follows: a control group of oxidized carboxymethyl chitosan/cellulose (O-CMC/CEL), a composite group with commercial hydroxyapatite (O-CMC/CEL/HA), and two experimental composite groups containing HA synthesized from sea urchin spine (O-CMC/CEL/HA (spine-derived)) and shell (O-CMC/CEL/HA (shell-derived)). Four groups of hydrogels melded on 3D print frames to evaluate the osteogenic differentiation of human adipose-derived mesenchymal stem cells (ADSCs). SEM, FTIR, water contact angle, swelling rate, and live/dead assay results indicated that the porous composite hydrogels possessed a suitable microarchitecture, featuring appropriate pore size and interconnectivity, which promotes nutrient permeability, cell attachment, cell survival, and proliferation. Furthermore, real-time PCR analysis indicated an upregulation of key osteogenic markers in ADSCs cultured on these composites, suggesting their potential to support osteogenic differentiation. The collective in vitro evidence indicates that the O-CMC/CEL/HA (spine-derived) composite hydrogel, with its suitable physicochemical properties and positive cellular responses, represents a promising biomaterial for future bone tissue engineering studies.

Keywords Sea urchin · Bioceramic · Hydroxyapatite · Hydrogel · Osteogenic differentiation

✉ Narges Amrollahi Biuki
amrollahi@hormozgan.ac.ir

[1] Department of Marine Biology, Faculty of Marine Science and Technology, University of Hormozgan, Bandar Abbas, Iran

[2] Department of Modern Technologies, Mangrove Forest Research Center, University of Hormozgan, Bandar Abbas, Iran

[3] Department of Chemistry, Faculty of Science, University of Hormozgan, Bandar Abbas, Iran

[4] Nanoscience, Nanotechnology and Advanced Materials Research Center, University of Hormozgan, Bandar Abbas, Iran

Introduction

The marine environment is one of the richest and most complex habitats, covering more than 70% of the Earth's surface. They do not only consist of salt water but are a most valuable birthplace of large group of organisms that represents an important resource for abundant biological and pharmacological substances and various bioactive chemical and mineral materials (Carroll et al. 2020; Carvalho et. 2024; Martinelli et al. 2025). In the last two decades, the development of novel materials has been considered important for

Published online: 29 January 2026

treatment of damaged teeth, bone implantation and tissue engineering and drug delivery devices. The study of new generation methods offered the advantage of reducing production costs and toxicity, an important requirement in tissue engineering (Salamanca et al. 2020).

Bioceramics have been developed for the purpose to repair, and regenerate diseased and damaged components of both the skeletal system and periodontal anomalies. Also, bioceramics have the ability to promote biomineralization, osteoconductivity, resistance to chemical corrosion and a rigid surface (Hasan et al. 2013; Ruffini et al. 2021; Sivakumar et al. 2023). Hydroxyapatite (HA), consisting of calcium, phosphorus and hydrogen atoms ($Ca_{10}(PO_4)_6(OH)_2$) with a hexagonal crystal structure, is considered in the medical field as a bioactive compound (Parisi et al. 2020; Guo et al. 2022; Xing et al. 2024). This structure has a chemical composition and crystallography similar to the biomineral content (70%) found in bones (Li et al. 2019; Witzler et al. 2019). In addition, HA offers a high percentage of biocompatibility due to its non-toxic and non-inflammatory properties (Lett et al. 2019; Sorkhi et al. 2019; Kavasi et al. 2021).

Calcite and aragonite, which are the main crystalline polymorphs of calcium carbonate, found in abundant marine sources, serve as sustainable and viable calcium precursors for the synthesis of calcium phosphate bioceramics such as hydroxyapatite (Silva et al. 2012; Macha et al. 2015; Choi et al. 2017). Despite the various chemical techniques used in the production of HA, the precipitation method, microwave processing, hydrothermal techniques, wet chemical precipitation and calcium phosphate (CaP) hydrolysis have proven to be notable methods (Agbeboh et al. 2020; Kavasi et al. 2021). Numerous studies have reported the successful synthesis of hydroxyapatite (HA) from marine skeletal wastes, which can be broadly categorized based on their intrinsic mineral composition. Fish bones and scales, which naturally contain biological apatite, can be directly converted to HA with crystal sizes ranging from 85 to 119 nm (Naga et al. 2015), 100–250 nm (Shi et al. 2018), and up to 8 µm (Ashwitha et al. 2020). On the other hand, calcareous shells, primarily composed of calcium carbonate polymorphs (calcite/aragonite), require chemical conversion to produce HA. Examples include 100–200 nm from oyster shells (Yang et al. 2011), 76–134 nm from clamshells (Shi et al. 2018; Suresh Kumar et al. 2020), 293 nm from crab shell (Irfan et al. 2020), and 10–300 µm from kina shell (Shavandi et al. 2016). In contrast, calcareous shells composed of calcium carbonate require chemical transformation to produce HA (Mancilla-Sanchez et al. 2019). Therefore, these results highlight the potential of using different natural sources for the synthesis of HA with different crystal sizes and demonstrate the, versatility and sustainability of this approach as well as rapid and low cost synthesis method.

Chitosan possesses desirable properties for the fabrication of flexible hydrogels and organized networks as well as biological and mechanical compatibility. Chitosan, a natural copolymer of glucosamine and N-acetylglucosamine, is typically obtained from crustacean shells through the process of partial deacetylation of chitin (Merzendorfer and Cohen 2019). This biomaterial has been used alone or together with other polymers due to its biocompatible, biodegradable and bacteriostatic properties (Malik et al. 2020). Numerous studies have shown the potential of chitosan in dental and bone treatment and regeneration (Gupta et al. 2023; Tang et al. 2023b). Additionally, cellulose is widely known for its applications in the food and pharmaceutical industries. Due to its gradual degradability and biocompatibility, cellulose is used together with chitosan and HA for the regeneration of hard tissues (Yar et al. 2016). Due to the importance of CaP bioceramics, the primary objective of this study is to utilize sea urchin's skeletal structure (shell and spine), a rich and sustainable source of calcium carbonate, as a precursor for the synthesis of hydroxyapatite via the chemical treatment, aiming to explore its properties for potential biomedical applications. Additionally, the composite hydrogels were synthesized by combining chitosan, cellulose and synthesized HA. Subsequently these hydrogels were utilized in the fabrication of a three-dimensional printed model made of polycaprolactone (PCL), allowing for further investigation of its potential applications in tooth and bone reconstruction.

Materials and Methods

Materials

The exoskeleton of sea urchins, consisting of shell and spine, was used as a precursor for the production of CaP bioceramic. The chemical process included the use of distilled or deionized water (DW) with phosphoric acid (H_3PO_4) 85% (Merck, Germany). High molecular weight chitosan (molecular weight range of 310,000–375,000 Da, Sigma catalog number 9012-76-4), was employed alongside acetic acid, sodium hydroxide, monochloroacetic acid, sodium dodecyl sulfate, ethanol, and various reagents such as phosphate-buffered saline (PBS), DMEM/High glucose (Dulbecco's Modified Eagle Medium), fetal bovine serum (FBS), antibiotics (penicillin, streptomycin), and trypsin (Gibco, Germany). Additionally, PCL with a molecular weight of 45,000 (Sigma-Aldrich, USA), HA (Sigma-Aldrich, USA), and human adipose derived mesenchymal stem cells (hADSC) were utilized. Lastly, the Acridine Orange/Propidium Iodide (AO/PI) staining solution (Nexcelom Bioscience, CS2-0106) was used.

Synthesis of Natural HA Bioceramic

Sample Preparation

In the present study, an exoskeleton (shell and spine) of sea urchin (*Echinometra mathaei*) weighing between 7 and 9 g was used as a precursor for CaPs bioceramic synthesis. The samples were collected from the seashore of Bandar-e Lengeh (Persian Gulf, Hormozgan, Iran). Following a thorough cleaning procedure involving mechanical agitation with DW at a temperature of 90 °C, the exoskeleton samples were subsequently pulverized into fine particles and comminuted using a grinder mill. The resulting milled powder was then subjected to a 100 µm sieve in order to isolate particles less than 100 µm in diameter. Subsequently, the obtained product samples were calcined in an electric furnace to produce calcium oxide (CaO), which would be utilized for subsequent chemical processes (Komalakrishna et al. 2017; Gómez Vázquez et al. 2020).

Chemical reactions process involved in the synthesis of hydroxyapatite are as follows (Miculescu et al. 2017):

$$CaCO_3 \rightarrow CaO + CO_2 \quad (1)$$

$$CaO + H_2O \rightarrow Ca(OH)_2 \quad (2)$$

$$10Ca(OH)_2 + 6H_3PO_4 \rightarrow Ca_{10}(PO_4)_6(OH)_2 + 18H_2O \quad (3)$$

For CaPs synthesis, the reagents were first evaluated according to the stoichiometric reaction described by Rahtje method, as follows: According to stoichiometric reaction, to obtain 10 g of powder from the heat treatment of the sea urchin skeleton (shell and spine), 200 mL of DW and 5.5 mL of H_3PO_4 85% were used (Rathje 1939; Ferraz et al. 2004; Miculescu et al. 2017). In relation to the objective of the ongoing investigation, the optimization of the synthesis conditions was examined as follows: (1) A hot plate and ultrasonic stirring; (2) Variation of the stoichiometric acid quantity (SA: abbreviation of mentioned phrase): 1.0 × 5.5 (1.0 SA) and 1.2 × 5.5 (1.2 SA) to in order to achieve the appropriate Ca/P ratio of HA; (3) Pyrolysis process temperature based on TGA analysis. The appropriate amount of acid was determined in the duration of the conversion process at 8 h.

Bioceramic Synthesis Method

The raw powders of samples calcination were performed in electric furnace for 2 h at 720 °C and 740 °C for shell and spine sample respectively. Then produced materials as CaO powders were immersed in DW and then subjected to a gradual addition of H_3PO_4 in the form of drops using different quantities of H_3PO_4 (1.0 SA and 1.2 SA), until a stoichiometric ratio of Ca/*P* = 1.667 was achieved. The suspended samples were subjected to stirring at temperatures of 80 °C for 8 h in both methods of hot plate and ultrasonic agitation for each skeleton samples, in order to facilitate the completion of the reaction. Lastly, the required material were obtained by subjecting the dried final product to an electric furnace and heating it for a duration of 2 h at a temperature of 600 °C (Karacan et al. 2018).

Hydrogel Synthesis

To generate modified cellulose, a first step involved the dissolution of 0.5 g of cellulose in 5 mL of distilled water, followed by the addition of 0.5 g of sodium metaperiodate in powdered form. This mixture was then stored at room temperature, protected from light for 4 h. Subsequently, 1 mL of diethylene glycol was added, and the solution was refrigerated for 24 h. Afterward, the solution underwent dialysis for a period of 4 days and final step concluding with a freeze-drying. In this study, O-carboxymethyl chitosan (O-CMC) was used (Fattahi et al. 2023). To dissolve 5 g of O-CMC, 2.5 mL of acetic acid (10%) was used. Similarly, 0.25 g of cellulose was dissolved in 5 mL of acetic acid (10%). These two solutions were combined and subsequently supplemented with 5 g of three types of HA (4%) in powdered form. In this study, HA synthesized from sea urchin was used in hydrogel fabrication. The hydrogels were fabricated of O-CMC/CEL, O-CMC/CEL/HA, O-CMC/CEL/HA (spine-derived), and O-CMC/CEL/HA (shell-derived).

Three-dimensional (3D) Printing of Polycaprolactone

The frames in Fig. 1 was constructed using a 3D plotting device that was prepared within a laboratory setting. The PCL substance underwent a process of melting within a container composed of stainless steel at a specified temperature of 80 °C. For the fabrication process, a pneumatic pressure measuring at 600 ± 10 kilopascals, along with a feed rate of 1 mL per second, were used. The diameter of the frames was 8 mm with internal diameter of 3 mm. After synthesis, the hydrogels are molded into these frames and used to fallow a further process in current research (Fig. 1).

Material Characterization

Information on the crystalline phase of the bulk minerals was obtained by performing X-ray diffraction (XRD) analysis on samples before and after the chemical reaction. To evaluate the stability of the samples, weight loss and

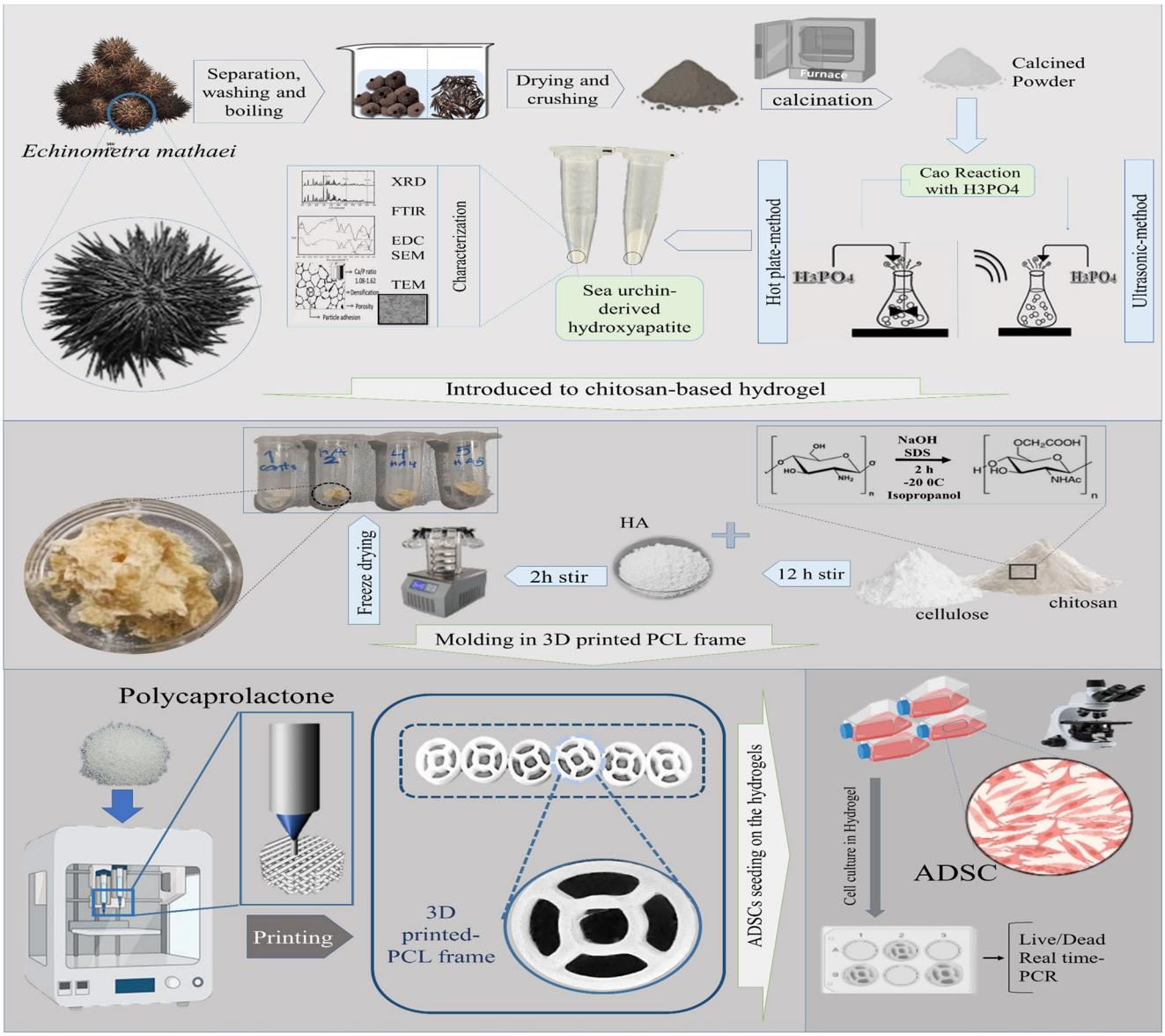

Fig. 1 Schematic figure of research process

responses during heating were determined using a differential thermogravimetry analyzer (DTA/TG). Subsequently, TG curves were recorded under nitrogen gas flow at a rate of 10 °C/min from room temperature to 1000 °C. Scanning electron microscopy (SEM) along with energy-dispersive X-ray spectroscopy (EDS) was used to study the morphology and porosity as well as to identify the elemental composition of the materials. The prepared samples were analyzed using Fourier transform infrared spectroscopy (FTIR). Furthermore, transmission electron microscopy (TEM) was used to characterize the crystal size and morphology of the HA samples. The calcium to phosphate ratio of the CaPs synthesized in the present study were evaluated based on previous studies examining the chemical compositions of various CaPs (Dorozhkin 2009a; Pina et al. 2015).

Hydrogel Characterization

SEM

A scanning electron microscope (model XL30, manufactured by PHILIPS) was used to determine and measure the surface morphologies of hydrogels composed of O-CMC/CEL (Control group), O-CMC/CEL/HA, O-CMC/CEL/HA (spine-derived), and O-CMC/CEL/HA (shell-derived). All

samples were mounted on aluminum stubs, sputter-coated with gold–palladium and viewed in a Philips XL-30 SEM with an accelerating voltage of 10 kV.

FTIR

Fourier transform infrared spectroscopy (FTIR) was performed on the O-CMC/CEL (Control group), O-CMC/CEL/HA, O-CMC/CEL/HA (spine-derived), and O-CMC/CEL/HA (Shell-derived), to investigate their structure to check properties. The FTIR spectrum (Bomem, model MB-102, Quebec, Canada) was obtained in the range of 4000 to 450 cm^{-1}.

Contact Angle

Water-contact angle measurements were performed on dried hydrogels using a G10 Kruss goniometer to assess surface hydrophilicity at room temperature. for this purpose, a drop of distilled water (5 µL) is placed on the surface of the dry hydrogels above it and drop shape recorded using camera after 3 s from the drop on the grid. lastly, interaction between water and the dry hydrogels was performed by quantifying the angle at which the water droplet adheres to the surface of the hydrogels.

Swelling Behavior

The hydrogel pieces were carefully measured for weight (M1) and then immersed in a solution of 50 mL of phosphate-buffered saline (PBS) for 24 h at a temperature of 20 °C. At various intervals, the samples were removed from the PBS and the moisture on their surfaces was carefully removed with a tissue, then they were weighed again (M2). Then the water absorption (WS) was calculated using the following formula:

$$WS\ (\%) = \frac{M2 - M1}{M1} \times 100$$

Cell Seeding

Human adipose derived stem cells (ADSCs) used in this study were obtained from the laboratory of tissue engineering (Department of Tissue engineering and Applied Cell Sciences, School of Advanced Technologies in Medicine, Shahid Beheshti University of Medical Sciences, Tehran, Iran) as already ADSC isolation from adipose tissue performed by Fattahi et al. (2023). The experiments for this study were performed using third passage ADSC. Synthesized hydrogels were molded into 3D print frames and placed in wells. First, float it in 70% alcohol for 40 min, then remove the alcohol and expose the hydrogels to UV light for 30 min to sterilize them. We then added the culture medium to the hydrogels and placed them in the incubator for 24 h. After that, the culture medium is removed and the number of cells with a density of 50×10^4 cells were planted on the hydrogels. Ultimately, we add culture medium (DMEM-HG) supplemented with 15% FBS and 1% antibiotics (penicillin/streptomycin) in each well and put it under incubation condition (5% CO_2, 95% humidity at 37 °C).

Cell Viability Assay

Cell viability assessment was performed on days 1, 3, and 15 using AO/PI solution (Nexcelom, CS2-0106) and Live/Dead staining on hydrogel samples according to the manufacturer's instructions. The hydrogels were molded into 3D frames, sterilized and placed in wells. Equal amounts of staining solution and PBS were added to the wells of the plate containing the hydrogel and incubated for 20 min in the dark at room temperature. To examine the viability, hydrogels were observed under a fluorescent microscope. Finally, the number of live cells in the hydrogels was determined using Image J software after the imaging process was performed with a fluorescence microscope.

RNA Isolation and Real-Time PCR Analysis

The hydrogels were molded into 3D frames, sterilized and placed into the wells. After the cells were seeded on the hydrogels, they were kept in an incubator for 21 days. The culture medium was changed every two days. Finally, after 21 days, the expression of bone-specific genes was analyzed using the real-time PCR technique. The real-time PCR method was used to examine the differentiation of mesenchymal stem cells into bone cells in hydrogels as well as the expression of collagen I and Runx2, which are bone target genes. Trizol lysed the cells, extracted the RNA, and the protocol included in the kit (Qiagen, Japan) was used for cDNA synthesis. The synthesized cDNA (40 ng) was mixed with Power SYBER Green Master Mix (10 µL) (Qiagen, Japan), and each primer (0.5 µL) designed with Gene Runner software was added. The primer sequences are listed in Table 1. Normalization for each sample was performed using the ACTIN gene and calculated using Step One software.

Table 1 Primer sequences for polymerase chain reaction

Gene	Sequence 5′–3′
Collagen F	TGGAGCATCACCCTTAGAG
Collagen R	CACCAGCATCACCCTTAGC
RUNX2 F	GAACCCAGAAGGCACAGACA
RUNX2 R	ACTTGGTGCAGAGTTCAGGG
Actin F	ATGCCTGCCGTGTGAAC
Actin R	ATCTTCAAACCTCCATGATG

Statistical Analysis

All data collected in this study were repeated three times, and all data are mean ± standard deviation and analyzed by analysis of variance (two-way ANOVA).

Results and Discussion

Material Charecterization

Thermal Gravimetric Analysis (TGA)

Pyrolysis represents a fundamental step in evaluating the thermal resistance of samples to determine the calcination temperature required for the decomposition of $CaCO_3$ or aragonite in a raw sample. These parameters were determined from the weight reduction of the sample using the formula below (Walsh et al. 2008):

$$MS = M_0 - Mx/M_0 \times 100$$

This parameter determines the optimal conditions for eliminating organic compounds from the skeletal component of sea urchin. In addition, it serves to protect the integrity of the microporous structures and prevent their damage from high temperatures or heating. Figure 2 illustrates the thermogravimetric (TG) curves of the samples in a temperature range spanning from room temperature to 1000 °C. TGA results showed the spine sample exhibits greater stability compared to the shell sample. So, the shell indicated a faster weight loss within the range of room temperature to 550 °C, resulting in a weight loss of approximately 10%. This weight reduction may be due to greater endothermic by chemical or physical removal of water (Sha et al. 2011; Ikeda et al. 2014). The gradual decline in weight between temperatures of 550 to 740 °C (for the spine sample) and 630 to 720 °C (for the shell sample) may be attributed to the elimination of organic matter (Kusmanto et al. 2008). Excessive weight loss 35% at temperatures of 720 and 740 °C for the shell and spine samples respectively, could have a detrimental impact on the structural integrity of the specimens, leading to their potential collapse into fine CaO powder (Heidari et al. 2015). In one study, the weight loss of the similar samples was evaluated in three phases: In the initial phase, which ranged from 70 to 100 °C, the HA containing composite experienced a weight loss of 11.06 to 15.98%. This phenomenon was attributed to the surface burning of the samples. The gradual weight loss in the second stage was probably due to water evaporation (Ghaemy and Naseri 2012). At the final stage, the weight loss of the samples is due to the thermal degradation of organic compounds in composite material (Bahrololoom et al. 2009). Previous studies have reported mass losses of Kina shells between 10 and 35%. This can be attributed to the removal of organic matter and the decomposition of $CaCO_3$ and its conversion to CaO (Wilton et al. 2016). As a result, in this study, by choosing the temperature range of 630 to 720 °C (for the shell sample) and 550 to 740 °C (for the spine sample), not only the normal shell structure and spine, but also obtained calcium-rich $CaCO_3$/CaO in the pyrolysis experiment.

XRD Analysis

The phase composition of the materials was analysed by X-ray diffraction (XRD) at different stages of processing. The XRD patterns of the raw, uncalcined powders of sea urchin spine and shell are shown in Figs. 3A and D, respectively. The observed peaks were exclusively indexed to aragonite, a polymorph of calcium carbonate ($CaCO_3$), with the characteristic peak at $2\theta = 26.2°$ confirming this identification. The characteristic aragonite peaks in the XRD patterns clearly identify the mineral phase present in the untreated starting materials. The transformation of $CaCO_3$

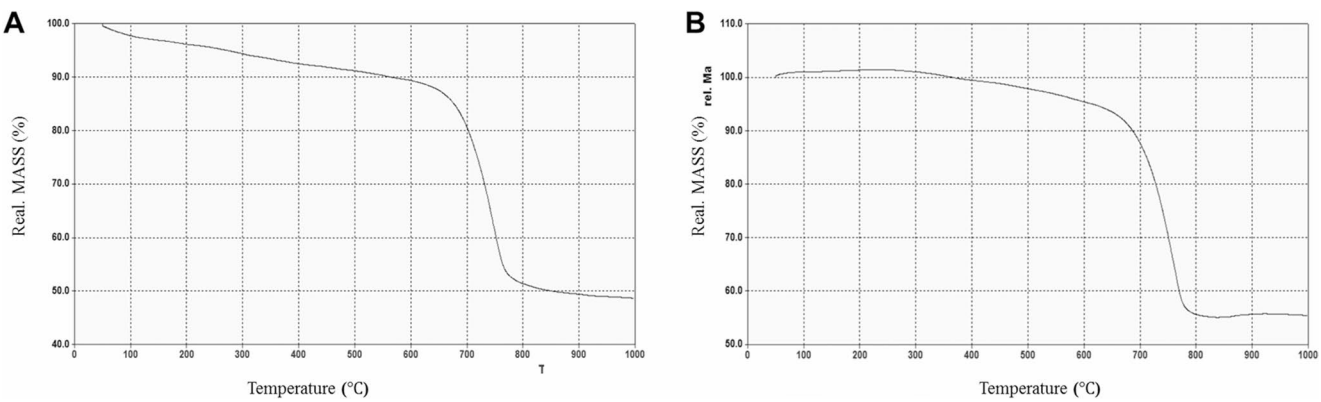

Fig. 2 Thermogram curves of raw powders. **A** Shell sample and **B** Spine sample

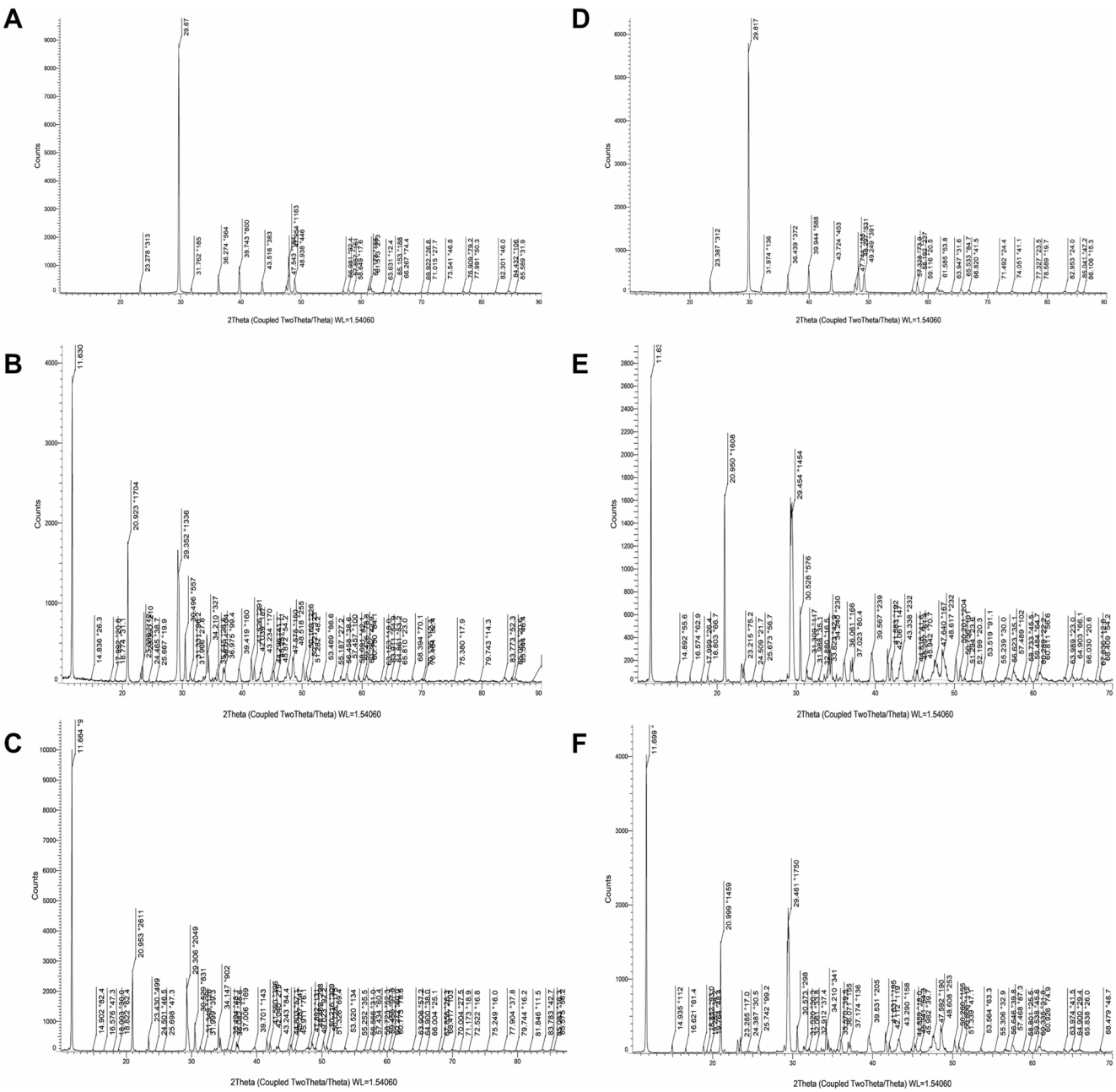

Fig. 3 X-ray diffraction patterns of sea urchin skeletal materials. Left side shows spine samples: **A** raw spine, **B** after calcination at 550 °C, and **C** after calcination at 740 °C. Right side shows shell samples: **D** raw shell, **E** after calcination at 630 °C, and **F** after calcination at 720 °C

to CaO occurs through the heat treatment process in the furnace during calcination (Wilton et al. 2016). Furthermore, the organic matrix within the sample structure appears to facilitate the ion exchange process during the subsequent chemical reaction, as supported by previous research (Vecchio et al. 2007).

The phase evolution during calcination was tracked by comparing the XRD patterns of the skeletal samples after heat treatment. For the spine samples (Fig. 3B and C), calcination at 550 °C resulted in the partial conversion of $CaCO_3$ to CaO, while treatment at 740 °C resulted in an effective conversion. A similar progression was observed for the shell samples (Fig. 3E and F), with effective conversion achieved at 720 °C. The XRD results thus clearly demonstrate the temperature-dependent conversion of calcium carbonate ($CaCO_3$) to calcium oxide (CaO). Furthermore, no significant differences were observed in the final products obtained from calcination within the 720–740 °C range.

SEM-EDS

In Fig. 4 the analysis of the treated samples using energy-dispersive X-ray spectroscopy (EDS) in both synthesis methods with 8 h of treatment revealed that the samples primarily consist of calcium (Ca), phosphorus (P), oxygen (O), carbon (C), and a small amount of sodium (Na). To evaluate the calcium-phosphorus atomic ratio (Ca/P) in the samples, a comparative analysis was performed on the samples treated with different amounts of H_3PO_4 (Table 2). The Ca/P atomic ratio calculated from the EDS results was between 1.0 and 3.12. The results showed that the increase in H_3PO_4 used during the synthesis process resulted in a decrease in the Ca/P ratio due to the greater presence of phosphate. Additionally, these findings revealed that the deviation from the stoichiometric value of 1.67 decreased as the concentration of the treatment solution increased due to heightened acidity (1.2 SA). Various studies have reported a Ca/P ratio for HA synthesized from marine sources, in the different range from the 1.67 value of stoichiometric HA (Dorozhkin 2009b; Akram et al. 2014; Wang et al. 2019; Miculescu et al. 2020; Hussain and Sabiruddin 2021). These studies suggested the existence of brushite/monetite/calcium pyrophosphate phases during CaP bioceramic synthesis. The synthesis of hydroxyapatite (HA, $Ca_{10}(PO_4)_6(OH)_2$) performed from shell and spine samples was confirmed by Ca/P ratio of 1.54 and 1.64 respectively, using hot plate method, with acid amount of 1.2 SA. Additionally, ACP (Amorphous calciumphosphate), whitlockite or β-tricalcium phosphate and monetite detected in the treated spine and shell samples as shown in Table 2 (Macha et al. 2013; Rosa Cegla et al. 2014; Karacan et al. 2018).

XRD

In Fig. 5, the presence of hydroxyapatite (HA) was confirmed by XRD diagram. Most calcium carbonate were converted into bioceramic, especially HA (Walsh et al. 2008). With an extended conversion in exoskeleton samples, HA peaks appeared and showed diffraction intensities, confirming the HA phase in the samples specially in spine-derived sample. Crystalline HA phases and purity depending on the source and conversion process, thus different research performed accordingly and indicating that more crystallinity and purity observed in calcination temperature above 600 °C and by using wet chemical process (Laonapakul 2015; Khiri et al. 2019). Furthermore, highly crystalline phases lead to improve bioactivity and osteointegration properties of HA (Hernández-Ruiz et al. 2022). XRD pattern of HA derived from waste kina (*Evechinus chloroticus*) shells as a marine waste demonstrated that sharp bands at 2θ = 26° and 2θ = 30° between the processed kina shell and commercial

Fig. 4 EDS results of HA synthesised by hot plate-method with acid quantity equal to 1.2 SA in **A** shell and **B** spine; EDS results of monetite and withlockite synthesised by ultrasonic method with acid quantity of 1.2 SA, **C** shell and **D** spine

HA samples (Ziani et al. 2014; Shavandi et al. 2016). Waste green mussel shells from Auckland, New Zealand, were converted to rod like nano-crystalline HA confirmed by bands at 2θ = 26°–34° using XRD pattern analysis (Shavandi et al. 2015). The findings of the X-ray analysis in current research are similar to fabrication of nanohydroxyapatite from the sea snail *Cerithium vulgatum* which indicate comprise HA peak (Gunduz et al. 2014).

FTIR

The FTIR spectrum of the calcined powders and synthesized CaPs from sea urchin shell and spine samples, is shown in Figs. 6A and B. Specific peaks at 1032 and 1072 cm^{-1} of the HA samples, indicating PO_4^{-3} ions related to the formation of hydroxyapatite. In addition, the symmetric PO stretching vibration of the PO_4^{-3} ion is shown at 563–717 cm^{-1}. This illustrates the changes in functional groups and development of phosphate within the samples and the conversion from calcium carbonate to HA (Kumar et al. 2012; Nandi et al. 2015). FTIR spectra evaluated in current research are similar to those observed by previous study on sea urchin (*Strongylocentrotus purpuratus*) and Sea Snail (*Cerithium vulgatum*) shell (Gunduz et al. 2014; Gómez Vázquez et al. 2020). Furthermore, the presence of bands at 1445 and 1072 cm^{-1} confirms the existence of carbonate ions in the HA crystals, which depicted the presence of some residual CO_3^{-2} group in process sample (Heidari et al. 2015; Nandi et al. 2015; Shavandi et al. 2016). However, carbonate-containing HA is chemically similar to the biological apatite found in bones, and is reported to have high bioactivity (Sabu et al. 2019). Furthermore, in Fig. 6A, the peaks at 1629 cm^{-1} correspond to H_2O adsorbed on surface (Nandi et al. 2015; Trinkunaite-Felsen et al. 2016). In comparison, the reduction or elimination of bands 3000–3500 cm^{-1} of the hydroxyl group (Rehman and Bonfield 1997), is attributed to the increase in carbonate substitution in process samples (Heidari et al. 2015).

Electron Microscopic Analysis

Figure 7 shows the scanning electron microscope (SEM) images of the shell-derived HA (Fig. 7A), spine-derived HA (Fig. 7B), and the commercial hydroxyapatite (Fig. 7C). The surface of the spine-synthesized HA material has various shapes of microstructures with a size of 1 to 5 µm. Compared to previous findings, these particles consist of rod-shaped crystals or needle-like structures as well as small

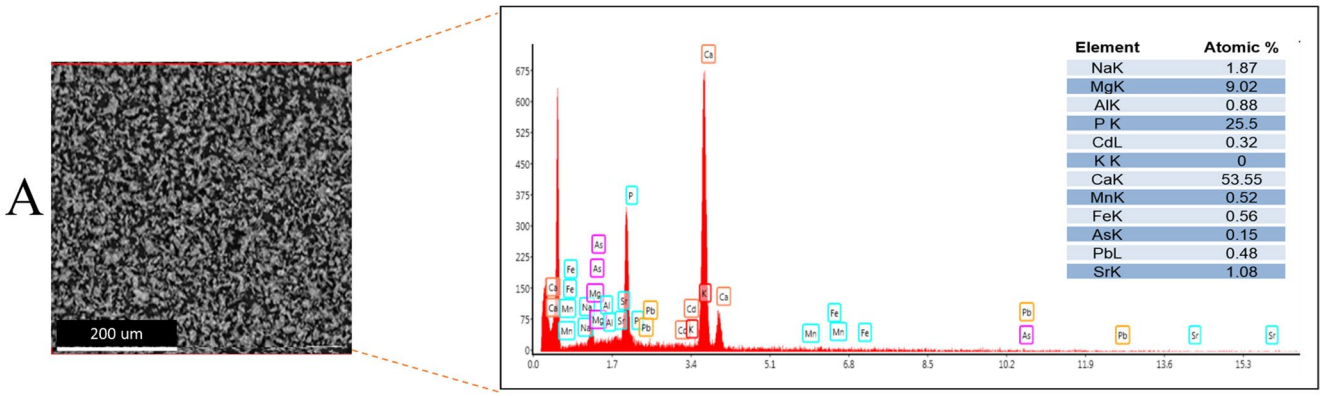
A
200 um
Element Atomic %
NaK 1.87
MgK 9.02
AlK 0.88
P K 25.5
CdL 0.32
K K 0
CaK 53.55
MnK 0.52
FeK 0.56
AsK 0.15
PbL 0.48
SrK 1.08

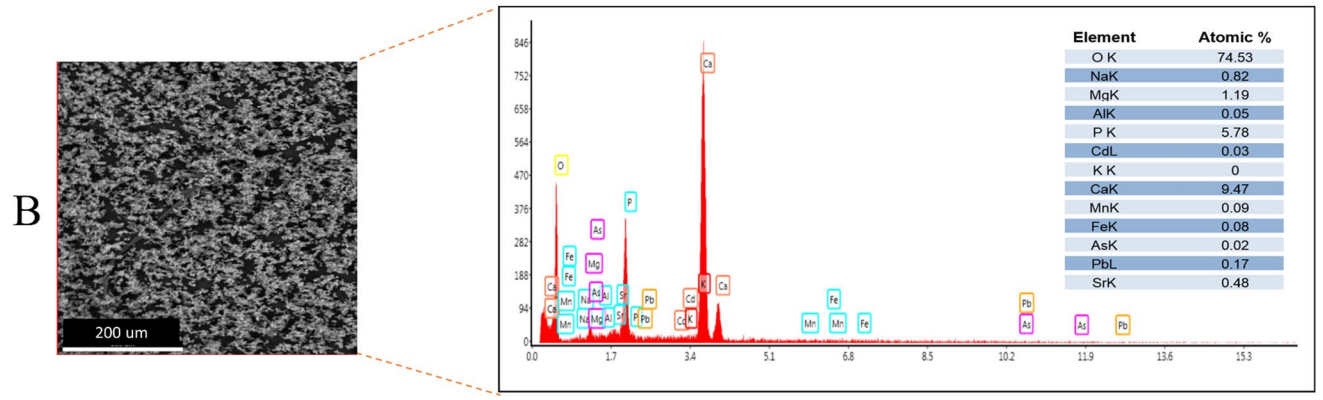
B
200 um
Element Atomic %
O K 74.53
NaK 0.82
MgK 1.19
AlK 0.05
P K 5.78
CdL 0.03
K K 0
CaK 9.47
MnK 0.09
FeK 0.08
AsK 0.02
PbL 0.17
SrK 0.48

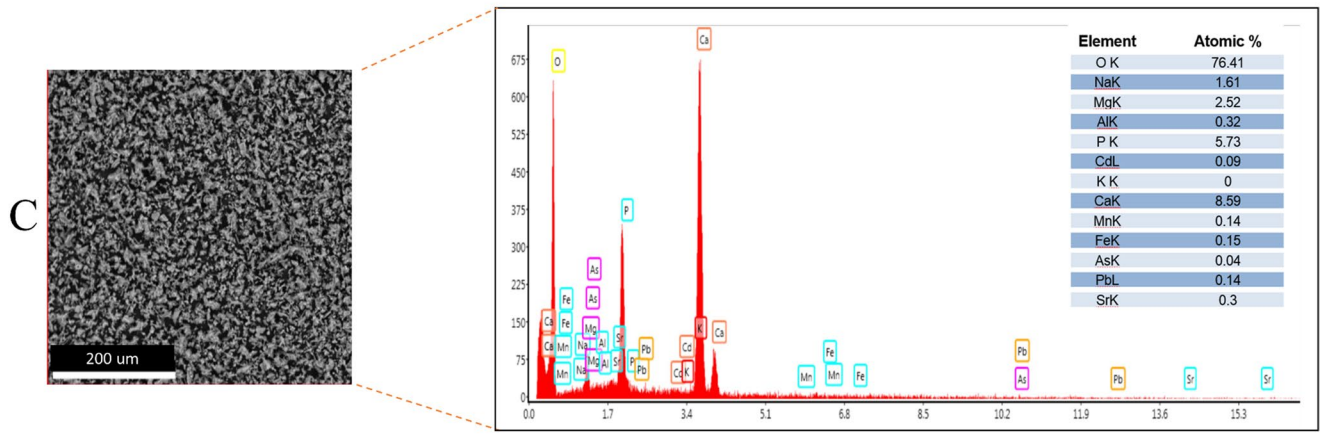
C
200 um
Element Atomic %
O K 76.41
NaK 1.61
MgK 2.52
AlK 0.32
P K 5.73
CdL 0.09
K K 0
CaK 8.59
MnK 0.14
FeK 0.15
AsK 0.04
PbL 0.14
SrK 0.3

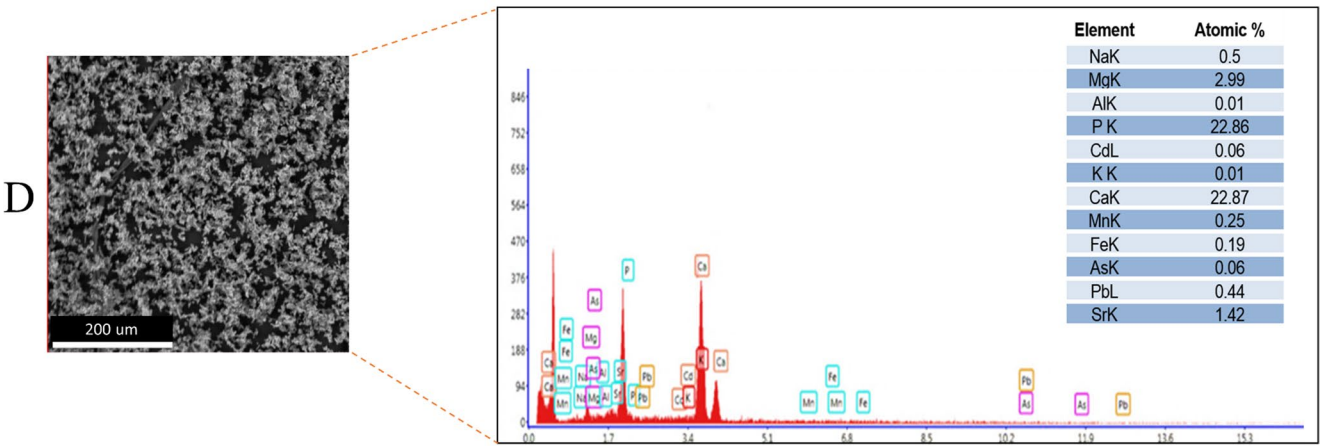
D
200 um
Element Atomic %
NaK 0.5
MgK 2.99
AlK 0.01
P K 22.86
CdL 0.06
K K 0.01
CaK 22.87
MnK 0.25
FeK 0.19
AsK 0.06
PbL 0.44
SrK 1.42

Table 2 Evaluation of Ca/P atomic ratio of synthesised samples using different quantities of H_3PO_4, by EDS analysis in both methods

Sample	Ca/*P* atomic ratio			
	Hot Plate Method		Ultrasonic Method	
	1.0 SA	1.2 SA	1.0 SA	1.2 SA
Shell	2.1	1.54	3.12	1.02
Spine	2.08	1.64	2.1	1.50

spheres, with large, dense and thick particles agglomerating in specific areas (Fig. 7B) (Akram et al. 2014). In contrast, commercial HA powders exhibit agglomeration and a nearly regular shape (Fig. 7C). Bioceramics with unstable structure and interconnected porous morphology, such as rod-shaped crystals are more desirable than cube-shaped crystals for bone tissue engineering and medical applications. The

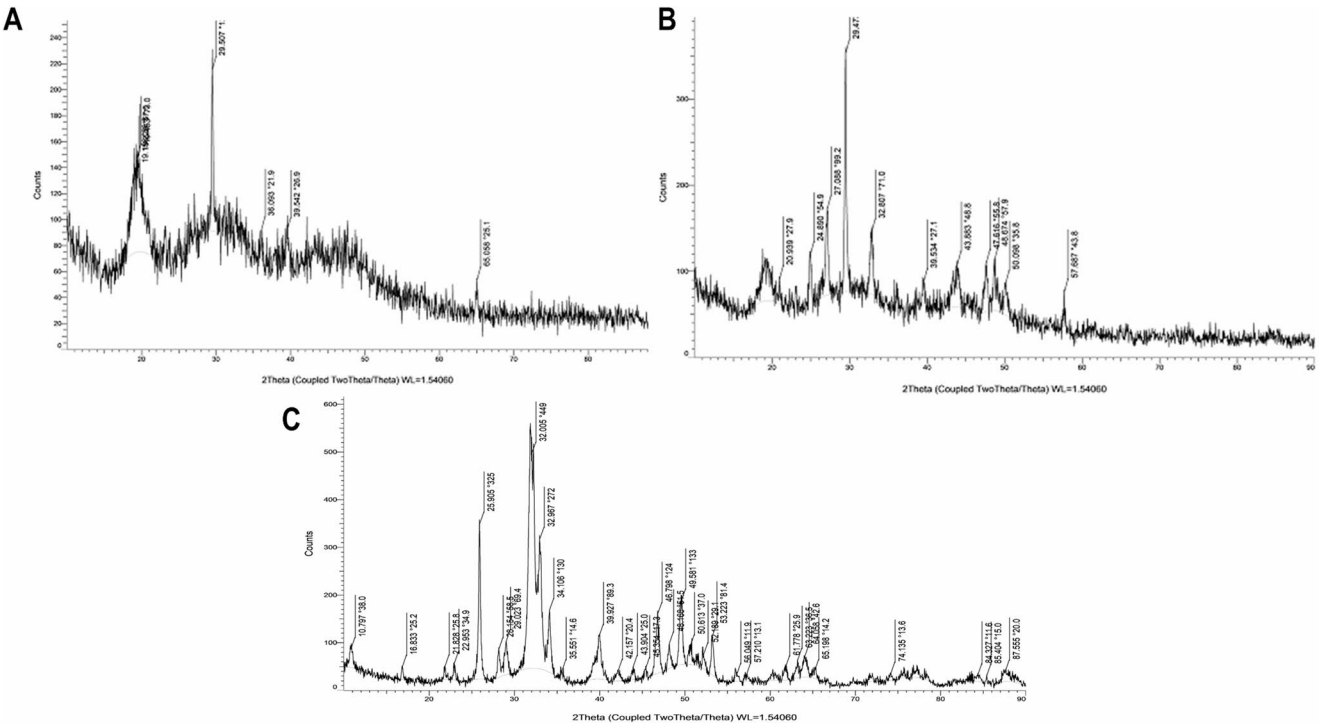

Fig. 5 XRD pattern of synthesised HA from exoskeleton samples, **A** shell and **B** spine; **C** Commercial HA

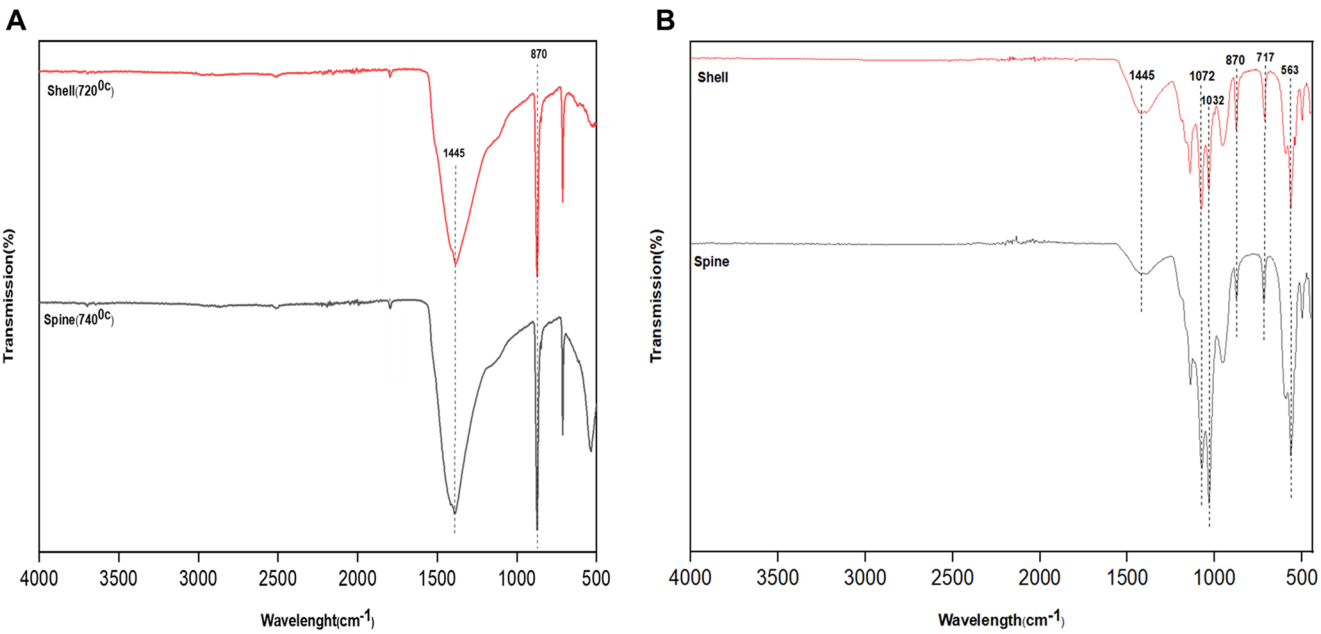

Fig. 6 FTIR spectra of **A** pyrolysed shell and spine samples at 720 °C and 740 °C respectively; **B** HA synthesized from shell and spine samples

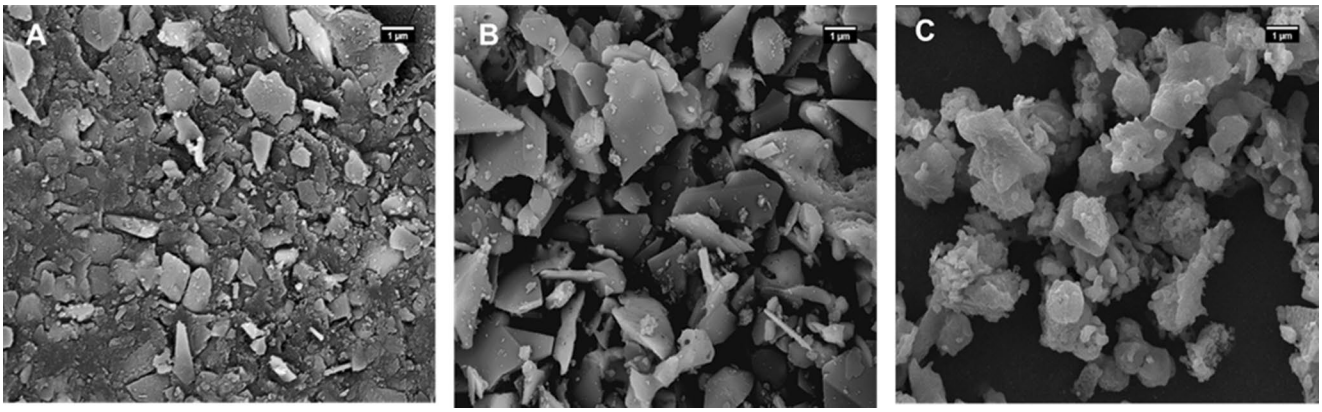

Fig. 7 SEM images of **A** shell-derived HA, **B** spine-derived HA and **C** commercial HA. scale 1 µm

formation of these HA microstructures during the synthesis process is due to the tendency of the particles to crystallize and agglomerate at high temperatures. In general, it can be concluded that high temperatures reduce the probability of grain growth and improve compaction (Fu et al. 2005; Herliansyah and Muzafar 2012).

Figure 8 shows the transmission electron microscope (TEM) images of the commercial HA (Fig. 8A) and spine-derived HA (Fig. 8B) in this study. The TEM image of the commercial HA sample shows narrower size distributions with nanorod morphology and faceted surfaces in the range of 50–100 nm. The TEM image of the spine-derived HA shows spherical particles with a size of 20–50 nm and an agglomerative morphology with irregular shapes. These results suggest that the spine-derived HA has better and larger crystallization structures, which is consistent with the XRD results discussed above and the findings of other researchers (Shavandi et al. 2015).

Hydrogel Characterization

SEM

The microstructure of scaffolds is very effective in their efficiency for bone tissue repair (Ge et al. 2022). Figure 9 shows the morphological properties of the structures of the O-CMC/CEL, O-CMC/CEL/HA, O-CMC/CEL/HA (spine-derived), and O-CMC/CEL/HA (shell-derived) hydrogels. The images showed the 3D porous structures in the hydrogels fabricated from spine-derived HA (Figs. 9C, G) and shell-derived HA (Figs. 9D, H). The distribution and size of pores appeared to be more interconnected and regular in the O-CMC/CEL/HA (spine-derived) hydrogel (Nazeer et al. 2017). The introduction of modified cellulose changes the morphology of chitosan and creates additional cross-links, creating a stronger structure in the hydrogels. This interaction contributes to the formation of stronger and stiffer polymer chains between chitosan and cellulose and subsequently increases the three-dimensional structure and mechanical properties (Phan et al. 2019). Furthermore, the surface of the hydrogels showed a regular distribution of HA crystals (Zhou et al. 2018). Compared to control and commercial HA, the skeleton-derived HA containing hydrogels showed a more porous structure with an average pore size of approximately 105 µm, which facilitate cell adhesion within the hydrogels (Dorozhkin 2009a).

FTIR

In the Fourier transform infrared (FTIR) spectrum of hydrogels in Fig. 10, it is observed that the bands at 1000 cm^{-1} are due to the vibrational motion of the phosphate group (PO_4) within the structure of hydroxyapatite (Danylchenko et al. 2009; Bakan et al. 2013). Furthermore, the peak at

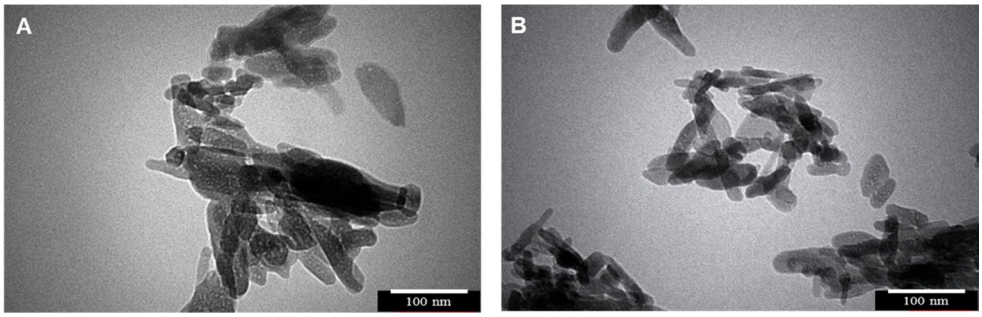

Fig. 8 TEM micrographs of the HA powders of **A** commercial HA and **B** spine-derived HA. scale 100 nm

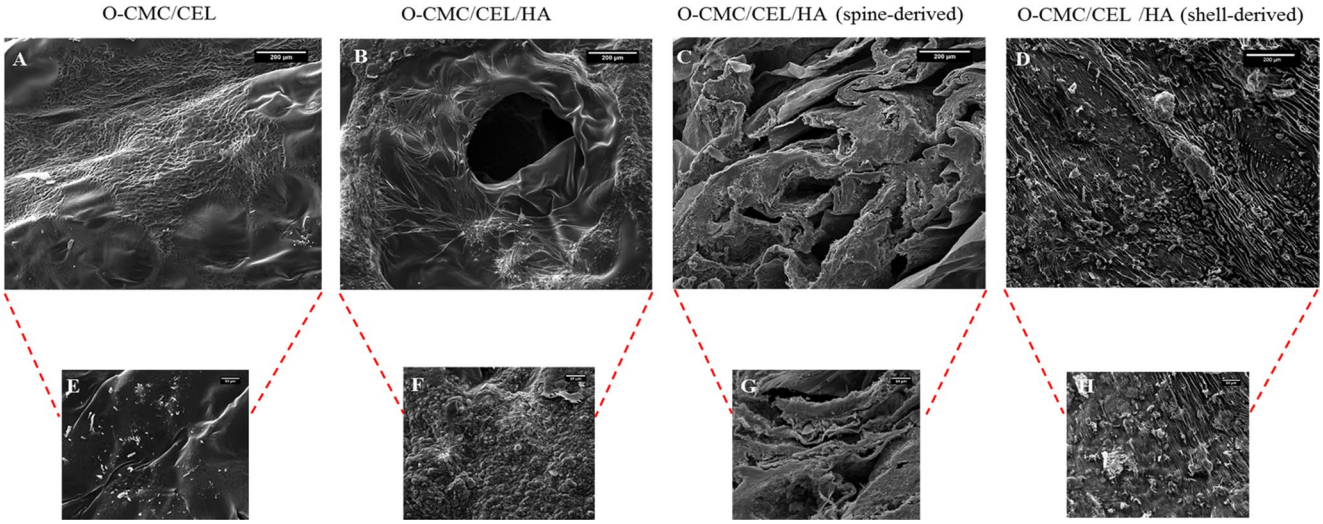

Fig. 9 SEM Images of the structures of the hydrogels. **A** and **E** O-CMC/CEL, **B** and **F** O-CMC/CEL/HA, **C** and **G** O-CMC/CEL/HA (spine-derived) and **D** and **H** O-CMC/CEL/HA (shell-derived) with different magnification at 200 µm and 50 µm

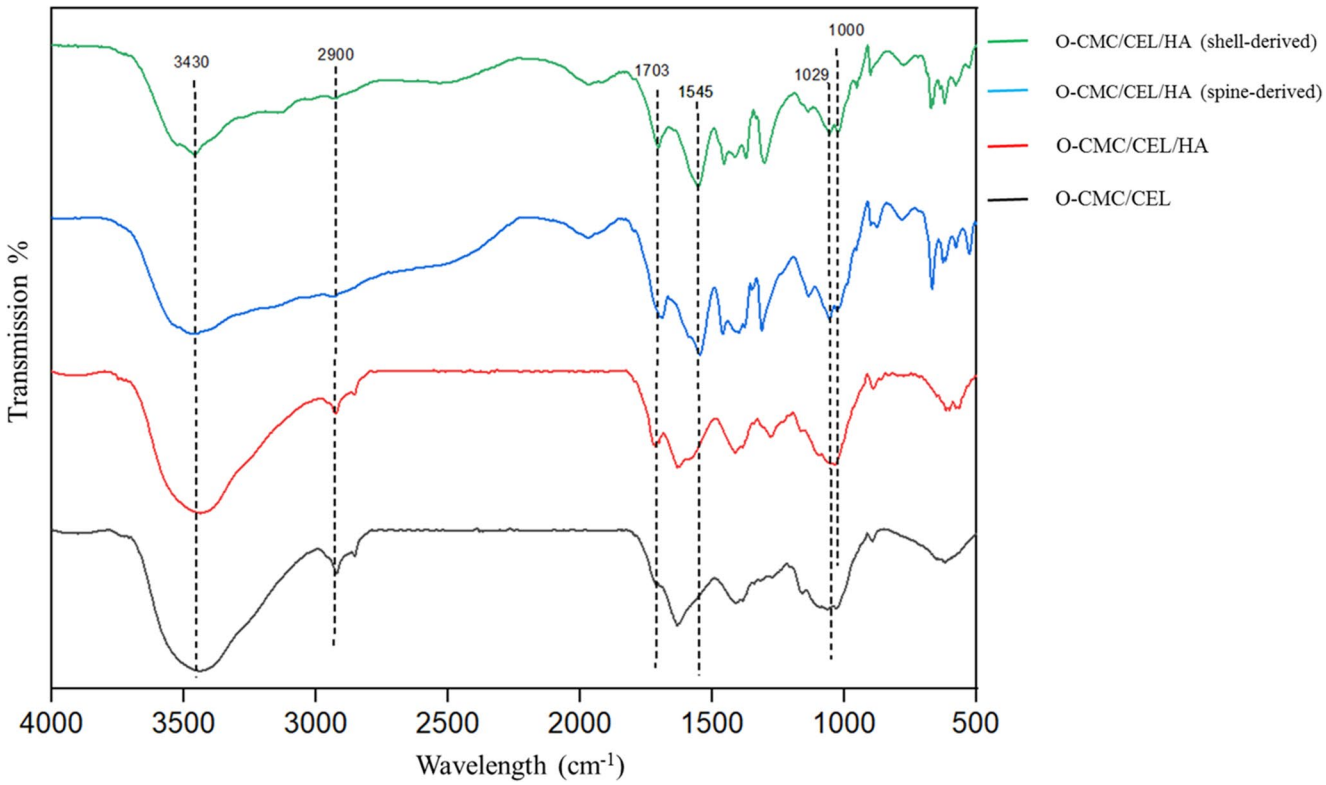

Fig. 10 Fourier transform infrared spectrum (FTIR) of O-CMC/CEL, O-CMC/CEL/HA, O-CMC/CEL/HA (spine-derived) and O-CMC/CEL/HA (shell-derived) hydrogels

a wavelength of 1050 cm^{-1} could be related to the presence of chitosan-hydroxyapatite compounds (CS-HA) (Tanase et al. 2009). The presence of a peak at 1640 cm^{-1} is attributed to the amide I group and also corresponds to the bending vibrations of NH_2 at 1545 cm^{-1} (Kumar-Krishnan et al. 2014). The changes in the position and intensity of the peaks between 3400 cm^{-1} and 3276 cm^{-1} provide evidence for a reaction between the amino and hydroxyl groups on the surface of HA (Sanchez et al. 2018). Furthermore, the peak observed at 1545 cm^{-1} is suggestive then an interaction between the NH_2 groups of chitosan and HA (Kumar-Krishnan et al. 2014). The symmetrical stretching

vibration of CH-CH_2 is observed at around 2900 cm^{-1}. The bands associated with cellulose are in the spectral range of 1000∼1200 cm^{-1} (Ibrahim et al. 2011).

Contact Angle

This particular test was chosen for its ability to accurately measure the contact angle of water on solid surfaces. By performing these experiments at room temperature, the influence of thermal effects on the water contact angle could be minimized, ensuring that the results obtained are mainly due to the intrinsic properties of the dry hydrogels. As shown in Fig. 11, the average contact angle with water on the hydrogels included: O-CMC/CEL (30.540), O-CMC/CEL/HA (24.440), O-CMC/CEL/HA (shell-derived) (20.420) and O-CMC/CEL/HA (spine-derived) (17.400). The addition of HA to the hydrogel resulted in an irregular surface, which is due to the inherent properties of HA (Jiang et al. 2013). However, the incorporation of chitosan with HA led to an improvement in the hydrophilicity of the hydrogel due to the presence of polar groups in the chitosan. This improvement in hydrophilicity was further confirmed by the decrease in water contact angle in the HA (shell-derived) and HA (spine-derived) containing hydrogels. Notably, all hydrogels, including those containing skeleton-derived HA, showed significant differences ($p<0.0001$) compared to the control group. Furthermore, the HA (spine-derived)-containing hydrogel exhibited the lowest contact angle among all hydrogels. Such results suggest that the addition of HA to hydrogels influences not only the surface properties but also the hydrophilic properties, thus providing potential advantages in various applications (Jolly et al. 2021; Tang et al. 2023a).

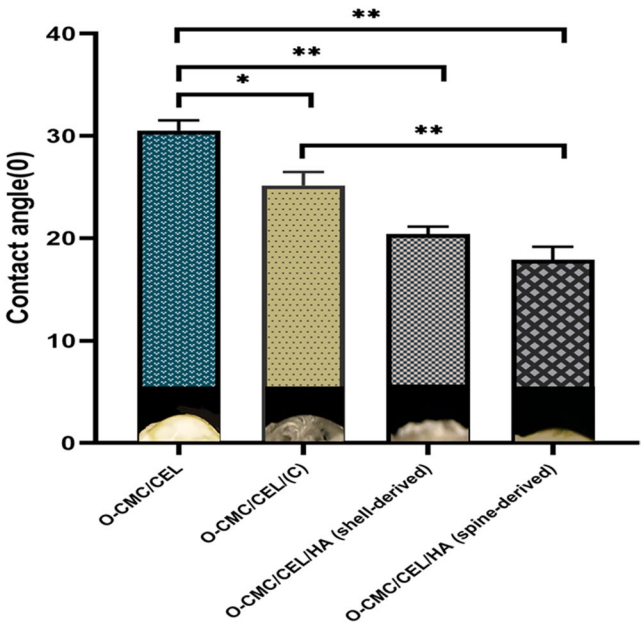

Fig. 11 Water contact angle in hydrogels with different HA

Swelling

Figure 12 shows the swelling ability of the synthesized hydrogels. Water absorption in hydrogels was calculated at 15 min interval for one hour and then at 1 h intervals. All hydrogels had a high water absorption between 50 and 80% in the first 15 min and their swelling rate remained almost constant until the end of the period. In the first 15 min, the O-CMC/CEL hydrogel showed the highest water absorption and the O-CMC/CEL/HA hydrogel showed the lowest (80% vs. 50%). The O-CMC/CEL/HA (spine-derived) and O-CMC/CEL/HA (shell-derived) hydrogels exhibited approximately 75% swelling in the first 15 min. The analysis showed that the swelling ratio of hydrogels containing HA is lower than that of hydrogels without HA. This is likely due to the presence of calcium carbonate in HA. HA components influence the formation of cross-links between chitosan and cellulose. The decrease in hydrophilicity of hydrogels containing hydroxyapatite is due to the cross-linking of calcium and phosphate with hydrophilic OH or NH_2 groups. In addition, by binding the NH_2 of chitosan to the calcium groups, it prevents the formation of hydrogen bonds in the OH groups, so that the swelling ratio of the hydrogels decreases (Peter et al. 2010; Zhou and Lee 2011). At a high swelling ratio, the liquid can penetrate the scaffold more easily (Cao et al. 2015), which causes the hydrogel to decompose more quickly and reduces its stability. The ability of swelling to transfer calcium and phosphate ions to the hydrogel is important for the formation of new tissue (Ghorbani and Roshangar 2021). During hydrolysis and hydrogel stability, swelling promotes nutrient transport and optimal cell attachment, which is important for the bone regeneration process (Liu et al. 2020).

Biological Characterization

Live & Dead

Figure 13A shows the culture of ADSC cells in hydrogels on the 1 st, 3rd and 15th days. Cell viability was evaluated by live/dead staining, with live cells scored with green color and dead cells scored with red color. In addition, the green color indicates cell penetration into the hydrogel and survival. The number of cells increased after 15 days in all groups, demonstrating cell viability and increased proliferation (Moreira et al. 2016). The cell proliferation tendency was greater in the O-CMC/CEL/HA (spine-derived) and O-CMC/CEL/HA (shell-derived) scaffolds than in the O-CMC/CEL and O CMC/CEL/HA scaffolds,

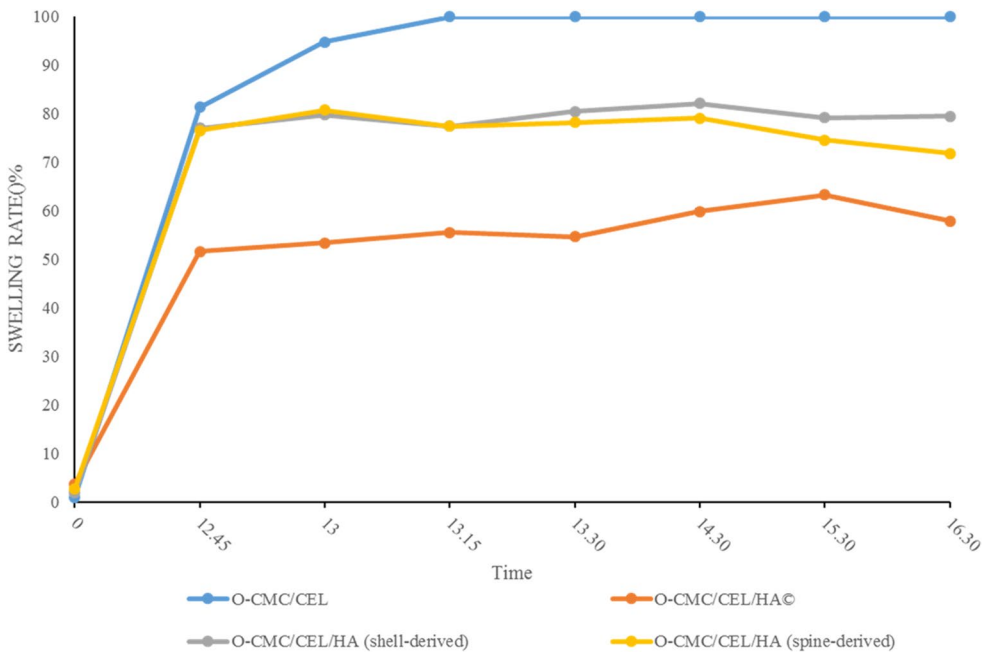

Fig. 12 Swelling ratio for each hydrogel after 4 h of immersion. The first hour with a time interval every 15 min, from the second hour onwards with a time interval every 1 h

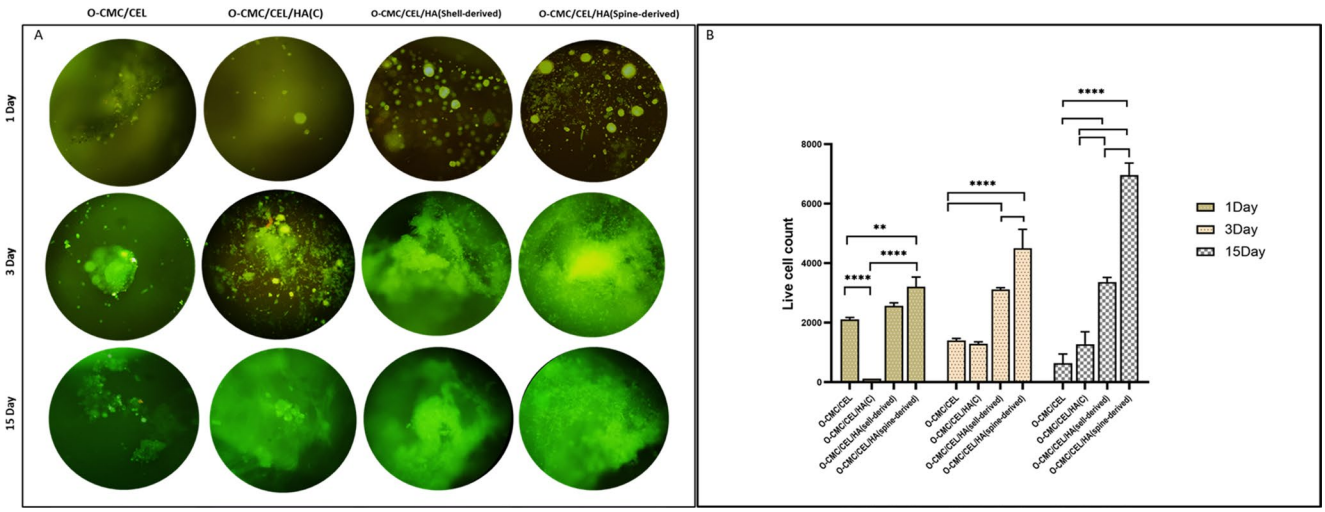

Fig. 13 Viability of ADSCs cultured in hydrogels after 1, 3, and 15 days. **A** The green color in the live and dead staining shows the density of living cells; and **B** counting the number of live cells in live/dead staining with software ($P < 0.05$). scale 10 µm

that confirming sufficient cell adhesion (Fig. 13B). Live cell counting with the software showed that the number of live cells on the O-CMC/CEL/HA (spine-derived) scaffold compared to the O-CMC/CEL/HA (shell-derived) scaffold on days 1, 3 and 15 increased significantly ($P \leq 0.0001$). On the third day, survival and cell proliferation on the O-CMC/CEL/HA (spine-derived) and O-CMC/CEL/HA (shell-derived) scaffolds were significantly increased compared to O-CMC/CEL ($P \leq 0.0001$). Furthermore, cell proliferation at day 3 in CMC/CEL/HA (spine-derived) hydrogel was also significant ($P \leq 0.0001$) compared to O-CMC/CEL/HA (shell-derived). At day 15, the increase in cell proliferation on O-CMC/CEL/HA (spine-derived) and O-CMC/CEL/HA (shell-derived) scaffolds is significant compared to O-CMC/CEL ($P \leq 0.0001$). There was a homogeneous cell distribution throughout the entire trabecular of the scaffold and an increase in cell number during the culture period. In addition, the surface properties and electrostatic charge of the scaffolds cause cell orientation, which plays an important role in cell adhesion and proliferation. Chitosan is a natural hydrophilic polymer that contains special amino groups that attract special cell-binding proteins. Through the deposition of apatite and chitosan, increases bone formation in the body and also causes the growth of osteoblasts in vitro (Bushra et

al. 2023). The alignment of cells around the HA particles has a positive effect on increasing cell number, which may be due to the effect of bioactivity (Bacakova et al. 2011; Walker et al. 2013; Uswatta et al. 2016). The increase in the number of viable cells indicates that composite scaffolds with interconnected pores facilitate the distribution of nutrients and oxygen to cells (Iqbal et al. 2017). The number of cells on pure chitosan scaffolds and on scaffolds containing sea urchin-derived HA was calculated, and it was confirmed that the addition of HA matrix to chitosan is beneficial for cell colonization. The number of cells in the HA-containing composites synthesized from the spine of the sea urchin is greater than that of its shell and the pure chitosan structure. Therefore, it is possible to confirm the positive effect of hydroxyapatite on cell proliferation as a bioactive component (Rogina et al. 2016; Przekora et al. 2021). In fact, these results suggested that HA synthesized from sea urchin spine as a marine resource can be introduce as a bioactive material promote positive biological properties or capabilities for tissue engineering especially bone tissue.

Real-Time PCR

The expression of key osteogenic markers, RUNX2 and type I collagen (COL1), was evaluated after 21 days of culture on the fabricated scaffolds to assess their osteogenic potential (Fig. 14). RUNX2 gene expression was a significant difference in the O-CMC/CEL/HA, O-CMC/CEL/HA (spine-derived), and O-CMC/CEL/HA (shell-derived) scaffolds when Comparison with the O-CMC/CEL group ($P = 0.0001$). Among the composite materials, the O-CMC/CEL/HA (spine-derived) scaffold showed higher gene expression than the other hydrogels. Furthermore, three scaffolds, O-CMC/CEL/HA, O-CMC/CEL/HA (spine-derived), and O-CMC/CEL/HA (shell-derived), showed a significant increase in the RUNX2 gene ($P < 0.0001$). The observed changes in collagen1 gene expression in the O-CMC/CEL/HA (spine-derived) scaffold were also significant ($P < 0.02$) compared to the O-CMC/CEL group.

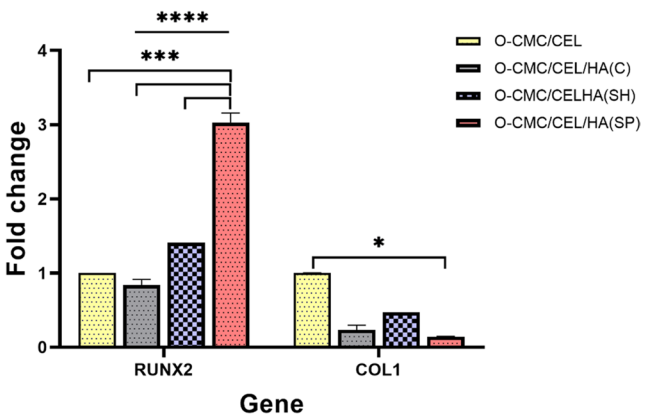

Fig. 14 Evaluation of changes in the expression of osteogenic genes in 21 days from ADSCs cultured on hydrogels ($P < 0.05$)

The process of bone formation involves three phases, namely proliferation, extracellular matrix maturation and mineralization, and collagen secretion in the cancellous bone increases during the phase of primary osteoblast differentiation. RUNX2 is widely recognized as a master transcription factor for early osteoblast commitment (Li et al. 2011; Huang et al. 2020). The observed upregulation of this gen suggests that the HA-containing scaffolds, particularly those derived from sea urchin spines, can improve bone regeneration more effectively than other composite materials (Franceschi and Xiao 2003; Moshaverinia et al. 2014). Furthermore, the use of chitosan promote the expression of osteogenic genes, especially RUNX2, compared to the control group (Fattahi et al. 2023). Hydroxyapatite (HA) plays a critical role in bone metabolism by actively promoting osteogenic activity and providing essential cues for bone regeneration (Parisi et al. 2019, 2020). Also, the cellulose and O-CMC matrix creates a nanofibrous architecture resembling collagen fibrils, activating mechanotransduction pathways that converge on osteogenic transcription factors (Narayanan 2025). Variations in osteogenesis-related gene expression results could potentially be due to discrepancies in HA composition within composite materials.

The sustained RUNX2 expression at day 21, while typical of early differentiation, indicates distinctly different kinetics in our 3D system. Cells were cultured in culture medium (DMEM-HG) supplemented with 15% FBS and 1% antibiotics (penicillin/streptomycin), without osteogenic supplements, meaning the scaffold provided the intrinsic cues for differentiation (Noory et al. 2025). The porous, three-dimensional architecture of the O-CMC/CEL/HA hydrogel creates a heterogeneous microenvironment where cells in deeper regions may exhibit delayed differentiation kinetics compared to those on the surface (Edmondson et al. 2014). This spatial asynchrony, a well-documented phenomenon in 3D cultures (Catoira et al. 2019; Shen et al. 2021), can account for the sustained RUNX2 expression at this later time point. Moreover, in such complex scaffold environments, RUNX2's continued presence can remain crucial for maintaining the osteogenic phenotype and regulating late-stage markers, as differentiation timelines are prolonged due to structural complexity (Komori 2024). Furthermore, the persistence of RUNX2 at this stage as a transitional phase from maturation to mineralization, indicates that the transcriptional machinery for osteogenesis remains active, ensuring progression toward mineralization (Teplyuk et al. 2009; Chan et al. 2021; Komori 2024). This pattern is logically complemented by the observed state of COL1 expression, as its natural decline aligns with the cellular shift from

matrix synthesis to mineralization. The combination of sustained RUNX2 and modulated COL1 thus suggests a coordinated progression through the osteogenic lineage, consistent with studies on similar composite scaffolds (Moshaverinia et al. 2014; Mazzoni et al., 2021; Noory et al. 2025).

The expression of these markers at day 21, while indicative of osteogenic commitment, does not constitute definitive evidence of terminal differentiation. To fully establish the osteoinductive efficacy of these scaffolds, future work must include a more comprehensive analysis. Some limitations of this study include the absence of a positive control group cultured in an osteogenic medium, the lack of assessment of late-stage differentiation markers, such as Osteocalcin, Alkaline Phosphatase activity, and matrix mineralization (e.g., via Alizarin Red staining), which are needed to confirm the progression to mature bone formation in future studies (Suchanecka et al. 2025).

Conclusion

This study successfully demonstrated the synthesis of hydroxyapatite (HA) from sea urchin exoskeletal components (shell and spine), utilizing their calcium carbonate content as a sustainable precursor. Material characterization indicated the effective conversion of the precursor to HA, with the resulting powder exhibiting a suitable microstructure. The resulting HA was incorporated into chitosan-cellulose hydrogels and melded into 3D-printed PCL frames to evaluate their physicochemical properties and biological performance. SEM analysis indicated that composite hydrogels possessed a suitable morphology, characterized by a porous and interconnected structure capable of supporting nutrient transport. FTIR analysis of the hydrogels indicated the presence of hydroxyapatite in combination with chitosan. Among the tested composites, the O-CMC/CEL/HA (spine-derived) hydrogel exhibited suitable microstructural features and enhanced hydrophilicity, as evidenced by its lowest measured water contact angle. Furthermore, it supported cell attachment and proliferation, and led to the upregulation of osteogenic markers such as Runx2 and COL1 in ADSCs cultured on the hydrogel, as measured by real-time PCR, suggesting a potential for osteogenic support. Overall, the composite hydrogels demonstrated biocompatibility based on the observed cellular responses and represent an eco-friendly platform for bone tissue engineering. However, due to the absence of a defined differentiation medium and the late expression of Runx2, further studies using controlled differentiation protocols and in vivo models are recommended to validate their osteogenic potential and clinical applicability.

Acknowledgements The study was performed with the cooperation of the Faculty of Marine Science and Technology of the University of Hormozgan, Bandar Abbas, Iran. This study was funded by the Iran National Science Foundation under the 98024691 Program. Also, the authors would like to thank Dr. Hakimeh Zali (Unite of Advanced Technologies in Medicine, Shahid Beheshti University of Medical Sciences, Tehran, Iran).

Author Contributions Sara Jamshidizadeh, Writing – original draft, Investigation, Formal analysis, Data curation; Narges Amrollahi Biuki, Writing– review & editing, Supervision, Project administration, Methodology, Funding acquisition, Conceptualization; Maroof Zarei, Supervision, Formal analysis.

Data Availability Data will be made available on request.

Declarations

Competing Interests The authors declare no competing interests.

References

Agbeboh N, Oladele I, Daramola O, Adediran A, Olasukanmi O, Tanimola M (2020) Environmentally sustainable processes for the synthesis of hydroxyapatite. Heliyon. https://doi.org/10.1016/j.heliyon.2020.e03765

Akram M, Ahmed R, Shakir I, Ibrahim WAW, Hussain R (2014) Extracting hydroxyapatite and its precursors from natural resources. J Mater Sci 49:1461–1475

Ashwitha A, Thamizharasan K, Bhatt P (2020) Optimization of hydroxyapatite (HAp) extraction from scales of sardinella longiceps and its conjugative effect with immunostimulants. SN Appl Sci 2:1–8

Bacakova L, Filova E, Parizek M, Ruml T, Svorcik V (2011) Modulation of cell adhesion, proliferation and differentiation on materials designed for body implants. Biotechnol Adv 29:739–767

Bahrololoom M, Javidi M, Javadpour S, Ma J (2009) Characterisation of natural hydroxyapatite extracted from bovine cortical bone ash. J Ceram Process Res 10:129–138

Bakan F, Lacin O, Sarac H (2013) A novel low temperature sol–gel synthesis process for thermally stable nano crystalline hydroxyapatite powder. Technology 233:295–302

Bushra A, Subhani A, Islam N (2023) A comprehensive review on biological and environmental applications of chitosan-hydroxyapatite biocomposites. Open Access, Composites Part C, p 100402

Cao H et al (2015) Fish collagen-based scaffold containing PLGA microspheres for controlled growth factor delivery in skin tissue engineering. Colloids and Surfaces B: Biointerfaces 136:1098–1106

Carroll AR, Copp BR, Davis RA, Keyzers RA, Prinsep MR (2020) Marine natural products natural product. Reports 37:175–223

Carvalho DN, Gonçalves C, Sousa RO, Reis RL, Oliveira JM, Silva TH (2024) Extraction and purification of biopolymers from marine origin sources envisaging their use for biotechnological applications. Mar Biotechnol 26:1079–1119

Catoira MC, Fusaro L, Di Francesco D, Ramella M, Boccafoschi F (2019) Overview of natural hydrogels for regenerative medicine applications. J Mater Sci Mater Med 30:115

Chan WCW, Tan Z, To MKT, Chan D (2021) Regulation and role of transcription factors in osteogenesis. Int J Mol Sci 22:5445

Choi AH, Macha IJ, Akyol S, Cazalbou S, Ben-Nissan B (2017) Nanostructured calcium phosphates for drug, gene, DNA and protein delivery and as anticancer chemotherapeutic devices. Clinical Applications of Biomaterials: State-of-the-Art Progress, Trends, and Novel Approaches. pp 227–256

Danylchenko SM, Kalinkevich OV, Pogorelov MV (2009) Chitosan–hydroxyapatite composite biomaterials made by a one step co-precipitation method: preparation, characterization and in vivo tests

Dorozhkin SV (2009a) Calcium orthophosphate-based biocomposites and hybrid biomaterials. J Mater Sci 44:2343–2387

Dorozhkin SV (2009b) Calcium orthophosphates in nature, biology and medicine. Materials 2:399–498

Edmondson R, Broglie JJ, Adcock AF, Yang L (2014) Three-dimensional cell culture systems and their applications in drug discovery and cell-based biosensors. Assay Drug Dev Technol 12:207–218

Fattahi R, Soleimani M, Khani M-M, Rasouli M, Hosseinzadeh S (2023) A three-dimensional structure with osteoconductive function made of O-carboxymethyl Chitosan using aspirin as a cross-linker international. J Polym Mater Polym Biomaterials:1–17

Ferraz M, Monteiro F, Manuel C (2004) Hydroxyapatite nanoparticles: a review of preparation methodologies. J Appl Biomater Biomech 2:74–80

Franceschi RT, Xiao G (2003) Regulation of the osteoblast-specific transcription factor, Runx2: responsiveness to multiple signal transduction pathways. J Cell Biochem 88:446–454

Fu B, Sun X, Qian W, Shen Y, Chen R, Hannig M (2005) Evidence of chemical bonding to hydroxyapatite by phosphoric acid esters. Biomaterials 26:5104–5110

Ge Y-W, Chu M, Zhu Z-Y, Ke Q-F, Guo Y-P, Zhang C-Q, Jia W-T (2022) Nacre-inspired magnetically oriented micro-cellulose fibres/nano-hydroxyapatite/chitosan layered scaffold enhances pro-osteogenesis and angiogenesis. Mater Today Bio 16:100439

Ghaemy M, Naseri M (2012) Synthesis of chitosan networks: swelling, drug release, and magnetically assisted BSA separation using Fe3O4 nanoparticles. Carbohydr Polym 90:1265–1272

Ghorbani M, Roshangar L (2021) Construction of collagen/nanocrystalline cellulose based-hydrogel scaffolds: synthesis, characterization, and mechanical properties evaluation. Int J Polym Mater Polym Biomater 70:142–148

Gómez Vázquez NS, Luque Morales PA, Gomez Gutierrez CM, Nava Olivas OdJ, Villarreal Sánchez RC, Vilchis Nestor AR, Chinchillas Chinchillas MdJ (2020) Hydroxyapatite biosynthesis obtained from sea urchin spines (*strongylocentrotus purpuratus*): effect of synthesis temperature. Processes 8:486

Gunduz O, Sahin Y, Agathopoulos S, Ben-Nissan B, Oktar FN (2014) A new method for fabrication of nanohydroxyapatite and TCP from the sea snail *Cerithium vulgatum*. J Nanomater 2014:1–1

Guo P, Liu X, Zhang P, He Z, Li Z, Alini M, Richards RG, Grad S, Stoddart MJ, Zhou G, Zou X (2022) A single-cell transcriptome of mesenchymal stromal cells to fabricate bioactive hydroxyapatite materials for bone regeneration. Bioact Mater 9:281–298

Gupta P, Sharma S, Jabin S, Jadoun S (2023) Chitosan nanocomposite for tissue engineering and regenerative medicine: A review. Int J Biol Macromol :127660

Hasan MS, Ahmed I, Parsons AJ, Rudd CD, Walker GS, Scotchford CA (2013) Investigating the use of coupling agents to improve the interfacial properties between a resorbable phosphate glass and polylactic acid matrix. J Biomater Appl 28:354–366

Heidari F, Bahrololoom ME, Vashaee D, Tayebi L (2015) In situ preparation of iron oxide nanoparticles in natural hydroxyapatite/chitosan matrix for bone tissue engineering application. Ceram Int 41:3094–3100

Herliansyah MK, Muzafar C (2012) Tontowi AE Natural bioceramics bone graft: A comparative study of calcite hydroxyapatite, gypsum hydroxyapatite, bovine hydroxyapatite and cuttlefish shell hydroxyapatite. In: Proceedings of the asia pacific industrial engineering & Management systems conference, pp 1137–1146

Hernández-Ruiz KL, López-Cervantes J, Sánchez-Machado DI, del Rosario Martínez-Macias M, Correa-Murrieta MA, Sanches-Silva A (2022) Hydroxyapatite recovery from fish byproducts for biomedical applications sustainable. Chemistry and Pharmacy 28:100726

Huang Z et al (2020) Strontium/chitosan/hydroxyapatite/norcantharidin composite that inhibits osteosarcoma and promotes osteogenesis in vitro. BioMed Research International 2020

Hussain S, Sabiruddin K (2021) Effect of heat treatment on the synthesis of hydroxyapatite from Indian clam seashell by hydrothermal method. Ceram Int 47:29660–29669

Ibrahim M, Osman O, Mahmoud AA (2011) Spectroscopic analyses of cellulose and chitosan: FTIR and modeling approach. J Comput Theor Nanosci 8:117–123

Ikeda T, Kasai M, Tatsukawa E, Kamitakahara M, Shibata Y, Yokoi T, Ioku K (2014) A bone substitute with high affinity for vitamin D-binding protein-relationship with niche of osteoclasts. J Cell Mol Med 18(1):170–180

Iqbal H et al (2017) Chitosan/hydroxyapatite (HA)/hydroxypropylmethyl cellulose (HPMC) spongy scaffolds-synthesis and evaluation as potential alveolar bone substitutes. Colloids and Surfaces B: Biointerfaces 160:553–563

Irfan M, Suprajaa P, Baraneedharan P, Reddy B (2020) A comparative study of nanohydroxyapetite obtained from natural shells and wet chemical process. J Mater Sci Surf Eng 7:938–943

Jiang H, Zuo Y, Zou Q, Wang H, Du J, Li Y, Yang X (2013) Biomimetic spiral-cylindrical scaffold based on hybrid chitosan/cellulose/nano-hydroxyapatite membrane for bone regeneration. ACS Appl Mater Interfaces 5:12036–12044

Jolly R et al (2021) Synthesis and characterization of β-cyclodextrin/carboxymethyl chitosan/hydroxyapatite fused with date seed extract nanocomposite scaffolds for regenerative bone tissue engineering. Mater Adv 2:5723–5736

Karacan I, Gunduz O, Ozyegin LS, Gökce H, Ben-Nissan B, Akyol S, Oktar FN (2018) The natural nano-bioceramic powder production from organ pipe red coral (*Tubipora musica*) by a simple chemical conversion method. J Aust Ceram Soc 54:317–329

Kavasi R-M, Coelho CC, Platania V, Quadros PA, Chatzinikolaidou M (2021) In vitro biocompatibility assessment of nano-hydroxyapatite. Nanomaterials 11:1152

Khiri MZA et al (2019) Crystallization behavior of low-cost biphasic hydroxyapatite/β-tricalcium phosphate ceramic at high sintering temperatures derived from high potential calcium waste sources. Results Phys 12:638–644

Komalakrishna H, Jyoth TS, Kundu B, Mandal S (2017) Low temperature development of nano-hydroxyapatite from *Austromegabalanus psittacus*, Star fish and Sea urchin. Mater Today Proc 4:11933–11938

Komori T (2024) Regulation of skeletal development and maintenance by Runx2 and Sp7. Int J Mol Sci 25:10102

Kumar GS, Thamizhavel A, Girija E (2012) Microwave conversion of eggshells into flower-like hydroxyapatite nanostructure for biomedical applications. Mater Lett 76:198–200

Kumar-Krishnan S et al (2014) Novel gigahertz frequency dielectric relaxations in chitosan films. Soft Matter 10:8673–8684

Kusmanto F et al (2008) Development of composite tissue scaffolds containing naturally sourced mircoporous hydroxyapatite. Chem Eng J 139:398–407

Laonapakul T (2015) Synthesis of hydroxyapatite from biogenic wastes. Eng Appl Sci Res 42:269–275

Lett JA et al (2019) Drug leaching properties of Vancomycin loaded mesoporous hydroxyapatite as bone substitutes. Processes 7:826

Li S et al (2011) The role of runt-related transcription factor 2 (Runx2) in the late stage of odontoblast differentiation and dentin formation. Biochem Biophys Res Commun 410:698–704

Li T-T, Ling L, Lin M-C, Jiang Q, Lin Q, Lin J-H, Lou C-W (2019) Properties and mechanism of hydroxyapatite coating prepared by electrodeposition on a braid for biodegradable bone scaffolds. Nanomaterials 9:679

Liu Y, Gu J, Fan D (2020) Fabrication of high-strength and porous hybrid scaffolds based on nano-hydroxyapatite and human-like collagen for bone tissue regeneration. Polymers 12:61

Macha IJ, Ozyegin L, Chou J, Samur R, Oktar F, Ben-Nissan B (2013) An alternative synthesis method for Di calcium phosphate (Monetite) powders from mediterranean mussel (*Mytilus galloprovincialis*) shells. Journal of the Australian Ceramic Society

Macha IJ, Boonyang U, Cazalbou S, Ben-Nissan B, Charvillat C, Oktar FN, Grossin D (2015) Comparative study of coral Conversion, part 2: microstructural evolution of calcium phosphate. Journal of the Australian Ceramic Society

Malik MH et al (2020) Thyroxine-loaded chitosan/carboxymethyl cellulose/hydroxyapatite hydrogels enhance angiogenesis in in-ovo experiments. Int J Biol Macromol 145:1162–1170

Mancilla-Sanchez E, Gómez-Gutiérrez CM, Guerra-Rivas G, Soto-Robles CA, Vilchis-Nestor AR, Vargas E, Luque PA (2019) Obtaining hydroxyapatite from the exoskeleton and spines of the purple sea urchin *Strongylocentrotus purpuratus*. Int J Appl Ceram Technol 16:438–443

Martinelli G, Marzorati S, Roncoroni M, Magro L, Brilli M, Beretta G, Colombo G, Melotti L, Carolo A, Zivelonghi G, Farris S (2025) Seas of renewal: turning sea urchin waste into Polyhydroxynaphtoquinone-Collagen biomaterials for regenerative medicine. Mar Biotechnol 27:1–17

Mazzoni E, Mazziotta C, Iaquinta MR, Lanzillotti C, Fortini F, D'Agostino A, Trevisiol L, Nocini R, Barbanti-Brodano G, Mescola A, Alessandrini A (2021) Enhanced osteogenic differentiation of human bone marrow-derived mesenchymal stem cells by a hybrid hydroxylapatite/collagen scaffold. Front Cell Dev Biol 8:610570

Merzendorfer H, Cohen E (2019) Chitin/chitosan: versatile ecological, industrial, and biomedical applications Extracellular Sugar-Based Biopolymers. Matrices:541–624

Miculescu F et al (2017) Facile synthesis and characterization of hydroxyapatite particles for high value nanocomposites and biomaterials. Vacuum 146:614–622

Miculescu F et al (2020) Considerations and influencing parameters in EDS microanalysis of biogenic hydroxyapatite. J Funct Biomater 11:82

Moreira CD, Carvalho SM, Mansur HS, Pereira MM (2016) Thermogelling chitosan–collagen–bioactive glass nanoparticle hybrids as potential injectable systems for tissue engineering. Mater Sci Eng C Mater Biol 58:1207–1216

Moshaverinia A, Chen C, Xu X, Akiyama K, Ansari S, Zadeh HH, Shi S (2014) Bone regeneration potential of stem cells derived from periodontal ligament or gingival tissue sources encapsulated in RGD-modified alginate scaffold. Tissue Eng Part A 20:611–621

Naga S, El-Maghraby H, Mahmoud E, Talaat M, Ibrhim A (2015) Preparation and characterization of highly porous ceramic scaffolds based on thermally treated fish bone. Ceram Int 41:15010–15016

Nandi SK, Kundu B, Mukherjee J, Mahato A, Datta S, Balla VK (2015) Converted marine coral hydroxyapatite implants with growth factors: in vivo bone regeneration. Mater Sci Eng C Mater Biol 49:816–823

Narayanan KB (2025) Nanotopographical features of polymeric nanocomposite scaffolds for tissue engineering and regenerative medicine: a review. Biomimetics 10:317

Nazeer MA, Yilgör E, Yilgör I (2017) Intercalated chitosan/hydroxyapatite nanocomposites: promising materials for bone tissue engineering applications. Carbohydr Polym 175:38–46

Noory P, Farmani AR, Ai J, Bahrami N, Bayat M, Ebrahimi-Barough S, Noory P, Farmani AR, Ai J, Bahrami N, Bayat M, Ebrahimi-Barough S, Farzin A, Shojaie S, Hajmoradi H, Mohamadnia A, Goodarzi A (2025) Enhancing in vitro osteogenic differentiation of mesenchymal stem cells via sustained dexamethasone delivery in 3D-printed hybrid scaffolds based on polycaprolactone-nanohydroxyapatite/alginate-gelatin for bone regeneration. J Biol Eng 19:48

Parisi JR, Fernandes KR, Avanzi IR, Dorileo BP, Santana AD, F, Andrade AL, Gabbai-Armelin PR, Fortulan CA, Trichês EDS, Granito RN, Renno ACM (2019) Incorporation of collagen from marine sponges (spongin) into hydroxyapatite samples: characterization and in vitro biological evaluation. Mar Biotechnol 21:30–37

Parisi JR, Fernandes KR, de Almeida Cruz M, Avanzi IR, de França Santana A, do Vale GCA, de Andra ALM, de Góes CP, Fortulan CA, de Sousa Trichês E, Granito RN (2020) Evaluation of the in vivo biological effects of marine collagen and hydroxyapatite composite in a tibial bone defect model in rats. Mar Biotechnol 22:357–366

Peter M, Ganesh N, Selvamurugan N, Nair S, Furuike T, Tamura H, Jayakumar R (2010) Preparation and characterization of chitosan–gelatin/nanohydroxyapatite composite scaffolds for tissue engineering applications. Carbohydr Polym 80:687–694

Phan D-N, Lee H, Huang B, Mukai Y, Kim I-S (2019) Fabrication of electrospun chitosan/cellulose nanofibers having adsorption property with enhanced mechanical property. Cellulose 26:1781–1793

Pina S, Oliveira JM, Reis RL (2015) Natural-based nanocomposites for bone tissue engineering and regenerative medicine: a review. Adv Mater 27:1143–1169

Przekora A, Kazimierczak P, Wojcik M (2021) Ex vivo determination of chitosan/curdlan/hydroxyapatite biomaterial osseointegration with the use of human trabecular bone explant: new method for biocompatibility testing of bone implants reducing animal tests. Materials Science and Engineering: C 119:111612

Rathje W (1939) Zur Kenntnis der Phosphate I: Über Hydroxylapatit. Bodenkunde und Pflanzenernährung 12:121–128

Rehman I, Bonfield W (1997) Characterization of hydroxyapatite and carbonated apatite by photo acoustic FTIR spectroscopy. J Mater Sci Mater Med 8:1–4

Rogina A, Rico P, Gallego Ferrer G, Ivanković M, Ivanković H (2016) In situ hydroxyapatite content affects the cell differentiation on porous chitosan/hydroxyapatite scaffolds. Ann Biomed Eng 44:1107–1119

Rosa Cegla R-N, Macha IJ, Ben-Nissan B, Grossin D, Heness G, Chung R-J (2014) Comparative study of conversion of coral with ammonium dihydrogen phosphate and orthophosphoric acid to produce calcium phosphates. J Aust Ceram Soc 50:154–161

Ruffini A, Sandri M, Dapporto M, Campodoni E, Tampieri A, Sprio S (2021) Nature-inspired unconventional approaches to develop 3D bioceramic scaffolds with enhanced regenerative ability. Biomedicines 9:916

Sabu U, Logesh G, Rashad M, Joy A, Balasubramanian M (2019) Microwave assisted synthesis of biomorphic hydroxyapatite. Ceram Int 45:6718–6722

Salamanca E, Hsu CC, Yao WL, Choy CS, Pan YH, Teng N-C, Chang W-J (2020) Porcine collagen–bone composite induced osteoblast differentiation and bone regeneration in vitro and in vivo. Polymers 12:93

Sanchez AG et al (2018) Chitosan-hydroxyapatite nanocomposites: effect of interfacial layer on mechanical and dielectric properties. Mater Chem Phys 217:151–159

Sha L, Liu Y, Zhang Q, Hu M, Jiang Y (2011) Microwave-assisted co-precipitation synthesis of high purity β-tricalcium phosphate crystalline powders. Mater Chem Phys 129:1138–1141

Shavandi A, Bekhit AE-DA, Ali A, Sun Z (2015) Synthesis of nano-hydroxyapatite (nHA) from waste mussel shells using a rapid microwave method. Mater Chem Phys 149:607–616

Shavandi A, Wilton V, Bekhit AE-DA (2016) Synthesis of macro and micro porous hydroxyapatite (HA) structure from waste kina (*Evechinus chloroticus*) shells. J Taiwan Inst Chem Eng 65:437–443

Shen BY, Li JX, Wang XF, Zhou Q (2021) Impact of different proportions of 2D and 3D scaffolds on the proliferation and differentiation of human adipose-derived stem cells. J Oral Maxillofac Surg 79:1580-e1

Shi P, Liu M, Fan F, Yu C, Lu W, Du M (2018) Characterization of natural hydroxyapatite originated from fish bone and its biocompatibility with osteoblasts. Mater Sci Engineering: C 90:706–712

Silva TH et al (2012) Materials of marine origin: a review on polymers and ceramics of biomedical interest international. Mater Reviews 57:276–306

Sivakumar PM, Yetisgin AA, Demir E, Sahin SB, Cetinel S (2023) Polysaccharide-bioceramic composites for bone tissue engineering: a review. Int J Biol Macromol. https://doi.org/10.1016/j.ijbiomac.2023.126237

Sorkhi L, Farrokhi-Rad M, Shahrabi T (2019) Electrophoretic deposition of hydroxyapatite–chitosan–titania on stainless steel 316. L Surf 2:458–467

Suchanecka M, Grzelak J, Farzaneh M, Azizidoost S, Dari MAG, Józkowiak M, Kempisty B (2025) Adipose derived stem cells–sources, differentiation capacity and a new target for reconstructive and regenerative medicine. Biomed Pharmacother 186:118036

Suresh Kumar C, Dhanaraj K, Vimalathithan R, Ilaiyaraja P, Suresh G (2020) Hydroxyapatite for bone related applications derived from sea shell waste by simpleprecipitation method. J Asian Ceam Soc 8:416–429

Tanase C, Popa M, Verestiuc L (2009) Chitosan-hydroxyapatite composite obtained by biomimetic method as new bone substitute. In: 2009 Advanced Technologies for Enhanced Quality of Life, IEEE, pp 42–46

Tang S, Jiang L, Jiang Z, Ma Y, Zhang Y, Su S (2023a) Preparation and characterization of a novel Tragacanth Gum/Chitosan/Sr-Nano-Hydroxyapatite. composite membrane. Polymers 15:2942

Tang W et al (2023b) Application of Chitosan and its derivatives in medical materials. Int J Biol Macromol :124398

Teplyuk NM, Zhang Y, Lou Y, Hawse JR, Hassan MQ, Teplyuk VI, Pratap J, Galindo M, Stein JL, Stein GS, Lian JB (2009) The osteogenic transcription factor runx2 controls genes involved in sterol/steroid metabolism, including CYP11A1 in osteoblasts. Mol Endocrinol 23:849–861

Trinkunaite-Felsen J, Birkedal H, Zarkov A, Tautkus S, Stankeviciute Z, Kareiva A (2016) Environmentally benign fabrication of calcium hydroxyapatite using seashells collected in Baltic sea countries: a comparative study. Phosphorus Sulfur Silicon Relat Elem 191:919–925

Uswatta SP, Okeke IU, Jayasuriya AC (2016) Injectable porous nano-hydroxyapatite/chitosan/tripolyphosphate scaffolds with improved compressive strength for bone regeneration. Mater Sci Eng C Mater Biomim Supramol Syst 69:505–512

Vecchio KS, Zhang X, Massie JB, Wang M, Kim CW (2007) Conversion of sea urchin spines to Mg-substituted tricalcium phosphate for bone implants. Acta Biomater 3:785–793

Walker J, Shadanbaz S, Woodfield TB, Staiger MP, Dias G (2013) The in vitro and in vivo evaluation of the biocompatibility of Mg alloys. Biomed Mater 9:015006

Walsh P, Buchanan F, Dring M, Maggs C, Bell S, Walker G (2008) Low-pressure synthesis and characterisation of hydroxyapatite derived from mineralise red algae. Chem Eng J 137:173–179

Wang Z, Jiang S, Zhao Y, Zeng M (2019) Synthesis and characterization of hydroxyapatite nano-rods from oyster shell with exogenous surfactants. Mater Sci Eng C Mater Biomim Supramol Syst 105:110102

Wilton V, Shavandi A , Bekhit A (2016) Synthesis of three dimensional Mg-HA scaffolds from New Zealand sea urchin (*Evechinus chloroticus*) waste shells. In: 10th world biomaterials congress, Montréal, QC, Canada, pp 17–22

Witzler M, Ottensmeyer PF, Gericke M, Heinze T, Tobiasch E, Schulze M (2019) Non-cytotoxic agarose/hydroxyapatite composite scaffolds for drug release. Int J Mol Sci 20:3565

Xing Z, Pang Y, Li E, Zhang JY, Xu D (2024) Preparation and characterisation of zirconia/hydroxyapatite bioactive composites as potential dental implants. J Mater Sci Mater Eng 19:1–13

Yang Y, Yao Q, Pu X, Hou Z, Zhang Q (2011) Biphasic calcium phosphate macroporous scaffolds derived from oyster shells for bone tissue engineering. Chem Eng J 173:837–845

Yar M et al (2016) Production of chitosan PVA PCL hydrogels to bind heparin and induce angiogenesis. Int J Polym Mater Polym Biomater 65:466–476

Zhou H, Lee J (2011) Nanoscale hydroxyapatite particles for bone tissue engineering. Acta Biomater 7:2769–2781

Zhou J, Yao T, Cao D, Lian J, Lu F (2018) In-situ TEM study of radiation-induced amorphization and recrystallization of hydroxyapatite. J Nucl Mater 512:307–313

Ziani S, Meski S, Khireddine H (2014) Characterization of magnesium-doped hydroxyapatite prepared by sol-gel process. Int J Appl Ceram Technol 11:83–91

ARTICLES FOR FACULTY MEMBERS

BONE-DERIVED HYDROXYAPATITE TOOTHPASTE FOR SUSTAINABLE PHARMACEUTICAL AND BIOMEDICAL APPLICATIONS

Microwave-assisted hydrothermal synthesis of hydroxyapatite from fermented fish by-product for removal of lead from contaminated water / Chaiyachet, W., Junggoth, R., Donprajum, T., Yasaka, S., Chaiyachet, R., & Kanchanatip, E.

Beni-Suef University Journal of Basic and Applied Sciences
Volume 14 Issue 116 (2025) Pages 1-22
https://doi.org/10.1186/s43088-025-00704-z
(Database: Springer Nature Link)

Chaiyachet *et al.*
Beni-Suef Univ J Basic Appl Sci (2025) 14:116
https://doi.org/10.1186/s43088-025-00704-z

Beni-Suef University Journal of Basic and Applied Sciences

RESEARCH

Open Access

Microwave-assisted hydrothermal synthesis of hydroxyapatite from fermented fish by-product for removal of lead from contaminated water

Wipada Chaiyachet[1], Rittirong Junggoth[1], Tongpak Donprajum[1*], Sudawadee Yasaka[2], Rungsan Chaiyachet[3] and Ekkachai Kanchanatip[4*]

Abstract

Background Lead contamination in water is a critical global issue, with severe health and environmental impacts. Conventional treatment methods typically rely on chemical precipitation and adsorption using activated carbon. However, these approaches can be costly and prone to generating secondary waste. Hydroxyapatite offers a cleaner alternative for heavy metal adsorption due to its strong affinity for lead and its environmental benignity. Importantly, fish bone waste from Thailand's fermented fish industry is an abundant, sustainable calcium-rich feedstock that can be converted into hydroxyapatite via hydrothermal process. Valorizing this by-product into an effective adsorbent not only addresses waste disposal challenges but also supports circular-economy goals.

Results Hydroxyapatite was successfully synthesized from fermented fish bone using a hydrothermal process, optimizing conditions at 210 °C and a Ca/P ratio of 2 (sample HT9). Characterization revealed that HT9 had the high crystallinity, featuring a thin, porous sheet-like morphology with a specific surface area of 14.08 m^2/g and pore volume of 0.0975 cm^3/g. Key functional groups (PO_4^{3-}, OH^-, CO_3^{2-}) critical for heavy metal adsorption were confirmed. The synthesized HT9 demonstrated excellent lead removal efficiency, achieving 99.6% removal within 60 min at pH 7 and an adsorbent dosage of 2.0 g/L. Pb adsorption on HT9 followed the Langmuir isotherm model ($R^2 = 0.9997$), indicating monolayer adsorption with a maximum capacity of 2.20 mg/g. Kinetic analysis showed the process adhered to a pseudo-second-order model, suggesting chemisorption as the rate-limiting step, with a rate constant of 1.2012 g/mg·min.

Conclusion The results highlight the potential of hydroxyapatite from fermented fish bone waste as a cost-effective, eco-friendly adsorbent for efficient lead removal and promote sustainable water-treatment solutions.

Keywords Hydrothermal, Hydroxyapatite, Adsorption, Heavy metal, Sustainable, Circular economy

*Correspondence:
Tongpak Donprajum
tongdo@kku.ac.th
Ekkachai Kanchanatip
ekkachai.kan@ku.th
Full list of author information is available at the end of the article

1 Introduction

Lead (Pb) contamination in potable and industrial wastewater poses a persistent global health and environmental challenge. High Pb concentrations have been linked to neurological damage, impaired cognitive development, and long-term ecological harm [1]. Traditional remediation methods such as chemical precipitation, ion exchange resins, and activated carbon adsorption have shown varying degrees of success, but their widespread deployment is often constrained by high operational costs, secondary waste production, and limited reusability capacities [2]. Consequently, there is a growing demand for innovative, economically viable, and environmentally benign materials that can efficiently capture lead ions under realistic conditions, especially those derived from by-products and waste streams, to reduce production costs and environmental impacts [3].

Among the diverse adsorbent materials used for water purification, hydroxyapatite (HAp; $Ca_{10}(PO_4)_6(OH)_2$) has gained significant attention as an environmentally friendly solution for removing pollutants from water [4]. HAp is composed primarily of calcium and phosphate, which can be sourced from both synthetic methods and biogenic wastes like chicken bones, eggshells, and fish bones. HAp has demonstrated remarkable efficiency in binding with various heavy metals such as lead (Pb^{2+}), cadmium (Cd^{2+}), copper (Cu^{2+}), and arsenic (As^{5+}) through mechanisms like ion exchange and dissolution–precipitation [5]. Synthetic HAp can be produced via chemical routes; however, such approaches frequently rely on energy-intensive conditions or harsh chemicals, potentially undermining their sustainability advantages [6]. Consequently, the search for alternative, cost-effective, and environmentally benign raw materials for HAp production remains a critical area of research [7]. This has urged a growing interest in converting biogenic waste into valuable HAp, a strategy that aligns with circular-economy principles by turning potential pollutants into functional materials [8].

Thailand is one of Southeast Asia's leading producers of fermented fish products such as Pla-ra. The processing activities generate substantial amounts of by-products, most notably fish bones, which are often discarded as waste. Accumulation of this waste poses persistent environmental and disposal challenges. Because the fermented fish bone waste retains residual flesh, proteins, and lipids, their decomposition releases a high-strength leachate rich in soluble organics (high BOD/COD), nutrients, and fats. Uncontrolled discharge can rapidly depress dissolved oxygen and degrade water quality. Under anaerobic conditions, putrefaction also releases strong odor and nuisance gases like ammonia, hydrogen sulfide, and volatile mercaptans, often prompting community complaints and regulatory action. Additionally, the waste's high salinity inhibits its conventional biological treatment by suppressing microbial activity and reducing removal efficiency. From a resource recovery perspective, however, these same fish bones are intrinsically rich in calcium and phosphorus, making them an excellent precursor for HAp. Converting the waste into HAp transform liability into a value-added material, providing a low-cost adsorbent for water treatment while mitigating odor, and leachate generation and reducing landfill pressures, this valorization pathway aligns with circular-economy principles and green chemistry approaches by closing material loops, reducing on mined precursors, and lowering the environmental footprint of both waste management and water purification.

Technologically, hydrothermal processes can effectively convert calcium-rich biogenic materials such as eggshells, animal bones, and fish bones into high-quality HAp with tunable crystallinity, porosity, and particle morphology [9]. Building on this foundation, microwave-assisted hydrothermal synthesis delivers volumetric, homogeneous heating that accelerates nucleation and crystal growth, enabling shorter reaction times and lower energy input than conventional hydrothermal heating [10]. With microwave-assisted hydrothermal processing, it may be possible to produce high-quality HAp from fish bone waste under milder conditions [11], potentially enhancing the adsorption kinetics, capacity, and reusability of the final material.

Despite these environmental liabilities and the clear promise of resource recovery, a focused knowledge gap remains for fermented fish bone waste specifically. Most studies on biogenic HAp have used non-fermented bones or other calcium-rich precursors [12], leaving the unique chemistry of fermented residues largely unexamined. This underexplored feedstock therefore presents a compelling direction for advancing sustainable materials. Moreover, while the adsorption capabilities of biogenic HAp have been well-documented [13], comparatively few investigations have systematically examined how synthesis conditions, especially microwave-assisted hydrothermal parameters and the resulting Ca/P ratios in HAp affect the physicochemical properties of the HAp and its Pb removal performance. To the best of our knowledge, this is the first study to report the use of fermented fish bone waste as a precursor for hydroxyapatite synthesized via microwave-assisted hydrothermal processing and its application as an adsorbent for Pb removal from water. This novelty not only addresses an untapped waste stream but also demonstrates the potential of combining microwave processing with circular-economy valorization strategies.

To address this gap, the present study develops a microwave-assisted hydrothermal route to convert fermented fish bone waste into HAp, aiming to study the effect of synthesis conditions to tune Ca/P ratios and microstructure, and then evaluate how these changes affect morphology and crystallinity of the resulting HAp as well as the performance in Pb adsorption through kinetics and isotherm analyses, with attention to reusability. This work provides a practical guideline for fermented fish industry residues valorization and advances sustainable Pb-remediation technologies aligned with circular-economy objectives.

2 Materials and methods

This study presents a sustainable method for synthesizing hydroxyapatite (HAp) from fish bone waste, targeting lead adsorption from contaminated water. The processes included preparing and calcining fish bone waste to use as a precursor for HAp synthesis via microwave-assisted hydrothermal process under controlled conditions. The diagram of the experiments is presented in Fig. 1.

2.1 Preparation and pretreatment of fish bone waste

The preparation of fermented fish bones began with an initial rinse using deionized (DI) water to remove surface debris and loose particulates. The fish bones were then boiled in a 0.1 M acetic acid (CH_3COOH, Sigma-Aldrich) solution for 1 h to achieve thorough cleaning to eliminate residual fats and proteins, followed by extensive rinsing with DI water until the effluent reached a neutral pH [14]. After completing the cleaning processes, the treated bone material was dried in an oven at 105 °C overnight to ensure complete moisture removal.

The dried and cleaned bone samples were transferred into alumina crucibles and placed in a muffle furnace (Carbolite Gero CWF 11/13,) for calcination. The furnace was programmed to heat the samples at a rate of 10 °C/min to a target temperature of 900 °C, and maintained for 3 h to facilitate the conversion of bone mineral constituents into calcium oxide (CaO) [15]. Upon completion of the calcination process, the furnace was allowed to cool naturally to room temperature before the samples were retrieved. The samples were then ground into a fine powder using an agate mortar and pestle to ensure uniformity. The resulting calcined fish bone powder was stored in airtight containers to prevent moisture and contamination for subsequent synthesis processes.

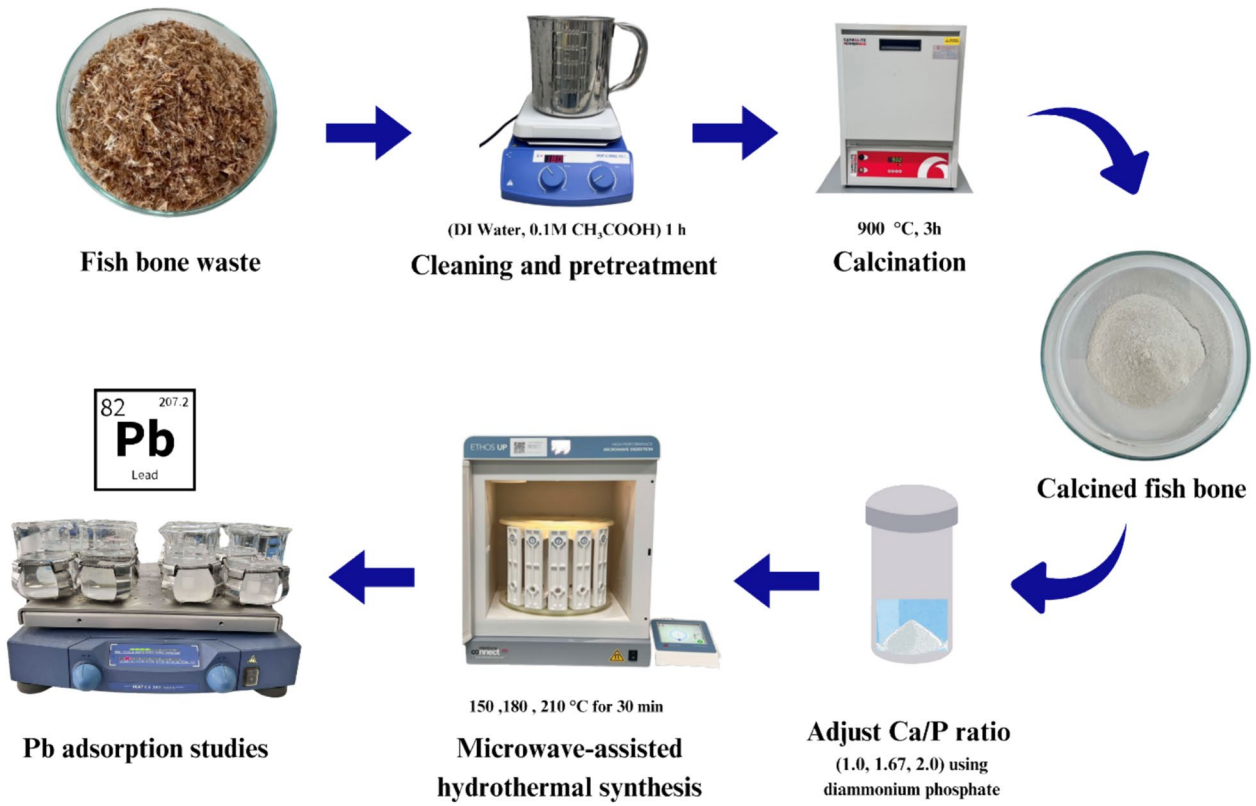

Fig. 1 Flow diagram of HAp synthesis process from fish bone waste

2.2 Synthesis of hydroxyapatite (HAp)

Five grams of calcined fish bone powder were weighed and mixed with a diammonium phosphate ($(NH_4)_2HPO_4$, ≥ 99% purity, Sigma-Aldrich) solution dissolved in DI water. The required mass of $(NH_4)_2HPO_4$ was calculated to achieve target Ca/P molar ratios of 1.0, 1.67, and 2.0, based on the Ca and P content of the calcined fish bone from prior characterization using XRF, as presented in Table 1. The pH of the mixture was then adjusted to 10 using 1 M sodium hydroxide (NaOH, Sigma-Aldrich) to create an alkaline environment favorable for HAp synthesis [16]. This precise control of the Ca/P ratio and pH ensures optimal conditions for forming HAp with the desired properties. The preweighed calcined fish bone powder and prepared phosphate solution were transferred into a Teflon digestion vessel compatible with a microwave digestion system (Milestone ETHOS™). The microwave-assisted hydrothermal synthesis was conducted by heating the mixture to 150, 180, and 210 °C, and maintaining the temperature for 30 min. After the hydrothermal reaction, the vessel was allowed to cool naturally to room temperature. The resulting HAp samples were dried overnight in an oven at 60 °C and stored in airtight containers to preserve their properties for subsequent characterization and testing.

2.3 Material characterization

The synthesized HAp adsorbents were examined by various characterization techniques. Elemental composition was quantified by X-ray fluorescence (XRF, Shimadzu EDX-7200). Crystalline phase identity and lattice were determined by powder X-ray diffraction (XRD, Rigaku SmartLab). BET surface area and porosity were assessed by nitrogen-sorption analyzer (Quantachrome NOVA 2200e). Functional groups were examined by Fourier transform infrared spectroscopy (FT-IR, PerkinElmer SpectrumTwo). Surface chemical states and atomic compositions were resolved by X-ray photoelectron spectroscopy (XPS, Kratos Axis Ultra DLD).

2.4 Lead adsorption experiments

The synthetic Pb-contaminated water was prepared by diluting Pb Lead AA Standard: 1000 µg/mL Pb in 5% HNO_3 (Agilent) in DI water to achieve the desired initial concentrations for adsorption studies. For the study of effect of pH, 1 M NaOH was used to adjust the pH of the solution, as the pH level plays a critical role in the adsorption process and can significantly influences the uptake of lead ions by HAp [17]. This preparation ensured consistency and accuracy for subsequent adsorption experiments.

Batch equilibrium adsorption tests were conducted by introducing a preweighed mass of HAp powder, ranging from 0.5 to 3.0 g/L in the Erlenmeyer flasks containing 5 mg/L Pb-contaminated water. The flasks were placed on an orbital shaker set to operate at 150 rpm to ensure consistent mixing at room temperature for up to 60 min. The samples were periodically taken to evaluate adsorption kinetics and establish equilibrium conditions. At predetermined intervals (0–60 min; 0, 10, 20, 30, 40, 50, 60 min), 10 mL aliquots were withdrawn, and filtered through a 0.45 µm PTFE syringe filter to remove any suspended solids, and analyzed for residual Pb(II) concentration by atomic absorption spectrometer (AAS, Agilent 240FS AA).

The performance of the synthesized HAp samples was evaluated in terms of Pb removal efficiency and adsorption capacity. The Pb removal efficiency (%) was calculated using the following equation:

$$\text{Removal Efficiency}(\%) = \frac{(C_0 - C_e)}{C_0} \times 100 \quad (1)$$

where C_0 and C_e refer to initial concentration (mg/L) and final concentration at equilibrium (mg/L), respectively.

Table 1 Synthesis parameters and elemental analysis of the HAp samples

Sample	HT temperature (°C)	Expected Ca/P	Ca (%)	*P* (%)	Actual Ca/P
Calcined fish bone	–	–	77.22	22.78	2.62
HT1	150	1.0	58.62	41.38	1.09
HT2	180	1.0	61.45	38.55	1.23
HT3	210	1.0	65.95	34.05	1.50
HT4	150	1.67	70.13	29.87	1.81
HT5	180	1.67	69.85	30.15	1.79
HT6	210	1.67	69.62	30.38	1.78
HT7	150	2.0	71.12	28.88	1.92
HT8	180	2.0	71.33	28.67	1.92
HT9	210	2.0	71.83	28.17	1.97

Equilibrium adsorption capacity (q_e) of the adsorbent is the amount of adsorbate adsorbed per mass of adsorbent at equilibrium and was calculated by using the following equation:

$$\text{Adsorption capacity}(q_e; mg/g) = \frac{(C_0 - C_e) \times V}{m} \quad (2)$$

where C_0 and C_e refer to initial concentration (mg/L) and final concentration at equilibrium (mg/L), respectively, V is solution volume (L), and m is adsorbent mass (g).

2.5 Adsorption kinetic study

In this study, time-dependent Pb(II) uptake data from batch experiments of nine HAp adsorbents were fitted to the pseudo-first-order (PFO) and pseudo-second-order (PSO) kinetic models [18]. The linearized forms of PFO and PSO kinetic formulations are given in Eq. (3) and (4), respectively. The model goodness-of-fit was assessed by the coefficient of determination (R^2).

$$\ln(q_e - q_t) = \ln q_e - k_1 t \quad (3)$$

$$\frac{t}{q_t} = \frac{1}{k_2 q_e^2} + \frac{t}{q_e} \quad (4)$$

where t is time (min), q_t is the amount of adsorbate adsorbed per mass of adsorbent at time t (mg/g), q_e is the amount of adsorbate adsorbed at equilibrium (mg/g), k_1 is the the pseudo-first-order rate constant (min^{-1}), k_2 is the pseudo-second-order rate constant (g/mg·min).

To elucidate the pH-dependent adsorption behavior of Pb on the synthesized HAp (sample HT9), batch tests were conducted at pH 3 and 10. In each test, 0.125 g of HT9 was dosed into 500 mL of a 5 mg/L Pb(II) solution for 1 h. The spent adsorbent was recovered by centrifugation at 6000 rpm for 5 min, oven-dried at 105 °C overnight, and characterized by X-ray photoelectron spectroscopy (XPS).

2.6 Adsorption isotherm study

Adsorption isotherm models, including Langmuir and Freundlich, were applied to quantify adsorption capacity and equilibrium parameters. These analyses provided critical insights into the efficiency and behavior of the synthesized HAp under varying conditions [19]. Lead working solutions (C_0 = 2–6 mg/L as Pb^{2+}) were prepared by dilution of an analytical-grade Pb(II) stock solution with deionized water. pH was adjusted to 3.0 using dilute HNO_3 and NaOH. For each initial Pb(II) concentration, 0.025 g of HT9 was added to 50.0 mL of Pb(II) solution, corresponding to a dosage of 0.5 g/L. Suspensions were agitated at 150 rpm for 60 min at room temperature, then centrifuged at 6000 rpm for 5 min. Supernatants were filtered through a 0.45 µm PTFE syringe filter, and Pb(II) concentration was quantified by atomic absorption spectrometry (AAS).

It should be noted that concentrations above 6 mg/L were not employed because, with our matrix and instrument settings, the AAS calibration did not sustain acceptable linear regression quality beyond this level. In addition, preliminary trials at 2.0 g/L adsorbent dosage yielded nearly 100% removal across 2–6 mg/L, collapsing isotherm resolution as multiple points converged to essentially the same C_e. To avoid this ceiling effect with adequate spread in C_e, the adsorbent dosage was reduced to 0.5 g/L.

The Langmuir isotherm is based on the assumption that adsorption occurs as a monolayer on a uniform surface of the adsorbent, where adsorption happens only at specific, identical sites. The equation representing this model is:

$$\frac{C_e}{q_e} = \frac{1}{q_e K_L} + \frac{C_e}{q_m} \quad (5)$$

where:

q_m is the maximum amount of lead adsorbed per gram of adsorbent (mg/g) to form a complete monolayer,

C_e is the equilibrium concentration of lead in solution (mg/L),

q_e is the amount of lead adsorbed at equilibrium per gram of adsorbent (mg/g),

K_L is the Langmuir constant (L/mg), reflecting the affinity between the adsorbent and lead ions.

The value of q_m indicates the theoretical adsorption capacity when all surface sites are saturated with lead ions. The K_L constants can be determined from the slope and intercept of the linear plot of C_e/q_e versus C_e.

In contrast, the Freundlich isotherm is used to describe adsorption on heterogeneous surfaces. Its empirical form is given as follows:

$$\log q_e = \frac{1}{n} \log C_e + \log K_F \quad (6)$$

The parameters K_F and n represent the Freundlich constants related to adsorption capacity and intensity, respectively. These values can be derived from a linear regression analysis of the plot between log q_e and log C_e.

Additionally, the constants obtained from both the Langmuir and Freundlich isotherm models, including their correlation coefficients (R^2), are computed and presented in Table 4. These values help assess the suitability of each model in describing the adsorption behavior observed in the experiment.

3 Results

3.1 Material characterization

Elemental composition analysis of the synthesized samples using X-ray fluorescence spectroscopy (XRF) revealed variations in the measured Ca/P molar ratios compared to the expected values, which ranged from 1.0 to 2.0 as defined in the synthesis process. The results can be categorized into three main groups, and the elemental composition of each sample is summarized in Table 1.

The first group includes samples with an expected Ca/P ratio of 1.0 (HT1, HT2, and HT3), with measure ratios ranging from 1.09 to 1.5. HT1 exhibited the closest value to the expected ratio (1.09), followed by HT2 (1.23) and HT3 (1.50). The second group comprised samples HT4, HT5, and HT6, synthesized with an expected Ca/P ratio of 1.67, with measured ratios ranging from 1.78 to 1.81. The third group included samples HT7, HT8, and HT9, synthesized with an expected Ca/P ratio of 2.0, with measured ratios ranging from 1.92 to 1.97.

The X-ray diffraction (XRD) patterns in Fig. 2 indicated distinct crystallinity differences between the calcined fish bone and the synthesized HAp. All the synthesized HAp samples exhibited high crystallinity, evidenced by sharp and well-defined peaks. XRD patterns of HT1-HT9 revealed distinct peaks at 2θ angles corresponding to hydroxyapatite, matching the standard reference (JCPDS 09–0432). Main peaks at 25.99° (002), 31.78° (211), and 32.28° (112) and 49.49° (213) confirmed the crystalline nature of HAp [20]. Secondary phases of merrillite were detected with peaks at 28.06° (214) and 34.75° (220) [21]. In addition, a prominent diffraction peak around 2θ = 45° was observed in samples HT1 to HT3, attributed to β-tricalcium phosphate (β-TCP; $Ca_3(PO_4)_2$), which has a Ca/P ratio of 1.51.

The surface and porous properties of HAp adsorbent materials were analyzed using the Brunauer–Emmett–Teller (BET) technique, which provided data on specific surface area, total pore volume, and average pore size as shown in Table 2.

Nitrogen-sorption analysis showed mesoporous structures (average pore diameter 5.078–26.008 nm) across all samples. Specific surface area ranged from 9.646 to 14.083 m^2/g, with a mean of 11.961 m^2/g. HT9 exhibited the highest specific surface area (14.083 m^2/g), followed by HT1 (13.212 m^2/g) and HT8 (12.576 m^2/g). Total pore volumes were in the range of 0.0624–0.0975 cm^3/g, with HT6 (0.1023 cm^3/g), HT8 (0.0998 cm^3/g), and HT9 (0.0975 cm^3/g) forming the high total pore volume group. The smallest pores were found in HT4 (5.078 nm) and HT7 (5.941 nm), and the largest in HT6 (26.008 nm) and HT9 (23.742 nm).

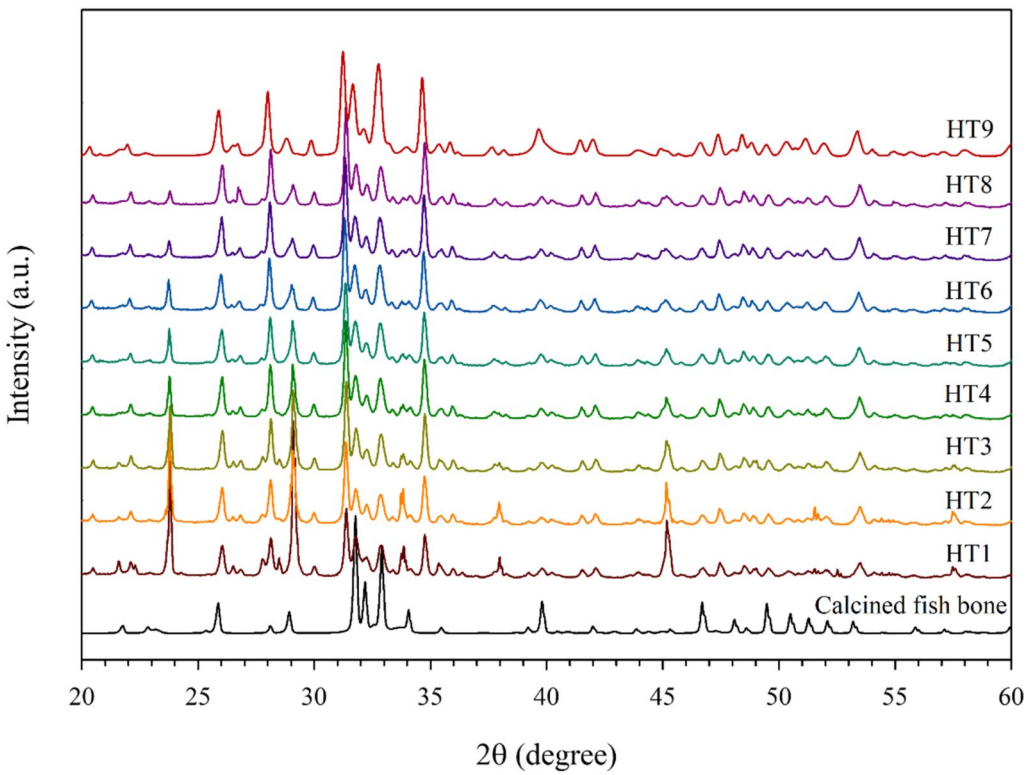

Fig. 2 XRD patterns of calcined fish bone and the synthesized HAp samples

Table 2 Surface and porous properties of the HAp samples

Sample	Specific surface area (m^2/g)	Total pore volume (cm^3/g)	Average pore diameter (nm)
HT1	13.212	0.0620	10.388
HT2	10.432	0.0832	8.695
HT3	11.643	0.0632	10.256
HT4	11.651	0.0651	5.078
HT5	12.129	0.0629	10.245
HT6	12.274	0.1023	26.008
HT7	9.646	0.0604	5.941
HT8	12.576	0.0998	9.964
HT9	14.083	0.0975	23.742

Figure 3 presents SEM images illustrating the morphological evolution of synthesized HAp samples across hydrothermal temperatures ranging from 150 to 210 °C and varying Ca/P molar ratios. At 150 °C, the particles appeared loosely aggregated with a porous morphology and indistinct crystalline structure. Increasing the temperature to 180 °C resulted in denser particle packing, more uniform size and shape, and the onset of crystallization. At the highest temperature of 210 °C, significant particle growth and tight aggregation were observed, indicating a well-developed crystalline phase.

The FT-IR analysis of calcined fish bone waste and the synthesized hydroxyapatite samples are shown in

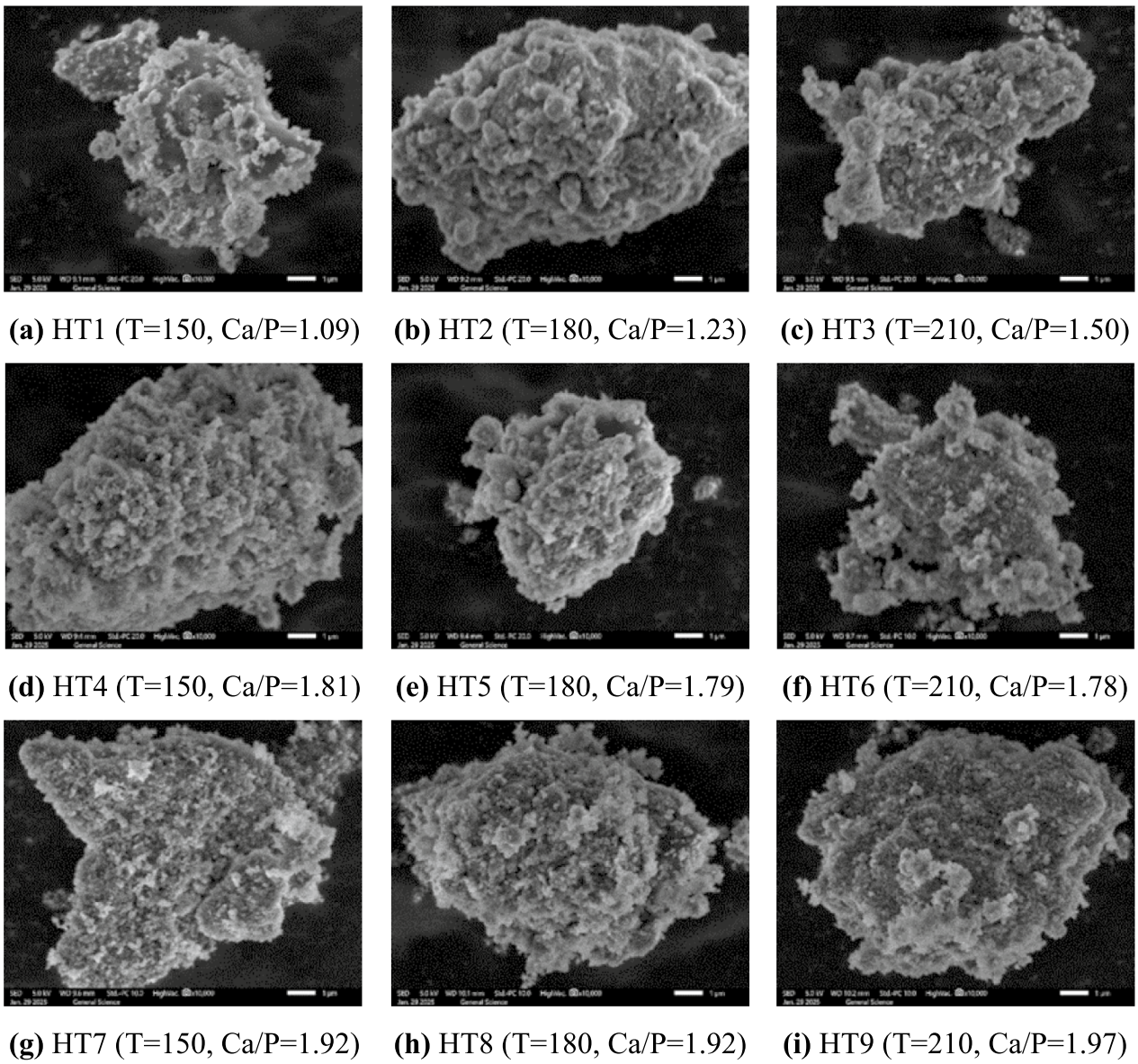

Fig. 3 SEM images of the nine HAp synthesized under different conditions

Fig. 4. The FT-IR spectra confirmed the formation of hydroxyapatite through its characteristic functional groups such as phosphate (PO_4^{3-}), hydroxyl (OH^-), and carbonate (CO_3^{2-}) [22]. A prominent hydroxyl (OH^-) peak at around 3400 cm^{-1} indicated the presence of hydroxyl groups within the HAp structure. Additionally, a distinct peak at approximately 630 cm^{-1} corresponded to hydroxyl vibrational modes within the HAp crystal lattice [23]. Phosphate (PO_4^{3-}) functional groups were identified through peaks at around 1030 cm^{-1} and 960 cm^{-1}, attributed to P–O stretching vibrations [24]. These signals were particularly intense in samples HT3 through HT9, indicating the progressive formation of a well-crystallized HAp phase with increasing hydrothermal temperature. Peaks at around 1450 cm^{-1} and 870 cm^{-1} suggested carbonate (CO_3^{2-}) substitution for phosphate, a phenomenon characteristic of biologically derived HAp [25]. Such substitution was more pronounced in the samples with higher Ca/P ratios, such as HT8 and HT9.

3.2 Effect of synthesis conditions on Pb removal

A 3D mesh plot was constructed to visualize the relationship between synthesis temperature (x-axis), Ca/P ratio (y-axis), and Pb removal efficiency (z-axis) for the nine synthesized HAp as shown in Fig. 5. The data revealed clear trends in how synthesis temperature influenced the removal of Pb as the removal efficiency increased with synthesis temperature at nearly all Ca/P ratios. For example, at a Ca/P ratio around 2.0, Pb removal rose from 67.2% at 150 °C (HT7) to 97.8% at 210 °C (HT9). The influence of Ca/P ratio on Pb removal is subtle. At 150 °C, Pb removal decreased slightly with increasing Ca/P ratio, while at higher temperatures (180 °C and 210 °C), Pb removal generally improved or remains high as Ca/P ratio increased.

3.3 Effect of contact time

The effect of contact time on lead adsorption performance was evaluated on nine HAp adsorbents under the experimental conditions of initial Pb concentration of 5 mg/L, an adsorbent dosage of 2.0 g/L, and a pH of 3. As can be observed in Fig. 6, all samples show a very fast initial drop in C/C_0 within the first 10 min, indicating rapid Pb(II) uptake. Estimated removals at 10 min ranged from 64.4–95.2%. After 10 min, the curves flattened, showing a slow approach to equilibrium. Most samples changed only modestly between 20–60 min. The results revealed that Pb removal efficiency after 60 min spanned 67.2 – 97.8%. Among all tested samples, the highest performance was obtained with HT9, achieving 97.8%

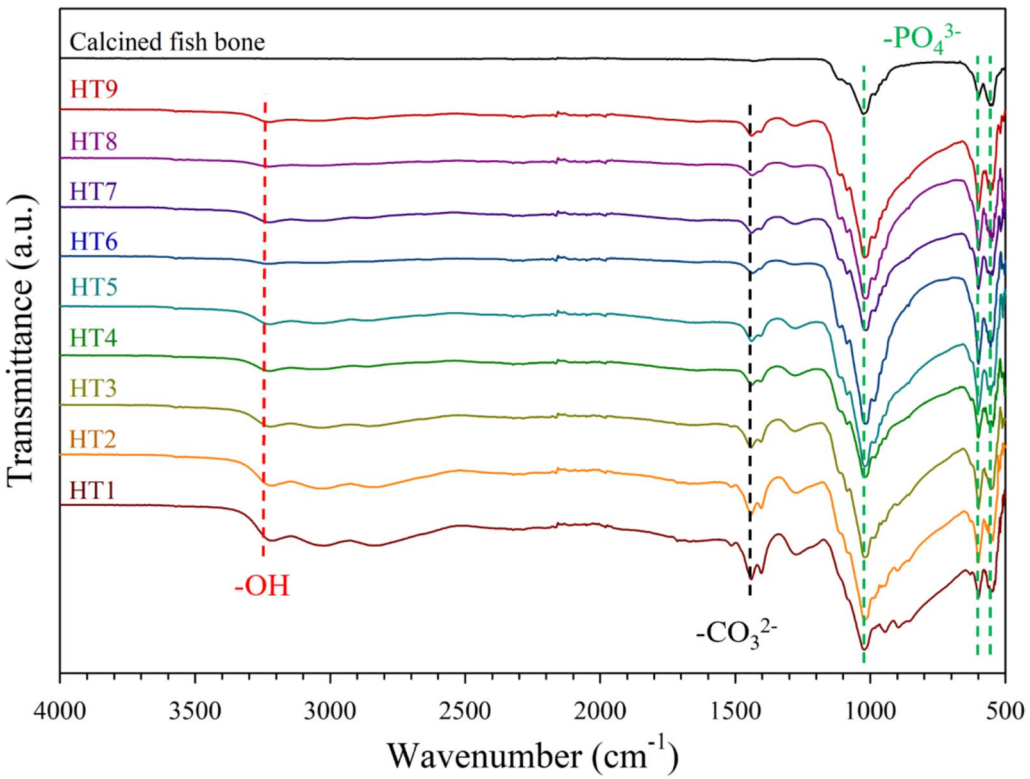

Fig. 4 FT-IR spectra of calcined fish bone and the synthesized HAp adsorbents

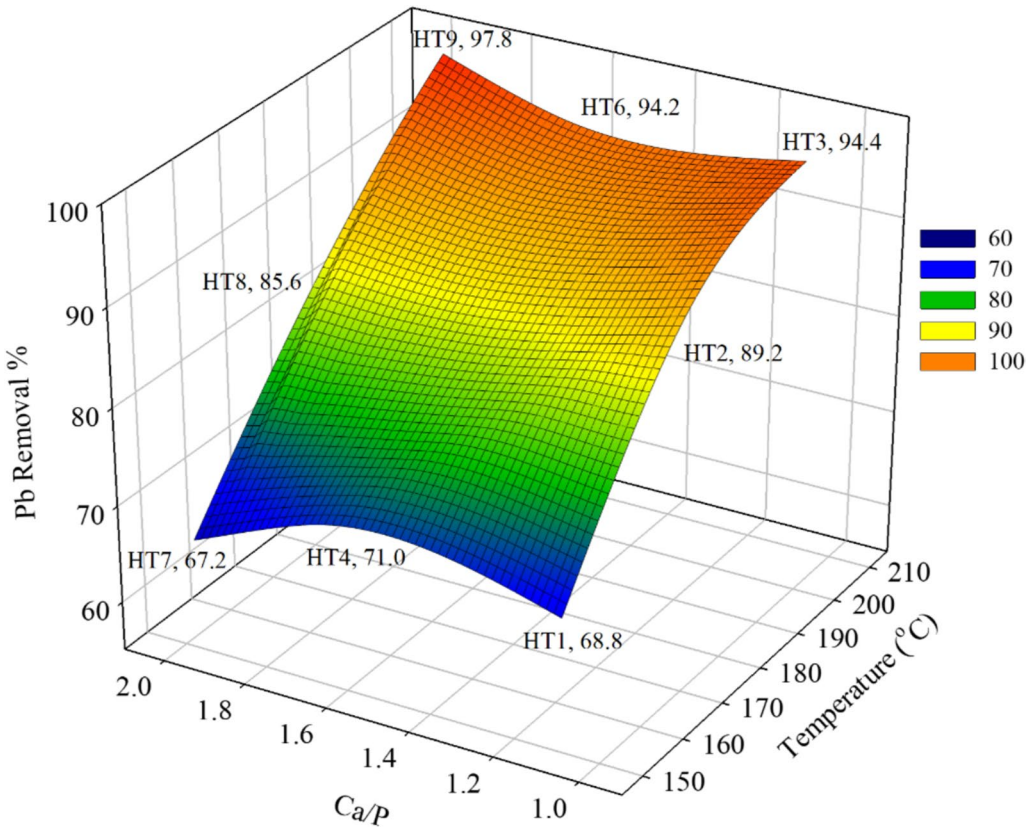

Fig. 5 Effect of synthesis temperature and Ca/P ratio on the Pb removal performance

removal, followed by HT3 (94.4%), and HT6 (94.2%). In contrast, HT7 was the least effective, having 67.2% removal.

The transient behavior of the lead adsorption process was analyzed using the pseudo-first-order (PFO) and pseudo-second-order (PSO) kinetic models. The test plots for PFO ($\ln(q_e\text{-}q_t)$ vs t) and PSO (t/q_t vs t) are shown in Fig. 7a, b, respectively. The kinetic parameters including rate constants and correlation coefficients obtained from kinetic plots are presented in Table 3.

Linearized kinetic fits revealed a clear preference for the pseudo-second-order (PSO) model (Fig. 7a) over the pseudo-first-order (PFO) model (Fig. 7b) for all adsorbents. PFO rate constants (k_1) were in the range of 0.0499–0.0750 min^{-1} with $R^2 = 0.8659–0.9966$, whereas PSO rate constants (k_2) were in the range of 0.4499–1.2012 g/mg·min with $R^2 = 0.9994–0.9999$. The near-unity R^2 values of PSO model, together with internally consistent capacities, indicate that PSO model provides the most reliable description of the uptake kinetics in this concentration regime. The best-performing sample HT9 combined the highest removal (97.8%), largest k_2 of 1.2012 g/mg·min, and highest q_e of 2.4588 mg/g, implying the fastest approach to equilibrium among the series. High-performing HT3 and HT6 also exhibited large q_e (around 2.38 mg/g) with strong PSO fits ($R^2 \geq 0.9994$). In contrast, lower-efficiency materials (HT1, HT4, HT7) showed the smallest (≤ 1.80 mg/g) and lower PFO R^2 while still conforming closely to PSO kinetic model.

3.4 Effect of adsorbent dosage

The effect of adsorbent dosage on lead removal efficiency (Initial Pb concentration = 5 mg/L, and pH 3) was evaluated using HT9 adsorbent based on its highest performance from the previous experiments, and the results are presented in Fig. 8. The results showed a clear increasing trend with dosage. Lead removal efficiency rose from 14.6% at 0.5 g/L to 96.5% at 2.0 g/L, and reached the highest value of 97.0% at 2.5 g/L, and then slightly decreased to 95.4% at 3.0 g/L. The corresponding adsorption capacity (q_e) peaked at 3.630 mg/g at 1.0 g/L and declined with further dosage, 3.020, 2.413, 1.940, 1.590 mg/g at 1.5, 2.0, 2.5, and 3.0 g/L, respectively, reflecting greater site availability but lower per-mass utilization at higher dosages.

3.5 Effect of pH

The influence of pH on lead adsorption efficiency was investigated on HT9 adsorbent at an initial lead

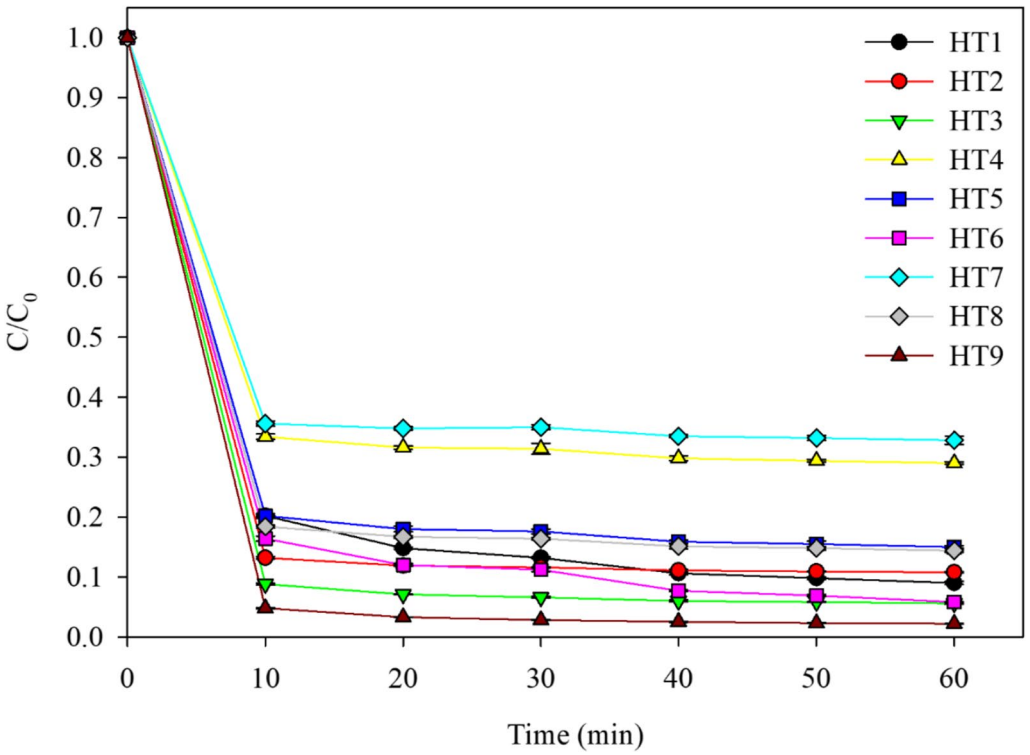

Fig. 6 Effect of contact time on Pb removal using different HAp adsorbents (C_0 = 5 mg/L, dosage = 2 g/L, pH 3)

concentration of 5 mg/L with an adsorbent dosage of 2.0 g/L at pH levels of 3, 7, and 10, as illustrated in Fig. 9. The results showed that Pb removal and adsorption capacity both peaked at neutral pH. Removal efficiency increased from 96.5% (q_e = 2.413 mg/g) at pH 3 to 99.6% (q_e = 2.490 mg/g) at pH 7, then decreased to 79.0% (1.975 mg/g) at pH 10. A more detailed mechanistic interpretation of these pH-dependent behaviors is provided in the Discussion section.

The surface charge of the adsorbent was analyzed using the acid–base titration method to determine the point of zero charge (pH_{PZC}), the pH at which the material has a neutral net surface charge [26]. Briefly, 20 mL of deionized water was prepared in Erlenmeyer flasks and the initial pH was adjusted across 3–11 using 0.01 M sodium hydroxide (NaOH) and 0.01 M hydrochloric acid (HCl). After that, 0.02 g of the adsorbent was then added to the flasks and agitated on a shaker at 200 rpm for 24 h, after which the final pH of the suspension was measured. The relationship between initial pH and final pH was subsequently plotted to determine the pH at the point of zero charge of the adsorbent as shown in Fig. 10. The analysis revealed that the adsorbent had a pH_{PZC} value of 6, indicating that at pH 3, the surface of the material carries a positive charge, while at pH 7 and 10, the surface carries a negative charge [27].

3.6 Effect of initial concentration

The experimental adsorption results of HT9 (0.5 g/L, pH 3) in Fig. 11 show that increasing the initial Pb(II) concentration from 2 to 6 mg/L led to a monotonic decrease in fractional removal from 40.5 to 17.0%, while the equilibrium uptake (q_e) increased by 26% from 1.62 to 2.04 mg/g. Correspondingly, the residual concentration (C_e) rose from 1.19 mg/L to 4.98 mg/L, and the absolute amount removed per liter increased slightly from 0.81 to 1.02 mg/L.

3.7 Adsorption isotherm study

The Langmuir and Freundlich adsorption isotherms were used to fit the adsorption data, as illustrated in Fig. 12a, b, respectively. The calculated parameters from the models are also tabulated in Table 4. Adsorption isotherm analysis revealed that the Langmuir isotherm best described the adsorption process by HT9, indicating monolayer adsorption on a homogeneous adsorbent surface, where all adsorption sites possess equal energy [28]. The model exhibited an exceptionally high correlation coefficient (R^2 = 0.9997), demonstrating its accuracy in describing the adsorption behavior. The maximum adsorption capacity (q_m) was determined to be 2.20 mg/g. In contrast, the Freundlich model, representing adsorption on heterogeneous surfaces and follows a multilayer

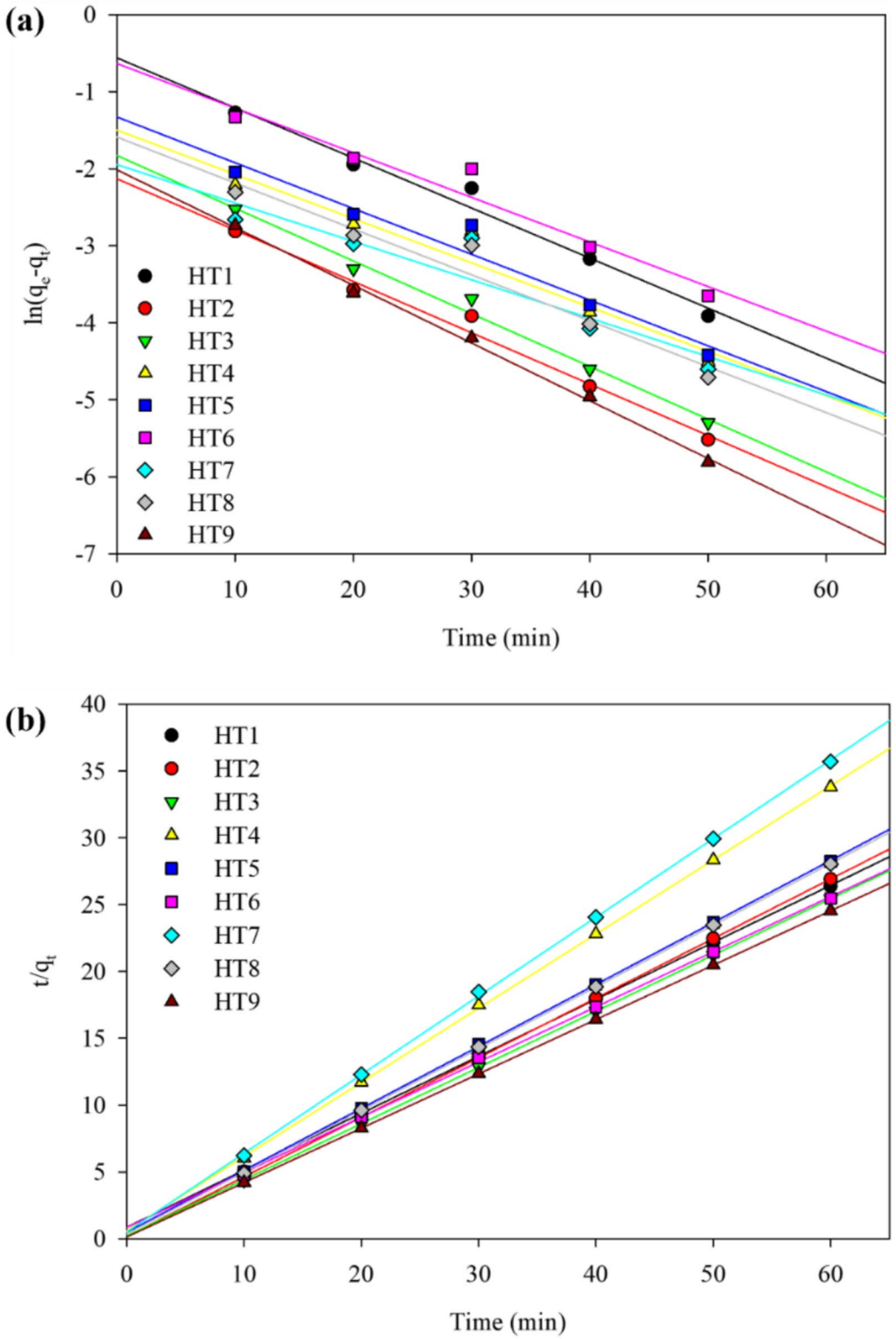

Fig. 7 Test plots for Pb adsorption onto different synthesized HAp; **a** pseudo-first-order and **b** pseudo-second-order kinetic models

Table 3 Lead removal efficiency and kinetics parameters for the Pb adsorption on the synthesized adsorbents

Sample	Pb removal (%)	Pseudo-first-order		Pseudo-second-order		
		k_1 (min^{-1})	R^2	k_2 (g/mg·min)	R^2	q_e (mg/g)
HT1	68.8 ± 2.1	0.0650	0.9856	0.4630	0.9998	1.7489
HT2	89.2 ± 2.8	0.0667	0.9892	1.0502	0.9999	2.2452
HT3	94.4 ± 2.1	0.0685	0.9393	0.8926	0.9999	2.3759
HT4	71.0 ± 2.5	0.0575	0.9512	0.5120	0.9998	1.8018
HT5	85.0 ± 1.2	0.0595	0.9512	0.4499	0.9998	2.1561
HT6	94.2 ± 2.3	0.0579	0.9510	0.6141	0.9994	2.3804
HT7	67.2 ± 2.4	0.0499	0.8659	0.6450	0.9997	1.7001
HT8	85.6 ± 2.5	0.0597	0.9498	0.5964	0.9999	2.1636
HT9	97.8 ± 1.6	0.0750	0.9966	1.2012	0.9999	2.4588

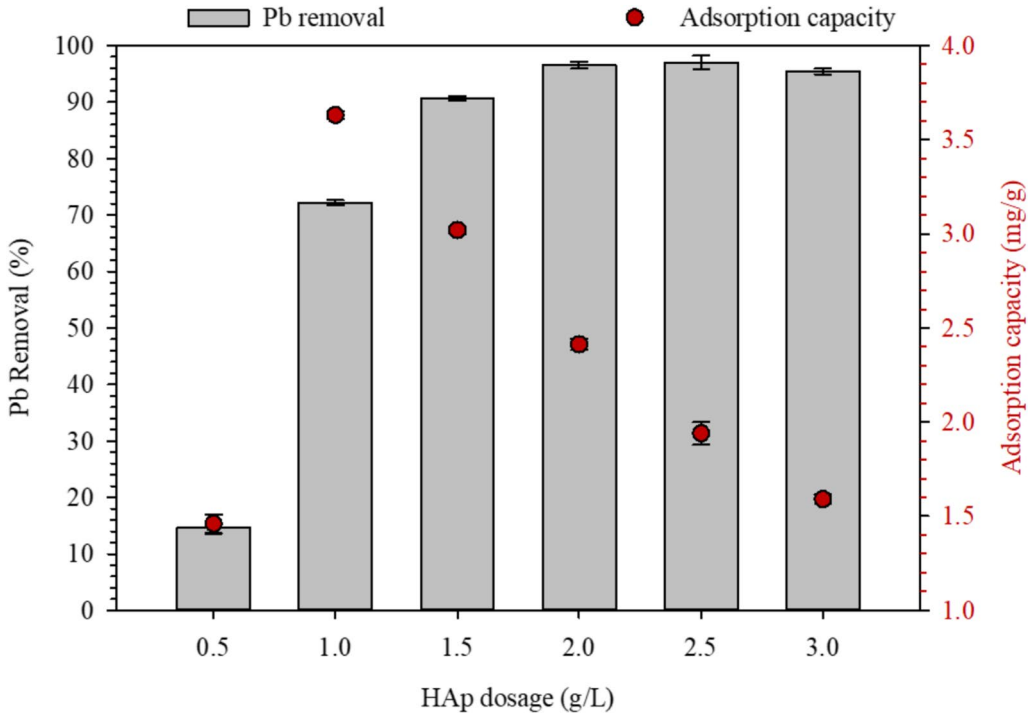

Fig. 8 Effect of HAp dosage on Pb removal and adsorption capacity of HT9 (pH 3)

adsorption mechanism, yielded a correlation coefficient of $R^2 = 0.9253$. This value suggested a relatively good fit, though not as strong as the Langmuir model. The results indicated that while some degree of surface heterogeneity exists, the overall adsorption behavior aligns more closely with the Langmuir model [29].

3.8 Reusability assessment

Reusability of HT9 adsorbent was assessed over five successive cycles using a simulated Pb-contaminated solution (5 mg/L, pH 3). In each cycle, 0.125 g of HT9 was contacted with 500 mL of Pb solution for 60 min. After adsorption, the solid was recovered by centrifugation at 6000 rpm for 5 min, oven-dried at 105 °C for 1 h, and redeployed under identical conditions. Residual Pb concentrations were quantified by atomic absorption spectroscopy (AAS), and adsorbent mass loss per cycle was determined using a 4-digit analytical balance (Sartorius BCA224i-1S). Figure 13 shows Pb removal by the HT9 adsorbent over five successive reuse cycles. Pb removal was essentially quantitative in cycle 1 (above 99%). With continued reuse, efficiency declined modestly to 95.6% and 87.0% in cycles 2 and 3, respectively, then declined more markedly to 84.4% and 70.6% in cycles 4 and 5.

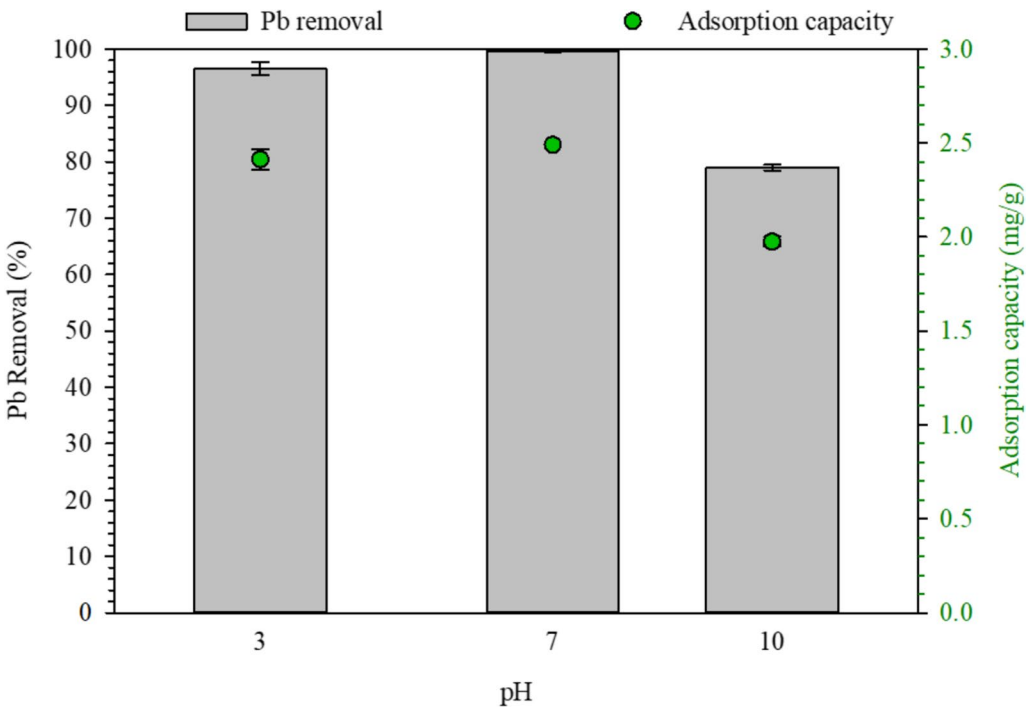

Fig. 9 Effect of pH on Pb removal and adsorption capacity of HT9 (2.0 g/L)

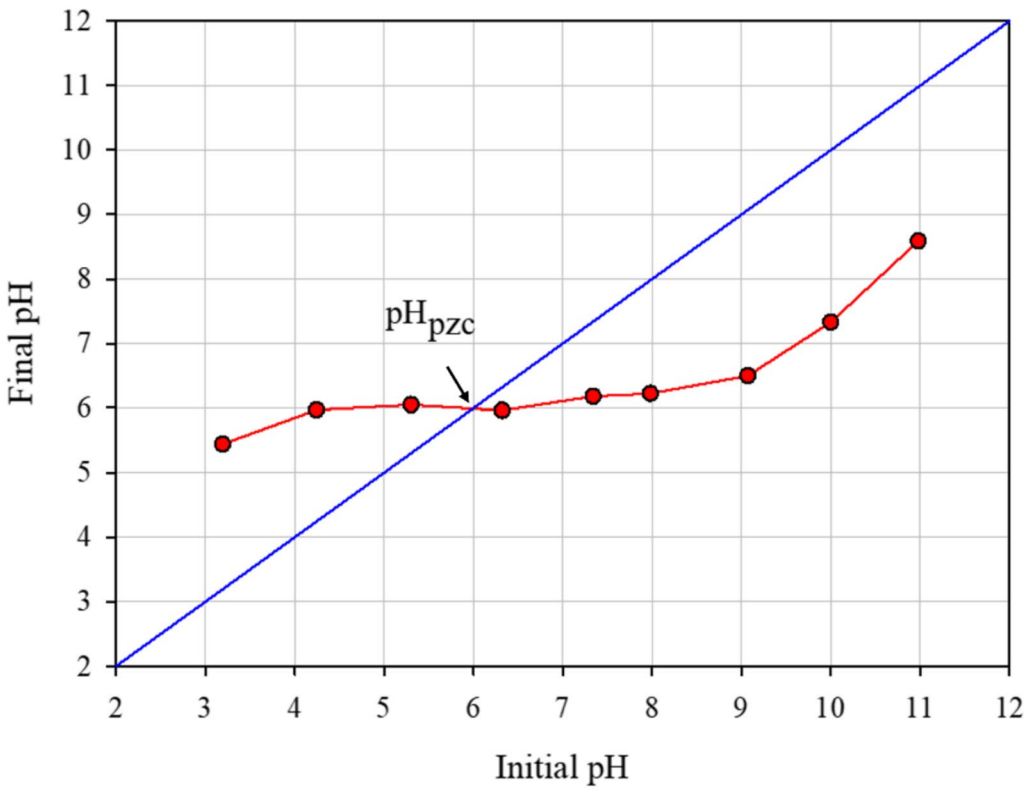

Fig. 10 Surface charge analysis of the adsorbent using acid–base titration

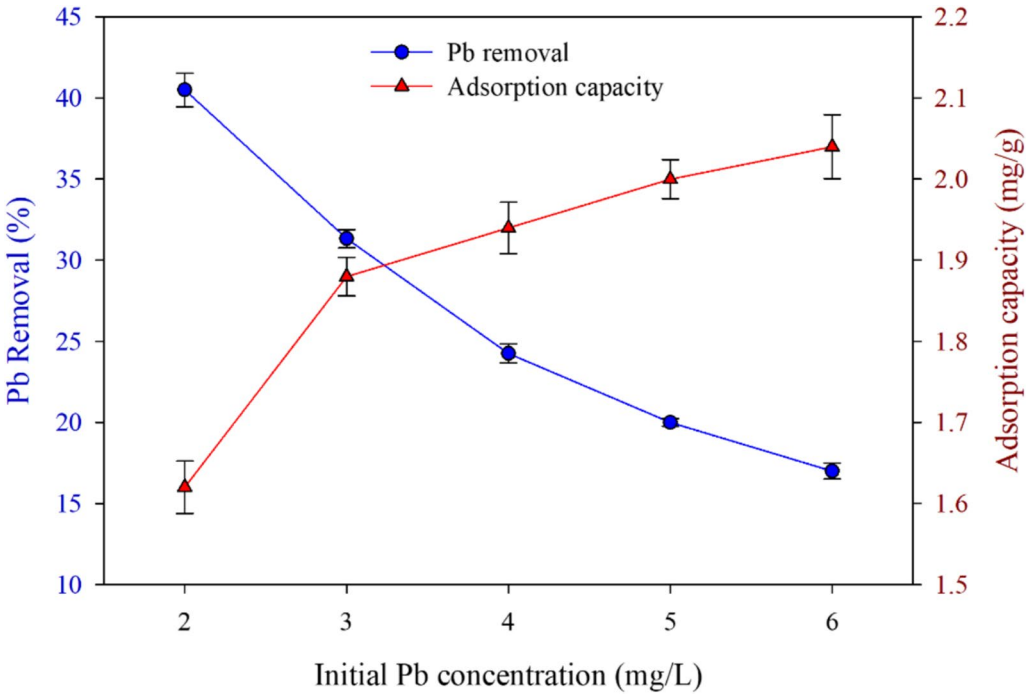

Fig. 11 Effect of initial Pb concentration on Pb removal and adsorption capacity of HT9

This monotonic decrease indicates a progressive loss of adsorption capacity. Concurrently, the observed mass loss of approximately 4.5–6.5% per cycle was consistent with particle attrition and handling losses intrinsic to centrifugation, which would diminish accessible surface area and active sites [30].

3.9 Adsorption mechanism study

The adsorption mechanisms of Pb on HAp were studied on the spent HT9 adsorbent after Pb adsorption at two different pH values, pH 3 and pH 10 using XPS and XRD. The XPS spectra in Fig. 14a, b represented the surface of HT9 after exposure to Pb. The key findings were the changes in peak intensity and position, which revealed the dominant adsorption mechanisms at each pH. At pH 3, the Pb 4f envelope signal was significantly more intense than at pH 10, indicating a greater amount of lead on the surface. Specifically, the atomic concentration of lead at pH 3 was 0.23%, compared to 0.09% at pH 10. In addition, there was a distinct shift in the binding energy of the lead peaks. The peak of Pb $4f_{7/2}$ at pH 3 was centered at 139.02 eV and shifted lower to 138.82 eV at pH 10. Both values lied within the characteristic range for lead in its + 2 oxidation state, confirming that lead is present predominantly as Pb^{2+} under both conditions [31]. Figure 14c shows powder XRD patterns of the Pb-contacted HT9 recovered from pH 3 and pH 10. There were no resolvable new reflections attributable to crystalline Pb-bearing phases compared to the fresh HT9. The diffractograms were dominated by the hydroxyapatite pattern and are essentially indistinguishable within the scan resolution and counting statistics. The absence of obvious XRD differences was fully consistent with the XPS results where Pb was present at low surface atomic concentrations, and suggested that any Pb-containing products lied below the detection limit of laboratory XRD [32].

4 Discussion

The hydrothermal synthesis conditions significantly influenced the composition and structure of the HAp materials. Variations between the measured and expected Ca/P ratios in the synthesized samples can be attributed to several factors inherent to the synthesis process. For samples with an expected Ca/P ratio of 1.0 (HT1, HT2, and HT3), the measured values (1.09–1.50) were higher than anticipated. This discrepancy may result from excess phosphate ions that were not fully incorporated into the HAp crystal lattice [33], and the formation of side-phases such as monetite ($CaHPO_4$), which has a lower Ca/P ratio than HAp [34]. In samples targeting a stoichiometric Ca/P ratio of 1.67 (HT4, HT5, and HT6), the measured ratios (1.78–1.81) were slightly above the ideal 1.67, suggest partial substitution of phosphate ions by carbonate (CO_3^{2-}) in the HAp structure [35]. Conversely, samples with an expected Ca/P ratio of 2.00 (HT7, HT8, and HT9) yielded marginally lower measured ratios

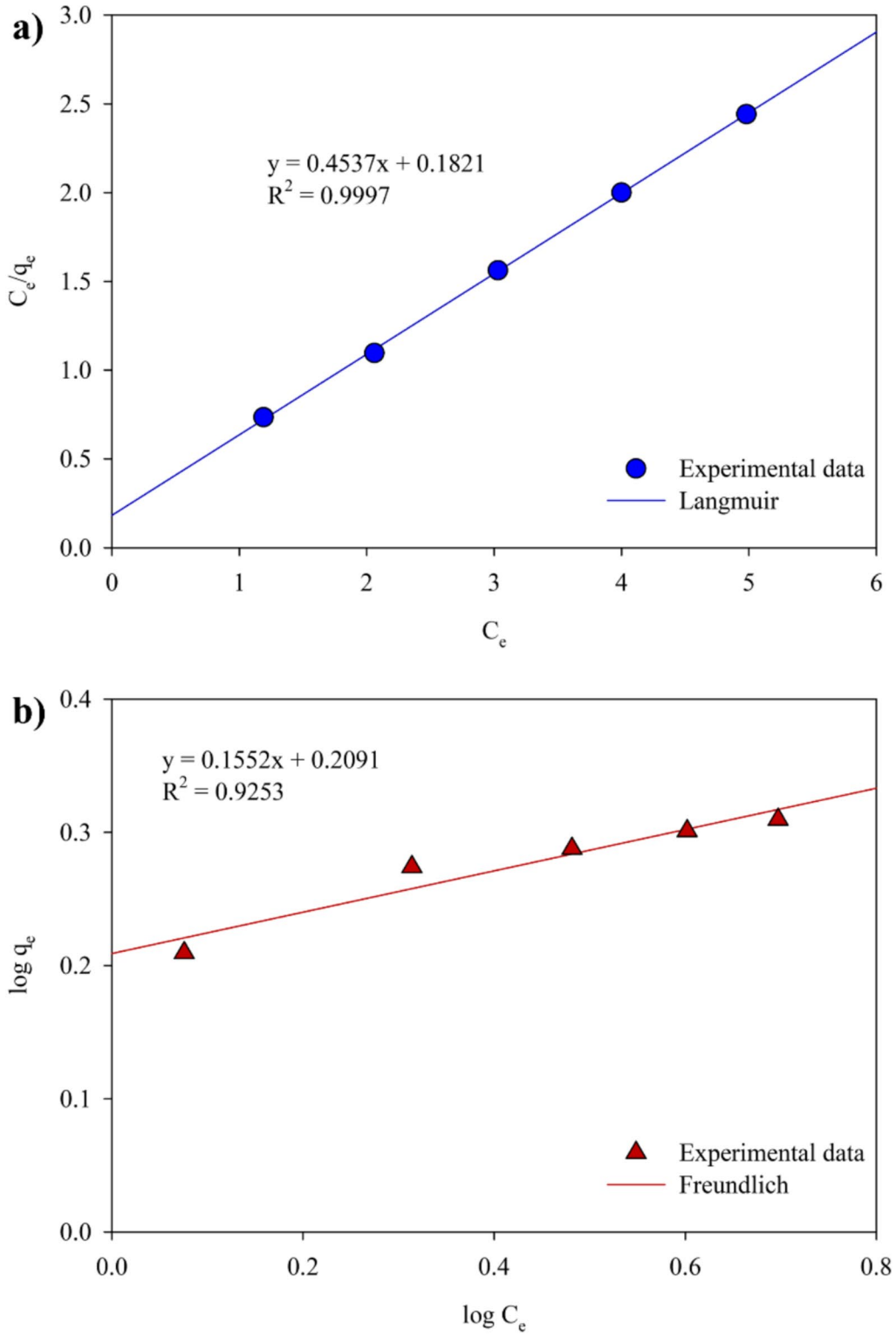

Fig. 12 Experimental data of Pb adsorption by HT9 fitted with **(a)** Langmuir and **(b)** Freundlich isotherms

Table 4 Calculated parameters from Langmuir and Freundlich isotherm models

Parameter	Value
Langmuir isotherm	
q_m (mg/g)	2.20
K_L (L/mg)	2.49
R^2	0.9997
Freundlich isotherm	
K_F	1.62
n	6.44
R^2	0.9253

(1.92–1.97) than expected, which can be explained by the incorporation of trace metal ions such as magnesium (Mg^{2+}) or zinc (Zn^{2+}) replacing calcium ions (Ca^{2+}) in the crystal lattice of biogenic HAp [36]. X-ray diffraction (XRD) analysis revealed that higher synthesis temperature (210 °C) and with Ca/P ratios near or above the stoichiometric value of 1.67 produced more crystallinity, phase-pure hydroxyapatite. Elevated hydrothermal synthesis temperatures promote the well-crystallized HAp formation, as reported in previous studies [37]. In contrast, samples with low Ca/P ratios (HT1–HT3) showed secondary β-tricalcium phosphate (β-TCP) phases, consistent with literature noting that β-TCP appears when calcium availability is insufficient to produce stoichiometric HAp [38]. These β-TCP peaks gradually vanished as the Ca/P ratio approaches 1.67, indicating that an excess calcium coupled with higher temperature favors the synthesis of phase-pure HAp.

Textural characterization of the best-performing sample (HT9) showed a mesoporous structure (average pore 23.742 nm) with a specific surface area of 14.083 m^2/g and total pore volume of 0.0975 cm^3/g. Such porosity is expected to facilitate intraparticle diffusion and improve access to active adsorption sites, enhancing the of Pb uptake rate within the contact time [39]. The larger surface area increases the number of available adsorption sites, while the greater pore volume enhanced ion retention. Additionally, prior studies showed that Pb removal by HAp can occur via a combination of $Ca^{2+} \leftrightarrow Pb^{2+}$ ion exchange and dissolution–reprecipitation [40]. Thus, the favorable mesoporous architecture and high surface area of HT9 likely support these processes, ultimately contributing to its superior performance.

Lead adsorption behavior reflected these synthesis-derived attributes. Performance improved systematically with synthesis temperature at each Ca/P ratio. For example, at Ca/P around 2.0, Pb removal rose from 67.2% (150 °C, HT7) to 85.6% (180 °C, HT8) and 97.8% (210 °C, HT9). The Ca/P effect was more subtle at 150 °C, increasing Ca/P slightly reduced removal, possibly because of incomplete HAp phase formation

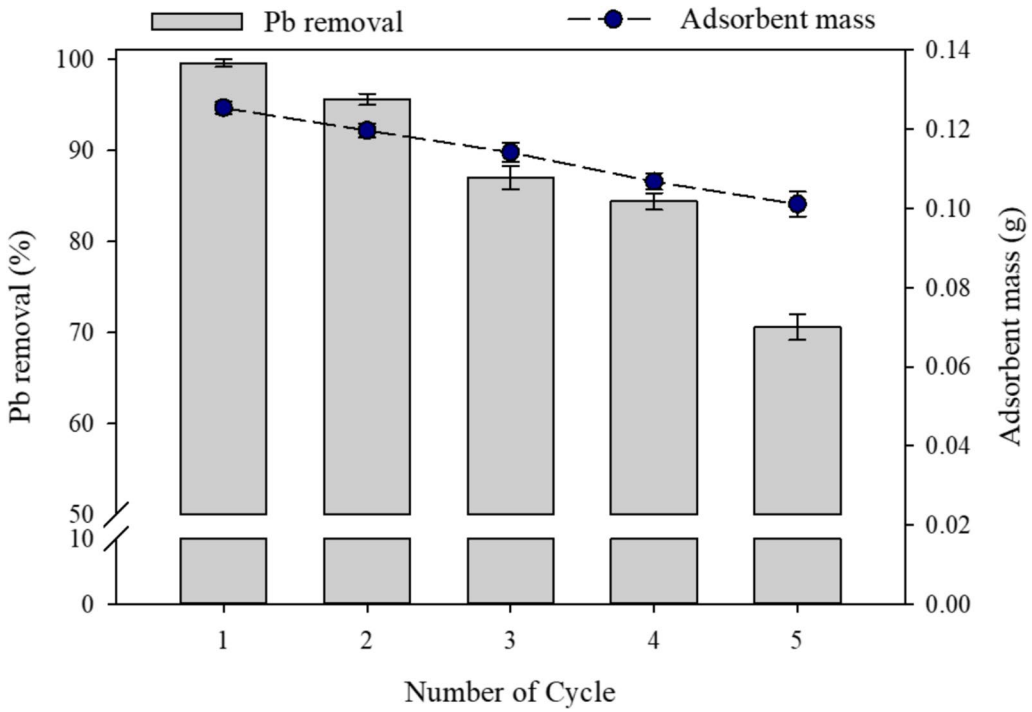

Fig. 13 Pb removal efficiency on HT9 over successive reuse cycles (pH 3)

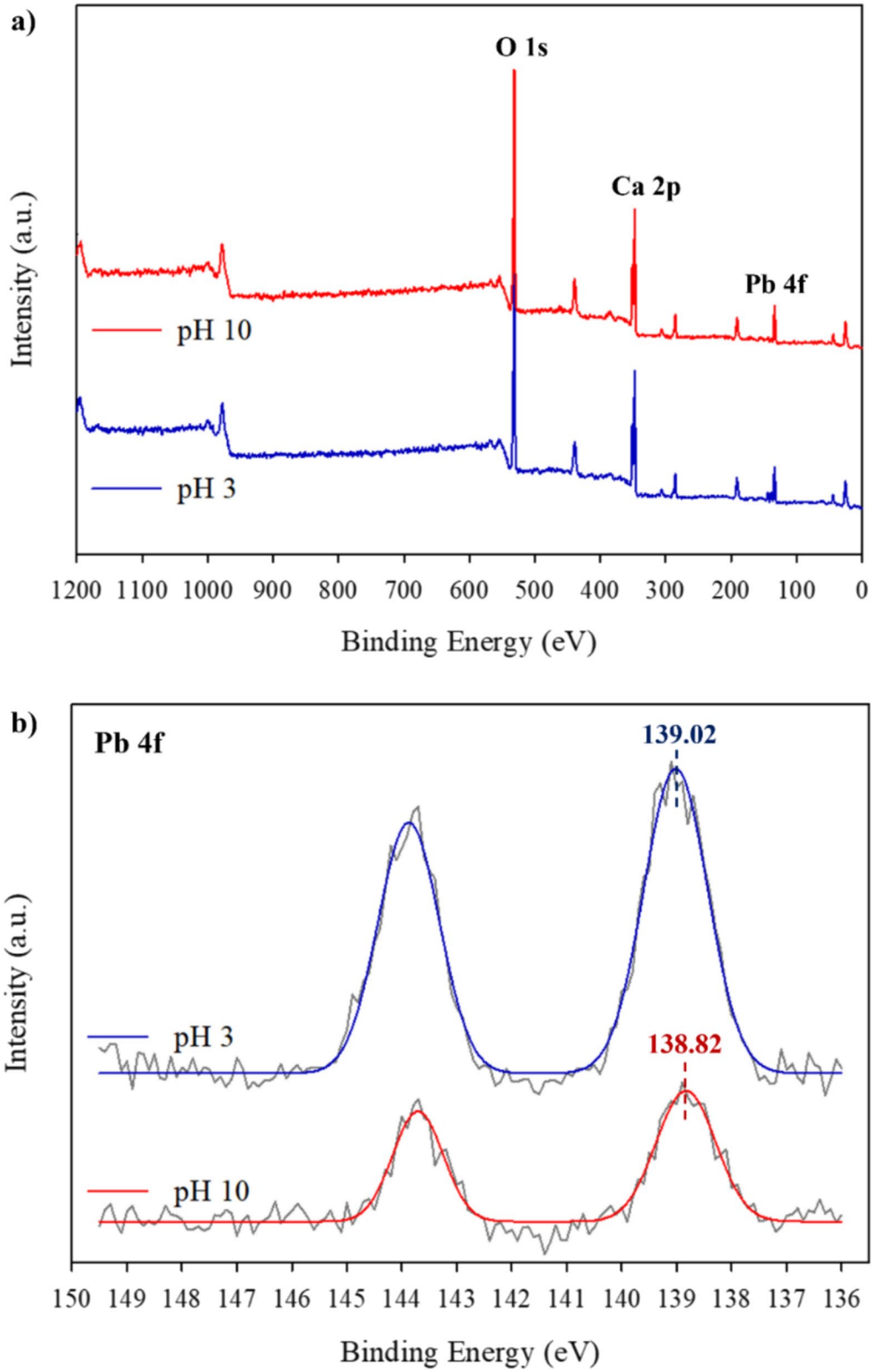

Fig. 14 Survey XPS spectra **(a)** and binding energies of Pb 4f **(b)** and XRD spectra **(c)** of Pb-contacted HT9 at pH 3 and pH10

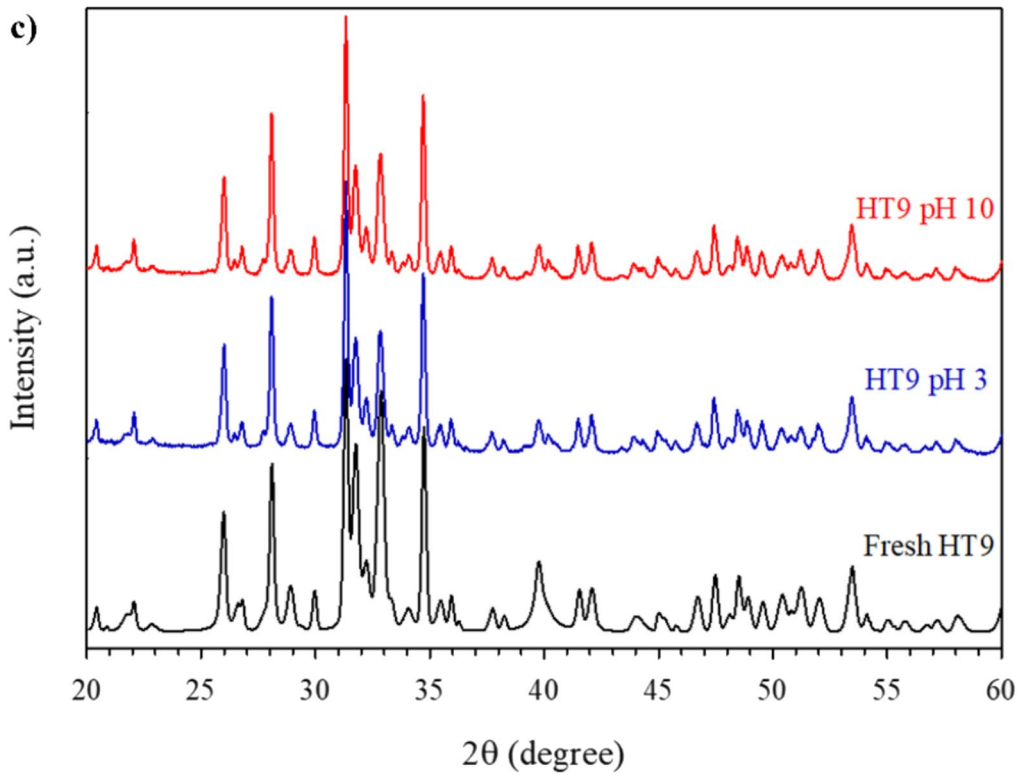

Fig. 14 continued

when the precursor ratio was far from the stoichiometric balance [41], whereas at 180–210 °C removal generally improved or remained high as Ca/P increased. These trends align with the suppression of β-TCP and enhancement of HAp crystallinity at higher temperature [42], coupled with favorable textural properties at Ca-excess conditions.

Kinetic analysis further supports a surface-reaction-controlled process. Pb uptake was rapid initially and approached equilibrium within 20–60 min, a behavior commonly observed for HAp and similar adsorbents [43], and the pseudo-second-order (PSO) model provided excellent fits across adsorbents, indicating that chemisorption governs the rate-limiting step, consistent with literature for HAp–Pb systems [44]. In practical terms, the steep early-time uptake followed by gradual plateau is consistent with a sequence of film diffusion, rapid site occupation, and a slower intraparticle-diffusion tail. Nevertheless, the overall rate law is captured best by the PSO expression. Notably, HT9 combined the highest equilibrium capacity (q_e = 2.4588 mg/g) with the fastest apparent rate constant (k_2 = 1.2012 g/mg·min), while HT5 showed the slowest kinetics (k_2 = 0.4499 g/mg·min), underscoring the role of synthesis-modified site accessibility and affinity. These results underscore the importance of carefully controlling both the synthesis temperature and the Ca/P ratio to optimize the structural and surface properties of biogenic HAp for lead adsorption [45].

Another key operational parameter is the adsorbent dosage. Operationally, adsorbent dosage exhibited the expected trade-off between total removal and per-mass utilization. Using HT9 (pH 3, C_0 = 5 mg/L), removal increased sharply from 14.6 to 96.5%, when the dosage increased from 0.5 to 2.0 g/L. Increasing the HAp dosage from 2.0 to 2.5 g/L slightly improved Pb uptake from 96.5 to 97.0%, but a further increase to 3.0 g/L led to a slight decrease to 95.4% removal. This trend suggested that while more adsorbent provides more active sites, beyond an optimal dosage particle agglomeration can reduce the effective surface area and thus the adsorption capacity [46]. Given the negligible performance gain (about 0.5%) versus a 20% increase in adsorbent usage at 2.5 g/L, the dosage of 2.0 g/L was selected as the optimal dosage to balance removal efficiency and material consumption.

Solution pH significantly also influenced the lead removal mechanism and efficiency. Experimentally, Pb^{2+} uptake followed the trend pH 7 (99.6% removal) > pH 3 (96.5%) > pH 7 (79.0%), highlighting how Pb speciation and HAp surface chemistry are affected by pH. The measured pH_{PZC} of approximately 6.0 implied a positively charged surface at pH 3 and a negatively charged surface at pH 7 and 10 [47]. At near-neutral pH, the HAp

surface carries only a mild charge and there is minimal proton competition, so most surface sites are readily available for Pb^{2+} binding. Under these conditions, lead is quickly sequestered through inner-sphere complexation with surface hydroxyl and phosphate groups, as well as through efficient $Ca^{2+} \leftrightarrow Pb^{2+}$ ion exchange. At acidic pH 3, the HAp surface becomes significantly protonated, which can reduce the number of binding sites and cause direct competition between H^+ and Pb^{2+}. However, the reduction in adsorption at low pH was partially offset by a dissolution–precipitation mechanism, maintaining high removal. Protons in the solution induced HAp dissolution, releasing phosphate species (H_2PO_{4-}/HPO_4^{2-}) into solution, which then combined with Pb^{2+} to precipitate highly insoluble lead-phosphate phases such as hydroxypyromorphite ($Pb_{10}(PO_4)_6(OH)_2$) [48]. In contrast, at pH 10, the removal efficiency dropped markedly. Although the HAp surface is strongly negative, Pb^{2+} ions tend to form soluble hydroxo complexes such as $Pb(OH)_3^-$, $Pb(OH)_4^{2}$ that are not as effectively incorporated at the HAp surface, and the limited HAp dissolution suppresses phosphate-driven precipitation; overall removal therefore declines [49].

To resolve the equilibrium curve at acidic pH without collapsing residual concentrations toward the detection limit, additional tests with HT9 at pH 3 were conducted at a reduced dose (0.5 g/L) across $C_0 = 2–6$ mg/L. As C_0 increased, the fractional removal decreased (from 40.5% to 17.0%), whereas the equilibrium uptake per gram (q_e) increased modestly (from 1.62 to 2.04 mg/g) and tended toward a shallow plateau near 2.0 mg/g. This behavior is consistent with a finite site density at fixed dose where higher concentration supplied greater driving force and raised q_e slightly [50]. However, because the number of sites per liter was fixed, the fraction of Pb removed necessarily declined.

Equilibrium isotherms acquired for HT9 under the studied conditions was fitted exceptionally by the Langmuir model ($R^2 = 0.9997$) with q_m of 2.20 mg/g and K_L of 2.49 L/mg, whereas the Freundlich fit ($R^2 = 0.9253$) was reasonable but inferior. This very tight Langmuir fit implied predominantly monolayer adsorption onto a relatively homogeneous population of sites, with negligible lateral interactions, consistent with mechanisms for HAp–Pb systems such as surface complexation on PO_4/OH groups and ion exchange with lattice Ca^{2+} [51].

The reusability of HT9 adsorbent was assessed over five consecutive batch-adsorption cycles without chemical regeneration. After each run, the spent adsorbent was recovered by centrifugation and oven-dried, no acid/base washing, chelating agent, or high-temperature desorption was applied. Under the identical conditions ($C_0 = 5$ mg/L, pH 3, contact time = 60 min), Pb removal efficiency dropped from above 99% in cycle 1 to 95.6%, 87.0%, 84.4%, and 70.6% in cycle 2–5. The decline is consistent with progressive occupation/occlusion of active sites by strongly bound or reprecipitated Pb-phosphate species on HAp [52], together with cumulative material loss between cycles. Additionally, the repeated oven-drying may induce microstructural changes such as microcracks or particle agglomeration that reduce the effective surface area and active site accessibility [53]. Despite this attenuation, HT9 maintained above 87% removal through cycle 3, indicating practical reusability without regeneration for applications that can tolerate moderate performance decay. Future work should evaluate targeted regeneration protocols to restore capacity.

Surface-sensitive analyses clarified the dominant immobilization pathways. XPS of spent HT9 confirmed Pb in the + 2 oxidation state under both acidic and alkaline conditions (binding energies around 139 eV for Pb $4f_{7/2}$ [54]. There was no evidence of Pb^{4+} or other oxidation states, which is expected since the chemistry of lead in aqueous adsorption typically involves Pb^{2+} binding. The intensity of the Pb 4f signal was substantially higher for the sample used at pH 3 than that at pH 10, consistent with the greater Pb uptake at low pH. Quantitatively, the surface atomic concentration of Pb on HAp was about 0.23% after adsorption at pH 3, compared to 0.09% at pH 10. Interestingly, the Pb $4f_{7/2}$ peak position shifted slightly between the two samples from 139.02 eV at pH 3 to 138.82 eV at pH 10. Both values are characteristic of Pb^{2+}, but the roughly 0.2 eV lower binding energy at pH 10 may indicate a slightly different chemical environment or bonding state for the lead. One possibility is that at pH 3, a significant portion of Pb^{2+} is present as surface phosphate species such as $Pb_3(PO_4)_2$ or precipitated as $Pb_5(PO_4)_3OH$ on the HAp surface [55], whereas at pH 10, Pb might be bonded more with hydroxyl groups (Pb–OH bonds), and possibly precipitated $Pb(OH)_2$ phase on or near the surface. This interpretation is consistent with the earlier discussion of mechanisms where low pH fosters formation of Pb–phosphate solids via HAp dissolution and reprecipitation, while high pH could lead to $Pb(OH)_2$ formation [56]. Powder XRD analysis of the Pb-loaded adsorbents revealed no new crystalline phases within the detection limits of XRD. This absence of new peaks, together with the low Pb concentrations detected by XPS, suggested that Pb was being immobilized in a highly dispersed form. The lead may be present as amorphous or nano-crystalline deposits on the HAp, or it may be incorporated into the HAp crystal lattice as a Pb–Ca substitution [57].

Looking ahead, further optimization of the HAp synthesis, for example, controlling particle size and morphology, and strategic ion doping with cations like Mg^{2+},

Sr^{2+}, or Si^{4+} could be explored to enhance adsorption performance and stability. Evaluating the material under multimetal conditions would also be valuable to determine selectivity and potential competition effects in real-world water-treatment scenarios. Finally, conducting long-term regeneration studies and life-cycle assessments will be important to ensure that the use of biogenic HAp for lead remediation is not only effective but also sustainable and economically viable in the context of circular-economy principles.

5 Conclusion

This study demonstrated an efficient, waste-to-resource route for producing hydroxyapatite (HAp) from fermented fish by-products via microwave-assisted hydrothermal synthesis, specifically targeting lead removal from contaminated water. The study identified optimal conditions for synthesizing HAp from fish bone waste, with a hydrothermal temperature of 210 °C and a Ca/P ratio of 2.0 yielding the most effective adsorbent (HT9), with a surface area of 14.08 m2/g and pore volume of 0.098 cm^3/g. SEM and XRD analyses revealed thin, porous sheet-like morphologies with the high crystallinity and well-ordered structure. Under optimal conditions (2.0 g/L dosage, pH 7), the synthesized HT9 achieved up to 99.6% lead removal within 60 min, where more than 90% of lead was removed within the first 10 min. Equilibrium adsorption data followed the Langmuir isotherm, indicating monolayer behavior, and chemisorption described by pseudo-second-order kinetics ($k = 1.2012$ g/mg·min, $q_e = 2.4588$ mg/g). XPS showed that Pb removal by HAp is strongly pH-dependent: Under acidic conditions (pH 3), it proceeded mainly via ion exchange and dissolution-driven reprecipitation of Pb-phosphate on the HAp surface, whereas under alkaline conditions, hydroxide precipitation and strong complexation to deprotonated surface groups predominated. Importantly, HT9 exhibited credible operational stability in reuse tests, maintaining the Pb removal of above 84% through 3 consecutive reuse cycles. Collectively, these results show that fermented fish bone-derived HAp can deliver high-efficiency Pb removal with promising short-term reusability, while advancing circular-economy goals by converting an abundant waste into a valuable water-treatment material, offering significant environmental and public health benefits.

Abbreviations

AAS	Atomic absorption spectroscopy
BET	Brunauer–Emmett–Teller
Ca/P	Calcium to phosphorus molar ratio
DI water	Deionized water
FT-IR	Fourier transform infrared spectroscopy
HAp	Hydroxyapatite
HT	Hydrothermal (used as a sample code prefix)
JCPDS	Joint Committee on Powder Diffraction Standards
Pb	Lead
PFO	Pseudo-first-order
pH_{PZC}	Point of zero charge
PSO	Pseudo-second-order
SEM	Scanning electron microscopy
TCP	Tricalcium phosphate
XPS	X-ray photoelectron spectroscopy
XRD	X-ray diffraction spectroscopy
XRF	X-ray fluorescence spectroscopy

Acknowledgements
The authors extend their sincere appreciation to the Department of Occupational Safety and Environmental Health, Faculty of Public Health, Khon Kaen University, and the Faculty of Science and Engineering, Kasetsart University Chalermphrakiat Sakon Nakhon Province Campus.

Author's contribution
E.K. and T.D. contributed to research concept and methodology. E.K., W.C., and R.C. were involved in experiment and instrumental analyses. T.D., R.J., R.C., and S.Y. provided technical support. E.K. and W.C. wrote and revised the manuscript. All authors contributed to data interpretation and validation, review, and final approval of the manuscript.

Funding
Not applicable.

Data availability
All data generated or analyzed during this study are included in this published article.

Declarations

Ethics approval and consent to participate
Not applicable.

Competing interests
The authors declare no competing interests.

Author details
[1]Department of Occupational Safety and Environmental Health, Faculty of Public Health, Khon Kaen University, Khon Kaen, Thailand. [2]Environmental Health Division, Faculty of Public Health, Naresuan University, Phitsanulok, Thailand. [3]Department of Mechanical and Manufacturing, Faculty of Sciences and Engineering, Kasetsart University Chalermphrakiat Sakon Nakhon Province Campus, Sakon Nakhon, Thailand. [4]Department of Civil and Environmental Engineering, Faculty of Science and Engineering, Kasetsart University Chalermphrakiat Sakon Nakhon Province Campus, Sakon Nakhon, Thailand.

Received: 16 June 2025 Accepted: 17 October 2025
Published online: 25 October 2025

References

1. Li X, Shen X, Jiang W, Xi Y, Li S (2024) Comprehensive review of emerging contaminants: detection technologies, environmental impact, and management strategies. Ecotoxicol Environ Saf 278:116420. https://doi.org/10.1016/j.ecoenv.2024.116420
2. Renu ST (2024) A review on regeneration of adsorbent and recovery of metals: adsorbent disposal and regeneration mechanism. S Afr J Chem Eng 50:39–50. https://doi.org/10.1016/j.sajce.2024.07.006
3. El Haddad M, Mamouni R, Saffaj N, Lazar S (2016) Evaluation of performance of animal bone meal as a new low cost adsorbent for the removal of a cationic dye Rhodamine B from aqueous solutions. J Saudi Chem Soc 20:S53–S59. https://doi.org/10.1016/j.jscs.2012.08.005
4. Bhushan B, Kotnala S, Nayak A (2024) Biogenic magnetic nanocomposite of hydroxyapatite and dextran: synthesis, characterization, and enhanced

removal of 2,4-D from aqueous environment. Environ Sci Pollut Res 31(27):39331–39349. https://doi.org/10.1007/s11356-024-33819-4
5. Nayak A, Bhushan B (2021) Hydroxyapatite as an advanced adsorbent for removal of heavy metal ions from water: focus on its applications and limitations. Mater Today Proc 46:11029–11034. https://doi.org/10.1016/j.matpr.2021.02.149
6. Alam MK, Sahadat Hossain M, Kawsar M, Bahadur NM, Ahmed S (2024) Synthesis of nano-hydroxyapatite using emulsion, pyrolysis, combustion, and sonochemical methods and biogenic sources: a review. RSC Adv 14(5):3548–3559. https://doi.org/10.1039/D3RA07559A
7. Bee S-L, Hamid ZAA (2020) Hydroxyapatite derived from food industry bio-wastes: syntheses, properties and its potential multifunctional applications. Ceram Int 46(11):17149–17175. https://doi.org/10.1016/j.ceramint.2020.04.103
8. Ibrahim M, Labaki M, Giraudon J-M, Lamonier J-F (2020) Hydroxyapatite, a multifunctional material for air, water and soil pollution control: a review. J Hazard Mater 383:121139. https://doi.org/10.1016/j.jhazmat.2019.121139
9. Castro MAM, Portela TO, Correa GS, Oliveira MM, Rangel JHG, Rodrigues SF et al (2022) Synthesis of hydroxyapatite by hydrothermal and microwave irradiation methods from biogenic calcium source varying pH and synthesis time. Bol Soc Esp Cerám Vidrio 61(1):35–41. https://doi.org/10.1016/j.bsecv.2020.06.003
10. Nayak A, Bhushan B, Gupta V, Kotnala S (2021) Fabrication of microwave assisted biogenic magnetite-biochar nanocomposite: a green adsorbent from jackfruit peel for removal and recovery of nutrients in water sample. J Ind Eng Chem 100:134–148. https://doi.org/10.1016/j.jiec.2021.05.028
11. Irfan M, Suprajaa PS, Praveen R, Reddy BM (2021) Microwave-assisted one-step synthesis of nanohydroxyapetite from fish bones and mussel shells. Mater Lett 282:128685. https://doi.org/10.1016/j.matlet.2020.128685
12. Etinosa PO, Osuchukwu OA, Anisiji EO, Lawal MY, Mohammed SA, Ibitoye OI et al (2024) In-depth review of synthesis of hydroxyapatite biomaterials from natural resources and chemical regents for biomedical applications. Arab J Chem 17(12):106010. https://doi.org/10.1016/j.arabjc.2024.106010
13. Ivanets AI, Kitikova NV, Shashkova IL, Roshchina MY, Srivastava V, Sillanpää M (2019) Adsorption performance of hydroxyapatite with different crystalline and porous structure towards metal ions in multicomponent solution. J Water Process Eng 32:100963. https://doi.org/10.1016/j.jwpe.2019.100963
14. Liu M, Li Z, Chen Q, Yang X, Chen J, Zhang L et al (2024) Preparation and characterization of grouper bone peptides-calcium complex by lactic acid bacteria fermentation. LWT 201:116224. https://doi.org/10.1016/j.lwt.2024.116224
15. Petrat P, Klomklao S, Visessanguan W, Benjakul S, Kishimura H (2025) Biocalcium phosphate powders prepared from threadfin bream (*Nemipterus hexodon*) bone: properties and comparison with calcined fish bone powder. J Agric Food Res 22:102041. https://doi.org/10.1016/j.jafr.2025.102041
16. Malau ND 2024 Synthesis and characterization of hydroxyapatite derived from limestone. 46 1 7 https://doi.org/10.52155/ijpsat.v46.1.6505
17. Kavand M, Eslami P, Razeh L (2020) The adsorption of cadmium and lead ions from the synthesis wastewater with the activated carbon: optimization of the single and binary systems. J Water Process Eng 34:101151. https://doi.org/10.1016/j.jwpe.2020.101151
18. Revellame ED, Fortela DL, Sharp W, Hernandez R, Zappi ME (2020) Adsorption kinetic modeling using pseudo-first order and pseudo-second order rate laws: a review. Cleaner Eng Technol 1:100032. https://doi.org/10.1016/j.clet.2020.100032
19. Gupta P, Nagpal G, Gupta N (2021) Fly ash-based geopolymers: an emerging sustainable solution for heavy metal remediation from aqueous medium. Beni-Suef Univ J Basic Appl Sci 10(1):89. https://doi.org/10.1186/s43088-021-00179-8
20. Sánchez-Campos D, Reyes Valderrama MI, López-Ortíz S, Salado-Leza D, Fernández-García ME, Mendoza-Anaya D et al (2021) Modulated monoclinic hydroxyapatite: the effect of pH in the microwave assisted method. Minerals 11(3):314
21. Daupor H (2021) Extraction of hydroxyapatite by alkaline acid from Budu waste and synthesis using calcination method. J Phys: Conf Ser 2049(1):012041. https://doi.org/10.1088/1742-6596/2049/1/012041
22. Koutsopoulos S (2002) Synthesis and characterization of hydroxyapatite crystals: a review study on the analytical methods. J Biomed Mater Res 62(4):600–612. https://doi.org/10.1002/jbm.10280
23. Vinoth Kumar KC, Jani Subha T, Ahila KG, Ravindran B, Chang SW, Mahmoud AH et al (2021) Spectral characterization of hydroxyapatite extracted from Black Sumatra and Fighting cock bone samples: a comparative analysis. Saudi Bio Sci 28(1):840–846. https://doi.org/10.1016/j.sjbs.2020.11.020
24. Ebrahimi S, Stephen Sipaut@ Mohd Nasri C, Bin Arshad SE (2021) Hydrothermal synthesis of hydroxyapatite powders using Response Surface Methodology (RSM). PLOS ONE. 16 5:e0251009. https://doi.org/10.1371/journal.pone.0251009
25. Zhang T, Xiao X (2020) Hydrothermal synthesis of hydroxyapatite assisted by gemini cationic surfactant. J Nanomater 2020(1):6173867. https://doi.org/10.1155/2020/6173867
26. Balderas-Hernández P, Ibanez J, Godinez-Ramirez J, Almada-Calvo F (2006). Microscale environmental chemistry: Part 7. Estimation of the point of zero charge (pzc) for simple metal oxides by a simplified potentiometric mass titration method. Chem Educator. 11:267–70. https://doi.org/10.1333/s00897061012a
27. Jiang F, Liu M, Li S, Liang M, Hu X, Li F (2024) Mechanism study on the immobilization of Cu2+/Pb2+ in aqueous phase by mineral co-milling-modified biochar. Langmuir 40(34):17897–17908. https://doi.org/10.1021/acs.langmuir.4c00948
28. Mousa SM, Ammar NS, Ibrahim HA (2016) Removal of lead ions using hydroxyapatite nano-material prepared from phosphogypsum waste. J Saudi Chem Soc 20(3):357–365. https://doi.org/10.1016/j.jscs.2014.12.006
29. Hayati B, Maleki A, Najafi F, Daraei H, Gharibi F, McKay G (2017) Adsorption of Pb2+, Ni2+, Cu2+, Co2+ metal ions from aqueous solution by PPI/SiO2 as new high performance adsorbent: preparation, characterization, isotherm, kinetic, thermodynamic studies. J Mol Liq 237:428–436. https://doi.org/10.1016/j.molliq.2017.04.117
30. Mudhoo A, Chu KH, Mondal P (2023) Attrition resistance, a sporadically studied factor in aqueous adsorption: status quo and research outlook towards creating better adsorbents. Particuology 77:71–78. https://doi.org/10.1016/j.partic.2022.08.013
31. Huang Y, Luo X, Liu C, You S, Rad S, Qin L (2023) Effective adsorption of Pb(ii) from wastewater using MnO2 loaded MgFe-LD(H)O composites: adsorption behavior and mechanism. RSC Adv 13(28):19288–19300. https://doi.org/10.1039/D3RA03035K
32. Guan D-X, Ren C, Wang J, Zhu Y, Zhu Z, Li W (2018) Characterization of lead uptake by nano-sized Hydroxyapatite: a molecular scale perspective. ACS Earth Space Chem 2(6):599–607. https://doi.org/10.1021/acsearthspacechem.8b00020
33. Giocondi JL, El-Dasher BS, Nancollas GH, Orme CA (2010) Molecular mechanisms of crystallization impacting calcium phosphate cements. Philos Trans A Math Phys Eng Sci 368(1917):1937–1961. https://doi.org/10.1098/rsta.2010.0006
34. Zhou H, Yang L, Gbureck U, Bhaduri SB, Sikder P (2021) Monetite, an important calcium phosphate compound–its synthesis, properties and applications in orthopedics. Acta Biomater 127:41–55. https://doi.org/10.1016/j.actbio.2021.03.050
35. Balu S, Sundaradoss MV, Andra S, Jeevanandam J (2020) Facile biogenic fabrication of hydroxyapatite nanorods using cuttlefish bone and their bactericidal and biocompatibility study. Beilstein J Nanotechnol 11:285–295. https://doi.org/10.3762/bjnano.11.21
36. Mondal S, Hoang G, Manivasagan P, Moorthy MS, Kim HH, Vy Phan TT et al (2019) Comparative characterization of biogenic and chemical synthesized hydroxyapatite biomaterials for potential biomedical application. Mater Chem Phys 228:344–356. https://doi.org/10.1016/j.matchemphys.2019.02.021
37. Szterner P, Biernat M (2022) The synthesis of hydroxyapatite by hydrothermal process with calcium lactate pentahydrate: the effect of reagent concentrations, pH, temperature, and pressure. Bioinorg Chem Appl 2022(1):3481677. https://doi.org/10.1155/2022/3481677
38. Bertocco A, Capela M, Caetano APF, Nito A, Quarta A, Seabra MP et al (2025) Porous hydroxyapatite - β-tricalcium phosphate ceramics produced from a rapid sol-gel process. Sci Rep 15(1):16422. https://doi.org/10.1038/s41598-025-01253-2
39. Elkady MF, Mahmoud MM, Abd-El-Rahman HM (2011) Kinetic approach for cadmium sorption using microwave synthesized

nano-hydroxyapatite. J Non-Cryst Solids 357(3):1118–1129. https://doi.org/10.1016/j.jnoncrysol.2010.10.021
40. Iconaru SL, Motelica-Heino M, Guegan R, Beuran M, Costescu A, Predoi D (2018) Adsorption of Pb (II) ions onto hydroxyapatite nanopowders in aqueous solutions. Materials 11(11):2204
41. Fitriana D, Mudasir M, Siswanta D (2025) The modification of coal fly ash adsorbent using dithizone immobilization for Cd(II) ions removal. J Kim Sains dan Apl 2025:10. https://doi.org/10.14710/jksa.28.4.215-224
42. Yang X, Zhou Y, Hu J, Zheng Q, Zhao Y, Lv G et al (2024) Clay minerals and clay-based materials for heavy metals pollution control. Sci Total Environ 954:176193. https://doi.org/10.1016/j.scitotenv.2024.176193
43. Googerdchian F, Moheb A, Emadi R (2012) Lead sorption properties of nanohydroxyapatite–alginate composite adsorbents. Chem Eng J 200–202:471–479. https://doi.org/10.1016/j.cej.2012.06.084
44. Hamad AA, Hassouna MS, Shalaby TI, Elkady MF, Abd Elkawi MA, Hamad HA (2020) Electrospun cellulose acetate nanofiber incorporated with hydroxyapatite for removal of heavy metals. Int J Biol Macromol 151:1299–1313. https://doi.org/10.1016/j.ijbiomac.2019.10.176
45. Bailliez S, Nzihou A, Bèche E, Flamant G (2004) Removal of lead (Pb) by hydroxyapatite sorbent. Process Saf Environ Prot 82(2):175–180. https://doi.org/10.1205/095758204322972816
46. Balasooriya IL, Chen J, Korale Gedara SM, Han Y, Wickramaratne MN (2022) Applications of nano hydroxyapatite as adsorbents: a review. Nanomaterials 12(14):2324
47. Bell LC, Posner AM, Quirk JP (1973) The point of zero charge of hydroxyapatite and fluorapatite in aqueous solutions. J Colloid Interface Sci 42(2):250–261. https://doi.org/10.1016/0021-9797(73)90288-9
48. Mavropoulos E, Rossi AM, Costa AM, Perez CAC, Moreira JC, Saldanha M (2002) Studies on the mechanisms of lead immobilization by hydroxyapatite. Environ Sci Technol 36(7):1625–1629. https://doi.org/10.1021/es0155938
49. Chowdhury IR, Chowdhury S, Mazumder MAJ, Al-Ahmed A (2022) Removal of lead ions (Pb2+) from water and wastewater: a review on the low-cost adsorbents. Appl Water Sci 12(8):185. https://doi.org/10.1007/s13201-022-01703-6
50. de Souza RF, de Almeida RRR, Omori EK, de Souza RT, Lenzi EK, Evangelista LR et al (2023) Role of the number of adsorption sites and adsorption dynamics of diffusing particles in a confined liquid with langmuir kinetics. Physchem 3(1):1–12
51. Hajiahmadi Z, Moheb A, Mohammadi M, Marzban N, Scheufele FB (2024) Surface and mass transfer kinetic and equilibrium modeling of Pb(II) ions adsorption on hydroxyapatite scaffold: batch and fixed-bed column studies. Sep Purif Technol 343:127141. https://doi.org/10.1016/j.seppur.2024.127141
52. Zhou M, Yan X, Zou H, Zhao Y, Yin N, Zhang C et al (2019) Enhanced adsorption of Pb(II) from aqueous solution by magnesium- incorporated hydroxyapatite with poor crystalline structure. Desalin Water Treat 171:183–195. https://doi.org/10.5004/dwt.2019.24762
53. Xu W-l, Sun X-h, Xue D, Guo J-z, Yan X-k, Sun P-j et al (2025) Effect of heat-treatment on microstructure of hydroxyapatite porous microspheres for enhanced biocompatibility. J Saudi Chem Soc 29(3):8. https://doi.org/10.1007/s44442-025-00010-4
54. López EO, Bernardo PL, Checca NR, Rossi AL, Mello A, Ellis DE et al (2022) Hydroxyapatite and lead-substituted hydroxyapatite near-surface structures: Novel modelling of photoemission lines from X-ray photoelectron spectra. Appl Surf Sci 571:151310. https://doi.org/10.1016/j.apsusc.2021.151310
55. Li X, Feng J, Zhu F, Ke W, Huang Y, Wu C et al (2025) Remediation of Pb, Cd, and As contaminated soils by phosphate-solubilizing bacteria and iron-doped hydroxyapatite: multi-pathway immobilization mechanisms. Chem Eng J 522:167445. https://doi.org/10.1016/j.cej.2025.167445
56. Kim SH, Chung H, Jeong S, Nam K (2021) Identification of pH-dependent removal mechanisms of lead and arsenic by basic oxygen furnace slag: relative contribution of precipitation and adsorption. J Clean Prod 279:123451. https://doi.org/10.1016/j.jclepro.2020.123451
57. Ellis DE, Terra J, Warschkow O, Jiang M, González GB, Okasinski JS et al (2006) A theoretical and experimental study of lead substitution in calcium hydroxyapatite. Phys Chem Chem Phys 8(8):967–976

Publisher's Note

ARTICLES FOR FACULTY MEMBERS

BONE-DERIVED HYDROXYAPATITE TOOTHPASTE FOR SUSTAINABLE PHARMACEUTICAL AND BIOMEDICAL APPLICATIONS

Natural sources of hydroxyapatite for biomedical applications / Suresh, N., Sweety, V. K., Suresh, N., Suraj, A. R., Waltimo, T., & Anil, S.

Ceramics International
Volume 52 Issue 2 (2026) Pages 1383-1391
https://doi.org/10.1016/j.ceramint.2025.12.019
(Database: ScienceDirect)

Ceramics International 52 (2026) 1383–1391

Contents lists available at ScienceDirect

Ceramics International

journal homepage: www.elsevier.com/locate/ceramint

Review article

NATURAL sources of hydroxyapatite for biomedical applications

Nandita Suresh [a,b,*], Vishnupriya K. Sweety [c], Namrata Suresh [d], Amartya Raj Suraj [c], Tuomas Waltimo [a,e], Sukumaran Anil [f,g]

[a] Department of Oral and Maxillofacial Diseases, Helsinki University and University Hospital, Helsinki, Finland
[b] Global Research Cell, Dr. D. Y. Patil Dental College & Hospital, Dr. D. Y. Patil Vidyapeeth (Deemed to be University), Pimpri, Pune 411018, India
[c] Pushpagiri Institute of Medical Sciences and Research Centre, Mendicity, Perumthuruthy, Tiruvalla, Kerala, India
[d] Department of Dental Research Cell, Dr. D. Y. Patil Dental College and Hospital, Dr. D. Y. Patil Vidyapeeth, Pune 411018, India
[e] Faculty of Medicine, University of Basel, Switzerland
[f] Oral Health Institute, Hamad Medical Corporation, Doha, Qatar
[g] College of Dental Medicine, Qatar University, Doha, Qatar

ARTICLE INFO

Keywords:
Natural hydroxyapatite
Calcium phosphate bioceramics
Bone tissue engineering
Controlled drug delivery
Dental biomaterials
Orthopedic implants
Biogenic materials
Osteoconduction

ABSTRACT

Hydroxyapatite (HAp, $Ca_{10}(PO_4)_6(OH)_2$) is a calcium phosphate bioceramic that constitutes approximately 70 % of the mineral phase in bone and teeth, making it a critical biomaterial for clinical applications. While synthetic hydroxyapatite has demonstrated clinical success, its limitations, including energy-intensive production processes, suboptimal crystallinity, and reduced biological activity compared to biogenic alternatives, have driven the investigation of naturally derived sources. This review aims to provide a quantitative comparison of natural HAp sources and extraction methods, critically evaluate biomedical applications with performance metrics, assess toxicological and regulatory challenges, and establish specific research priorities for clinical translation. Natural sources, including mammalian bone (bovine, porcine), marine resources (fish scales, fish bone), avian eggshells, and marine corals, yield HAp with inherent trace element substitutions (Mg^{2+}, Sr^{2+}, Na^{+}, CO_3^{2-}) and hierarchical micro-nanostructures that more closely approximate native bone composition, potentially enhancing osteoconductivity, osteointegration, and remodeling kinetics. We systematically analyze extraction protocols (thermal decomposition, alkaline hydrolysis, subcritical water processing), evaluate clinical applications spanning bone regeneration, periodontal therapy, and controlled drug delivery, and critically assess barriers including batch-to-batch variability, pathogen transmission risks, and regulatory complexities. Emerging strategies encompass green extraction technologies, surface functionalization with bioactive molecules, composite fabrication with synthetic polymers, and integration with additive manufacturing for patient-specific implants. This review identifies knowledge gaps in long-term biocompatibility, degradation kinetics, and clinical translation, providing a roadmap for advancing natural hydroxyapatite toward standardized, sustainable biomedical applications.

1. Introduction

Hydroxyapatite ($Ca_{10}(PO_4)_6(OH)_2$) is a naturally occurring calcium phosphate mineral that constitutes the primary inorganic phase of mammalian bone and teeth. Composed of calcium, phosphate, and hydroxyl ions, this bioceramic exhibits excellent bioactivity, biocompatibility, and osteoconductivity, which enable it to form a direct bond with living bone. These properties have established hydroxyapatite (HAp) as a cornerstone material in regenerative medicine, with wide-ranging biomedical applications including orthopedic implants, dental restorations, maxillofacial reconstruction, bone graft substitutes, and tissue engineering scaffolds [1]. Although synthetic HAp has been extensively investigated and employed, several limitations restrict its widespread clinical use. Conventional synthesis techniques—such as sol–gel, precipitation, and solid-state reactions—often require stringent conditions, expensive precursors, and high energy inputs. This not only elevates production costs but also results in variability in stoichiometry, crystallinity, and particle morphology across batches. More importantly, synthetic HAp frequently lacks trace bioactive elements and microstructural complexity present in natural bone mineral, which can limit

* Corresponding author. Department of Oral and Maxillofacial Diseases, Helsinki University and University Hospital, Helsinki, Finland:
E-mail address: nandita.suresh@helsinki.fi (N. Suresh).

https://doi.org/10.1016/j.ceramint.2025.12.019
Received 1 June 2025; Received in revised form 23 November 2025; Accepted 2 December 2025
Available online 5 December 2025

its biological performance, particularly in long-term integration and remodeling [2]. These challenges have stimulated growing interest in naturally derived hydroxyapatite, obtained from sustainable biological and mineral resources.

Naturally derived HAp can be sourced from diverse origins. Terrestrial animal bones (e.g., bovine, camel, horse) are widely used, offering high yields of calcium phosphate with physicochemical properties similar to human bone. Marine-derived materials such as fish bones, scales, and shells from clams, cockles, and oysters provide abundant and low-cost sources that also contain trace elements beneficial for osteogenesis. Eggshells, a common by-product of the poultry industry, offer a sustainable and eco-friendly precursor for HAp synthesis. Emerging research has also explored plant and algal matter as unconventional sources, expanding the scope of natural precursors. Additionally, mineral resources like limestone provide an abundant geological alternative for HAp production [3].

A distinguishing advantage of naturally sourced HAp is the presence of biologically relevant trace elements including magnesium, sodium, strontium, and zinc, which play critical roles in bone metabolism, mineralization, and remodeling. These trace ions improve physicochemical stability, enhance osteoblast activity, and modulate the immune response at the host–implant interface, resulting in improved bone regeneration and functional integration with host tissue. Natural HAp also exhibits porosity and hierarchical structures more closely resembling native bone, offering advantages in mechanical performance and vascularization [4,5].

Despite these promising features, systematic evaluation and standardization of natural HAp remain limited. Many studies report extraction and characterization of HAp from individual sources, yet comprehensive comparisons of different origins and methods are lacking. Moreover, while several reviews exist, most focus on either the chemistry of synthesis or broad applications, without critically addressing clinical translatability and the regulatory landscape. This review seeks to address these gaps by providing (i) a systematic comparison of natural HAp sources, supported by quantitative performance data; (ii) a critical analysis of extraction and processing techniques, highlighting their advantages, limitations, and scalability; (iii) a comprehensive assessment of biomedical applications across orthopedics, dentistry, and drug delivery; and (iv) an evidence-based discussion of challenges and future directions, with recommendations for clinical translation.

By integrating recent advances and highlighting unresolved issues, this review aims to establish a roadmap for harnessing the full potential of natural hydroxyapatite as a sustainable, high-performance biomaterial for regenerative medicine.

2. Natural sources and extraction methods

2.1. Natural sources

Natural hydroxyapatite (HAp) occurs primarily in mineralized tissues across diverse biological systems, offering sustainable alternatives to synthetic production with inherent advantages including native trace-element substitutions, hierarchical micro/nanostructures, and enhanced biocompatibility [6]. HAp sources are systematically categorized into four principal groups: mammalian hard tissues, aquatic/marine organisms, shell derivatives, and plant-based materials (Fig. 1, Table 1).

Mammalian sources (bovine, porcine, camel bones) represent the most commercially established category, comprising 60–70 % HAp, with the remainder being primarily collagen [7,8]. These sources closely match human bone composition (Ca/P ratio: 1.65–1.67) and contain biologically relevant trace,elements (Mg^{2+}, Na^{+}, Zn^{2+}, Sr^{2+}) that enhance osteogenic potential. Bovine bone dominates commercial production due to its availability in the meat industry [9]. The extraction from bovine bone involves sequential pre-treatment and high-temperature calcination. Fresh bone is mechanically cleaned,

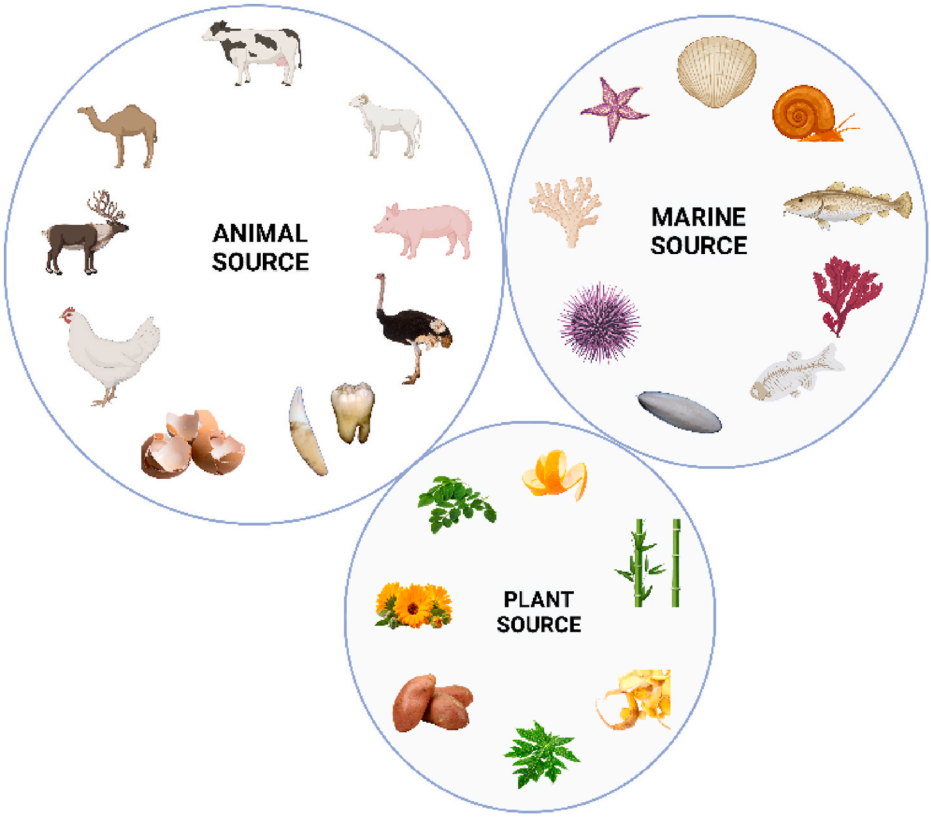

Fig. 1. A diagram illustrating the various natural sources of hydroxyapatite.

Table 1
Comprehensive characterization of natural hydroxyapatite sources.

Category/ Specific Source	HAp Content (%)	Ca/P Molar Ratio	Key Trace Elements (wt %)	Advantages
MAMMALIAN				
Bovine femur [9]	65–70	1.65–1.67	Mg, Na, Sr, Zn	High availability, structural similarity to human bone
Camel bone [8]	60–65	1.67–1.69	Mg, Na, Sr	High crystallinity, cultural acceptability
Porcine bone [7]	62–68	1.64–1.66	Mg, Na, Zn, Fe	Good mechanical properties
MARINE				
Fish scales [13,14]	45–55	1.65–1.70	Sr, Mg, Na, K	Abundant waste utilization, eco-friendly
Fish bones [12]	60–70	1.64–1.68	Sr, Mg, Na, F	High-purity potential, waste valorization
Coral [60]	85–95	1.67–1.69	Mg, Sr, Ba, F	Rapid microwave synthesis potential
SHELLS				
Chicken eggshell [16]	$CaCO_3$: 94–96 %	1.67–1.69	Mg, Sr	Abundant availability, low cost
Cockle shell [61]	$CaCO_3$ (90 %)	1.60–1.65	Mg, Na	Cost-effective processing
PLANT/ALGAL				
Moringa oleifera leaf [62]	Low Ca/P content	1.70–1.75	Various organics	Sustainable, renewable source
Citrus peels [63]	Organic matrix, 85–90 %	Variable	Limonene, vitamins	Agricultural waste utilization
Red algae [64]	$CaCO_3$: 75–85 %	1.55–1.72	Mg, Sr	Renewable marine resource; High Mg substitution; Natural bioactivity

reduced to 1–2 cm fragments, and subjected to lipid extraction using an acetone-chloroform mixture (1:1 v/v, 24h), followed by deproteinization with 1M NaOH at 80 °C for 4 h to remove collagen and proteins [10]. The pre-treated bone is calcined at 900 °C for 4 h with controlled cooling (5 °C/min) to prevent thermal shock. The resulting HAp exhibits Ca/P ratio of 1.67 ± 0.02, crystallinity of 85–90 %, and particle sizes tunable within 20–80 μm through grinding [11].

Marine sources leverage seafood processing waste for environmental sustainability. Fish scales and bones (45–70 % HAp) uniquely incorporate marine-specific elements, particularly strontium, promoting osteoblast differentiation [12,13]. cFish scales undergo optimized processing: an HCl wash (0.5 M, 2 h) removes surface organics, followed by alkaline hydrolysis with 2 M NaOH at 250 °C for 5 h, effectively decomposing organic fractions and facilitating mineral release. The resulting HAp exhibits a rod-like morphology with a high aspect ratio, particle size of 5–15 μm, and an enhanced surface area (80–120 m^2/g), providing superior drug adsorption capacity. Coral skeletons offer the highest HAp content (85–95 %) with interconnected porosity (200–500 μm) mimicking cancellous bone, though conservation regulations limit their use [14,15].

Shell-based sources primarily consist of calcium carbonate, requiring chemical conversion to HAp. Eggshells generate 8.5 million tons of waste annually, providing the most abundant and cost-effective source despite conversion yield losses [16]. Marine shells offer regional alternatives in coastal areas with established shellfish industries. Shell processing involves initial cleaning, size reduction to powder, acid treatment for decalcification, and subsequent phosphatization through hydrothermal or precipitation methods to achieve HAp conversion [17].

Plant and algal sources remain largely experimental, requiring external calcium and phosphate supplementation because of their low intrinsic mineral content [18]. However, they offer renewable templates with unique organic-mineral interfaces for specialized applications. Processing begins with the collection and washing of dried plant matter, followed by calcination at 600–900 °C to decompose organics and concentrate inorganic fractions [19]. Additional phosphoric acid treatment or hydrothermal reaction achieves the desired Ca/P stoichiometry. Rice husk ash treated with $Ca(OH)_2$ and phosphoric acid yields nanoscale HAp with Ca/P ratio approaching 1.67 [20]. Algal sources rich in calcium carbonate convert to HAp via direct reaction with phosphate precursors under hydrothermal conditions [3]. Plant-derived HAp typically displays nanoscale particles (20–100 nm) with high specific surface areas, incorporating trace ions (Mg, K, Si) that enhance bioactivity and stimulate osteoblast differentiation [21].

Extraction methods vary significantly in their efficiency and product characteristics (Table 2). Thermal decomposition (calcination) at 600–1000 °C for 2–6 h yields 85–95 % purity with 70–90 % extraction efficiency, producing microcrystals (1–10 μm) with high crystallinity (Fig. 2). Alkaline hydrolysis using 1–4 M NaOH at 60–100 °C for 4–24 h achieves 75–85 % purity and 60–75 % efficiency, generating submicron particles (0.5–5 μm) at low cost [22]. Microwave synthesis at 100–150 °C for 0.5–2 h provides rapid processing with 88–95 % purity and 55–70 % efficiency, producing nanoparticles (20–70 nm) [23]. Hydrothermal methods at 150–200 °C for 6–24 h yield high-quality crystals (50–200 nm) with 92–97 % purity and 65–80 % efficiency [24].

Source selection depends on multiple factors: compositional similarity to human bone, processing complexity, regulatory requirements, and intended application. Mammalian sources excel in structural applications due to compositional similarity; marine sources offer unique trace elements beneficial for bioactivity; shell sources provide cost-effective options for composite materials. The main advantages of plant-derived HAp include sustainability, abundance, and environmental friendliness, though challenges remain, including compositional variability and the need for standardized extraction protocols [25].

3. Biomedical applications of hydroxyapatite

Hydroxyapatite (HAp) is highly sought after in the biomedical field due to its excellent biocompatibility, bioactivity, osteoconductivity, and its likeness to the mineral component of human bone. Here are some major applications of HAp in the biomedical field.

3.1. Bioactive coatings of hydroxyapatite (HAp)

Applying HAp coatings onto orthopedic and dental implants brings several significant benefits. Firstly, HAp coatings enhance the osseointegration of implants, promoting bone growth at the bone-implant interface and reducing the risk of implant loosening or failure [26]. They provide a bioactive surface for osteoblasts (bone-forming cells) to proliferate, leading to faster healing and enhanced implant stability. HAp coatings also serve as a promising platform for drug delivery. The large surface area and porous nature of HAp coatings enable the loading of various therapeutic agents. For instance, antibiotics can be incorporated into the HAp coating to prevent postoperative infections [27].

Additionally, anti-inflammatory drugs or growth factors can be embedded within the coating for localized delivery, enhancing healing and reducing systemic side effects. Furthermore, HAp coatings regulate the dissolution rate of metallic implants. Since HAp is similar to the mineral component of bone, it dissolves at a rate that can match new bone growth. This property is essential in maintaining the mechanical stability of the implant over time and avoiding any possible detrimental effects from excessive ion release into the surrounding tissues [28]. Deposition of HAp coatings onto implants has been achieved through various techniques, each offering distinct advantages and challenges.

Plasma Spraying: Currently the most prevalent commercial method, the plasma spray technique employs an electric arc to generate a high-temperature plasma jet into which HAp powder is fed. The heat causes the HAp particles to melt, then sprayed onto the implant surface to form

Table 2
Quantitative comparison of HAp extraction methods.

Method	Temperature (°C)	Time	Extraction Efficiency (%)	Particle Size	Purity (%)	Yield (%)	Cost	Key Advantages
Thermal Calcination [38]	600–1000	2–6 h	70–90	1–10 μm	85–95	60–85	Low	Simple, high crystallinity
Alkaline Hydrolysis [44]	60–100	4–24 h	60–75	0.5–5 μm	75–85	50–70	Low	Low temperature preserves structure
Enzymatic Hydrolysis [45]	37–50	12–24 h	60–75	<10 μm	85–92	50–65	Low	Nanomedicine applications
Sol-gel Precipitation [5]	60–100	4–12 h	50–70	1–10 μm	85–93	40–60	Low	Coatings, thin films
Microwave Synthesis [36]	100–150	0.5–2 h	65–80	20–70 nm	88–95	55–70	Medium	Rapid processing, nanoparticles
Hydrothermal [37]	150–200	6–24 h	80–90	50–200 nm	92–97	65–80	Medium	High-quality crystals

Fig-2. Schematic diagram demonstrating the procedure for the preparation of hydroxyapatite.

the coating. This method allows high deposition rates and the ability to coat complex geometries [29]. However, the high processing temperatures can lead to phase transformations in HAp, possibly affecting its bioactivity.

Sol-gel Deposition: The sol-gel process involves the transition of a solution system from a liquid 'sol' into a solid 'gel.' By controlling the sol composition, a gel-like network of HAp is formed, which can be coated onto the implant [30]. The advantages include a uniform coating, excellent control over coating thickness, and low processing temperatures. The primary challenge is the requirement for post-deposition heat treatment to enhance coating adhesion.

Electrochemical Deposition: This method uses an electric current to deposit HAp onto the implant surface. The benefits of this approach include excellent control over the coating composition, crystallinity, and thickness. However, precise control of the electrolyte composition and processing conditions is essential, complicating the technique [31].

Biomimetic Deposition: It mimics the natural biomineralization process in which the implant is immersed in a simulated body fluid containing ions in human plasma. Over time, a carbonated HAp layer forms on the implant surface [32]. Although this process is time-consuming, it creates a highly bioactive coating similar to the mineral phase of natural bone.

Hydroxyapatite coatings represent a promising strategy to enhance the bioactivity of orthopedic and dental implants, offering a harmonious interface between the synthetic implant and the natural tissue [33]. With their exceptional biocompatibility, osteoconductivity, and capability to deliver therapeutic agents, HAp coatings could significantly improve patient outcomes in orthopedic surgery [33]. Although challenges persist in optimizing the deposition process and long-term stability of the coatings, ongoing research, and technological advancements provide a hopeful trajectory toward developing sophisticated, bioactive implant surfaces.

3.2. *Hydroxyapatite as a potential vehicle for gene therapy*

Gene therapy has emerged as a promising strategy for treating various diseases, including genetic disorders, cancers, and infectious diseases. However, the success of gene therapy is contingent upon the development of safe and efficient gene delivery systems. Hydroxyapatite has shown promise as a non-viral vector for gene delivery due to its positive surface charge, which allows for the adsorption of negatively charged DNA molecules. This interaction protects DNA from degradation and facilitates cellular uptake via endocytosis, subsequently leading to gene expression [34]. Moreover, HAp nanoparticles can be easily

functionalized, enabling the attachment of various targeting ligands for cell-specific delivery. This property is particularly beneficial for cancer gene therapy, where specific targeting of cancer cells is crucial to minimize damage to healthy cells. HAp has been investigated in various areas of gene therapy. For instance, HAp has been used in bone tissue engineering to deliver bone morphogenetic proteins (BMPs) genes, which encode proteins that stimulate bone growth and differentiation [35]. The local delivery of BMP genes using HAp scaffolds has demonstrated enhanced bone regeneration in several preclinical studies. In cancer gene therapy, HAp nanoparticles have been used to deliver tumor suppressor genes, indicating an inhibitory effect on tumor growth in animal models. Moreover, the delivery of immune-modulating genes using HAp has shown promise in triggering an immune response against cancer cells [36].

3.3. Hydroxyapatite (HAp) in biosensors

Biosensors, analytical devices that convert a biological response into a quantifiable and processable signal, have attracted significant attention due to their potential applications in various fields, including medical diagnostics, food safety, and environmental monitoring. Hydroxyapatite (HAp) has been extensively studied for biosensor applications owing to its unique properties, such as biocompatibility, bioactivity, and ability to interact with various biomolecules [37]. HAp, known for its excellent biocompatibility and versatile surface chemistry, is pivotal as a transducer material in biosensor development. It can be used as a matrix to immobilize various biomolecules, including enzymes, antibodies, and DNA, which are responsible for the selective recognition of analytes. Moreover, HAp exhibits strong adsorption characteristics towards a wide range of molecules due to its positively charged surface and high surface area-to-volume ratio, particularly in the case of nanoscale Hap [38]. These properties make HAp an excellent candidate for various biosensors, including enzymatic biosensors, immunosensors, and DNA biosensors.

Enzymatic Biosensors: HAp can support enzyme immobilization, providing a stable and biocompatible environment that preserves the enzyme's activity. For instance, glucose biosensors based on glucose oxidase immobilized on HAp have shown high sensitivity and stability [39].

Immunosensors: HAp can also serve as a matrix for antibody immobilization in immunosensors. The biocompatibility of HAp and its ability to maintain the biological activity of antibodies makes it an excellent material for detecting various antigens [40].

DNA Biosensors: HAp has been used as a transducer material in DNA biosensors due to its ability to bind DNA via electrostatic interactions [41]. HAp-based DNA biosensors have demonstrated high sensitivity in detecting DNA hybridization events, showing potential for use in genetic diagnostics and research.

3.4. Hydroxyapatite in medical imaging

Medical imaging is crucial in clinical decision-making, from disease diagnosis to treatment monitoring. As such, developing novel imaging agents that provide improved sensitivity and specificity is an active area of research. Firstly, HAp can serve as a contrast agent for various imaging modalities. For instance, in X-ray and computed tomography (CT), HAp provides high radiopacity due to its high atomic number of elements (calcium and phosphorus), allowing for improved visualization of structures or processes of interest [42]. Secondly, HAp nanoparticles can act as carriers for imaging agents, facilitating targeted imaging. The ability of HAp to adsorb various molecules on its surface enables the loading of specific contrast agents or tracers, enhancing imaging sensitivity and specificity [43]. Finally, the bioactive nature of HAp makes it a promising platform for theranostics, a field that combines diagnostics and therapeutics. HAp nanoparticles can simultaneously deliver imaging agents and therapeutic drugs, enabling real-time monitoring of drug delivery and treatment response [44].

Bone Imaging: Given its presence in bone, HAp has been widely used in bone imaging. Synthetic HAp can mimic bone minerals in radiographic images, diagnosing bone diseases and assessing bone regeneration.

Cancer Imaging: HAp nanoparticles can serve as carriers for cancer-specific tracers or contrast agents. By tagging these nanoparticles with cancer-targeting ligands, targeted imaging of cancer cells can be achieved, improving the early detection and monitoring of cancers.

Theranostic Applications: The integration of HAp into theranostic systems has shown promising results. HAp can co-deliver imaging agents and therapeutic drugs, providing real-time feedback on drug delivery and therapeutic response. This approach holds great potential for personalized medicine, where treatment can be tailored based on individual patient responses.

3.5. Hydroxyapatite in antimicrobial applications

Antimicrobial resistance is a pressing global health concern, necessitating the development of new strategies and materials for antimicrobial applications. Known for its biocompatibility, bioactivity, and potential for functionalization, HAp provides an intriguing platform for the development of antimicrobial applications. The antimicrobial action of HAp can be attributed to its unique physicochemical properties and ability to be doped with antimicrobial agents. HAp exhibits limited antimicrobial activity [45]. However, it can be an effective antimicrobial material when modified or combined with other substances. Nanoscale HAp, for instance, demonstrates increased antimicrobial activity compared to its bulk counterpart due to its high surface area-to-volume ratio and enhanced interaction with microbial cells [46]. Additionally, HAp can be doped with various antimicrobial agents such as silver, zinc, or copper ions, or loaded with antibiotics or antimicrobial peptides, to produce composites with enhanced antimicrobial.

Bone Infections: Bone infections or osteomyelitis, often caused by bacteria such as *Staphylococcus aureus*, are challenging to treat due to the difficulty in delivering antibiotics to the site of infection. HAp can be an effective delivery system to treat bone infections [47].

Implant-associated Infections: Bacterial colonization on the surface of medical implants can lead to implant-associated infections. Coating the implants with antimicrobial HAp can prevent bacterial adhesion and biofilm formation, thereby reducing the risk of infection. Hydroxyapatite offers exciting possibilities in the fight against microbial infections. Its ability to be doped with antimicrobial agents and its excellent biocompatibility make it a promising material for various applications, including treating bone and implant-associated infections and dental health [27]. Despite the challenges that need to be addressed, ongoing research and technological advancements hold the potential to significantly enhance the antimicrobial performance of HAp, offering a promising route to combat the pressing issue of antimicrobial resistance.

3.6. Hydroxyapatite in drug delivery

The delivery of therapeutic agents to specific body sites in a controlled manner is a critical aspect of modern healthcare. Hydroxyapatite (HAp), a calcium phosphate mineral found naturally in bone, is gaining momentum as a potent material in the drug delivery field. First, its nanostructured form exhibits high surface area and porosity, providing ample space for drug loading [38]. Second, HAp's surface chemistry allows for the adsorption and desorption of various drugs, enabling controlled drug release [48]. Finally, its biodegradability ensures HAp can safely degrade and release its drug load in the body over time. Additionally, HAp's properties can be manipulated to meet specific delivery needs. For example, by adjusting the particle size, morphology, and crystallinity or doping it with different ions, the drug loading capacity and release kinetics can be tailored.

Bone Disorders: Given HAp's affinity for bone tissue, it has been

extensively used to deliver drugs for bone disorders. Antibiotics, anti-inflammatory drugs, and bone growth factors loaded onto HAp have been employed to treat osteomyelitis, arthritis, and osteoporosis, respectively [49].

Cancer Therapy: HAp nanoparticles have been exploited as carriers for anticancer drugs. Their ability to adsorb and gradually release drugs helps maintain therapeutic levels over extended periods, improving the treatment efficacy and reducing side effects [36].

Dental Applications: HAp has been employed in dental applications to deliver various therapeutics [50]. For example, fluoride or antibacterial agents loaded onto HAp have been incorporated into toothpaste or mouthwashes to prevent tooth decay and gum diseases.

Hydroxyapatite is carving a niche in the drug delivery arena, leveraging its unique properties and tunable characteristics. Its current applications in treating bone disorders, cancer, and dental diseases highlight its potential, and ongoing research continues to push the boundaries of what HAp can achieve in drug delivery. Although challenges exist, the future of HAp in drug delivery looks promising, offering new avenues for the effective treatment of various diseases.

3.7. Bone tissue engineering applications

Hydroxyapatite (HAp) has wide applications in bone tissue engineering due to its chemical similarity to natural bone, excellent biocompatibility, and osteoconductive properties [51]. In spinal fusion, HAp acts as a scaffold for new bone growth, promoting mineralization and stability with success rates of 85–92 % and integration times of 8–12 weeks [52]. In maxillofacial reconstruction, its moldability into blocks, granules, or pastes makes it ideal for complex craniofacial defects, achieving success rates of 88–95 % with rapid integration and high patient satisfaction [53]. Orthopedic defect repair also benefits from HAp's structural integrity and ability to guide bone ingrowth, with success rates of 82–89 % though requiring longer integration times of 10–16 weeks [54]. Its effectiveness is based on the mechanism of controlled calcium and phosphate ion release, protein adsorption, cellular adhesion, angiogenesis stimulation, and stable scaffold support during remodeling. These properties make HAp a reliable and versatile material across a range of clinical bone regeneration applications [3].

4. Advantages of naturally derived hydroxyapatite

Hydroxyapatite (HAp) derived from natural sources holds several advantages, especially in biomedicine. HAp, a naturally occurring mineral form of calcium apatite, is recognized for its remarkable biocompatibility, bioactivity, and osteoconductivity. While synthetic HAp has been utilized widely, there is a growing interest in naturally derived HAp due to its superior biological performance.

4.1. Composition of naturally derived HAp

Naturally derived HAp is generally obtained from bovine bone, fish bone, or eggshells and processed through various steps such as degreasing, deproteination, demineralization, and calcination to extract pure HAp. Synthetic HAp, on the other hand, is produced via several methods, including wet chemical precipitation, sol-gel, hydrothermal, and biomimetic deposition. In terms of composition, naturally derived HAp resembles human bone minerals more closely, containing trace elements like magnesium, zinc, and fluoride that are typically absent in synthetic HAp. These trace elements can significantly influence the biological and mechanical properties of HAp, often resulting in enhanced bioactivity and strength in naturally derived HAp [55,56].

4.2. Mechanical strength and durability

A notable advantage of naturally derived HAp over synthetic is its superior mechanical strength and durability. This advantage stems from its higher degree of crystallinity and the presence of trace elements which contribute to its inherent strength. Moreover, the porous nanostructure of natural HAp mimics the architecture of human bone, thereby offering better stress distribution and mechanical compatibility when used in bone grafts and implants. On the other hand, synthetic HAp generally exhibits lower mechanical strength due to its lesser degree of crystallinity and lack of trace elements [57]. This poses a challenge in applications where load-bearing capacity is critical. Thus, the mechanical superiority of naturally derived HAp positions it as a more favorable option for orthopedic and dental implants.

4.3. Bioactivity and osteoconductivity

Bioactivity, or the ability of a material to form a bond with living tissues, is a key attribute for biomaterials used in bone grafting or tissue engineering. Naturally derived HAp, due to its compositional and structural similarity to human bone, demonstrates excellent bioactivity. This is evidenced by the faster formation of bone-like apatite on its surface when soaked in simulated body fluid, indicating a superior bone-bonding ability [26].

In addition, naturally derived HAp exhibits enhanced osteoconductivity (the property that allows bone growth on its surface), which is crucial for successful bone regeneration. Studies have shown improved osteoblast (bone-forming cells) adhesion, proliferation, and differentiation on naturally derived HAp surfaces, suggesting its potential for enhanced bone tissue integration and regeneration [57,58]. While synthetic HAp also possesses bioactivity and osteoconductivity, these properties are often inferior to naturally derived HAp due to the absence of trace elements and the disparity in the nanostructure. Trace elements and inherent nanostructure in naturally derived HAp promote enhanced cellular responses. Moreover, the drug-loading capacity and release kinetics of naturally derived HAp have shown promising results, particularly in drug delivery [38,48]. The natural porosity and high surface area of naturally derived HAp allows for higher drug loading and sustained release, offering advantages over synthetic HAp.

4.4. Structural differences and implications

The structural similarity of naturally derived HAp to human bone tissue can result in a more natural integration with the body, potentially reducing the risk of complications or implant failure. The structure of HAp at the nanoscale is critical in dictating its interaction with biological systems [49]. Naturally derived HAp, owing to its organic origin, typically exhibits a highly crystalline nanostructure that closely mimics the nanoscale architecture of human bone. This high degree of crystallinity contributes to its superior mechanical properties and enhanced thermal stability compared to synthetic HAp. On the contrary, synthetic HAp often exhibits a less crystalline structure, making it less stable thermally and mechanically. Additionally, despite various fabrication methods, the highly porous nanostructure observed in naturally derived HAp is challenging to replicate in synthetic HAp [59]. This inherent porosity is pivotal in promoting cell adhesion, proliferation, and nutrient exchange, enhancing tissue regeneration. q.

5. Challenges and future perspectives

The clinical translation of naturally derived hydroxyapatite poses fundamental scientific challenges that must be addressed through innovative research. The primary challenge involves compositional variability inherent in biological sources. Variations in Ca/P ratios (1.55–1.75), crystallinity indices, and trace element profiles directly affect mechanical properties, dissolution kinetics, and cellular responses. This heterogeneity stems from species differences, dietary factors, age, and environmental conditions of source materials, making standardization of biological performance particularly challenging. Additionally, while processing methods such as calcination

(600–1000 °C) and alkaline hydrolysis effectively remove organic components, they may also eliminate beneficial bioactive molecules and alter the native nanostructure, which contributes to superior biological performance. Processing optimization represents a critical research frontier. Current extraction methods often involve trade-offs among purity, yield, and the preservation of beneficial characteristics. High-temperature treatments ensure pathogen elimination but may cause sintering, reducing specific surface area from 80 to 120 m^2/g to 10–30 m^2/g, thereby diminishing protein adsorption capacity and cellular interaction. Scale-up from the laboratory to industrial production frequently results in decreased crystallinity (from 85-90 % to 60–70 %) and broader particle-size distributions, affecting both mechanical properties and biological responses. Understanding the relationship between processing parameters and final material properties remains incomplete, particularly regarding the retention of trace elements (Sr, Mg, Zn) that enhance osteogenesis and angiogenesis.

Future research should prioritize several strategic directions. Advanced characterization techniques, including high-resolution transmission electron microscopy, solid-state NMR, and synchrotron-based X-ray analysis, could elucidate the precise structural features responsible for enhanced bioactivity. Machine learning algorithms analyzing multi-parametric datasets may identify optimal processing conditions for specific clinical applications. Surface functionalization strategies offer transformative potential—incorporating growth factors (BMP-2, VEGF, FGF), antimicrobial peptides, or gene delivery systems could create multifunctional platforms. Development of biomimetic composites combining natural HAp with biodegradable polymers (PCL, PLGA) or bioactive glasses may overcome mechanical limitations while preserving superior biocompatibility.

Emerging processing technologies warrant intensive investigation. Supercritical CO_2 extraction, enzymatic processing, and microwave-assisted synthesis show promise for preserving native structure while ensuring sterility. Low-temperature plasma treatment could enable surface modification without altering bulk properties. Understanding degradation mechanisms and ion release kinetics in physiological environments remains crucial for predicting long-term performance. Advanced in vitro models, including microfluidic organ-on-chip systems and 3D co-culture platforms, could better predict in vivo behavior. The convergence of natural HAp with cutting-edge technologies presents unprecedented opportunities. Integration with 3D bioprinting enables the fabrication of patient-specific scaffolds with controlled architecture and porosity. Incorporation of pH-, temperature-, or magnetic-field-responsive materials could enable triggered drug release or enhanced imaging capabilities. Development of gradient structures mimicking the natural bone interface (cortical-cancellous transition) may improve implant integration. Success requires interdisciplinary collaboration combining materials science, biology, and clinical expertise to translate laboratory innovations into therapeutic solutions. By addressing these scientific challenges through systematic research, naturally derived HAp can fulfill its potential as a superior alternative to synthetic biomaterials in regenerative medicine applications.

6. Conclusion

Naturally derived hydroxyapatite represents a promising alternative to synthetic variants, offering superior biocompatibility, inherent trace element composition, and structural similarity to native bone tissue. However, successful clinical translation faces critical challenges that require systematic resolution. Primary concerns include batch-to-batch variability arising from source heterogeneity, which affects Ca/P ratios, trace element profiles, and biological performance—posing significant barriers to regulatory approval and clinical standardization. Despite rigorous processing via calcination and alkaline hydrolysis, complete elimination of biological contaminants remains difficult to verify, as residual organic components may trigger adverse immunological responses. While preliminary studies demonstrate favorable cytocompatibility, comprehensive data on hemocompatibility, systemic immunogenicity, and long-term tissue responses remain limited.

Regulatory pathways introduce additional complexities, as agencies require extensive documentation of source traceability, processing validation, and batch consistency—requirements that are particularly challenging given the inherent heterogeneity of biological materials. The risk of disease transmission, especially from mammalian sources, necessitates stringent controls exceeding those for synthetic materials. Furthermore, critical gaps persist in understanding the long-term kinetics of degradation, chronic inflammatory responses, and the in vivo fate of degradation products.

Future advancement requires four strategic priorities: (1) establishing standardized extraction protocols with defined quality attributes to minimize variability; (2) conducting comprehensive toxicological and immunological assessments across multiple preclinical models; (3) developing sustainable, scalable manufacturing processes that maintain quality while reducing environmental impact; and (4) fostering collaborative frameworks between academia, industry, and regulatory bodies to establish clear clinical pathways. Addressing these challenges through continued investment in fundamental research, process optimization, and rigorous clinical validation will position naturally derived HAp as a transformative biomaterial in regenerative medicine. Only through the systematic resolution of current limitations can naturally HAp transition from a promising research material to a validated therapeutic option, ultimately improving patient outcomes in bone regeneration applications.

CRediT authorship contribution statement

Nandita Suresh: Writing – review & editing, Writing – original draft, Data curation, Conceptualization. **Vishnupriya K. Sweety:** Formal analysis, Data curation. **Namrata Suresh:** Resources, Data curation. **Amartya Raj Suraj:** Resources, Data curation. **Tuomas Waltimo:** Writing – review & editing, Supervision, Conceptualization. **Sukumaran Anil:** Writing – review & editing, Supervision, Data curation, Conceptualization.

Declaration of competing interest

The authors declare that they have no known competing financial interests or personal relationships that could have appeared to influence the work reported in this paper.

References

[1] R. Kareem, O. Kaygili, Hydroxyapatite Biomaterials: a Comprehensive Review of Their Properties, Structures, Medical Applications, and Fabrication Methods, vol. 6, 2024, pp. 1–26, https://doi.org/10.48309/JCR.2024.415051.1253.

[2] P. Forero, B. Segura-Giraldo, B. Garcia, E. Parra, P.J. Arango, Comparative study between natural and synthetic hydroxyapatite: structural, morphological and bioactivity properties, Materia 23 (2018), https://doi.org/10.1590/s1517-707620180004.0551.

[3] N.A.S. Mohd Pu'ad, P. Koshy, H.Z. Abdullah, M.I. Idris, T.C. Lee, Syntheses of hydroxyapatite from natural sources, Heliyon 5 (5) (May 2019) e01588, https://doi.org/10.1016/j.heliyon.2019.e01588 (in eng).

[4] A. Yasukawa, K. Gotoh, H. Tanaka, K. Kandori, Preparation and structure of calcium hydroxyapatite substituted with light rare Earth ions, Colloids Surf. A Physicochem. Eng. Asp. 393 (2012/01/05/2012) 53–59, https://doi.org/10.1016/j.colsurfa.2011.10.024.

[5] J. Venkatesan, R. Anchan, S. Subramanian, S. Anil, S.-K. Kim, Natural hydroxyapatite-based nanobiocomposites and their biomaterials-to-cell interaction for bone tissue engineering, Discover Nano 19 (2024), https://doi.org/10.1186/s11671-024-04119-0.

[6] S. Mondal, et al., Hydroxyapatite: a journey from biomaterials to advanced functional materials, Adv. Colloid Interface Sci. 321 (2023/11/01/2023) 103013, https://doi.org/10.1016/j.cis.2023.103013.

[7] X. Bui, T. Linh, The Extraction of pure hydroxyapatite from porcine bone by thermal process, Metallurgical and Materials Engineering 25 (2019), https://doi.org/10.30544/410.

[8] Z. Khurshid, et al., Extraction of hydroxyapatite from camel bone for bone tissue engineering application, Molecules 27 (22) (2022), https://doi.org/10.3390/molecules27227946 (in eng).

[9] C. Rodrigues, et al., Characterization of a bovine collagen-hydroxyapatite composite scaffold for bone tissue engineering, Biomaterials 24 (2004) 4987–4997, https://doi.org/10.1016/S0142-9612(03)00410-1.
[10] M.R. Ayatollahi, M.Y. Yahya, H. Asgharzadeh Shirazi, S.A. Hassan, Mechanical and tribological properties of hydroxyapatite nanoparticles extracted from natural bovine bone and the bone cement developed by nano-sized bovine hydroxyapatite filler, Ceram. Int. 41 (9, Part A) (2015) 10818–10827, https://doi.org/10.1016/j.ceramint.2015.05.021.
[11] J. Ratnayake, N. Ramesh, M.L. Gould, M.R. Mucalo, G.J. Dias, Silicate-substituted bovine-derived hydroxyapatite as a bone substitute in regenerative dentistry, J. Appl. Biomater. Funct. Mater. 23 (2025) 22808000251314302, https://doi.org/10.1177/22808000251314302.
[12] R.N. Granito, A.C. Muniz Renno, H. Yamamura, M.C. de Almeida, P.L. Menin Ruiz, D.A. Ribeiro, Hydroxyapatite from fish for bone tissue engineering: a promising approach (in eng), Int J Mol Cell Med 7 (2) (2018) 80–90, https://doi.org/10.22088/ijmcm.Bums.7.2.80. Spring.
[13] D. Ayala-Barajas, V. González-Vélez, M. Vélez-Tirado, J. Aguilar-Pliego, Hydroxyapatite extraction from fish scales of Tilapia, in: 2020 42nd Annual International Conference of the IEEE Engineering in Medicine & Biology Society (EMBC), 2020, pp. 2206–2208, https://doi.org/10.1109/EMBC44109.2020.9176479, 20-24 July 2020.
[14] I. Zainol, N.H. Adenan, N.A. Rahim, C.N.A. Jaafar, Extraction of natural hydroxyapatite from tilapia fish scales using alkaline treatment, Mater. Today Proc. 16 (2019/01/01/2019) 1942–1948, https://doi.org/10.1016/j.matpr.2019.06.072.
[15] F.N. Oktar, et al., Marine-derived bioceramics for orthopedic, reconstructive and dental surgery applications, Journal of the Australian Ceramic Society 59 (1) (2023/02/01 2023) 57–81, https://doi.org/10.1007/s41779-022-00813-3.
[16] J.S. Swarup, R. Thomas, J. Rucharitha, V.R. Arunkumar, V. V, Eggshell-derived hydroxyapatite as a biomaterial in dentistry: a scoping review of synthesis, properties and applications, Evid. Base Dent. 26 (3) (2025/09/01 2025) 153, https://doi.org/10.1038/s41432-025-01146-3, 153.
[17] F.L. Muntean, et al., Hydroxyapatite from mollusk shells: characteristics, production, and potential applications in dentistry, Dent. J. 12 (12) (2024) 409 [Online]. Available: https://www.mdpi.com/2304-6767/12/12/409.
[18] M. Prakash, H.K. Rajan, M.N. Chandraprabha, S. Shetty, T. Mukherjee, S. Girish Kumar, Recent developments in green synthesis of hydroxyapatite nanocomposites: relevance to biomedical and environmental applications, Green Chem. Lett. Rev. 17 (1) (2024/12/31 2024) 2422409, https://doi.org/10.1080/17518253.2024.2422409.
[19] A. Ruksudjarit, K. Pengpat, G. Rujijanagul, T. Tunkasiri, Synthesis and characterization of nanocrystalline hydroxyapatite from natural bovine bone, Curr. Appl. Phys. 8 (2008) 270–272, https://doi.org/10.1016/j.cap.2007.10.076.
[20] A. Bianco, I. Cacciotti, M. Lombardi, L. Montanaro, G. Gusmano, Thermal stability and sintering behaviour of hydroxyapatite nanopowders, Journal of Thermal Analysis and Calorimetry 88 (2007), https://doi.org/10.1007/s10973-006-8011-6.
[21] N.I. Agbeboh, I.O. Oladele, O.O. Daramola, A.A. Adediran, O.O. Olasukanmi, M. O. Tanimola, Environmentally sustainable processes for the synthesis of hydroxyapatite, Heliyon 6 (4) (2020/04/01/2020) e03765, https://doi.org/10.1016/j.heliyon.2020.e03765.
[22] A.L. Giraldo-Betancur, et al., Comparison of physicochemical properties of bio and commercial hydroxyapatite, Curr. Appl. Phys. 13 (7) (2013/09/01/2013) 1383–1390, https://doi.org/10.1016/j.cap.2013.04.019.
[23] A. Shavandi, A.E.-D.A. Bekhit, A. Ali, Z. Sun, Synthesis of nano-hydroxyapatite (nHA) from waste mussel shells using a rapid microwave method, Mater. Chem. Phys. 149–150 (2015/01/15/2015) 607–616, https://doi.org/10.1016/j.matchemphys.2014.11.016.
[24] S.-C. Wu, H.-K. Tsou, H.-C. Hsu, S.-K. Hsu, S.-P. Liou, W.-F. Ho, A hydrothermal synthesis of eggshell and fruit waste extract to produce nanosized hydroxyapatite, Ceram. Int. 39 (7) (2013/09/01/2013) 8183–8188, https://doi.org/10.1016/j.ceramint.2013.03.094.
[25] J. Venkatesan, Z.J. Qian, B. Ryu, N.V. Thomas, S.K. Kim, A comparative study of thermal calcination and an alkaline hydrolysis method in the isolation of hydroxyapatite from Thunnus obesus bone, Biomed Mater 6 (3) (Jun 2011) 035003, https://doi.org/10.1088/1748-6041/6/3/035003 (in eng).
[26] J. Chamrad, P. Marcian, J. Cizek, Beneficial osseointegration effect of hydroxyapatite coating on cranial implant - FEM investigation, PLoS One 16 (7) (2021) e0254837, https://doi.org/10.1371/journal.pone.0254837 (in eng).
[27] X. Chen, J. Zhou, Y. Qian, L. Zhao, Antibacterial coatings on orthopedic implants, Mater. Today Bio 19 (Apr 2023) 100586, https://doi.org/10.1016/j.mtbio.2023.100586 (in eng).
[28] B. Beig, U. Liaqat, M.F.K. Niazi, I. Douna, M. Zahoor, M.B.K. Niazi, Current challenges and innovative developments in hydroxyapatite-based coatings on metallic materials for bone implantation: a review, Coatings 10 (12) (2020) 1249 [Online]. Available: https://www.mdpi.com/2079-6412/10/12/1249.
[29] M. Roy, A. Bandyopadhyay, S. Bose, Induction plasma Sprayed Nano Hydroxyapatite coatings on titanium for orthopaedic and dental implants, Surf. Coat. Technol. 205 (8–9) (Jan 25 2011) 2785–2792, https://doi.org/10.1016/j.surfcoat.2010.10.042 (in eng).
[30] G.J. Owens, et al., Sol–gel based materials for biomedical applications, Prog. Mater. Sci. 77 (2016/04/01/2016) 1–79, https://doi.org/10.1016/j.pmatsci.2015.12.001.
[31] D.J. Blackwood, K.H.W. Seah, Electrochemical cathodic deposition of hydroxyapatite: improvements in adhesion and crystallinity, Mater. Sci. Eng. C 29 (4) (2009/05/05/2009) 1233–1238, https://doi.org/10.1016/j.msec.2008.10.015.
[32] L. Jonasova, F.A. Muller, A. Helebrant, J. Strnad, P. Greil, Biomimetic apatite formation on chemically treated titanium, Biomaterials 25 (7–8) (Mar-Apr 2004) 1187–1194, https://doi.org/10.1016/j.biomaterials.2003.08.009.
[33] D. Arcos, M. Vallet-Regi, Substituted hydroxyapatite coatings of bone implants, J. Mater. Chem. B 8 (9) (Mar 4 2020) 1781–1800, https://doi.org/10.1039/c9tb02710f (in eng).
[34] T.J. Levingstone, S. Herbaj, J. Redmond, H.O. McCarthy, N.J. Dunne, Calcium phosphate nanoparticles-based systems for RNAi delivery: applications in bone tissue regeneration, Nanomaterials 10 (1) (Jan 14 2020), https://doi.org/10.3390/nano10010146 (in eng).
[35] L. Zhu, et al., Application of BMP in bone tissue engineering, Front. Bioeng. Biotechnol. 10 (2022) 810880, https://doi.org/10.3389/fbioe.2022.810880 (in eng).
[36] S. Kargozar, et al., Hydroxyapatite nanoparticles for improved cancer theranostics, J. Funct. Biomater. 13 (3) (Jul 20 2022), https://doi.org/10.3390/jfb13030100 (in eng).
[37] A. Mushtaq, et al., Magnetic hydroxyapatite nanocomposites: the advances from synthesis to biomedical applications, Mater. Des. 197 (2021/01/01/2021) 109269, https://doi.org/10.1016/j.matdes.2020.109269.
[38] S. Lara-Ochoa, W. Ortega-Lara, C.E. Guerrero-Beltran, Hydroxyapatite nanoparticles in drug delivery: physicochemistry and applications, Pharmaceutics 13 (10) (Oct 9 2021), https://doi.org/10.3390/pharmaceutics13101642 (in eng).
[39] S. Salman, S. Soundararajan, G. Safina, I. Satoh, B. Danielsson, Hydroxyapatite as a novel reversible in situ adsorption matrix for enzyme thermistor-based FIA, Talanta 77 (2) (2008/12/15/2008) 490–493, https://doi.org/10.1016/j.talanta.2008.04.003.
[40] L. Yang, W. Wei, X. Gao, J. Xia, H. Tao, A new antibody immobilization strategy based on electrodeposition of nanometer-sized hydroxyapatite for label-free capacitive immunosensor, Talanta 68 (1) (Nov 15 2005) 40–46, https://doi.org/10.1016/j.talanta.2005.04.038 (in eng).
[41] Y.W. Hartati, et al., Recent advances in hydroxyapatite-based electrochemical biosensors: applications and future perspectives, Sens. Biosens. Res. 38 (2022/12/01/2022) 100542, https://doi.org/10.1016/j.sbsr.2022.100542.
[42] E. Olaret, I.C. Stancu, H. Iovu, A. Serafim, Computed tomography as a characterization tool for engineered scaffolds with biomedical applications, Materials 14 (22) (Nov 10 2021), https://doi.org/10.3390/ma14226763 (in eng).
[43] A. Adamiano, et al., On the use of superparamagnetic hydroxyapatite nanoparticles as an agent for magnetic and nuclear in vivo imaging, Acta Biomater. 73 (Jun 2018) 458–469, https://doi.org/10.1016/j.actbio.2018.04.040 (in eng).
[44] A.A. Barbosa, S.A. Junior, R.L. Mendes, R.S. de Lima, A. de Vasconcelos Ferraz, Multifunctional hydroxyapatite with potential for application in theranostic nanomedicine, Mater Sci Eng C Mater Biol Appl 116 (Nov 2020) 111227, https://doi.org/10.1016/j.msec.2020.111227.
[45] S.L. Iconaru, P. Chapon, P. Le Coustumer, D. Predoi, Antimicrobial activity of thin solid films of silver doped hydroxyapatite prepared by sol-gel method, Sci. World J. 2014 (2014) 165351, https://doi.org/10.1155/2014/165351.
[46] P.N. Silva-Holguin, S.Y. Reyes-Lopez, Synthesis of Hydroxyapatite-Ag composite as antimicrobial agent, Dose Response 18 (3) (Jul-Sep 2020) 1559325820951342, https://doi.org/10.1177/1559325820951342 (in eng).
[47] U. Joosten, A. Joist, G. Gosheger, U. Liljenqvist, B. Brandt, C. von Eiff, Effectiveness of hydroxyapatite-vancomycin bone cement in the treatment of Staphylococcus aureus induced chronic osteomyelitis, Biomaterials 26 (25) (Sep 2005) 5251–5258, https://doi.org/10.1016/j.biomaterials.2005.01.001.
[48] W. Sun, J. Fan, S. Wang, Y. Kang, J. Du, X. Peng, Biodegradable drug-loaded hydroxyapatite nanotherapeutic agent for targeted drug release in tumors, ACS Appl. Mater. Interfaces 10 (9) (Mar 7 2018) 7832–7840, https://doi.org/10.1021/acsami.7b19281.
[49] N.A. Abdul Halim, M.Z. Hussein, M.K. Kandar, Nanomaterials-Upconverted hydroxyapatite for bone tissue engineering and a platform for drug delivery, Int J Nanomedicine 16 (2021) 6477–6496, https://doi.org/10.2147/IJN.S298936 (in eng).
[50] K. O'Hagan-Wong, J. Enax, F. Meyer, B. Ganss, The use of hydroxyapatite toothpaste to prevent dental caries, Odontology 110 (2) (Apr 2022) 223–230, https://doi.org/10.1007/s10266-021-00675-4 (in eng).
[51] W. Liu, N. Cheong, Z. He, T. Zhang, Application of hydroxyapatite composites in bone tissue engineering: a review, J. Funct. Biomater. 16 (4) (Apr 2 2025), https://doi.org/10.3390/jfb16040127 (in eng).
[52] J. Litak, et al., Hydroxyapatite use in spine surgery-molecular and clinical aspect, Materials 15 (8) (Apr 15 2022), https://doi.org/10.3390/ma15082906 (in eng).
[53] J.W. Frame, C.L. Brady, The versatility of hydroxyapatite blocks in maxillofacial surgery, Br. J. Oral Maxillofac. Surg. 25 (6) (1987/12/01/1987) 452–464, https://doi.org/10.1016/0266-4356(87)90137-9.
[54] W. Liang, et al., Prospective applications of bioactive materials in orthopedic therapies: a review, Heliyon 10 (16) (Aug 30 2024) e36152, https://doi.org/10.1016/j.heliyon.2024.e36152 (in eng).
[55] S.S. Rahavi, O. Ghaderi, A. Monshi, M.H. Fathi, A comparative study on physicochemical properties of hydroxyapatite powders derived from natural and synthetic sources, Russ. J. Non-Ferrous Metals 58 (3) (2017/05/01 2017) 276–286, https://doi.org/10.3103/s1067821217030178.
[56] P.A.F. Sossa, B.S. Giraldo, B.C.G. Garcia, E.R. Parra, P.J.A. Arango, Comparative study between natural and synthetic Hydroxyapatite: structural, morphological and bioactivity properties, Materia 23 (4) (2018), https://doi.org/10.1590/s1517-707620180004.0551.
[57] B. Wan, et al., Biomimetically precipitated nanocrystalline hydroxyapatite, Nano TransMed 1 (2–4) (2022) e9130008, https://doi.org/10.26599/ntm.2022.9130008.

[58] A.R. Amini, C.T. Laurencin, S.P. Nukavarapu, Bone tissue engineering: recent advances and challenges, Crit. Rev. Biomed. Eng. 40 (5) (2012) 363–408, https://doi.org/10.1615/critrevbiomedeng.v40.i5.10 (in eng).
[59] S. Jiang, M. Wang, J. He, A review of biomimetic scaffolds for bone regeneration: toward a cell-free strategy, Bioeng. Transl. Med. 6 (2) (May 2021) e10206, https://doi.org/10.1002/btm2.10206 (in eng).
[60] I. Wahyudi, A. Tajrin, H. Mubarak, The potential use of hydroxyapatite from sea coral as a bone substitute: a systematic review, Arch Craniofac Surg 26 (5) (Oct 2025) 175–182, https://doi.org/10.7181/acfs.2025.0005 (in eng).
[61] S. Sri-o-sot, K. Vepulanont, C. Kamkit, T. Srichumpong, T. Chanadee, Fabrication, characterization, and properties of hydroxyapatite ceramics derived from cockle shell, Journal of the Australian Ceramic Society 58 (4) (2022/09/01 2022) 1081–1093, https://doi.org/10.1007/s41779-022-00757-8.
[62] D. Govindaraj, M. Rajan, Synthesis and spectral characterization of novel nano-Hydroxyapatite from moringaoleifera leaves, Mater. Today Proc. 3 (6) (2016/01/01/2016) 2394–2398, https://doi.org/10.1016/j.matpr.2016.04.153.
[63] M. Sumathra, et al., Sustainable pectin fascinating hydroxyapatite nanocomposite scaffolds to enhance tissue regeneration, Sustain. Chem. Pharm. 5 (2017/06/01/2017) 46–53, https://doi.org/10.1016/j.scp.2017.02.001.
[64] P.J. Walsh, F.J. Buchanan, M. Dring, C. Maggs, S. Bell, G.M. Walker, Low-pressure synthesis and characterisation of hydroxyapatite derived from mineralise red algae, Chem. Eng. J. 137 (1) (2008/03/15/2008) 173–179, https://doi.org/10.1016/j.cej.2007.10.016.

ARTICLES FOR FACULTY MEMBERS

BONE-DERIVED HYDROXYAPATITE TOOTHPASTE FOR SUSTAINABLE PHARMACEUTICAL AND BIOMEDICAL APPLICATIONS

Physicochemical analysis and application of sardinella fimbriata-derived hydroxyapatite in toothpaste formulations / Anwar, A. I., Ruslin, M., Marlina, E., & Hasanuddin, H.

BMC Oral Health
Volume 25 Issue 195 (2025) Pages 1-9
https://doi.org/10.1186/s12903-025-05557-7
(Database: Springer Nature Link)

BMC Oral Health

RESEARCH

Open Access

Physicochemical analysis and application of sardinella fimbriata-derived hydroxyapatite in toothpaste formulations

Ayub Irmadani Anwar[1*], Muhammad Ruslin[2], Erni Marlina[3] and H Hasanuddin[1]

Abstract

Background Toothpaste contains hydroxyapatite is a natural substance derived from fish bones. This study examines the physicochemical process of natural hydroxyapatite, conducts organoleptic testing, and assesses the homogeneity of Fringescale sardinella (*Sardinella fimbriata*) fish bone in toothpaste formulations.

Method The study employed laboratory experimental research in September 2021. The calcination technique was employed to acquire a calcium precursor to produce natural hydroxyapatite powder derived from the bones of Sardinella fimbriata fish. X-ray fluorescence (XRF) was investigated to analyze the element calcium (Ca)—the morphological evaluation involved using an X-ray diffractometer (XRD) to evaluate the crystallinity. Toothpaste was formulated using natural hydroxyapatite as an abrasive, with different concentrations of CaCO3: F0 (0%), F1 (30%), F2 (40%), and F3 (50%). The toothpaste formulation was evaluated by a sensory assessment conducted on ten persons. The toothpaste's attributes were evaluated for consistency, thickness, acidity level, foam generation, stability, and overall preference.

Results The calcium oxide content in fish bones was 60.25 m3/m%. The XRD of the natural fish bone hydroxyapatite compound has a crystallinity of 82.9%. The average hedonic test liked each toothpaste formula, but the F3 formula was preferred in color, aroma, taste, and texture.

Conclusion Hydroxyapatite extracted from Sardinella fimbriata fish bone can be incorporated into toothpaste formulated with F3, which includes a 50% hydroxyapatite concentration.

Keywords Physicochemical process, Toothpastes, Hydroxyapatite, Organoleptic test, Quality Test, Fish Bone

*Correspondence:
Ayub Irmadani Anwar
ayubanwar.dds@gmail.com
[1]Department of Dental Public Health and Preventive Dentistry, Faculty of Dentistry, Hasanuddin University, Makassar, South Sulawesi, Indonesia
[2]Department of Oral and Maxillofacial Surgery, Faculty of Dentistry, Hasanuddin University, Makassar, South Sulawesi, Indonesia
[3]Department of Oral Medicine, Faculty of Dentistry, Hasanuddin University, Makassar, South Sulawesi, Indonesia

Introduction

Fish bones are valuable for biomedical applications that benefit human health due to their high hydroxyapatite (HAp) content. HAp is an essential natural calcium-rich mineral from fish bones with significant potential for various health-related uses [1]. Fishbones contain 60–70% minerals with 30% collagen protein constituent components, mostly bioapatite, hydroxyapatite (HAp), and carbonated apatite [2–4]. They also comprise 60-70% inorganic substances, mainly calcium phosphate and hydroxyapatite [1, 4].

Fish bone meal offers several advantages as a calcium source compared to other natural CaCO3/CaO resources. Because of its similarities to the composition of human bones, the body can easily absorb the calcium contained in hydroxyapatite [1]. Further, fish bone meal also provides phosphorus, enhancing overall mineral absorption, and contains protein that can break down into plant-available nitrogen [2]. This sustainable source offers trace minerals and potential improvements in product characteristics, such as increased whiteness in some applications. Due to its adaptability and extensive nutrient composition, fish bone meal has the potential to be a promising option for a range of applications, including fertilizers and dietary supplements. It provides benefits that go beyond its calcium level alone. The fishbone meal has 1002.00 mg of calcium and 12.80 mg of phosphorus per 100 g [5, 6]. A viable option for acquiring CaCO3 that is safe for human consumption and does not rely on natural sources. Further, $CaCO_3$ in toothpaste functions as a cleaning compound to reduce the intensity of the brown layer on the tooth surface [7, 8].

Natural HAp, derived from Fringescale Sardine *(Sardinella fimbriata, S. fimbriata)* fish bones, typically have better osteoconductivity[1] than synthetic materials because it resemble human bone's mineral composition and structure. This similarity in composition and structure promotes better cell adhesion, proliferation, and integration with surrounding bone tissue, leading to more effective bone regeneration and healing [3, 4]. HAp from natural materials has better osteoconductivity than synthetic materials. *S. fimbriata* fish bones are a natural resource for synthesizing HAp and an organic bone replacement ingredient in the human body [9, 10]. Further, HAp from fishbones is an inexpensive natural source for bone regeneration [11–13]. Toothpaste has a variety of chemical compounds, including HAp, which is proficient at sealing dental cavities. Using mouthwash and toothpaste containing HAp can effectively be a preventive measure against dental caries. Toothpaste has a variety of chemical compounds, including HAp, which is proficient at sealing dental cavities. Consequently, using mouthwash and toothpaste containing HAp can effectively be a preventive measure against dental caries [15, 16].

HAp is a common and popular biomaterial for bone regeneration. About 70% of tooth enamel structure is HAp [17, 18]. HAp has been used in pharmaceutical fields such as tablet manufacturing, dental implants [19], and injection manufacturing [20]. In addition, several studies show that fish bones can be utilized in HAp. This HAp source can be absorbed effectively [11, 12, 21]. HAp has demonstrated significant effectiveness in various dental applications, particularly remineralization and caries prevention. Studies have shown that HAp toothpaste can effectively remineralize initial enamel lesions and reduce tooth sensitivity, with one clinical study reporting caries inhibition rates of 35.86% in boys and 55.93% in girls compared to non-HAp toothpaste [5]. Research has yielded promising results regarding absorption and bioavailability. A comparative study found that calcium absorption from fish bones containing HAp was comparable to standard calcium carbonate supplements, with absorption rates of 21.9% for cod bones and 22.5% for salmon bones versus 27.4% for CaCO3 [1].

Notably, the particle size of HAp influences its bioavailability, with both micro and nanoparticles of fish bone-derived HAp showing superior calcium bioavailability compared to standard supplements [6]. Natural HAp, such as that derived from fish bones, typically exhibits better biocompatibility and osteoconductivity than synthetic versions due to its closer resemblance to human bone composition [5, 7]. This similarity enhances cell adhesion and integration with surrounding bone tissue. Furthermore, nano-sized HAp particles have improved bioactivities and mechanical properties due to their increased surface area, enhancing protein binding and interaction with biological tissues [5, 6]. While these findings are promising, additional clinical studies are needed to fully establish HAp's long-term effectiveness and superiority over other calcium sources in various applications [5, 7].

This study explores the untapped potential of *S. fimbriata* fish bones as a source of natural HAp for toothpaste formulations. Unlike previous research, our approach focused on developing a chemical-free HAp extraction process, potentially eliminating contaminants that could compromise toothpaste quality. By conducting comprehensive physicochemical analyses on toothpaste containing this fish bone-derived HAp, we aim to establish a novel, sustainable method for repurposing fish bone waste into a valuable oral care ingredient. Our innovative formulation meets the stringent SNI 12-3524, 1995 toothpaste standards, ensuring product safety and

[1] Osteoconductivity is the ability of a material to support bone growth on its surface and allow the attachment, migration, and distribution of cells involved in bone formation.

efficacy. This research addresses the gap in HAp toothpaste studies using Sardinella fimbriata. It presents a unique opportunity to create eco-friendly, high-quality oral care products while promoting responsible waste management in the fishing industry.

Methods

The research was a laboratory experimental design focused on extracting and testing HAp at the Science Research and Development Laboratory and Biochemistry Laboratory in the Faculty of Mathematics and Natural Sciences at Hasanuddin University. Additionally, the research involved formulating toothpaste and conducting physicochemical analysis. The Pharmacy Laboratory lies in the Faculty of Pharmacy at Hasanuddin University. The projected timeframe for execution was September 2021.

The calcination process removed organic materials and metals other than Ca and decomposed calcium carbonate into calcium oxide, which was used as a Ca precursor to produce hydroxyapatite powder. Ca analysis was done by XRF, and morphological analysis of crystallinity was done using an X-ray diffractometer (XRD). In making toothpaste formulations, HAp was used as an abrasive for CaCO3, including F0 (0%), F1 (30%), F2 (40%), and F3 (50%).

The study conducted both organoleptic and physicochemical tests on the toothpaste preparations. Organoleptic tests, which rely on sensory evaluations, included the hedonic test performed on ten adult participants. This test likely assessed subjective qualities such as taste, texture, color, and overall acceptability of the toothpaste formulations. On the other hand, the physicochemical tests comprised a series of objective measurements to assess the quality and characteristics of the toothpaste. These included the homogeneity test (to ensure uniform distribution of ingredients), viscosity test (to measure the toothpaste's thickness and flow properties), pH measurement (to determine acidity or alkalinity), foam formation test (to evaluate the toothpaste's ability to create foam during use), and stability test (to assess the formulation's consistency over time). While the hedonic test falls under organoleptic evaluation, the homogeneity, viscosity, pH, foam formation, and stability tests were all considered physicochemical tests as they involved measurable, objective parameters rather than sensory perceptions. The official permission had been approved by the Health Research Ethics Committee of Hasanuddin University Dental Hospital (RSGM) Makassar, Indonesia (No. 0095/PL.09/KEPK-RSGM UNHAS/2021).

Table 1 Toothpaste formulations with HAp from *S. fimbriata* fish bones (parts by weight)

material	F0	F1	F2	F3
Hydroxyapatite	0	30	40	50
Natrium lauril sulfat	1	1	1	1
Gliserin	10	10	10	10
Carbomer	3	3	3	3
Sorbitol 70%	10	10	10	10
Menthol	0.3	0.3	0.3	0.3
Natrium Benzoat	0.05	0.05	0.05	0.05
Aqua Destilata Ad	100	100	100	100

Note: Aqua Destilata (distilled water) was added to bring the total to 100 parts for each formulation

HAp extraction

The process of extracting HAp started with producing vibrated fish bones, which were then subjected to sintering. Subsequently, the material was dried in an oven for six hours, maintaining a temperature of 60 °C [22]. The hydroxyapatite was extracted by calcination. It was then heated in a furnace at 1000 °C with a heating rate of 10 °C per minute for five hours. Subsequently, it was cooled isothermally for three hours. The fish bones were pulverized before calcination to generate a refined form of hydroxyapatite.

The calcination process was carried out to remove organic matter and other metals besides calcium (Ca) and decompose calcium carbonate ($CaCO_3$) into calcium oxide (CaO), which was used as a Ca precursor to produce hydroxyapatite powder. This method was modified from the research of Trilaksani et al. (2006) [23]. Crystallinity morphological analysis using an X-ray diffractometer (XRD).

Toothpaste formula

Four toothpaste formulations (F0, F1, F2, and F3) were prepared with varying concentrations of HAp derived from *S. fimbriata* fish bones. The compositions are shown in Table 1, with ingredients measured in parts by weight. F0 was the control with no HAp, while F1, F2, and F3 contained 30, 40, and 50 parts of hydroxyapatite, respectively, replacing an equivalent amount of the standard abrasive (calcium carbonate). Other ingredients remained constant across formulations. Distilled water was added to each formulation to bring the total to 100 parts, ensuring consistent composition.

Creating a revised toothpaste formulation began by dissolving the sodium carboxymethyl cellulose (Na. CMC) in hot distilled water in a glass beaker and allowing it to sit undisturbed for approximately 15 min until it expanded. Then, the ingredients were mixed until they formed a uniform and consistent mixture (mass 1). The combination of fishbone meal and sodium lauryl sulfate was mixed until they formed a uniform mixture, and then this mixture was to mass one (also known as mass 2). Glycerin was combined with mass two until a uniform mixture was achieved. The active compounds carbomer, sorbitol, and sodium benzoate were mixed with

the remaining distilled water, then added to mass two and agitated until the combination achieved a consistent and pasty texture. Blend the menthol into the pasta mixture, ensuring thorough blending, then transfer the pasta to a sterile and moisture-free container for assessment. The formulation of this composition was based on a commonly used toothpaste mixture.

Toothpaste evaluation

The toothpaste formulation contained the following ingredients: trembling fish bone meal as an active component, sodium lauryl sulfate as a cleanser or foam maker, glycerin as a humectant, sodium CMC as a binder, gelling agent carbomer, sorbitol as a sweetener, menthol as a flavoring, and sodium benzoate as a preservative. Solvents such as preservatives and aqua distillate were included.

The powdered *S. fimbriata* bone (CaO) production began with a 45-minute boiling procedure. Subsequently, the fish bones were immersed in a 0.1% NaOH solution for seven hours, followed by an eight-hour immersion in 50% acetone to decrease the fat content in the Sardinella fimbriata. The samples underwent calcination in a furnace at 800oC for three hours. This process aimed to eliminate carbonates that could hinder crystal formation and eliminate all organic components present in *S. fimbriata* fishbones.

Table 2 Analysis of *S. fimbriata* bone powder with XRF

Parameter	Results (m/m%)
CaO	60.25
P_2O_5	39.66
ZnO	0.0536
Nb_2O_5	0.0146
MoO_3	0.0075
SnO_2	0.0058

Results

As shown in Table 2, the bones of *S. fimbriata* contain 60.25 m/m% of calcium oxide. This indicates that calcium oxide can be utilized as a calcium precursor for the formation of HAp compounds.

Crystallinity analysis results

Figure 1 shows the X-ray diffraction (XRD) pattern of the hydroxyapatite compound extracted from *S. fimbriata* fish bone, demonstrating a crystallinity percentage of 82.9%. This high crystallinity was evidenced by the well-defined peaks and narrow peak widths observed in the XRD pattern. While our study used a single calcination temperature of 800 °C, the high crystallinity suggests that this temperature was effective for producing well-crystallized hydroxyapatite from *Sardinella fimbriata* fishbones. However, further studies would be needed to compare the effects of different calcination temperatures on crystallinity.

Based on the XRD pattern shown in Fig. 1, the analysis of HAp bone powder derived from *S. fimbriata* fish

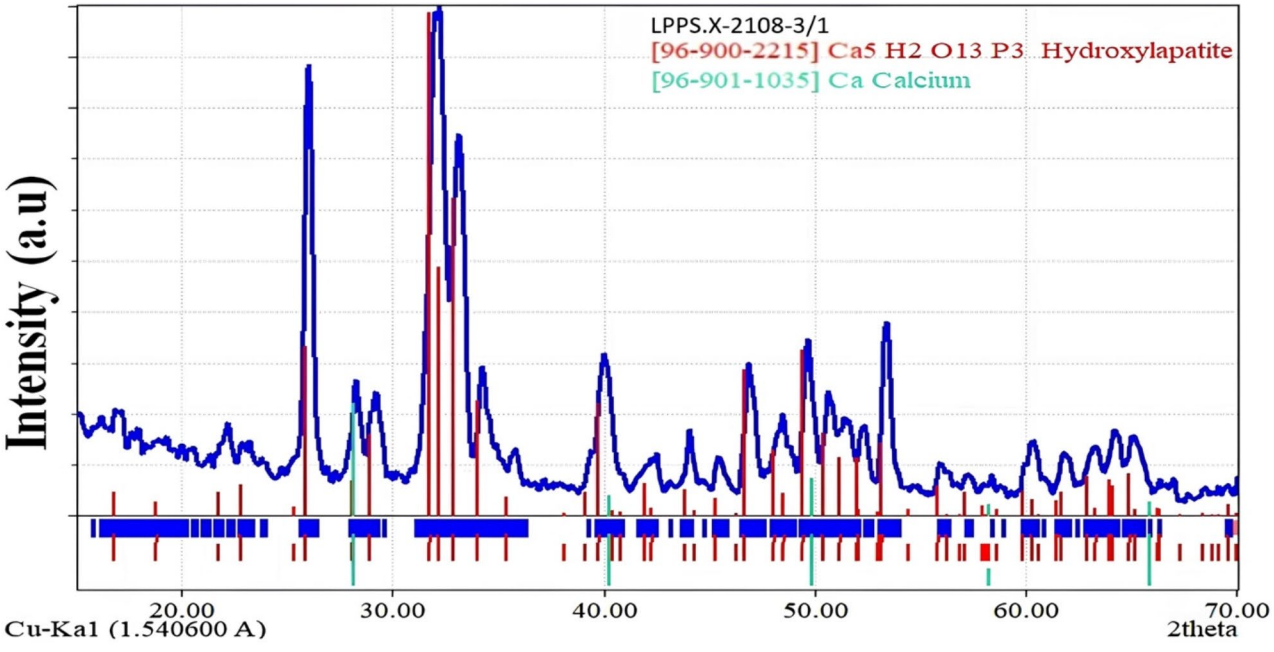

Fig. 1 XRD analysis of hydroxyapatite bone powder of *S. fimbriata* fish

reveals a complex crystalline structure. The diffraction pattern displays prominent peaks characteristic of HAp (Ca5(PO4)3(OH)), indicated in red, with significant peaks observed at approximately 26°, 32°, and 34°. These peaks align well with the standard reference pattern for HAp (JCPDS card 96-900-2215). Additionally, the presence of calcium peaks, shown in green (JCPDS card 96-901-1035), suggests the existence of residual elemental calcium in the sample. The sharp, well-defined peaks and their high intensities indicate a high degree of crystallinity in the sample. The x-axis represents the diffraction angle (2θ) ranging from 20° to 70°, while the y-axis shows the intensity in arbitrary units (a.u.). Cu-Kα1 radiation (λ = 1.540600 Å) is noted for the XRD analysis. This XRD pattern provides valuable insights into the crystalline composition of the fish bone-derived hydroxyapatite, demonstrating its potential as a source of high-quality HAp for various applications while highlighting some residual calcium that may require further consideration in purification processes. Previous investigations reported that the surface morphology of HAp was in the form of agglomerates [16].

Toothpaste evaluation

Organoleptic observations

Table 3 shows organoleptic assessment findings for *S. fimbriata* fish bone HAp toothpaste. The 21-day examination evaluated texture, fragrance, taste, and color on a five-point scale (1-very poor to 5-very good). Participants rated the control formulation (F0) five for texture 85.7–100% of the time. F0 aroma ratings rose from 42.9% on day one to 71.5% on day 21. Taste evaluations for F0 were initially robust, then fluctuated. However, formulations F1, F2, and F3 had more diversified responses across all characteristics. These formulas had lower and more diverse texture ratings than F0, although F1 improved with time. Aroma and taste ratings for F1-F3 varied throughout the research, showing reduced sensory constancy. Color evaluations were comparable across all formulations, with 100% of participants rating it two, demonstrating that adding fish bone-derived hydroxyapatite did not change the toothpaste's appearance. The XRD analysis shows high crystallinity, suggesting that hydroxyapatite may offer oral health benefits, but it also affects consumer sensory perception in nuanced ways that may affect product acceptance.

Organoleptic observations revealed a smell or aroma. The added aroma was menthol in this preparation because it could provide a fresh and clean aroma in the user's mouth. The results showed no difference in the aroma of HAp toothpaste. The preparation looks white; all respondents chose white in F1, F2, and F3. In line with previous findings , the ingredients used in toothpaste are white [16, 24, 25, 26].

Viscosity test

Table 4 shows a toothpaste viscosity study using *S. fimbriata* fish bone hydroxyapatite. The study tested four formulations (F0-F3) on days 1, 7, 14, and 21. Results reveal that hydroxyapatite concentration increases viscosity. The control formulation (F0) had the lowest viscosity, from 16.600 cP on day one to 5.200 cP on day 21. As hydroxyapatite concentration increased, formulations F1, F2, and F3 were more viscous. F3, having the most hydroxyapatite, had the highest viscosity, rising from 34.800 cP on day one to 41,000 cP on day 21. Due to its higher solid content and probable interactions with other components, hydroxyapatite appears to affect toothpaste rheology considerably.

The results of the pH measurement test on toothpaste added with *S. fimbriata* fishbone meal. The pH measurement was carried out using a pH meter. The result was no significant change in pH from the first day to the 21st day, which tended to be stable at an average of 10 alkaline pH. For each formula, the pH decreased but very little, often increasing with time. In conclusion, there was no significant change in pH (Table 5).

Environmental factors such as extreme temperatures, humidity, and storage containers can cause changes in pH values. A reaction between hydroxyapatite (HAp) and sodium may trigger base formation [27].

Foaming test

The results of the foaming power or formation test showed that each formula had almost the same foam formation at F0, F1, F2, and F3 after 21 days of storage without significant changes, but at F0, it showed a lower foam of 7.7 on the 21st day (Table 6).

The results indicate that the relationship between *S. fimbriata* fishbone meal concentration and foam production is not straightforward. While adding HAp generally increased foam production compared to the control (F0), the highest foam was observed at an intermediate concentration (30% in F1). This suggests that there may be an optimal HAp concentration for maximizing foam production, beyond which other factors, such as increased viscosity, might limit further foam enhancement. Toothpaste preparations are said to be good if they form foam. In HAp preparations, fishbones still meet the 60–70% requirements [28, 29].

The results of the high foam test indicate the detergent's ability to produce foam. There are no high foam requirements for toothpaste products, which is associated with the aesthetic value that consumers prefer [30, 31]. Based on the observation of foam height, F1, F2, and F3 have almost the same foam height. This is due to the same percentage of sodium lauryl sulfate being added. SLS is an anionic surfactant with characteristics such as a good foaming agent and high cleaning power [32].

Table 3 Results of organoleptic observations of *S. fimbriata* fish toothpaste

	Organoleptic results (%)																
Days to	**Texture Value**					**Aroma Value**					**Taste Value**						
F0	**1**	**2**	**3**	**4**	**5**	**1**	**2**	**3**	**4**	**5**	**1**	**2**	**3**	**4**	**5**	**1**	**2**
1	-	-	-	14.3	85.7	-	-	57.1	42.9	-	-	-	14.3	28.6	57.1	100	-
7	-	-	-	-	100	-	-	28.6	28.6	42.9	-	-	-	14.3	85.7	100	-
14	-	-	-	-	100	-	-	42.9	42.9	14.3	-	-	-	28.6	71.4	100	-
21	-	-	-	-	100	-	-	28.6	42.9	28.6	-	-	42.9	42.9	14.3	100	-
F1	**1**	**2**	**3**	**4**	**5**	**1**	**2**	**3**	**4**	**5**	**1**	**2**	**3**	**4**	**5**	**1**	**2**
1	-	42.9	57.1	-	-	-	-	42.9	57.1	-	-	-	42.9	57.1	-	-	100
7	-	28.6	14.3	57.1	-	-	14.3	57.1	28.6	-	-	57.1	-	28.6	14.3	-	100
14	-	14.3	57.1	28.6	-	-	14.3	42.9	42.9	-	-	14.3	-	42.9	42.9	-	100
21	-	14.3	57.1	28.6	-	-	28.6	28.6	28.6	14.3	-	-	28.6	57.1	14.3	-	100
F2	**1**	**2**	**3**	**4**	**5**	**1**	**2**	**3**	**4**	**5**	**1**	**2**	**3**	**4**	**5**	**1**	**2**
1	14.3	28.6	28.6	28.6	-	-	14.3	14.3	57.1	14.3	-	-	42.9	28.6	14.3	-	100
7	28.6	-	57.1	14.3	-	-	-	85.7	14.3	-	-	14.3	14.3	14.3	-	-	100
14	-	-	57.1	42.9	-	-	14.3	57.1	14.3	14.3	-	14.3	28.6	42.9	14.3	-	100
21	-	14.3	71.4	14.3	-	-	28.6	28.6	42.9	-	-	28.6	57.1	14.3	-	-	100
F3	**1**	**2**	**3**	**4**	**5**	**1**	**2**	**3**	**4**	**5**	**1**	**2**	**3**	**4**	**5**	**1**	**2**
1	14.3	14.3	57.1	14.3	-	-	-	28.6	57.1	14.3	-	28.6	57.1	14.3	-	-	100
7	28.6	14.3	57.1	-	-	-	57.1	14.3	28.6	-	-	-	57.1	28.6	14.3	-	100
14	-	14.3	57.1	28.6	-	-	28.6	28.6	42.9	-	-	28.6	57.1	14.3	-	-	100
21	-	28.6	42.9	28.6	-	-	28.6	28.6	42.9	-	-	28.6	71.4	-	-	-	100

Table 4 Viscosity test results of *S. Fimbriata* fish bone and pH measurement on toothpaste

Formula	Viscosity (cP)			
	1st day	7th day	14th day	21st day
F0	16.600	4.800	4.800	5.200
F1	28.000	11.600	14.000	18.200
F2	32.000	28.000	27.200	35.600
F3	34.800	32.800	36.800	41.000

Table 5 Test results for measurement of pH toothpaste *S. fimbriata* bone fish

Formula	Average pH			
	1st day	7th day	14th day	21st day
F0	7.56	7.69	7.47	7.43
F1	10.34	10.15	9.83	10.05
F2	10.36	10.02	10.09	10.07
F3	10.46	10.53	10.41	10.27

Table 6 Test results for *Sardinella fimbriata* hydroxyapatite toothpaste foaming

Formula	Average Foam height (cm)			
	1st day	7th day	14th day	21st day
F0	7.6	7.7	7.7	7.7
F1	15.8	15.9	16.0	16.2
F2	13.8	13.8	13.8	13.9
F3	15.5	15.6	15.6	15.7

Stability test

A stability test was carried out by storing hydroxyapatite (HAp) toothpaste from *S. fimbriata* fishbones at 40 °C, room temperature, and 40 °C for the 21st day. Then, continue to observe whether the organoleptic, pH, homogeneity, spreadability, and changes in the foam formed on the 7th, 14th, and 21st days [33].

The stability of the toothpaste formulations was assessed through storage at 40 °C for one minute. While water content was not directly measured, changes in viscosity were monitored as an indirect indicator of water loss. Viscosity measurements were taken on days 1, 7, 14, and 21, as shown in Table 4. A hedonic test was conducted with 7 participants to evaluate the organoleptic properties of the toothpaste. Participants rated texture, aroma, taste, and color on a 5-point scale (1 being very poor, five being very good) at four-time points over 21 days. The results of this organoleptic evaluation are presented in Table 3.

Hedonic test

In a hedonic test on hydroxyapatite toothpaste *Sardinella fimbriata* fishbone, 20 volunteers, on average, liked each toothpaste formula in terms of color, aroma, taste, and texture.

Discussion

Incorporating hydroxyapatite (HAp) derived from *Sardinella fimbriata* fish bones into toothpaste formulations has shown promising results regarding physicochemical properties and organoleptic characteristics. This research demonstrates that increasing HAp concentration increases toothpaste formulations' viscosity. The control (F0) showed the lowest viscosity, while F3 (50% HAp) consistently exhibited the highest viscosity throughout the 21-day study period. This trend aligns with findings by Hiller et al. (2018) and Dorozkin (2019), who reported that nano-hydroxyapatite particles increase the viscosity of dental materials due to their high surface area and interaction with other ingredients [8, 9]. The increased viscosity in HAp-containing formulations may improve stability and adherence to tooth surfaces, potentially enhancing the remineralization effect.

Our current study also reveals that *the organoleptic observations were* over 21 days. Interestingly, the control formulation (F0) consistently received high ratings for texture and taste, while HAp-containing formulations (F1, F2, F3) showed more varied responses. This variability in sensory perception is consistent with research by Hiller et al. (2017) and Dorozhkin (2018), who noted that the incorporation of bioactive materials like HAp can influence the organoleptic properties of oral care products [8, 9].

The aroma ratings for all formulations fluctuated over time, suggesting that the HAp content may interact with flavoring agents. Chen et al. (2021 and 2021) support this observation, discussing the challenges of maintaining consistent sensory properties in biomimetic oral care products [10, 11]. Color perception remained consistent across all formulations, indicating that HAp addition did not significantly alter the toothpaste's visual appeal. This is a positive finding, as consumer acceptance often hinges on familiar product appearance [12]. While direct water content measurements were not performed, the stability of viscosity measurements over 21 days suggests that the formulations maintained their integrity. This stability is crucial for commercial viability and shelf-life considerations.

As revealed by XRD analysis, the high crystallinity (82.9%) of the fish bone-derived HAp indicates its structural similarity to human tooth enamel. This similarity is a key factor in the toothpaste's potential remineralization efficacy. Rial et al. (2011) demonstrated that highly crystalline HAp particles show superior remineralization effects compared to amorphous calcium phosphates [13]. This finding aligns with studies by Boutinguiza et al. (2012) [14], who reported that fish-derived HAp exhibits structural properties similar to human bone and teeth. The work of Rial et al. (2011) further supports this, demonstrating that highly crystalline HAp particles show

superior remineralization effects compared to amorphous calcium phosphates [15, 16]. Pepla et al. (2014) corroborate this, noting that nano-hydroxyapatite has been shown to remineralize enamel subsurface lesions in vitro [17]. Amaechi et al. (2015) further emphasized that nano-hydroxyapatite has significant remineralizing effects on initial enamel lesions, superior to conventional fluoride [18].

The structural resemblance contributes to the biocompatibility of fish-derived HAp and its potential for better integration with natural tooth structures, as suggested by Shepherd et al. (2012) in their work on multi-substituted hydroxyapatites [19]. Moreover, the high crystallinity suggests that fish-derived HAp may offer advantages over synthetic versions, particularly due to the presence of trace elements that can enhance its properties for dental applications. While the crystallinity primarily relates to remineralization potential, it's worth noting that the organoleptic properties of HAp-based toothpaste can be improved through various additives, as discussed by Lippert (2013) in the literature on toothpaste formulations [20]. This combination of high crystallinity and potential for organoleptic enhancement opens up possibilities for developing effective, biomimetic, non-fluoride alternatives for caries prevention and enamel remineralization, a direction that Enax & Epple (2018) suggest is promising for the future of oral care products [21].

Future research should focus on (1) Quantifying the remineralization effects of these HAp-containing toothpaste through in vitro and in vivo studies, (2) Investigating the long-term stability of the formulations under various storage conditions, (3) Conducting clinical trials to evaluate the efficacy of these formulations in improving oral health outcomes, (4) Exploring the potential of different particle sizes and concentrations of HAp to optimize both efficacy and sensory properties, 5)Assessing the environmental impact and sustainability of using fish bone waste as a source of HAp for oral care products.

Conclusion

Hydroxyapatite from *Sardinella fimbriata* fish bones shows promise as a toothpaste component. Increasing hydroxyapatite content increased viscosity, with the 50% formulation (F3) having the maximum viscosity after 21 days. The control formulation (F0) scored better for texture and taste while hydroxyapatite-containing formulations (F1, F2, F3) had more varied reactions. The color perception was constant across all formulations. These data imply that toothpaste made with fish bone-derived hydroxyapatite can be effective, although sensory qualities and consumer acceptability need additional tuning. This research lays the groundwork for sustainable, biocompatible dental care products made from fish industry byproducts, which may improve the environment and oral health. Quantifying remineralization effects, assessing long-term stability, and performing clinical trials to improve oral health should be the focus of future research.

Supplementary Information

The online version contains supplementary material available at https://doi.org/10.1186/s12903-025-05557-7.

Supplementary Material 1

Author contributions

AIA: conceptualization; methodology; resources; investigation; data curation; visualization; funding; writing—original draft preparation; and editing. MR, EM, and HH: conceptualization; methodology; resources; investigation; writing—review and editing; project administration. All authors have read and approved the published version of the manuscript.
All authors wrote the main manuscript text and prepared figures and tables.
All authors reviewed the manuscript.

Funding

This research is supported by the Unhas Beginner Lecturer Research Grant Fund for the 2021 fiscal year.

Data availability

The authors confirm that the data supporting the findings of this study are available within the article.

Declarations

Competing interests

The authors declare no competing interests.

Received: 21 April 2024 / Accepted: 24 January 2025
Published online: 07 February 2025

References

1. Nemati M, Huda N, Ariffin F. Development of calcium supplement from fish bone wastes of yellowfin tuna (Thunnus albacares) and characterization of nutritional quality. Int Food Res J. 2017;24(6):2419–26.
2. Nawaz A, et al. Valorization of fisheries by-products: challenges and technical concerns to the food industry. Trends Food Sci Technol. 2020;99:34–43.
3. Kim S-K. Marine medicinal foods: implications and applications: animals and microbes. Volume 65. Academic; 2012.
4. Logesh A, et al. Calcium and phosphorus determination in bones of low-value fishes, Sardinella longiceps (Valenciennes) and Trichiurus savala (Cuvier), from Parangipettai, Southeast Coast of India. Asian Pac J Trop Disease. 2012;2:S254–6.
5. Mahnaz N, Huda N, Ariffin F. Development of calcium supplement from fish bone wastes of yellowfin tuna (Thunnus albacares) and characterization of nutritional quality. Int Food Res J. 2017;24(6):2419–26.
6. Kusumawati P, et al. Nano-calcium Powder properties from six commercial Fish Bone Waste in Indonesia. Squalen Bull Mar Fisheries Postharvest Biotechnol. 2022;17(1):1–12.
7. Devitasari SP, Hudiyati M, Anastasia D. *Effect of hydroxyapatite from waste of tilapia bone (Oreochromis niloticus) on the surface hardness of enamel*. in *Journal of Physics: Conference Series*. 2019. IOP Publishing.
8. Singh S et al. Sustainable processes for treatment and management of seafood solid waste. Sci Total Environ, 2022: p. 152951.
9. Hui P, et al. Synthesis of hydroxyapatite bio-ceramic powder by hydrothermal method. J Minerals Mater Charact Eng. 2010;9(8):683–92.
10. Curren E, et al. Marine microplastics in the ASEAN region: a review of the current state of knowledge. Environ Pollut. 2021;288:117776.

11. Hasan MR, Yasin NSM, Mohd MS. Proximate and morphological characteristics of nano hydroxyapatite (Nano HAp) extracted from fishbone. J Sustain Sci Manage. 2020;15(8):9–21.
12. Rosidi WNTM, Arshad NM, Mohtar NF. Characterization of Sardinella fimbriata and Clarias gariepinus bones. Biodiversitas J Biol Divers, 2021. 22(4).
13. Murtini NLA, Hamzah B. Analysis of calcium (ca) and potassium (K) levels in Mackerel (Rastrelliger sp.) bones. Volume 9. Jurnal Akademika Kimia; 2020. pp. 143–7. 3.
14. El Mhammedi MA, Achak M, Chtaini A. Ca10 (PO4) 6 (OH) 2-modified carbon-paste electrode for the determination of trace lead (II) by square-wave voltammetry. J Hazard Mater. 2009;161(1):55–61.
15. Jeong S et al. *Remineralization potential of new toothpaste containing nano-hydroxyapatite*. in *Key Engineering Materials*. 2006. Trans Tech Publ.
16. Anggresani L, Sari YN, Rahmadevi R. Hydroxyapatite (HAp) from Tenggiri Fish bones as Abrasive Material in Toothpaste Formula. Jurnal Kimia VALENSI Volume, 2021. 7(1).
17. Bains PS et al. *On the machinability and properties of Ti–6Al–4V biomaterial with n-HAp powder–mixed ED machining.* Proceedings of the Institution of Mechanical Engineers, Part H: Journal of Engineering in Medicine, 2020. 234(2): pp. 232–242.
18. McPherson R, Vickers P, Slater G. Bone grafting with coralline hydroxyapatite. EC Dent Sci. 2019;18:2413–23.
19. Sidiqa AN, et al. Surface modification of multilayer coatings Ti-Al-Cr and hydroxyapatite on calcium phosphate cement with sol-gel method. J Dentistry Indonesia. 2013;19(2):43–6.
20. Sofian FRM et al. *Biomaterials derived from tamban, Sardinella fimbriata bones as promising anodyne sunscreen.* 2017.
21. Ahuja I, et al. Fish and fish waste-based fertilizers in organic farming - with status in Norway: a review. Waste Manag. 2020;115:95–112.
22. Venkatesan J, Kim SK. Effect of temperature on isolation and characterization of Hydroxyapatite from Tuna (Thunnus obesus) bone. Mater (Basel). 2010;3(10):4761–72.
23. Trilaksani W, Salamah E, Nabil M. Utilization of Tuna Fish Bone Waste (Thunnus Sp.) as a source of calcium with protein hydrolysis method. Indonesian J Fish Prod Process. 2006;9(2):34–45.
24. Mutmainnah M, Chadijah S, Rustiah WO. Hidroksiapatit Dari tulang ikan tuna sirip kuning (tunnus albacores) dengan metode presipitasi. Al-Kimia. 2017;5(2):119–26.
25. Cahyanto A et al. *Fabrication of hydroxyapatite from fish bones waste using reflux method*. in *IOP Conference Series: Materials Science and Engineering*. 2017. IOP Publishing.
26. Andriana I, Murrukmihardi M, Ekowati D. The effect of tragacanth concentration on the physical quality of toothpaste preparations of ethanolic extract of Mahkota dewa leaves (Phaleria Papuana Warb var. Wichnannii) as an antibacterial for Streptococcus mutans. Jurnal Farmasi Indonesia. 2011;8(1):66–76.
27. Nuraskin C, et al. Toothpaste activity test of Laban Leaf methanol extract (Vitex pinnata) against the growth of Streptococcus mutans bacteria. Open Access Macedonian J Med Sci. 2021;9(F):95–100.
28. Fuller BT, et al. Fish δ13C and δ15N results from two Bronze/Iron age sites (tell Tweini & Sidon) along the levantine coast. J Archaeol Science: Rep. 2020;29:102066.
29. Caruso G, et al. Fishery wastes as a yet undiscovered treasure from the sea: Biomolecules sources, extraction methods and valorization. Mar Drugs. 2020;18(12):622.
30. Bouassida M, et al. Potential application of Bacillus subtilis SPB1 lipopeptides in toothpaste formulation. J Adv Res. 2017;8(4):425–33.
31. El-Khordagui L, Badawey SE, Heikal LA. *Application of biosurfactants in the production of personal care products, and household detergents and industrial and institutional cleaners*, in *Green Sustainable Process for Chemical and Environmental Engineering and Science.* 2021, Elsevier. pp. 49–96.
32. Enax J, et al. Modes of action and clinical efficacy of particulate hydroxyapatite in preventive oral health care – state of the art. Open Dentistry J. 2019;13:274–87.
33. Guntermann L, et al. Remineralization and protection from demineralization: effects of a hydroxyapatite-containing, a fluoride-containing and a fluoride- and hydroxyapatite-free toothpaste on human enamel in vitro. Head Face Med. 2022;18(1):1–11.

Publisher's note

ARTICLES FOR FACULTY MEMBERS

BONE-DERIVED HYDROXYAPATITE TOOTHPASTE FOR SUSTAINABLE PHARMACEUTICAL AND BIOMEDICAL APPLICATIONS

Preparation and characterization of hydroxyapatite obtained from bovine bones / Alvarado, C., Alfaro, A., Cisneros, M., & Alvarado-Quintana, H.

Proceedings of the 21st LACCEI International Multi-Conference for Engineering, Education and Technology
(2023) Pages 1-6
https://doi.org/10.18687/laccei2023.1.1.590
(Database: Latin American and Caribbean Consortium of Engineering Institutions)

ISBN: 978-628-95207-4-3. ISSN: 2414-6390. Digital Object Identifier: https://dx.doi.org/10.18687/LACCEI2023.1.1.590

Preparation and Characterization of Hydroxyapatite Obtained from Bovine Bones

Cinthya Alvarado, MSc[1], Akemy Alfaro, Eng[2], Maraid Cisneros, Eng[3], and Hernán Alvarado-Quintana, PhD[4]
[1]Universidad Privada del Norte, Perú, cinthya.alvarado@upn.edu.pe
[2,3,4]Universidad Nacional de Trujillo, Perú, alfaalva2198@gmail.com, cisnerosms98@gmail.com, halvarado@unitru.edu.pe

Abstract*– According to certain research, feedlots are a major source of unseparated solid and liquid organic wastes and residues, which contaminate the air, surface waters, and groundwater. Cattle bones are typically discarded before being fully exploited, therefore hydroxyapatite can be extracted from this bio-waste in an affordable, environmentally responsible way that adds value. The current research was carried out to examine the influence of the particle size of hydroxyapatite sintered at 1000 °C obtained from bovine bone to estimate its compressive strength and porosity in order to offer it a practical approach and enhance its long-term mechanical properties. The stoichiometry of the bovine bone powder was determined by a thermogravimetric analysis (TGA), which demonstrated that it is suitable for producing hydroxyapatite. Cleaning, boiling, drying at 150 °C, burning at 400 °C, and calcining at 900 °C were all performed on the cow bones. They were further crushed and sieved using screens of 300, 150, 75, and 53 μm aperture diameters. By uniaxially compacting specimens of hydroxyapatite powder at a pressure of 1 MPa and sintering them at 1000 °C, the specimens were created. By analyzing the sintered hydroxyapatite powders using X-Ray Diffraction (XRD) and Scanning Electron Microscopy (SEM), the powders were given a specific character. When samples with various grain sizes were evaluated, those with a grain size of 53 μm and a porosity of 44.24% had a greater compressive strength of 2.53 MPa.

Keywords*-- Hydroxyapatite, bovine bone, bioresidue, porosity, compressive strength.

I. Introduction

Because they produce a large amount of organic waste and residues that aren't usually segregated into solid and liquid forms, cattle slaughterhouses have recently emerged as highly polluting sources. These biological waste spills cause air pollution, surface, and groundwater contamination, and are a source of environmental risks. It should be mentioned that since these wastes can be used as a source of raw materials for the creation of biomaterials, attempts to valorize them are a helpful strategy for addressing these issues [1].

Engineering has been greatly impacted by the rise in environmental consciousness, and as a result, biomaterials are now more and more in demand. Hydroxyapatite (HA) is one of the most alluring biomaterials that have been used for many biomedical applications because of its characteristics that resemble those of natural bone. It is a kind of bioceramic made from calcium orthophosphate, a substance found in teeth and bones [2].

Digital Object Identifier: (only for full papers, inserted by LACCEI).
ISSN, ISBN: (to be inserted by LACCEI).
DO NOT REMOVE

Production of hydroxyapatite has been ongoing from natural sources, primarily from biowaste (mammalian skeletal remains, poultry eggshells, fish bones and scales). The extraction of hydroxyapatite from this bio-waste is cost-effective, ecologically benign, and adds value because bovine bones are typically thrown without being fully exploited [3]. Additionally, using trash to create biomaterial can be good for the environment as a method of managing biowaste and lowering waste output.

The qualities of the generated product will depend on the kind of precursor used, and the synthesis processes employed. There are various ways to make hydroxyapatite, including dry, wet, and high-temperature techniques. However, these synthesis processes can be challenging or dangerous for biological systems, therefore recently they have been extracted by synthesis from biological sources. The microstructure features, such as grain and pore size, which are dependent on the processing parameters (particle size reduction) and sintering temperature, are crucial because they may have an impact on the mechanical capabilities of the hydroxyapatite [4].

Using discarded chicken femur bone, reference [4] investigated the effects of calcination temperatures of 500 °C, 700 °C, and 900 °C on the characteristics of natural hydroxyapatite. This thermal treatment revealed that the morphology, content, and crystallinity of hydroxyapatite were substantially associated with the calcination temperature. Additionally, its crystallinity and crystallite size increased dramatically when the sintering temperature was raised. Furthermore, they said that 700 °C would be the ideal temperature to create hydroxyapatite and that temperatures between 250 and 800 °C totally eradicated the organic phase, making accurate temperature management of the calcination process crucial. This study contributes to the research by explaining the rationale for producing hydroxyapatite from food industry waste, realizing a thermal analysis of the bone to understand how it decomposes during the calcination process, and performing XRD and SEM tests to identify the composition and crystallinity of the produced hydroxyapatite.

A study published in Reference [5] compared the physical, chemical, and mechanical characteristics of natural hydroxyapatite made from catfish bones and unseparated animal bones that underwent 900 °C of heat treatment. Catfish bones and hydroxyapatite made from unseparated animal bones both showed Ca/P ratios of 1.58 and 1.63, respectively. Both hydroxyapatite formed from catfish bones and hydroxyapatite derived from unseparated animal bones had fracture toughness values of 2.35 MPa.m$^{1/2}$ and 5.72 MPa.m$^{1/2}$,

compressive strengths ranging from 0.47 to 1.92 MPa, and hardness values of 0.65 GPa and 0.48 GPa, respectively. The hardness values were also discovered to be in the range of human cortical bone, increasing the viability of catfish bone-derived hydroxyapatite for use in biomedical applications where compressive pressures are present. The exploration of the low pressure approach (1 MPa) for specimen compaction and the connection between porosity and the enhancement of particular mechanical qualities are both furthered by this work.

Reference [6] assessed the characteristics of hydroxyapatite ceramics produced by direct thermal conversion from catfish bones (CB) and unseparated animal bones (NB). Cold compaction was used to create representative scaffolds, which were subsequently sintered at temperatures of 900, 1000, and 1100 °C. They discovered that the CB-derived hydroxyapatite showed an increase in hardness (0.73 GPa) at 1000 °C, followed by a reduction. While NB-derived hydroxyapatite's hardness characteristics became less robust as the temperature rose. All samples' fracture toughness decreased as the sintering temperature increased from 900 to 1100 °C. Phase changes that occur during heat treatment are the causes of these gradients in mechanical measurements. This paper explains the rationale behind the sintering temperature of hydroxyapatite specimens and the tendency of high temperatures to reduce mechanical characteristics.

Reference [1] examined the effects of various sintering temperatures (900 °C, 1000 °C, and 1100 °C) on the mechanical and microstructural characteristics of naturally occurring hydroxyapatite biowaste produced by a cold compaction technique under low pressure (500 Pa). The characterization process employed XRD and SEM measurements. The hydroxyapatite powder demonstrated thermal stability while sintering at 1000 °C. Both 0.93 and 1.09 GPa of hardness, 4.28 and 6.20 GPa of Young's modulus, 1.87 and 2.21 $MPa.m^{1/2}$ of fracture toughness, and 0.84 and 0.69 MPa and 0.69 MPa, respectively, of compressive strength without pressure and with 500 Pa of compaction pressure were produced. Consistently observing increased mechanical qualities, except for compressive strength because of stress created during compaction of the hydroxyapatite particles.

Reference [7] produced natural hydroxyapatite from chicken, goat, and bovine bones using cold isostatic pressing techniques at temperatures of 1100 °C, 1200 °C, and 1300 °C. They were characterized using XRD and SEM analysis, and in terms of mechanical characteristics, their hardness and compressive strength were assessed both before and after sintering. According to the study, hydroxyapatite extracted from cattle had a higher production efficiency than that of chicken and goat; the greatest hardness was 3.7 GPa at 1300 °C, while the highest compressive strength (0.44 MPa) was for the sample sintered at 1200 °C. The relative density increased as the sintering temperature climbed, rising from 12.44% at 1100 °C to a maximum of 30.3% at 1300 °C. This study adds to the investigation of the natural source that, when compared to chicken, goat, and cattle bones, had the highest efficiency of hydroxyapatite formation, with the bovine bone source having the best outcomes.

Reference [8] employed a heat treatment in an air atmosphere at temperatures ranging from 600 °C to 1000 °C to generate hydroxyapatite from animal bone biowaste, specifically bovine, goat, and chicken bones. Following heat treatment above 700 °C, tricalcium phosphate (TCP) residues were found in the hydroxyapatite generated from goat and chicken bones, indicating phase instability, whereas hydroxyapatite derived from bovine bone shown good thermal stability. Energy-dispersive x-ray spectroscopy (EDS) was used to analyze the hydroxyapatite and determine its chemical composition. This method revealed that the sample's elemental composition is similar to that of natural bone. When the bovine bones were sintered at particular temperatures, a porous hydroxyapatite body with hardness values comparable to those of human cortical bone was created. The value of 387 MPa was obtained at a temperature of 750 °C, whereas the hardness of human cortical and cancellous bone is 396 MPa and 345 MPa, respectively. In comparison to the other two types of bones, the sintered chicken bone sample had higher levels of porosity and lower levels of hardness (200 MPa). This work adds to the body of knowledge regarding the characterization of hydroxyapatite, and in this instance, bovine bone was the natural source that produced the greatest outcomes.

Reference [9] investigated how particle size and calcination temperature affected the structural characterization of hydroxyapatite. The hydroxyapatite powders were sinter using the chemical precipitation technique. XRD, SEM, and Fourier-transform infrared spectroscopy (FTIR) were used for characterization. They acquired the increase in particle size, as well as the appearance and growth of grains, as a result of the rise in calcination temperature. They used X-rays to observe the presence of distinctive hydroxyapatite peaks at each of the three calcination temperatures, but due to thermal factors, they were unable to identify any hydroxyapatite disintegration phases. This study adds to the body of knowledge regarding the behavior of the hydroxyapatite grain size as well as the resulting crystallinity.

As a result, the goal of this study was to ascertain how particle size influenced the compressive strength and porosity of HA made from bovine bones that were sintered at 1000 °C. There has been limited research on the physical and mechanical properties of HA as a function of bio-residue particle size, despite some studies being done on the production and sintering of hydroxyapatite.

II. Material and Methods

A. Material

The object of study in this research was hydroxyapatite obtained by calcination and grinding of bovine bones. For its physical and mechanical characterization, 32 cubes of 25 mm of side were elaborated by uniaxial pressing.

B. *Experimental design*

A one-factorial experimental design was applied where the independent variable was grain size with four study levels, 300, 150, 75 and 53 µm and the dependent variables were compressive strength (MPa) and porosity (%). All tests were performed in quadruplicate.

C. *Synthesis*

10 kg of cattle bones were taken from the El Porvenir animal feedlot in Trujillo, Peru, and utilized as a source to make hydroxyapatite. Ten liters of distilled water were purchased and used throughout the procedure. To remove contaminants, distilled water was used to clean the raw bovine bones. The bone samples were then deproteinized by boiling them for 3 hours, rinsed once more with distilled water, and dried for 8 hours at 105 °C. They were then heated to 400 °C on a gas burner in order to burn off all organic material. Finally, the bones were calcined at 900 °C with a ramp rate of 5 °C/min in an electric oven, held for 2 hours, and then allowed to cool in the oven. The resulting samples were crushed with mortar and then sieved through 50 (300 µm), 100 (150 µm), 200 (75 µm) and 270 (53 µm) mesh.

D. *Characterization*

The XRD test was performed on the hydroxyapatite sample after the sintering process. A Rigaku diffractometer, model Miniflex 600 and a scanning speed of 2 theta of 2°/min was used.

The thermogravimetry test was performed on the bovine bone sample and the hydroxyapatite sample using Setsys Evolution TGA-DTA / DSC equipment.

The materials' microstructure was examined using a Tescan Vega 3 XMU SEM running at 10 kV. The microscope is fitted with an Oxford EDS detector for elemental analysis. The samples were prepared by sputtering gold at a low deposition rate onto their surface. Each sample was observed at 5000x and 7500x.

E. *Powder compaction*

With 5% water, 22 g of hydroxyapatite powder was prepared. It was put into a steel mold and compressed uniaxially with a Humboldt HM 3000 Press at 1 MPa and 1 mm/s. For experiments on compressive strength and porosity assessment, cube-shaped specimens measuring 25 mm on each side were obtained.

F. *Sintering*

The specimens were sintered in a muffle-type electric furnace at a temperature of 1000 °C for 2 hours at a heating rate of 5 °C/min.

G. *Porosity measurements*

The porosity of the sintered samples was determined by (1) [1,10].

$$\text{Porosity (\%)} = [1 - \text{Weight}/(\text{Volume} \times \text{Density})] \times 100 \quad (1)$$

The density of hydroxyapatite used was 3.16 g/cm^3 [1].

H. *Compressive strength*

Using a Humboldt HM 3000 testing apparatus with a 50 kN load cell, the compressive strength of the pressed cubes was measured.

III. Results and Discussion

A. *XRD analysis of sintered HA samples*

X-ray diffraction was performed to confirm the presence and crystallinity of hydroxyapatite in the sample obtained, as shown in Fig. 1, the test was performed on the hydroxyapatite sample sintered at 1000 °C.

The distinctive peaks of hydroxyapatite are seen in Fig. 1, demonstrating its presence and purity. The extremely sharp, narrow, intense, and well-defined peaks signify a higher degree of crystallinity in the compound's phases.

In the X-ray diffraction patterns, the presence of peaks characteristic of hydroxyapatite is observed. The main and highest intensity peak of hydroxyapatite is found at 2θ = 31.70°, corresponding to the (211) plane, it is accompanied by three nearby peaks; the one at 2θ = 32.20°, corresponding to the (112) plane, of lower intensity of the previous peak; the one at 2θ = 32.90°, corresponding to the (300) plane of almost equal intensity, but higher than the previous one and a peak at 2θ = 34.22°, smaller than the previous three, corresponding to the (202) plane. This set of four peaks and their respective relative intensities are indicative of pure hydroxyapatite of high crystallinity, as are the lower intensity peaks that are also present (ICCD-JCPDS data sheet # 9-0432).

This experiment proves that, as stated in [1], hydroxyapatite retains its purity phase up to a maximum sintering temperature of 1000 °C without disintegrating into biphasic hydroxyapatite.

B. *Thermogravimetric analysis*

Fig. 2 shows the graph of the TGA performed on two samples, bovine bone powder and sintered hydroxyapatite, obtained from the same bone.

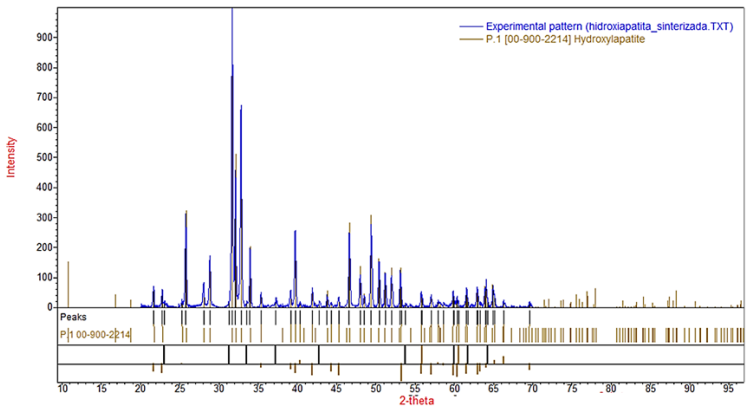

Fig. 1 X-ray diffraction patterns of the hydroxyapatite sample.

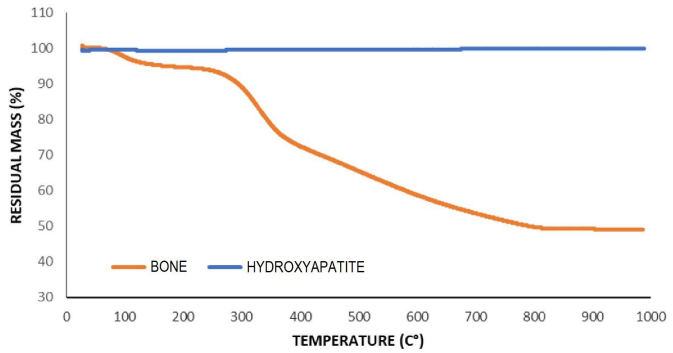

Fig. 2 TGA of bovine bone powder and hydroxyapatite powder.

The three stages of thermal decomposition can be seen in the orange-colored curve, which represents bovine bone powder. The first stage occurs between 100 – 200 °C, the second between 200 – 400 °C, and the third between 400 – 800 °C.

The first stage, occurring between 100 – 200 °C, results in a 10% mass loss due to desorption of water present in the bovine bone powder.

The second stage, occurring between 200 – 400 °C, results in a 22.22% mass loss attributed to the combustion of organic components (such as fats and collagen) in the bovine bone powder.

The third stage, occurring between 400 – 800 °C, results in 28.57% mass loss, which can be caused by residual organic matter and the decomposition of carbonate groups.

According to the results obtained, in the range of 200 – 400 °C, the incineration of all the organic components present in the bovine bone sample takes place. Reference [4] also indicates that from 250 °C onwards, the combustion of these components occurs. Due to this, a color change of the bone sample is observed, going from a brownish-yellow color to a gray powder that is attributed to the presence of ashes generated in the organic incineration process.

The blue line represents the hydroxyapatite obtained from the bovine bone powder, as shown in Fig. 2; as this material does not present mass loss, the curve is stable and remains constant throughout the thermogravimetric process.

C. *SEM microstructure*

Fig. 3 shows SEM micrographs of the hydroxyapatite sample sintered at 1000 °C at high magnification.

The grain boundaries can be seen in the densely packed surface morphology in Fig. 3. It confirms what is indicated in Reference [9], where they state that the phase transition starts at a temperature of 900 °C, where the β-TCP phase transforms to hydroxyapatite and there is a clearer formation of the grain.

According to Reference [11], the interconnection between the grain structures that are nearest to one another often defines the commencement of a definite crystalline grain structure of hydroxyapatite.

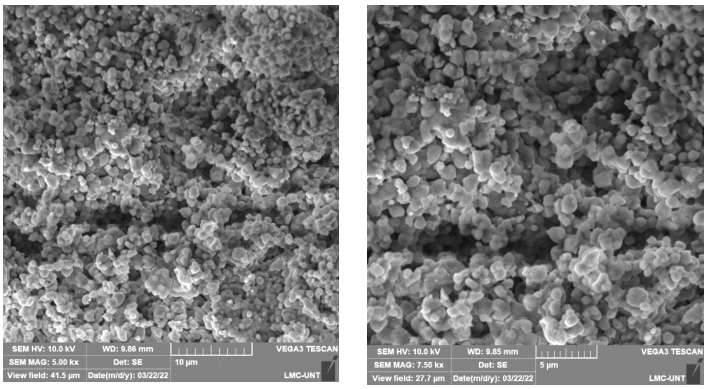

(a) (b)

Fig. 3 SEM micrograph of hydroxyapatite sintered at 1000 °C. a) Micrograph at 5000x. b) Micrograph at 7500x.

D. *EDS analysis*

Fig. 4 presents the results of the EDS investigation into the elemental makeup of sintered hydroxyapatite. With traces of trace elements like magnesium (Mg) and sodium (Na), the three elements calcium (Ca), phosphorus (P), and oxygen (O) makeup most of the sintered samples. The elemental makeup of the samples, according to Reference [8], is strikingly close to the chemical makeup of real bone.

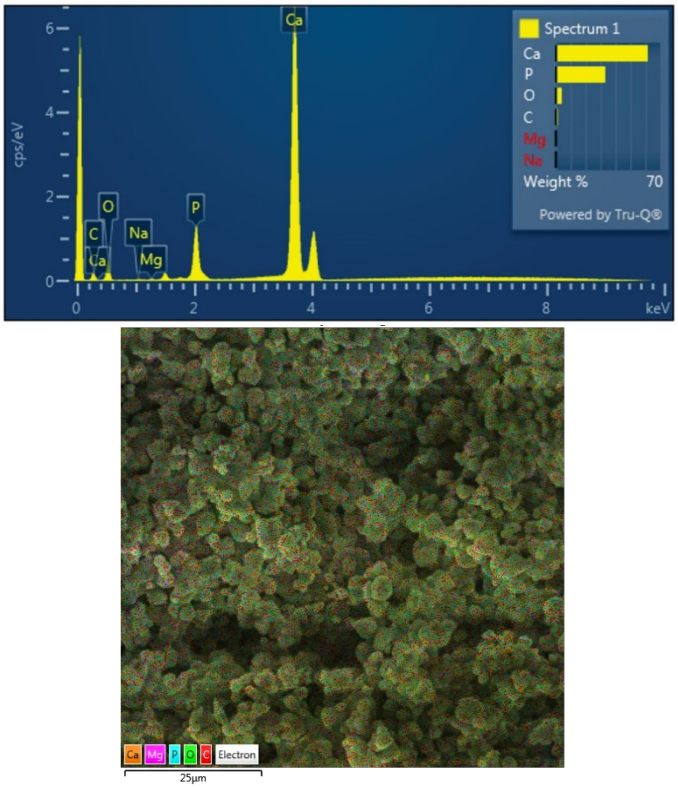

Fig. 4 EDS analysis of sintered hydroxyapatite at 1000°C.

TABLE I
ELEMENTAL COMPOSITION OF HYDROXYAPATITE SAMPLE

ELEMENT	Wt%
C	1.31
O	3.29
Na	0.02
Mg	0.07
P	36.23
Ca	59.08
Total	**100.00**

The elemental composition and weight percentage of the hydroxyapatite sample subjected to EDS analysis are shown in Table I. Calculated for the proportion of sample weight, the Ca/P ratio was 1.63. The predicted value for pure stoichiometric hydroxyapatite is 1.67, and the Ca/P ratio found in this experiment deviates somewhat from that value [12]. One of the variables that could explain this variation is the sintering temperature, which has an impact on the kind and composition of calcium-based compounds that would show up in the final hydroxyapatite bioceramic.

E. Compressive strength

The results of the compressive strength test of hydroxyapatite sintered at 1000 °C are shown in Fig. 5. The graph shows the variation of strength with respect to hydroxyapatite grain size.

The compression test was the type of test used on these materials. During this test, the specimen is subjected to compressive stresses in a direction parallel to the load application and more significant tensile stresses in a direction perpendicular to the load application. The specimen fails because of the stresses being greater than the material's strength.

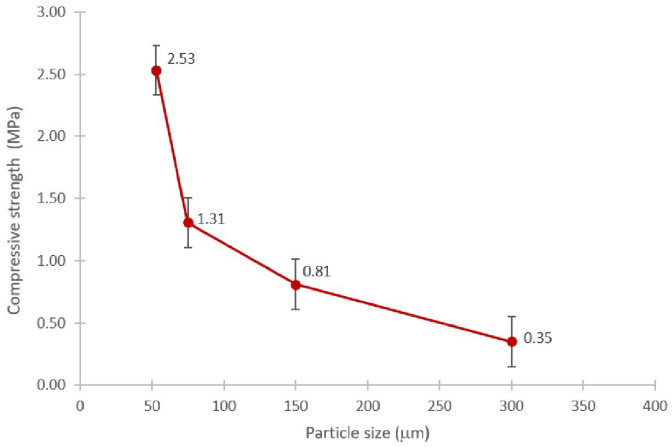

Fig. 5 Compressive strength test results of hydroxyapatite sintered at 1000 °C

Figure 5 demonstrates the relationship between compressive strength and particle size, demonstrating an 86% increase in strength from a minimum compressive strength of 0.35 MPa for a particle size of 300 μm to a maximum strength of 2.53 MPa for a 53 μm particle. The difference in compressive strength results from the fact that better compaction occurs with smaller particle sizes because there are fewer spaces between them (defects), which results in a better arrangement and a stronger material.

In their study, Reference [1] discovered that sintered hydroxyapatite samples with a particle size of 300 μm had compressive strengths that varied from 0.30 to 0.69 MPa. They found a compressive strength of 0.35 MPa with the same particle size. When comparing their results with the present study, it can be said that the strength grew as the particle size decreased, reaching a maximum value of 2.53 MPa at 53 μm.

It is confirmed that these results are better than those of Reference [7], who obtained a maximum compressive strength of 0.44 MPa for a hydroxyapatite sample sintered at 1200 °C. This improvement is attributed to the stability that hydroxyapatite exhibits at the sintering temperature of 1000 °C and that, at higher temperatures, it exhibits degradation.

F. Porosity

Fig. 6 shows the results of how the percent porosity of hydroxyapatite varies as a function of particle size.

Because larger particles leave more empty spaces in the formed specimens, the porosity of hydroxyapatite increases primarily as the particle size increases. For example, the porosity of hydroxyapatite was 44.89% at a particle size of 300 μm and 44.24% at a particle size of 53 μm.

A higher compaction pressure (1 MPa) was used in this study, resulting in lower porosity due to improved particle ordering. This is compared to Reference [1], whose research obtained a porosity percentage of 44.89% for a particle size of 300 μm sintered at 1000 °C at a compaction pressure of 500 Pa.

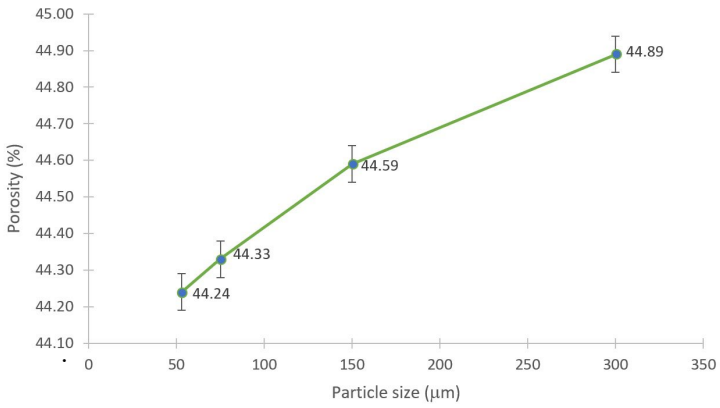

Fig. 6 Porosity results of hydroxyapatite sintered at 1000 °C

It may be inferred from Figs. 5 and 6 that porosity and compressive strength are closely related. The compressive strength of hydroxyapatite increases as the percentage of porosity decreases. The results are consistent with studies by other authors in References [1] and [10], which claim that the porosity of hydroxyapatite affects its mechanical properties and that a decrease in the porosity of the samples results in an increase in those properties. It was found that there is a relationship between the two by comparing the compressive strength results with the porosity results, as the compressive strength increases, the porosity decreases.

IV. Conclusions

The impact of particle size on the compressive strength and porosity of hydroxyapatite obtained from bovine bones sintered at 1000 °C was assessed. Results showed that a particle size of 53 μm had the highest compressive strength value of 2.5 MPa and a particle size of 300 μm had the highest value of 44.89% porosity.

The biological source synthesis technique was used to produce hydroxyapatite from the bones of cattle.

To assess the sample's purity and crystallinity, the XRD test was employed. The hydroxyapatite-specific peaks were seen in the diffraction patterns, and because they are very clearly defined, sharp, intense, and narrow, they suggest that the phases are more crystalline.

The TGA determined the hydroxyapatite's thermal stability, and in the bone sample under investigation, three stages of thermal decomposition were visible: the first stage, which takes place between 100 and 200 °C, is when water that is present in the powdered bovine bone is desorbed; the second, between 200 and 400 °C, is when the organic material is burned; and the third, between 400 and 800 °C, is when the carbonate groups are broken down.

The hydroxyapatite was found by SEM to have a surface that was densely packed, with grain boundaries visible in the morphology, as well as closer interconnectivity between the grain structure. In hydroxyapatite, this typically denotes the start of a distinct crystalline grain structure. According to the EDS test results, the three elements calcium (Ca), phosphorus (P), and oxygen (O) make up the majority of the sintered samples, with traces of other elements including sodium (Na) and magnesium (Mg). In terms of weight %, the sample's computed Ca/P ratio was 1.63, which deviates somewhat from the 1.67 theoretical value predicted for pure stoichiometric hydroxyapatite.

It was found that the compressive strength and porosity of hydroxyapatite made from bovine bone are considerably influenced by granulometry. Additionally, since the results demonstrate that the compressive strength obtained was higher (2.53 MPa) at a lower porosity (44.24%), it is possible to conclude that the compressive strength of hydroxyapatite depends on porosity.

Acknowledgment

The authors thank the Universidad Privada del Norte and the Universidad Nacional de Trujillo for the financial support received for the publication of this research and for providing the resources necessary to conduct this investigation.

References

[1] D. O. Obada, E. T. Dauda, J. K. Abifarin, D. Dodoo-Arhin, and N. D. Bansod, "Mechanical properties of natural hydroxyapatite using low cold compaction pressure: Effect of sintering temperature," *Mater Chem Phys*, vol. 239, Jan. 2020, doi: 10.1016/j.matchemphys.2019.122099.

[2] T. Varadavenkatesan, R. Vinayagam, S. Pai, B. Kathirvel, A. Pugazhendhi, and R. Selvaraj, "Synthesis, biological and environmental applications of hydroxyapatite and its composites with organic and inorganic coatings," *Prog Org Coat*, vol. 151, Feb. 2021, doi: 10.1016/j.porgcoat.2020.106056.

[3] N. A. M. Barakat, M. S. Khil, A. M. Omran, F. A. Sheikh, and H. Y. Kim, "Extraction of pure natural hydroxyapatite from the bovine bones bio waste by three different methods," *J Mater Process Technol*, vol. 209, no. 7, pp. 3408–3415, Apr. 2009, doi: 10.1016/j.jmatprotec.2008.07.040.

[4] S.-L. Bee, M. Mariatti, N. Ahmad, B. H. Yahaya, and Z. A. A. Hamid, "Effect of the calcination temperature on the properties of natural hydroxyapatite derived from chicken bone wastes," in *Materials Today: Proceedings*, 2019, vol. 16, pp. 1876–1885. doi: 10.1016/j.matpr.2019.06.064.

[5] E. S. Akpan, M. Dauda, L. S. Kuburi, D. O. Obada, and D. Dodoo-Arhin, "A comparative study of the mechanical integrity of natural hydroxyapatite scaffolds prepared from two biogenic sources using a low compaction pressure method," *Results Phys*, vol. 17, Jun. 2020, doi: 10.1016/j.rinp.2020.103051.

[6] E. S. Akpan, M. Dauda, L. S. Kuburi, D. O. Obada, N. D. Bansod, and D. Dodoo-Arhin, "Hydroxyapatite ceramics prepared from two natural sources by direct thermal conversion: From material processing to mechanical measurements," in *Materials Today: Proceedings*, 2020, vol. 38, pp. 2291–2294. doi: 10.1016/j.matpr.2020.06.391.

[7] F. Heidari, M. Razavi, M. Ghaedi, M. Forooghi, M. Tahriri, and L. Tayebi, "Investigation of mechanical properties of natural hydroxyapatite samples prepared by cold isostatic pressing method," *J Alloys Compd*, vol. 693, pp. 1150–1156, 2017, doi: 10.1016/j.jallcom.2016.10.081.

[8] S. Ramesh et al., "Characterization of biogenic hydroxyapatite derived from animal bones for biomedical applications," *Ceram Int*, vol. 44, no. 9, pp. 10525–10530, Jun. 2018, doi: 10.1016/j.ceramint.2018.03.072.

[9] A. Barrera Villatoro, J. Zarate Medina, T. Rivera Montalvo, and M. E. Contreras, "Efecto del Tamaño de Partícula en la Respuesta Termoluminiscente de la Hidroxiapatita," in *Proceedings of the ISSSD*, Sep. 2016, vol. 2, pp. 189–194.

[10] M. Munar, K. Udoh, K. Ishikawa, S. Matsuya, and M. Nakagawa, "Effects of Sintering Temperature Over 1,300°C on the Physical and Compositional Properties of Porous Hydroxyapatite Foam," *Dent Mater J*, vol. 25, no. 1, pp. 55–58, 2006.

[11] K. Haberko et al., "Natural hydroxyapatite - Its behaviour during heat treatment," *J Eur Ceram Soc*, vol. 26, no. 4–5, pp. 537–542, 2006, doi: 10.1016/j.jeurceramsoc.2005.07.033.

[12] K. Ishikawa, S. Matsuya, Y. Miyamoto, and K. Kawate, "9.05 Bioceramics," in *Bioengineering*, vol. 9, Elsevier Ltd., 2007, pp. 169–214. doi: 10.1016/B0-08-043749-4/09146-1.

ABOUT UMT FACULTY

SDI

Selective Dissemination of Information (SDI) service is a current-awareness service offered by the PSNZ for UMT Faculty Members. The contents selection criteria include current publications (last 5 years), highly cited and most viewed/downloaded documents. The contents with pdf full text from subscribed databases are organized and compiled according to a monthly theme which is determined based on the topics of specified interest.

For more information or further assistance, kindly contact us at 09-6684185/4298 or email to psnz@umt.edu.my/sh_akmal@umt.edu.my

Thank you.

Perpustakaan Sultanah Nur Zahirah
Universiti Malaysia Terengganu
21030 Kuala Nerus, Terengganu.

Tel. : 09-6684185 (Main Counter)
Fax : 09-6684179
Email : psnz@umt.edu.my